Modeling, analysis and simulation of 2D dynamic crack propagation

Von der Fakultät Mathematik und Physik der Universität Stuttgart
zur Erlangung der Würde eines Doktors der
Naturwissenschaften (Dr. rer. nat.) genehmigte Abhandlung

Vorgelegt von
Dipl.-Math. Adriana E. LALEGNAME
geboren in Tucumán, Argentinien

Hauptberichter: Apl. Prof. Dr. A.-M. Sändig

Mitberichter: Prof. Dr. G. Sewell, Prof. Dr-Ing. Dr. h.c. W. Wendland

Tag der Einreichung: 20 June 2009
Tag der mündlichen Prüfung: 22 July 2009

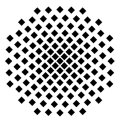

University of Stuttgart
Germany

Institut für Angewandte Analysis und Numerische Simulation.
University Stuttgart
2009

Dipl.-Math. Adriana Lalegname
Universität Stuttgart
Institut für Angewandte Analysis und Numerische Simulation
Pfaffenwaldring 57
70 569 Stuttgart
Germany
Stuttgart, den 22.07.2009

This document is typeset with LaTeX

I would like to dedicate this thesis to my loving parents

Isabel and Juan Carlos Lalegname

in honour of their lovely support during the time I spent on this work

Acknowledgements

This thesis has emerged from a DAAD Felloship for the project "*Dynamical crack propagation in a 2D elastic body*". It has been completed on my time as assistant at the Institut für Angewandte Analysis und Numerische Simulation, Department of Mathematics at the University of Stuttgart.

I would like to express my deep-felt gratitude to my supervisor appl. Prof. Dr. A.-M. Sändig, for her advice, encouragement, enduring patience and constant support, for the many interesting and not only mathematical discussions we had. She was never ceasing in her belief in me (though I was often doubting in my own abilities), always providing clear explanations when I was (hopelessly) lost, constantly driving me with energy when I was tired, and always, *always* giving me her time, in spite of anything else that was going on.
I would also thank Prof. Dr. G. Sewell for his encouragement, for his support over the whole period of time, I was working on this thesis, his valuable advice and review of this thesis. He taught me many things about computer science and life. Among the many things he showed me was that there really is science in computer science.
I also wish to thank Prof. Dr-Ing. Dr. h.c. W. Wendland. His suggestions, comments and additional guidance were invaluable to me. For many stimulating conversations, several helpful comments concerning to my work, I wish to express my thanks.
The author is greatly indebted to the members of my committee.

I gratefully acknowledge the financial support from the DAAD, who gave me the opportunity to interchange with many kind people in Germany and abroad from science and industry.
There are many colleagues from the *Institut für Angewandte Analysis und Numerische Simulation* whom I owe a lot of gratitude for their support and friendship. Among them Prof. Dr. Rohde, Dr. Werner Kolbe, all of the PhD students,

etc., etc.. The author gratefully acknowledges the many helpful suggestions and support of Dr. Heiko Schulz.
I wish to thank the University of Stuttgart, where this work was written, for financial support, for the invitation and hospitality.
Additionally, I want to thank the University of Tucumán, Argentinien and staff for all their hard work and dedication, to complete my goals.

Not least, I want to thank my family- parents, my sisters and my brother, for supporting me all the time in both counts: mentally and financially. I must thank for putting up with me during the development of this work with continuing, loving support.

Stuttgart, 2009

Contents

Zusammenfassung

Gegenstand der Bruchmechanik ist die Beschreibung der Phänomene, die bei der teilweisen oder vollständigen Trennung eines ursprünglich ganzen Körpers auftreten.
Physikalische Experimente und numerische Berechnungen zeigen, dass in einen Körper sehr hohe Spannungskonzentrationen in der Nähe von Rissen auftreten können. Solche Spannungskonzentrationen beeinflussen die Festigkeit und Lebensdauer des Körpers. So können sich zum Beispiel Mikrorisse bilden, wie das Beispiel von Bild 1(a) zeigt, die sich bei weiterer Belastung vereinigen und schließlich zum Versagen der gesamten Struktur führen. Zahlreiche Festigkeitshypothesen der Bruchmechanik basieren auf den Spannungsverteilungen im Körper, weshalb eine genaue Kenntnis der Spannungen notwendig ist.
Bruchprozesse sind jedem aus Natur und Technik hinlänglich bekannt. Sehr beeindruckend sind Risse und Brüche natürlicher Materialien wie Gestein und Eis, vor allem wenn sie uns in großen geologischen Formationen als Felseinstürze, Gletscherspalten und Erdbeben begegnen, siehe Bild 1(b).

Die in der Kontinuumsmechanik zur Beschreibung des mechanischen Verhaltens von Festkörpern verwendeten Größen wie Spannungen und Verzerrungen sind jedoch nicht immer unmittelbar für die Beschreibung von Bruchvorgängen geeignet. Aus diesem Grund werden in der Bruchmechanik zusätzliche Größen, wie zum Beispiel Spannungsintensitätsfaktoren oder Energiefreisetzungsraten, eingeführt, welche den lokalen Zustand an der Rissspitze beziehungsweise das globale Verhalten des Risses bei der Ausbreitung charakterisieren.

Zwei typische Probleme stehen im Vordergrund der Betrachtung der linearen Bruchmechanik: a) der stationäre (stehende) Riss unter einer dynamischen Belastung und b) der instationäre (schnell laufende) Riss.

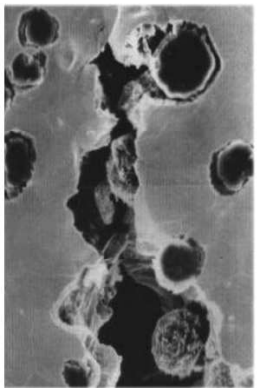

(a) Mikroriss im Gefüge von duktilem Gusseisen

(b) Makroriss (Spalte) im Fründelgletscher-Schweiz

Dieser Arbeit beschäftigt sich mit dem Punkt b), nämlich mit dem dynamischen Risswachstum. Es wird die Frage, wie weit sich ein Riss in einem Körper unter äußerem Welleneinfluss ausbreitet, diskutiert. Dabei hängt das Fortschreiten des Risses nicht nur von der Geometrie und dem Material des Körpers ab, sondern auch von der Art der äußerem Belastung.
Es soll unterstrichten werden, dass die Rissausbreitung in einem beschränkten Gebiet betrachtet wird, was zu zusätzlichen Schwierigkeiten im Vergleich zum üblichen Model in der gesamten Ebene führt.

Hinsichtlich der Deformation eines Risses werden drei verschiedene Rissöffnungsarten unterschieden (vgl. dazu Abbildung 2.2): *Modus I*, *Modus II* und *Modus III*. In dieser Arbeit wird unterschieden zwischen der *out-of-plane* und der *in-plane* Situation für die lineare Elastizität.
Im Falle linearer elastischer Materialien kann das Singulärverhalten schwacher Lösungen und deren Ableitungen in der Nähe von Rissspitzen vollständig durch eine asymptotische Entwicklung der Lösung charakterisiert werden.
In der Nähe der Rissspitze in einem zweidimensionalen Gebiet hat die asymptotische Entwicklung für ein Verschiebungsfeld $\vec{u} = (u_1, u_2, u_3)^\top$ folgende Struktur (Polarkoordinaten bezüglich Rissspitze):

$$\begin{pmatrix} u_1 \\ u_2 \end{pmatrix} = c_1\, r^{\frac{1}{2}}\, \vec{g}_1(\omega) + c_2\, r^{\frac{1}{2}}\, \vec{g}_2(\omega) + \vec{u}_{\text{reg}}.$$
$$u_3 = c_3\, r^{\frac{1}{2}}\, g_3(\omega) + u_{\text{reg}}.$$

Dabei sind die Singulärexponenten $\frac{1}{2}$ Eigenwerte eines zugehörigen Eigenwertproblems, die Funktionen $\vec{g}_1(\omega), \vec{g}_2(\omega)$ und $g_3(\omega)$ verallgemeinerte Eigenfunktionen und $\vec{u}_{\text{reg}}$, u_{reg} sind

glattere Funktionen. Die Eigenfunktionen können für gegebene Geometrie und Materialparameter explizit berechnet werden und hängen nicht von den äußeren Belastungen ab. Der Einfluss der äußeren Lasten spiegelt sich in den verallgemeinerten Spannungsintensitätsfaktoren c_i wider.

Ziel dieser Arbeit ist, das dynamische Risswachstum in einem linear elastischen, isotropen, homogenen zweidimensionalen Körper unter Einfluss einer Welle mathematisch zu untersuchen. Die Grundgleichungen der linearen Elastodynamik (Navier-Lamé-Gleichungen) sind hier zu verwenden:

$$\rho \vec{u}_{tt} - (\mu \Delta \vec{u} + (\lambda + \mu) \operatorname{grad}(\operatorname{div} \vec{u})) = \tilde{f} \tag{1}$$

wobei $\vec{u}(y,t) = \vec{u} = (u_1, u_2, u_3)^\top$ das Verschiebungsfeld, ρ die Massendichte, Δ den Laplace Operator, $\tilde{f}$ die Volumenkräfte und λ, μ die Lamé Konstanten beschreiben.

$$\lambda = \frac{\nu E}{(1+\nu)(1-2\nu)}, \quad \mu = \frac{E}{2(1+\nu)}.$$

Kommt es aufgrund äußerer Belastung zu einem Rissfortschritt in einem a-priori rissbehafteten Körper, so läßt sich das neue Rissproblem zu einem festen Zeitpunkt t als Transformation (Bewegung) des ursprünglichen Rissproblems zum Zeitpunkt Null auffassen. Mit Hilfe der Kontinuumsmechanik lassen sich aktuelle bruchrelevante Größen wie Verschiebungen, Spannungen, Spannungsintensitätsfaktoren, etc. durch eine Rück-Transformation auf eine Referenz Konfiguration ausdrücken.
Im Falle eines isotropen linear elastischen Körpers lassen sich die Spannungen σ als Asymptotiken der Form:

$$\begin{aligned} \sigma &= k_I(t,h,h')\, r^{-\frac{1}{2}} \widetilde{\sigma_{ij}}^{(1)}(\omega) + k_{II}(t,h,h')\, r^{-\frac{1}{2}} \widetilde{\sigma_{ij}}^{(2)}(\omega) + \sigma_{reg} \\ \nabla u_3 &= k_{III}(t,h,h')\, r^{-\frac{1}{2}} \widetilde{V_{ij}}^{(3)}(\omega) + \text{reg. Term} \end{aligned} \tag{2}$$

darstellen. r ist der Abstand zur Rissspitze und ω ist der Polarwinkel.
Dabei werden $\widetilde{\sigma_{ij}}^{(k)}$ bsw. $\widetilde{V_{ij}}^{(3)}$ aus den zu $\alpha = \frac{1}{2}$ gehörenden Eigenfunktionen berechnet.
Nähert man sich im Modus I der Rissspitze ($r \to 0$), so dominierten im Spannungsfeld die singuläre Terme, gewichtet durch den Spannungsintensitätsfaktoren $k_I(t) = k_I(t,h,h')$, $k_{II}(t) = k_{II}(t,h,h')$ und $k_{III}(t) = k_{III}(t,h,h')$.

Es gibt eine ganze Reihe von Bruchkriterien, bei denen Spannungen, Verzerrungen, die auftretende Energie oder die Spannungsintensitätsfaktoren zur Charakterisierung der Materialbeanspruchung und des Versagens herangezogen werden. Die wohl am häufigsten verwendeten Kriterien sind das *Griffith-Kriterium* und das *Irwin-Kriterium*. Im Fall dynamischer

Bruchvorgänge muss die kinetische Energie in die Energiebilanz bei der Rissausbreitung einbezogen werden. In dieser Arbeit betrachten wir ein verallgemeinertes dynamisches Griffith-Kriterium.
Das Bruchkriterium eines laufenden Risses hat deshalb die Form (unter geeigneten Voraussetzungen):

$$G(h,h') = \Gamma(h,h'). \tag{3}$$

Die rechte Seite $\Gamma(h,h')$ repräsentiert die dynamische Bruchzähigkeit (engl. dynamic toughness) und $G(h,h')$ die dynamische Energiefreisetzungsrate.
In der Arbeit werden zwei Aspekte untersucht.
Der erste Aspekt bezieht sich auf ein zweidimensionales Problem in dem angenommen wird, dass nur Scherwellen (Mode III), nichtebener Schubspannungszustand, auftreten und dass sich der Riss geradlinig ausbreitet. Damit ist es möglich von der klassischen Wellengleichung (Laplace-Operator) in der aktuellen Konfiguration auszugehen. Durch Aufstellen der Energiebilanz konnte eine gewöhnliche Differentialgleichung, "die Bewegungsgleichung", zur Bestimmung der Bewegung der Rissspitze $h(t)$ hergeleitet werden.
Die Kopplung der Wellengleichung mit der Bewegungsgleichung ist durch eine nichtlineare Relation zwischen $h(t)$, der Geschwindigkeit der Rissspitze $h'(t)$ und den sogenannten dynamischen Spannungsintensitätsfaktor $k_{III}(t) = k_{III}(t,h,h')$ dargestellt.

Der zweite Aspekt betrifft den ebenen Verzerrungszustand, "in-plane case", auf den die obige Methode übertragen wird. In diesem Fall treten zwei Ausbreitungsgeschwindigkeiten auf, die der Longitudinalwellen und der Transversalwellen und darüber hinaus die dynamischen Spannungsintensitätsfaktoren $k_I(t) = k_I(t,h,h')$ und $k_{II}(t) = k_{II}(t,h,h')$.

Wie in der Mechanik üblich, wurden ein elastodynamisches Skalarpotential ϕ und ein elastodynamisches Vektorpotential ψ_k in (1) so eingeführt, dass

$$\left.\begin{aligned} u_1 &= \partial_1\phi + \partial_2\psi_3 - \partial_3\psi_2, \\ u_2 &= \partial_2\phi + \partial_3\psi_2 - \partial_1\psi_3, \\ u_3 &= \partial_3\phi + \partial_1\psi_2 - \partial_2\psi_1. \end{aligned}\right\}$$

Es folgen die Helmholtzschen Wellengleichungen, die auf der aktuellen Konfiguration Ω_t definiert sind.
Es ergeben sich zwei hyperbolische Differentialgleichungen mit der Ausbreitungsgeschwindigkeit c_1 und c_2:

$$\ddot{\phi} - c_1^2\nabla^2\phi = 0 \text{ in } Q := \bigcup_{t=0}^{T} \Omega_t. \qquad \ddot{\psi} - c_2^2\nabla^2\psi = 0 \text{ in } Q := \bigcup_{t=0}^{T} \Omega_t,$$

$$c_1^2 = \frac{(\lambda + 2\mu)}{\rho}, \qquad c_2^2 = \frac{\mu}{\rho}.$$

Darin beschreibt das Skalarpotential ϕ eine Volumenänderung (Dilatation) und das Vektorpotential ψ_k eine reine Gestaltänderung bei konstantem Volumen (Distorsion). Entsprechend ist c_1 die Ausbreitungsgeschwindigkeit der Dilatationswellen (Longitudinalwellen) und c_2 die Ausbreitungsgeschwindigkeit der Distorsionswellen oder Scherwellen (Transversalwellen). Neben den Transversal- und den Longitudinalwellen spielen die Rayleigh-Wellen oder Oberflächenwellen eine wichtige Rolle bei dynamischen Rissproblemen. Es handelt sich dabei um Wellen, die sich entlang einer freien Oberfläche ausbreiten und die ins Innere hinein schnell abklingen. Die Ausbreitungsgeschwindigkeit c_R ergibt sich aus der Nullstelle der so genannten Rayleigh-Funktion D,

$$D := 4\,\alpha_1(t)\,\alpha_2(t) - (1 + \alpha_2(t)^2)^2,$$

$$\alpha_1(t)^2 = 1 - \frac{h'(t)^2}{c_1^2}, \qquad \alpha_2(t)^2 = 1 - \frac{h'(t)^2}{c_2^2}.$$

Das Rissspitzenfeld, d.h. die Spannungen und Deformation in einer Umgebung der Rissspitze sind von fundamentaler Bedeutung für das dynamische Risswaschstum. Dieses Feld beschreibt nicht direkt den Zustand in der Prozeßzone, bestimmt aber dennoch indirekt die Vorgänge, die in ihr ablaufen. Unter Prozeßzone, Bild 1(c), versteht man die Region in der Umgebung der Rissspitze, in welcher der mikroskopisch komplexe Prozeß der Bindungslösung stattfindet und die mit Mitteln der klassichen Kontinuumsmechanik nicht behandelbar ist. Es wird die

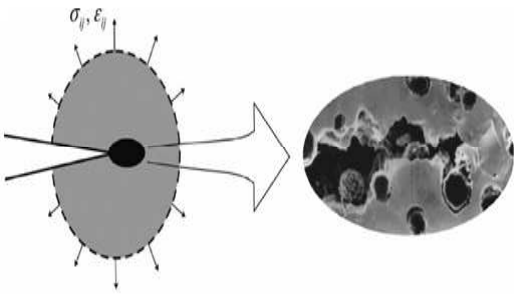

(c) Prozeßzone der mikromechanischen Bruchvorgänge an der Rissspitze

Energiebilanz in einem Körper mit Riss während der Rissausbreitung untersucht. Unter Verwendung eines verallgemeinerten *Griffithschen Bruchkriteriums* (3) wird auch diesem Fall eine gewöhnliche Differentialgleichung hergeleitet, die mit der Wellengleichung gekoppelt ist. Deren Lösungen beschreiben das gesuchte Risswachstum an der Rissspitze.
Die Bewegungsgleichung der Rissspitze kann auch im “in-plane“ Fall explizit hergeleitet

werden.
Die Vorhersage des Ausbreitungsvorgangs von Rissen ist für viele bruchmechanische Fragestellungen von Bedeutung. Die numerische Simulation bietet zur Lösung dieser Aufgaben hervorragende Möglichkeiten und hat sich zu einem unentbehrlichen Werkzeug entwickelt.
Die Lösungen der gekoppelten Probleme werden mit Hilfe des Programmpaketes PDE2D 8.6 berechnet. Diese Software ist ein FORTRAN-Programm.
Es geht hierbei um zeitabhängige Probleme, die man bei Aufteilung in mehrere Zeitintervalle mit unterschiedlichen Zeitschritten lösen kann. Am Ende jedes erfolgreichen PDE2D-Laufs wird die Lösung an den Knotenpunkten in einen 'restart'-File pde2d.res geschrieben. Die Möglichkeit von dump/restart erleichtert die Lösung nichtlinearer Probleme. Es wird von einem linearisierten Problem ausgegangen, dessen Lösung Startwert für ein neues, leicht modifiziertes lineares Problem ist. Weiterhin ist mit dump/restart der Aufruf von PDE2D in einer Schleife möglich.
Die vom Benutzer erstellte Anfangstriangulierung des Gebiets ist regulär.
Im Unterschied zu einer automatischen Vernetzung von Risskonfigurationen bzw. ausgewählten Teilbereichen, die mit herkömmlichen Netzgeneratoren erfolgt, spricht man von einer adaptiven Vernetzung dann, wenn der Algorithmus auf der Basis der FEM-Lösung selbst eine Anpassung der Diskretisierung an das behandelte Problem vornimmt. Als Kriterium für eine lokale Verfeinerung oder Vergröberung der Vernetzung dienen lokale Fehlerschätzer. Bei der adaptiven Triangulierung sind zwei oder mehr Läufe (mit einer unterschiedlichen Anzahl von Dreiecken in der Endtriangulierung) des Benutzerprogramms nötig. Beim ersten Lauf werden durch Setzen von TRIDEN Informationen über die Rechnung mit einer gleichmäßigen Triangulierung auf dem File *pde2d.adp* gespeichert. Diese dienen in den weiteren Läufen als Basis für die Netzerzeugung.
Auf sehr komfortable Weise wird das FEM-Netz in der Umgebung der Rissspitzen $(h(t),0)$ verfeinert, da hier der lokale Fehler der numerischen Lösung aufgrund der Spannungssingularität am höchsten ist. Für die Vernetzung der Rissumgebung ist ein sehr feines FEM-Netz erforderlich durch:

$$TRIDEN(y_1,y_2) = \frac{1.0}{\sqrt{(y_1-h)^2+y_2^2}}$$

Zur Berechnung unserer Rissprobleme werden isoparametrische Elemente vom Grad 3 generiert. Dadurch kann man viele derartige Elemente sektorförmig um die Rissspitze legen.
Für Elemente vom Grad 3 wird die Anzahl der benutzten Integrationsknoten so gewählt, dass die globale Genauigkeit von $O(h^4)$ für diese Elemente gewährleistet ist.
Es wird ein iteratives numerisches Verfahren zur Berechnung der unbekannten Verschiebungsfelds $u_3 = u_3(y,t)$, und $\vec{u} = \vec{u}(y,t)$ und von $h(t)$ aufgestellt. Daraus wird in Kapitel 7 ein

Algorithmus für den Modus III Fall hergeleitet und ein Flussdiagramm für den in-plane Fall aufgestellt.
Die größte Hürde ist dabei die Berechnung der dynamischen Spannungsintensitätsfaktoren während des Risswachstums. Diese können aus den FEM Verschiebungslösungen mit Hilfe von Extraktionsformeln errechnet werden. Für das Verschiebungenfeld bieten sich die Werte in den Knoten an. Hierbei treten folgende lokale Effekte auf:

- sehr nahe an der Rissspitze können die finiten Elemente die Singularität nur ungenau abbilden.
- Im mittleren Abstand ist die Güte der FEM-Lösung ausreichend.

Das bedeutet:

- erstens: je feiner wir vernetzen, desto höher wachsen die Spannungen in der Nähe der Rissspitze an,
- zweitens muss die Diskretisierung so fein sein, dass die Feldgrößen im Nahfeld der Rissspitze ausreichend genau berechnet werden. Dies ist Voraussetzung dafür, dass die Spannungsintensitätsfaktoren qualitativ gut extrahiert werden.

Die besten Erfahrungen mit dieser Auswertung gab es im folgenden Fall: die Spannungintensitätsfaktoren werden aus den FEM-Lösungen des Verschiebungsfeldes zweier gegenüberliegender Knoten auf den Rissspitze ermittelt, d.h. sei $(x_N, 0)$ Knotenpunkt der Rissspitze, dann werden die Verschiebungsfelder im Knotenpunkt $(x_{N-2}, 0)$ ausgewertet, um die Spannungsintensitätsfaktoren zu berechnen.
Bemerkung: Im allgemeinen Fall einer gemischten Modus-Beanspruchung des Risses müssen die unterschiedlichen Komponenten des Verschiebungsfeldes in der Nähe der Rissspitze entsprechend ausgewertet werden.
Um aus der FEM- Analyse der Randwertaufgabe am bewegten Riss die Rissspitzengeschwindichkeit $h'(t)$ ermitteln zu können, müssen Bruchkriterien herangezogen werden. Nachdem ein dynamischer Bruchvorgang gestartet ist, hängt der weitere Verlauf der Rissausbreitung vom Energieangebot und dem Energieverbrauch ab.

Zur numerischen Auswertung realistischer nichtgleichmäßiger Rissspitzengeschwindigkeiten $h'(t)$, wird die dynamische Bruchzähigkeit im verallgemeinerten dynamischen Griffith-Kriterium (3) nicht als konstant angesetzt, sondern als Funktion von t, $h = h(t)$ und $h' = h'(t)$.
Unsere numerische Resultate für die Rissspitzengeschwindigkeit stimmen mit dem Maximum

der Scherwellengeschwindigkeit in der Richtung der Rissausbreitung bis zu einer Geschwindigkeit $h'(t) < 0.65 * c_2$ überein, wie in der Literatur zu finden ist: für Modus III bildet die Scherwellengeschwindigkeit c_2 eine obere Grenze.

Ziele der Arbeit sind:

- Mathematische Modellierung und eine mathematische Herleitung der Bewegungsgleichung der Rissspitze unter dem Einfluss einer Welle für die sogennanten Fälle “out-of plane“ und ”in-plane” in endlichen Körpern.
- Herleitung von Singularitätsentwickungen für die Verschiebungs- und Spannungsfelder in der Nähe der Rissspitze in einem elastischen Körper.
- Analyse der Interaktion einer Belastungwelle mit einem sich fortpflanzenden Riss.
- Anwendung der bruchmechanischen Versagenskriterien und Konzepte auf rissbehaftete Konstruktionen, um quantitative Aussagen zur Bewegung der Rissspitze zu gewinnen.
- Entwicklung und Implementierung einer iterativen Methode zur Lösung des nichtlinearen gekoppelten Gleichungsystems.
- Interpretation der numerischen Rechnungen.

CHAPTER 1

Introduction

The object of fracture mechanics is to describe the behaviour of a body with crack under loading. Thereby a crack is a partial or complete macroscopic separation of a body. Pre-existing cracks are very common and virtually impossible to avoid in large structures. An important question is whether a pre-existing crack will grow for a given loading, Figure 1.1 shows the famous crack on the Liberty Bell, the crack was originally a hairline, and by the 1840s it was a threat to the bell.

Figure 1.1: The Bell (with crack)

Cracks are also frequently formed during manufacturing of the material or as the result of mechanical processes during manufacturing structural parts. Based on fracture mechanics investigations the safety and reliability of a body is estimated.
Modeling of fracture processes in structures and its simulations are challenging problems in mechanics as well as mathematics. Its understanding is important for the construction of structures and the development of new materials.
Typically the mathematical model consists of an idealized description of the geometrical configuration of the deformable body, an empirical relationship between internal stress and

deformation, and a corresponding balance law of physics dealing with mechanical quantities. Dynamic fracture mechanics is the subfield of fracture mechanics concerned with fracture phenomena in which inertia plays a role. Dynamic processes in a cracked body fall into two basic categories: dynamic crack propagation, and dynamic loading of bodies with stationary cracks. Often a mixture of these two kinds of processes appears, for example when dynamic loading on a body which contains a stationary crack causes dynamic crack propagation, or when dynamic crack propagation generates waves, which after reflection at an outer boundary of the body, impact on the crack.
Because an additional dimension, the time, enters when going from a static to a corresponding dynamic case, the mathematical models and the analysis are, of course, more difficult and complex. From the experimental point of view, the time dependence requires that many accurate sequential measurements of quantities of interest must be made in an extremely short time period in a such that there is no interference with the process being observed.

1.1 Motivation

In many cases, failure of engineering structures through fracture can be fatal. Often disasters occur because engineering structures contain cracks - arising either during production or during service (e.g. from fatigue).
In the beginning of the 1900's the interest increased in the behaviour of steel, the most used material at that time, after fractures were detected in various types of structures including ships, examples are Olympic (1911), Titanic (1912), several ships during World War I (1914-1918) and World War II, see Fig. 1.2.

Figure 1.2: Schip failure-Callister 1997

The ICE accident of Eschede, the heaviest tragedy in German rail, took place on June 3, 1998 on the track Hannover-Hamburg. It was caused by a single fatigue crack in one wheel, which when it finally failed, caused the train to derail, Figure 1.3.

(a) Cracks in sidewalk (b) Cracks in bone (c) Cracks in building

Figure 1.4: Cracks everyday

Lots of things crack, some just a little piece and some a whole lot. One can see cracks everyday, in the sidewalk, in a building, in a window, or maybe in a bone, Figure 1.4.

In the field of biomedical engineering we can quote as a typical problem the breaking of a bone. Fracture is another word for cracking or a crack. It is important to study how cracks behave because cracks can cause things to fail, something as small as a bone or as large as a ship. If a large structure, such as a building or a ship, cracks, this may lead to a catastrophic failure which could affect many people.

Experte hält Radsatzwellen für ungeeignet

ICE-Probleme: Bahn unter Druck

Ist der Riss, der an einer ICE -Radachse entdeckt wurde, wirklich als Einzelfall zu sehen? Ein angesehener Bahn-Gutachter widerspricht der Bahn und warnt: Die verwendeten Radsatzwellen entsprechen grundsätzlich nicht den Anforderungen.

Vatroslav Grubisic weiß, wovon er spricht: Der im Ruhestand lebende Professor wird als "Räder-Papst" bezeichnet und war für das Fraunhofer Institut Gutachter im Prozess um das ICE-Unglück von Eschede. Seit 2006 beschäftigt sich Grubisic intensiv mit den beim ICE verwendeten Radsatzwellen. Am Freitag (17.10.08) äußerte er sich gegenüber dem WDR äußerst kritisch zu den verwendeten →Radsatzwellen: Deren Lebenslaufzeit sei auf 15 Millionen Kilometer in 30 Jahren ausgelegt. Doch schon jetzt, nach einer Laufleistung von etwa sechs bis sieben Millionen Kilometern, gebe es die ersten Defekte.

Die Radsatzwellen werden kritisiert

Figure 1.3: Eschede train disaster

For analyzing the crack-tip behaviour theoretically, a number of approaches have been derived e.g. [7], [8], [17]. However, there are many unsolved problems in dynamic fracture mechanics.

Computational challenges

Since cracks cannot be eliminated, procedures must be devised to quantify and predict the behaviour of cracked structures under service conditions. Brittle materials, which can be modeled as linear elastic materials, require the prime characterization and evaluation of the

so-called stress intensity factors. The fundamental postulate of linear elastic fracture mechanics is that the behaviour of cracks, i.e. whether or not they grow and how fast they grow, is determined solely by the value of this stress intensity factor. The method for obtaining analytically as well as computationally stress intensity factor solutions to crack problems will be described in later chapters.
In this thesis, we focus on efficient solution techniques for the numerical simulation of crack propagation in 2D linear elastic formulations based on Finite Element Method.
The numerical solution procedure for the corresponding boundary value problem with changing boundaries conditions shall be made as efficient as possible. Thus, it is necessary to obtain high accurate solutions, particularly at larger times, surrounding the crack tip, including the asymptotic behavior, where the fracture process occurs. Away from the crack tip, the numerical solution does not require very high resolution. In fact, one needs adaptivity of the solution based on a posteriori error estimation together with effective capable solvers for the discrete solution system at each step of crack propagation.

1.2 Purpose of the thesis

The four building blocks of this thesis are: mathematical modeling, analysis, singular expansions and numerical simulations. We shall focus on the development of the following main goals:

- Mathematical modeling and a rigorous mathematical derivation of the crack tip motion under the influence of a wave for the out of- and in-plane cases.
- Study of the interaction of stress waves with a propagating crack and analysis of the displacement and stress fields of cracked elastic bodies which are subjected to external loadings. Here we consider the anti-plane/in-plane shear cracks in a finite body.
- Derivation of the displacement and stress fields of bodies with cracks near the crack tip.
- Resolution of mathematical models consisting of two coupled equations: a 2D scalar wave equation for the displacement fields in a cracked bounded domain and an ordinary differential equation for the crack position for the out-of plane case and the in-plane case respectively. Both cases are handled in a similar way, but the in-plane case, given by the Navier Lamé equations is more complicated.

- Presentation of an iterative method in order to solve the nonlinear coupled problems.
- Computation of a 2D dynamic crack propagation problem for the out of- and in-plane cases.

So far, to the author's knowledge, no such simulations for dynamical crack propagation in finite bodies have yet been done.

There are three basic modes of deformation for a cracked body. These modes are characterized by the movements of the upper and lower crack faces with respect to each other. We study the mode III, out of plane case, and the mode I and II, in-plane case, separately.
In the case of linear elastic materials, the singular behaviour of the displacement and stress fields near corners, edges or points with changing material parameters can be completely characterised by means of an asymptotic expansion of the solution near the crack tip.
The first step to compute local singularities is, as usual, to transform the problem into polar coordinates with respect to a corner point or an interior cross point S and use the fact that in the neighbourhood of S the solution for the displacement field $\vec{u}$ admits an expansion:

$$\vec{u} = \sum_{i=1}^{N} c_{\alpha_i} r^{\alpha_i} \vec{g}_i(\omega) + \vec{u}_{\text{reg}}. \tag{1.1}$$

(r, ω) are polar coordinates, centered at the singular point at the crack tip. Note that, we consider only those opening angles, where no logarithm terms occur.
The singular exponents $\alpha_i \in \mathbb{C}$ are eigenvalues of a corresponding nonlinear eigenvalue problem, and the functions $\vec{g}_i$ are eigenfunctions. The dominant singularity is given by the smallest positive real part of the eigenvalue α_i in a strip. The constants c_{α_i} are generalised stress intensity factors near the singular point. They can be obtained via postprocessing of the discrete finite solutions by using the eigenpairs $(\alpha_i, \vec{g}_i)$.
$\vec{u}_{\text{reg}}$ is a regular function. The regularity of the solution $\vec{u}$ is determined by the singular exponent α_i with the smallest positive real part. The c_{α_i} depend on the geometry, the elasticity parameters as well as on the boundary conditions. Additionally, c_{α_i} is influenced by the load.
Expansions like (1.1) have a long tradition in continuum mechanics for linear elastic materials. K. Wieghardt [43], studied the behaviour of stress fields near cracks with the help of an expansion like (1.1). Later, H.M. Westergaard [56], M.L. Williams [60] and G.R. Irwin [71] formulated new fracture criteria which are based on the representation (1.1) of the displacement and stress fields. In his fundamental work, V.A. Kondrat'ev [86] proved that the structure of solutions of linear elliptic equations near corner points is indeed completely

characterised by an asymptotic expansion, e.g. by (1.1).

The general strategy here is to describe the displacement fields in the medium subject to both, the boundary conditions as well as the externally applied stress.
For a single moving crack, the only energy sink existing in the system is located at the tip of the crack. Thus, an equation of motion can be obtained for a moving crack if one possesses detailed knowledge of the dissipative mechanisms in the vicinity of the tip.
Unfortunately, the processes that lead to dissipation in the tip's vicinity are far from simple. Fracture, together with the complex dissipative processes occurring in the vicinity of the tip, occurs due to intense values of the stress field that occur near to the tip.

This thesis deals with 2D problems and we restrict ourselves to straight cracks. In particular, we assume that the following assumptions are satisfied:

1 The material is homogeneous and isotropic and plane strain conditions hold.

2 The preexisting crack is part of a straight line and the crack can propagate along this line, only.

1.3 Thesis outline

The thesis is organized as follows:
Chapter 2 focuses on the mechanical and mathematical background of elasticity and fracture description on the basis of continuum mechanics. The two-dimensional Lamé equations, apply to the two cases of equilibrium of elastic bodies which are of considerable interest later on, namely the cases of *plane strain* and *plane stress*, are summarized. The Navier Lamé equations are introduced and the basic physical properties are discussed. The generalized Griffith energy criterion is presented. This discussion is very important in connection with the derivation of an equation of motion for a dynamic crack tip.
Chapter 3 is devoted to the study of the behavior of two-dimensional elastic fields near static cracks. The theory to which this chapter is devoted was develop through previous years. We have selected the material for this chapter in order to be able to present the main apparatus of the dynamic theory related to Navier-Lamé and Laplace operators used in Chapters 4-5, in a sufficiently detailed way. Furthermore, in order to motivate and explain some numerical aspects of the posteriori dynamic cases, we give short new strategy and overview on numerical computations of the eigenfunctions for the boundary value problem for Lamé equations

with conical points. The numerical results in this section were produced by a Fortran program solver and a PDE2D program (Appendix B). Both are designed to solve the more general problem (A.8), where $h'(t)$ is not necessarily 0, hence $\alpha_2(t) := \sqrt{1 - \frac{h'(t)^2}{c_2^2}}$ is not 1. This is an eigenvalue problem where the eigenvalue appears non-linearly. For the static case, $h'(t) = 0$, which implies $\alpha_2(t) = 1$, the problem reduces to (3.6). For the static state the results from the Fortran and PDE2D programs can be compared with analytical one from [23].

We split the investigation on dynamic crack propagation into the two fracture states.

Chapters 4-5 are devoted to the main results on dynamic crack propagation. In these chapters asymptotic formulas for displacement-, stress fields are derived. The significance of these computations particularly manifests itself later in deriving asymptotic formulas for solutions. An important role play the coefficients in asymptotics of solutions: the dynamic stress intensity factors.

The goal is to investigate mathematically the behaviour of a linear elastic, isotropic, homogeneous and finite body with a running crack under the influence of a wave. Here we concentrate on bounded crack velocities. Reducing the three-dimensional wave model given by Navier-Lamé equation system to a two-dimensional one we get an in-plane model for plane elastic waves and an out-of-plane model for shear waves, according to Chapter 2.

The main points are in both cases: the description of the behaviour of the elastic fields near the running crack tip and the derivation of the equations of motion of the crack tip.

The method: *Analysis of the transformed problem.*

A well-tried method in solid mechanics is to transform the current configuration (a noncylindrical space-time domain, space variables y_1, y_2) like in P. Destuynder and M. Jaoua, (1981), *Sur une interprétation mathématique de l'intégrale de Rice en théorie de la rupture fragile*. For this purpose it will be assumed there is a family of mapping $y = F_t(x) = x + h(t)\theta(x)$ which maps the reference configuration Ω_0, (space variables x_1, x_2, cylindrical domain) into the current configuration Ω_t. Additionally a further configuration (space variables z_1, z_2), where the isotropic Laplacian appears, is considered. The passage to the different configurations is described by corresponding coordinate transformations.

Roughly speaking, $h(t)$ describes the motion of the crack tip. Performing the above change of variables we get elastic wave equations with time-dependent coefficients and lower order terms in Ω_0. Using functional analysis arguments the solvability of the transformed initial boundary value problem is studied.

Derivation of the equation of motion. Starting from the rate of the total energy in the current

configuration we have to derive an equation of motion of crack tip, that means, a nonlinear ordinary differential equation for $h(t)$. In order to calculate the rate of the contributing energies we transform again the integrals into the reference configuration and use the results of the first item.

Most of the studies on the dynamic crack propagation from the viewpoint of the fracture mechanics postulate the body is infinite in a thickness direction because the mathematical treatment is simple. However this postulate is not pertinent to most practical cases. We report here an analytical study on the dynamic crack propagation in a finite configuration.

Chapter 4 begins with the simpler out-of-plane state.

Chapter 5 is devoted to the most interesting fracture case in applications, i.e. the in-plane state. A sizable portion of the material in this Chapter is discussed in [4].

For both cases the analytical solution is determined in the vicinity of a moving crack located in an isotropic medium. As specially, we are concerned with the variation of stress intensity factors and displacement fields near the crack tip. The extraction of the dynamical stress intensity factor from the current displacement field decomposition for the out-of-plane state, is given in Chapter 4.

In order to construct the asymptotics of the singular solutions for in-plane fracture case in Chapter 5, the matching procedure will be used once more. In contrast to the previous chapter 4, the method based on ideas [4], [77] is not directly applicable transforming the space variables x_1, x_2, to space variables z_1, z_2, where the singular solution of the Navier-Lamé could be obtained in easier way. This step is just a mathematical tool to start from an isotropic Laplacian near the crack tip and to use the known singular fields.

For getting these fields we introduce in Chapter 5 auxiliary potentials ϕ and ψ related to the in-plane motion of the crack which are separable into Mode I (opening mode) and Mode II (inplane sliding mode) crack problems.

Once such asymptotic fields near the tip of a propagating crack are determined, other important quantities of relevance in dynamic fracture mechanics, such as dynamic stress intensity factors and dynamic energy release rate can be determinated.

In **Chapter 6** we outline the crack tip energy flux in terms of the near tip mechanical fields for the in-plane fracture case. First of all, an expression for crack tip energy flux, is obtained by application of Reynolds's transport Theorem and the divergence theorem. The calculations thereby are long and technical but, we make them as practical as we can, computing the expressions in the more mathematically convenient reference configuration.

Here, the generalized fracture Griffith criterion and a generalized energy balance law are also used:

$$\hat{\Pi}(t) = \dot{D}(t) + \dot{E}(t) - \hat{A}(t) + \dot{K}(t) = 0$$

with the rate of the elastic energy $\dot{E}$, the external energy $\hat{A}$, the rate of the kinetic energy $\dot{K}$. $\dot{D} = \frac{d}{dt}D$ is then the rate of dissipative energy.

The expression derived for the crack tip energy flux holds for general material response. Then we restrict ourselves for the particular case the mode I fracture (it is assumed that $k_{II}(t,h,h') = 0$), for which some expression for the fracture toughness is found. Assuming small-scale yielding, rate independent behaviour under monotonically increasing stress intensity factors, it is possible also to write an equation of motion of the crack tip.

The corresponding expressions for the dynamic stress intensity factors $k_I(t,h,h')$ and $k_{II}(t,h,h')$ are extracted in the Chapter 6. The novelty is here that we use the solutions for the displacement field $\vec{u}$ given in the different configurations for determining the stress intensity factors in terms of displacement field, instead of the stress field as usual in the mechanics literature. That means, they are extracted by using a very precise knowledge of the solution at the crack tip.

Chapter 7 deals with the numerical simulation of a linear elastic, finite body with a crack influenced by a wave. Galerkin finite element method with isoparametric triangular elements of third degree is used for discretisation with respect to space and the Crank-Nicolson scheme for the time discretisation is applied.

The goal is the development of numerical methods that provide fast and reliable evaluation of the PDE input-output relationship.

At first the two-dimensional antiplane situation is analysed and simulated. Since we deal with time dependent problems, we have to analyse some preprocessing tasks. The corresponding initial displacement field and crack tip speed is computed according to:

$$\begin{aligned} u_0 &= u_{R0} + k_{III}(0)\ \eta\ S_N(x_1,x_2,0), \quad k_{III}(0) \in \mathbb{R},\ u_{R0} \in H^2(\Omega_0) \\ u_1 &= \partial_t u(0) \in H^1_D(\Omega_0), \end{aligned} \tag{1.2}$$

with

$$S_N(x_1,x_2,t) = \sqrt{\frac{r}{2\alpha_2(t)}}\sqrt{\sqrt{\cos^2\phi + \alpha_2^2(t)\sin^2\phi} - \cos\phi}$$

defined here in the reference configuration.

Numerical results for the coupled problems from chapters before togheter with initial conditions of the form (1.2), i.e. initial conditions depending also on the values of the stress intensity factors, are not explicitely known until now.

We deal with time-dependent problems, i.e. when the crack evolves, we require that the mesh evolves also and must conform to the crack geometry. As the crack is part of the mesh, this involves the update of the mesh, as well as the data structure associated with the crack geometry. One must treat a moving-singularity-boundary-value-problem.

Since the solution exhibits a strong singularity at the crack tip, a strongly refined mesh is required near the crack tip. This technique requires considerable computing time because of the nature of the iteration. Because of that, a parallel solver which runs efficiently on multiple processor machines, is used. Furthemore, the grids are most dense near the crack tip $(h(t),0)$. That is realized by a user-defined FORTRAN expression, here took as:

$$TRIDEN(y_1,y_2) = \frac{1.0}{\sqrt{(y_1-h)^2+y_2^2}}.$$

This controls the grading of the triangulation. Note that TRIDEN is largest where the triangulation is to be most dense, i.e at the crack tip $(h(t),0)$.

Since the mathematical analysis of the full coupled nonlinear problem for the wave equations with the equation of motion for the crack tip, described in Chapter 4 is not easy, we use an iterative approach starting from a given pre-crack position. Computing the wave-displacement and the dynamic stress intensity factor $k_{III}(t,h,h')$ at a certain time $t = t_i$, the solution of an ordinary differential equation is used to pass to the next time step $t = t_{i+1}$ and repeat the procedure.

Using the equation of motion of the crack tip, the crack propagation behaviour is given if the fracture toughness is provided. In contrast to the simpler case, constant quantity for the fracture toughness, we compute here more realistic model and we get non-uniform crack tip velocities.

These simulations are realized for different measures of resistance of the material to extension of a crack (fracture toughness). Finally, numerical simulations are presented, which show the influence of changing boundary conditions and the given triangulation on the growth of the advance of the crack.

Due to its great importance in dynamic fracture mechanics, the computation of the dynamic stress intensity factor has attracted much attention from engineers [14], [15], [83]. However, we mention that to our knowledge the analytical model proposed here and the numerical simulation of the crack tip motion $h(t)$ and the corresponding nonuniform crack tip speed $h'(t)$ are new.

The second part of this chapter is devoted to numerical treatment of the coupled problem for the in-plane fracture case, which becomes even more complicated. The same questions for mesh generation, control on the grading of the triangulation, moving-singularity are set forth in the in-plane case.

Now the initial conditions for the initial position and velocity of each point look like:

$$u_1(y,t_0) = k_I(h,h',t_0)\,\frac{(1+\alpha_2(t_0)^2)\,\sqrt{2r}}{\mu\,D}\left[\sqrt{\frac{\sqrt{\cos^2\varphi+\alpha_1(t_0)^2\sin^2\varphi}+\cos\varphi}{\cos^2\varphi+\alpha_1(t_0)^2\sin^2\varphi}}+\right.$$
$$\left.-\frac{2\,\alpha_1(t_0)\,\alpha_2(t_0)}{(1+\alpha_2(t_0)^2)}\sqrt{\frac{\sqrt{\cos^2\varphi+\alpha_2(t_0)^2\sin^2\varphi}+\cos\varphi}{\cos^2\varphi+\alpha_2(t_0)^2\sin^2\varphi}}\right],$$
$$u_2(y,t_0) = k_I(h,h',t_0)\,\frac{(1+\alpha_2(t_0)^2)\,\sqrt{2r}}{\mu\,D}\left[-\alpha_1(t_0)\sqrt{\frac{\sqrt{\cos^2\varphi+\alpha_1(t_0)^2\sin^2\varphi}-\cos\varphi}{\cos^2\varphi+\alpha_1(t_0)^2\sin^2\varphi}}+\right.$$
$$\left.+\frac{2\,\alpha_1(t_0)}{(1+\alpha_2(t_0)^2)}\sqrt{\frac{\sqrt{\cos^2\varphi+\alpha_2(t_0)^2\sin^2\varphi}-\cos\varphi}{\cos^2\varphi+\alpha_2(t_0)^2\sin^2\varphi}}\right]$$

and

$$\partial_t\vec{u}(y,t_0) = 0.$$

The strategy for solving this dynamic fracture problems is to obtain the dynamically admissible displacement fields from the Navier Lamé governing equations, subjected to the initial and boundary conditions, and then use the energy rate balance equation at the crack tip equation to determine the crack speed.
The chapter contains some conclusions. We also formulate some remarks, which are related to the problems discussed in this thesis.
The thesis closes with an appendix where we list some essential results and transformations on the different configurations, which are needed for the proofs.

This method was motivated in the Literature by Freund, [8], [13], [38], [45], [46], Gross, [15], [17], Aliabadi, [30], Rosakis A.J. Ravichandran G., [25].

CHAPTER 2

Fracture mechanics

2.1 Introduction

One of the most important, classical objectives of fracture mechanics is to understand the behavior of propagating of a pre-existing crack in a structure. Given an initial crack inside a structure, under which loading and environment conditions will it propagate; and if it does, which velocity at? To answer these questions, computational fracture mechanics uses the theory of failure analysis of material and structures containing cracks. Once the ingredients, the fields of displacement, strain, stress and energy of the structure, are obtained, it is possible to extract the information of the behavior of the crack numerically.

Because the process zone, which always appears in a small region near the crack tip and is subjected to very high load, cannot be treated as a continuum, fracture problems cannot be solved simply by calculating stress and strains in the body. The significant process in the process region is the nucleation and growth of micro-separations. By micro-separations it is meant a material separation on a micro-structural level.

On the other hand, knowledge of stress and strains in the continuum outside the process zone is essential for understanding the process of crack growth. Both analytical and numerical calculations play important roles. Due to the complexity of the real phenomena concerning cracks, analytical methods require the description of the body geometry, process zone and continuum constitutive equations.

In this chapter we shall review some fundamental concepts of fracture mechanics which we

shall use later on. We shall review the fundamental equations of linear elastic fracture mechanics, basic fracture mechanics concepts, and crack growth prediction theory.

2.1.1 Background of elasticity and mathematical preliminaries

Let a body occupy the domain $\Omega \subset \mathbb{R}^3$.
The solid particle coincides with the point $y = (y_1, y_2, y_3) \in \Omega$. An elastic solid is described by the following fields:

- the displacements $u(y) = (u_1(y), u_2(y), u_3(y))$;
- the strain tensor $\varepsilon_{ij}(y)$, $i, j = 1, 2, 3$;
- the stress tensor $\sigma_{ij}(y)$, $i, j = 1, 2, 3$

at the point $y \in \Omega$.
To formulate a model of the solid body, one needs the *constitutive law* $\sigma = \sigma(\varepsilon)$, *the geometrical equation* $\varepsilon = \varepsilon(u)$ and equilibrium or motion equations.

Let $f = (f_1, f_2, f_3)$ be a given function describing an external force in the domain Ω, the *static equilibrium equations* are as follows:

$$-\sigma_{ij,j}(y) = f_i(y), \quad i = 1, 2, 3,$$

where $\sigma_{ij,j} = \dfrac{\partial \sigma_{ij}}{\partial y_j}$; the repeated indices j mean the sum over j=1,2,3.
In the dynamical case all functions depend also on the time variable $t, t \geq 0$, and we have the *motion equations*

$$\rho \frac{\partial^2}{\partial t^2} u_i(t, y) - \sigma_{ij,j} = f_i(t, y), \quad i = 1, 2, 3.$$

2.1.2 Continuum fracture mechanics

In this subsection we attempt to review briefly the background and underlying assumptions to discuss the behaviour of a body in the framework of continuum fracture mechanics. There are many textbooks on the subject from many different points of view.
According to J. Betten, [37], continuum mechanics for solids may be divided into three fields: elasticity, plasticity and creep mechanics. For elasticity and plasticity it is assumed that the material behaviour of the body depends only on the chronological order of the applied loadings but not on the particular velocity which means that the processes are **rate independent**.

In contrast to that, creep mechanics deals with materials with a **rate dependent** behaviour, i.e., it depends on how fast the applied loadings change with time.
A body is **elastic**, if the deformation is reversible and vanishes immediately and rate independently if the loadings are removed. In contrast to that there remains a permanent strain after unloading in plastic bodies, where the process is irreversible.

We will discuss here the reduction of linear elasticity to two dimensions. Some basic concepts common to both static and dynamic cracks will be here discussed.
We will perform an asymptotic analysis for a straight crack near the crack tip.
The principal interest of analysis of dynamial crack propagation problems is to study how the elastic fields surrounding the moving tip evolve in time. Therefore it is appropiated to express the field equations, initial and boundary conditions with respect to a coordinate system which translates with the propagating crack and whose origin is attached to the moving tip.

We start with some useful definitions and the description of a deformation process of an elastic body as depicted in Figure 2.1, which occupies the domain Ω at the time $t = 0$.

Definition 1. *The particles of a body can occupy various positions in a 3-dimensional space. The complete specification of the positions of the particles of a body is called the configuration of a body.*

Definition 2. *The configuration of a body at the* ***reference time (initial or undeformed state)*** *and the* ***current time (or deformed state)*** *is the reference configuration denoted by Ω_0 and the current configuration denoted by Ω_t, respectively.*

To describe the two configurations, a *material* (Lagrangian) *coordinate system* denoted by x, and a *spatial* (Eulerian) *coordinate system*, denote by y, is introduced. For convenience, the undeformed configuration of a material element is often chosen as the reference configuration, but, any other configuration may also be serve as the reference configuration, if needed.

Definition 3. *A motion is a time-dependent family of configurations, written as*

$$y = F(x,t) = F_t(x),$$

see Figure 2.1.

The reference and the deformed configurations are distinguished in the following way:

- **Spatial/Euler view** The variables $y = F_t(x)$ in the deformed configuration are called Euler coordinates. They are part of the problem's solution. Volume and surface forces which load the body are given in those coordinates.

- **Material/Lagrange view** The so called Lagrange variables x of the reference configuration are given. Therefore it is desirable, to transform the equations of motion, which are given in Euler coordinates, back to the reference configuration which is achieved by the Piola transformation.
  Lagrange view means, that an observer follows each material point on its curve.

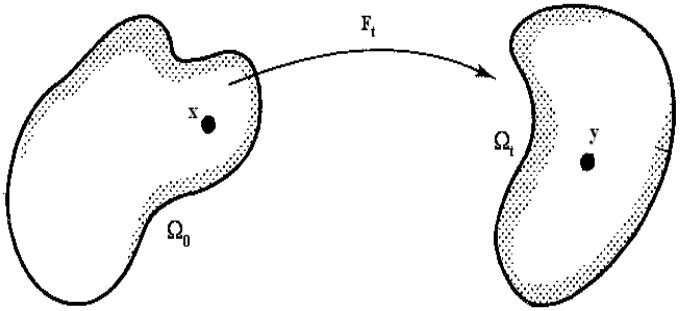

Figure 2.1: The reference configuration Ω_0 and the body after the time t, i.e. the current configuration Ω_t

The evolution of a spatial field is basically described by the Reynolds transport theorem. In case of a scalar field, like mass density, the Reynolds transport theorem reads as follows:

Theorem 1. ***Reynolds transport theorem***
Let $\phi : \Omega_t \to \mathbb{R}$ be a smooth scalar field in the current configuration. Furthermore, let $\upsilon : \Omega_t \to \mathbb{R}^d$ be the corresponding smooth spatial velocity and let $\widehat{\phi} : \Omega_t \to \mathbb{R}$ be a volume source of this field also in the current configuration. Then for any time $t \in (0,T)$ and any subdomain $\mathcal{P}_t \subset \Omega_t$ holds

$$\frac{d}{dt}\int_{\mathcal{P}_t} \phi d\boldsymbol{y} = \int_{\mathcal{P}_t} \left(\phi' + div_y(\phi\,\upsilon)\right) d\boldsymbol{y} = \int_{\mathcal{P}_t} \widehat{\phi} d\boldsymbol{y}.$$

In fact, this relation holds for all subdomains $\mathcal{P}_t \subset \Omega_t$ and we have almost everywhere

$$\phi' + div_y(\phi\,\upsilon) = \widehat{\phi}.$$

Proof. The proof basically uses transformation of integrals. For details see Gurtin, [59], page 78. □

Continuum mechanics for static problems is based on the stress principle, named so after the fundamental contributions by Euler [1757-1771] and Cauchy [1823-1827]. Cauchy's theorem guarantees the existence of a continuously differentiable tensor field

$$T^{F_t} : F_t(\Omega_0) \to \mathbb{R}^{3\times 3}$$

which allows us to write the following boundary value problem in the deformed configuration

$$\begin{aligned} -\mathrm{div} T^{F_t}(y) &= f^{F_t}(y), \quad \text{in } \Omega_t, \\ T^{F_t}(y) n^{F_t} &= g^{F_t}(y), \quad \text{on } \Gamma_1^{F_t} \subset \partial\Omega_t. \end{aligned}$$

We now formulate the field equations in the reference configuration. We use the *Piola transformation* $P : \mathbb{R}^{3\times 3} \to \mathbb{R}^{3\times 3}$ defined by

$$\begin{aligned} PT^{F_t}(y) = T(x) &= T^{F_t}(y)\mathrm{Cof}(DF_t) \\ &= T^{F_t}(y)\det(\nabla F_t)[DF_t(x)]^{-\top}. \end{aligned}$$

$T(x)$ is called the *first Piola-Kirchhoff-stress tensor*.
D is the derivative operator. Here we denote the operator ∇ as $\nabla = \mathrm{D}^\top$.

$$\nabla \vec{u} = (\mathrm{D}\vec{u})^\top = \begin{pmatrix} \partial_{y_1} u_1 & \partial_{y_2} u_1 & \partial_{y_3} u_1 \\ \partial_{y_1} u_2 & \partial_{y_2} u_2 & \partial_{y_3} u_2 \\ \partial_{y_1} u_3 & \partial_{y_2} u_3 & \partial_{y_3} u_3 \end{pmatrix}^\top.$$

Since

$$-\mathrm{div} T(x) = -\det(DF_t)\,\mathrm{div}(T^{F_t}(y)),$$

we get the following boundary value problem in the reference configuration:

$$-\mathrm{div} T(x) = f(x) := (\det DF_t(x)) f^{F_t}(F_t(x)), \quad \text{in } \Omega_0, \tag{2.1}$$

$$T(x)n(x) = g(x) := (\det DF_t(x))||(DF_t(x))^{-\top} n|| g^{F_t}(F_t(x)), \quad \text{on } \Gamma_1. \tag{2.2}$$

The *symmetric second Piola-Kirchhoff stress tensor* is defined as

$$\Sigma(x) = (\det DF_t(x))(DF_t(x))^{-1} T^{F_t}(y) DF_t(x)^{-\top} = (DF_t(x))^{-1} T(x).$$

It satisfies the following boundary value problem in the reference configuration:

$$-\mathrm{div}(DF_t(x)\Sigma) = f(x), \quad \text{in } \Omega_0 \tag{2.3}$$

$$DF_t(x)\Sigma(x)n(x) = g(x), \quad \text{on } \Gamma_1, \tag{2.4}$$

$$F_t(x) = F_0(x), \quad \text{on } \Gamma_0 = \partial\Omega_0 \backslash \overline{\Gamma_1}. \tag{2.5}$$

The constitutive equations near the reference configuration
For $F_t = \mathrm{id}$, i.e. $F_t(x) = x$ and $DF_t(x) = I$ the stress in the reference configuration is given by:

$$\Sigma(x) = T^{F_t}(y) = T(x).$$

Stress occur in the body if the distances between neighbored material points change during the deformation. A suitable measure for this change of distances is given by the Green-St. Venant or Lagrangian strain tensor

$$E(u) = \frac{1}{2}\left(Du + (Du)^\top + (Du)^\top (Du)\right).$$

Definition 4. ***St. Venant-Kirchhoff materials***
An isotropic and elastic material is a St. Venant-Kirchhoff material, if

$$\Sigma(x) = \lambda\, tr E(x) I + 2\mu E(x) \tag{2.6}$$

where λ and μ are the Lamé constants.

Under the assumption of a small gradient of the displacement field $\vec{u}$ one obtains the linearised strain tensor $\varepsilon(\vec{u})$ by cancelling the nonlinear term $(Du)^\top (Du)$ from E:

$$\varepsilon(\vec{u}) = \frac{1}{2}\left(\nabla\vec{u} + (\nabla\vec{u})^\top\right). \tag{2.7}$$

Instead of the nonlinear strain tensor E we consider the linearized strain tensor ε and as in the linear elasticity theory we consider the linear stress-strain relation, with the help of the generalization of Hooke's law, [28] (Robert Hooke 1635-1703):

$$\sigma_{jk}(y) = \sum_{l,m=1}^{n} c_{jklm}(y)\,\varepsilon_{lm}(y) = \lambda\varepsilon_{ii}\delta_{jk} + 2\mu\varepsilon_{jk}$$

or

$$\sigma(\varepsilon) = \lambda\,(\mathrm{tr}(\varepsilon))I + 2\mu\varepsilon. \tag{2.8}$$

This form of Hooke's law was first derived (1820s) by Claude Louis Marie Henri Navier (1785-1836). The Lamé constant μ is known as the shear modulus or rigidity: it is a measure of the resistance against shear or torsion of the medium. The shear modulus is large for very stiff materials, but is small for media with low viscosity ($\mu = 0$ for water or for liquid metallic iron in the outer core). The other Lamé constant, λ, does not have much (general) physical meaning by itself, but defines important elastic parameters in combination with the shear modulus μ.

The elasticity tensor c_{jklm} has the symmetry properties

$$c_{jklm} = c_{kjlm} = c_{jkml} = c_{mljk}.$$

Therefore, in case the case $n=3$ or $n=2$ there are only 21 or 6 different entries, respectively, the elasticites which define the symmetric positive definite $3(n-1)\times 3(n-1)$ Sommerfeld matrix, [28]

$$\widehat{C}(y)=\begin{pmatrix} c_{1111} & c_{1122} & c_{1133} & c_{1123} & c_{1131} & c_{1112} \\ . & c_{2222} & c_{2233} & c_{2223} & c_{2231} & c_{2212} \\ . & . & c_{3333} & c_{3323} & c_{3331} & c_{3312} \\ . & . & . & c_{2323} & c_{2331} & c_{2312} \\ . & . & . & . & c_{3131} & c_{3112} \\ . & . & . & . & . & c_{1212} \end{pmatrix} \quad \text{for } n=3, \tag{2.9}$$

and

$$\widehat{C}(y)=\begin{pmatrix} c_{1111} & c_{1122} & c_{1112} \\ . & c_{2222} & c_{2212} \\ . & . & c_{1212} \end{pmatrix} \quad \text{for } n=2.$$

For the isotropic material, the elasticities are explicitly given by

$$\begin{aligned} c_{1111}=c_{2222}=c_{3333} &= 2\mu+\lambda, \\ c_{2323}=c_{3131}=c_{1212} &= \mu, \\ c_{1122}=c_{1133}=c_{2223} &= \lambda \quad \text{and} \\ c_{jkml}=0 \quad &\text{for all remaining indices.} \end{aligned}$$

Hooke's law reads then in vector form:

$$\begin{aligned} \begin{pmatrix} \sigma_{11} \\ \sigma_{22} \\ \sigma_{33} \\ \sigma_{12} \\ \sigma_{23} \\ \sigma_{13} \end{pmatrix} &= \begin{pmatrix} 2\mu+\lambda & \lambda & \lambda & 0 & 0 & 0 \\ \lambda & 2\mu+\lambda & \lambda & 0 & 0 & 0 \\ \lambda & \lambda & 2\mu+\lambda & 0 & 0 & 0 \\ 0 & 0 & 0 & \mu & 0 & 0 \\ 0 & 0 & 0 & 0 & \mu & 0 \\ 0 & 0 & 0 & 0 & 0 & \mu \end{pmatrix} \begin{pmatrix} \varepsilon_{11} \\ \varepsilon_{22} \\ \varepsilon_{33} \\ 2\varepsilon_{12} \\ 2\varepsilon_{23} \\ 2\varepsilon_{13} \end{pmatrix} \\ &= \frac{E}{(1+\nu)(1-2\nu)} \begin{pmatrix} 1-\nu & \nu & \nu & 0 & 0 & 0 \\ \nu & 1-\nu & \nu & 0 & 0 & 0 \\ \nu & \nu & 1-\nu & 0 & 0 & 0 \\ 0 & 0 & 0 & \frac{1-2\nu}{2} & 0 & 0 \\ 0 & 0 & 0 & 0 & \frac{1-2\nu}{2} & 0 \\ 0 & 0 & 0 & 0 & 0 & \frac{1-2\nu}{2} \end{pmatrix} \begin{pmatrix} \varepsilon_{11} \\ \varepsilon_{22} \\ \varepsilon_{33} \\ 2\varepsilon_{12} \\ 2\varepsilon_{23} \\ 2\varepsilon_{13} \end{pmatrix}. \end{aligned} \tag{2.10}$$

From (2.10) it is possible to write ε in terms of σ by using the inverse matrix.

$$\begin{pmatrix} \varepsilon_{11} \\ \varepsilon_{22} \\ \varepsilon_{33} \\ 2\varepsilon_{12} \\ 2\varepsilon_{23} \\ 2\varepsilon_{13} \end{pmatrix} = \frac{1}{E} \begin{pmatrix} 1 & -\nu & -\nu & 0 & 0 & 0 \\ -\nu & 1 & -\nu & 0 & 0 & 0 \\ -\nu & -\nu & 1 & 0 & 0 & 0 \\ 0 & 0 & 0 & 2(1+\nu) & 0 & 0 \\ 0 & 0 & 0 & 0 & 2(1+\nu) & 0 \\ 0 & 0 & 0 & 0 & 0 & 2(1+\nu) \end{pmatrix} \begin{pmatrix} \sigma_{11} \\ \sigma_{22} \\ \sigma_{33} \\ \sigma_{12} \\ \sigma_{23} \\ \sigma_{13} \end{pmatrix}. \tag{2.11}$$

Following [72], we introduce the matrix $\mathcal{G}$ of differential operators generalizing the Nabla operator:

$$\mathcal{G} = \begin{pmatrix} \partial_1 & 0 & 0 \\ 0 & \partial_2 & 0 \\ 0 & 0 & \partial_3 \\ \partial_2 & \partial_1 & 0 \\ 0 & \partial_3 & \partial_2 \\ \partial_3 & 0 & \partial_1 \end{pmatrix} \quad \text{for } n = 3, \tag{2.12}$$

whereas for n=2, delete the rows containing ∂_3 and the last column.

Remark 1. *For convenience, we rewrite $\mathcal{G}$ in the form*

$$\mathcal{G} = \sum_{k=1}^{n} \mathcal{G}_k \frac{\partial}{\partial y_k}$$

where, for each fixed $k = 1, \cdots, n$, $\mathcal{G}_k = (\mathcal{G}_{lmk})_{l=1,\cdots,3(n-1)}$ is a constant $3(n-1) \times n$ matrix of the same form as $\mathcal{G}$.

Therefore the following vector form for $\vec{\varepsilon}$ holds:

$$\vec{\varepsilon} = \begin{pmatrix} \partial_1 & 0 & 0 \\ 0 & \partial_2 & 0 \\ 0 & 0 & \partial_3 \\ \partial_2 & \partial_1 & 0 \\ 0 & \partial_3 & \partial_2 \\ \partial_3 & 0 & \partial_1 \end{pmatrix} \begin{pmatrix} u_1 \\ u_2 \\ u_3 \end{pmatrix}. \tag{2.13}$$

We use now the constitutive relation (2.6) in the boundary value problem (2.3)-(2.4), and we get along with $F_t = I$ a non linear boundary problem.
The linearized boundary problem is obtained via (2.8) and reads:

$$-\text{div}\sigma = f(x), \quad \text{in } \Omega_0 \tag{2.14}$$

$$\sigma(x)n(x) = g(x), \quad \text{on } \Gamma_1, \tag{2.15}$$

$$u = 0, \quad \text{on } \Gamma_0. \tag{2.16}$$

Lemma 1. *For the displacement field $\vec{u}$, the linearized boundary value problem (2.14)-(2.16) reads:*
Find $\vec{u} = (u_1, u_2, u_3)^\top$ such that:

$$-(\mu\Delta\vec{u} + (\lambda+\mu)\, grad\, div\vec{u}) = f(x), \quad in\, \Omega_0 \tag{2.17}$$

$$\sigma(\vec{u})\, n = g, \quad on \Gamma_1, \tag{2.18}$$

$$\vec{u} = 0. \quad on \Gamma_0. \tag{2.19}$$

Proof. The proof is an elementary consequence of (2.14).

$$
\begin{aligned}
-\mathrm{div}\sigma(\vec{u}) &= -\mathrm{div}\begin{pmatrix} \lambda\,\mathrm{div}u + 2\mu\partial_1 u_1 & \mu(\partial_1 u_2 + \partial_2 u_1) & \mu(\partial_1 u_3 + \partial_3 u_1) \\ \mu(\partial_1 u_2 + \partial_2 u_1) & \lambda\,\mathrm{div}u + 2\mu\partial_2 u_2 & \mu(\partial_2 u_3 + \partial_3 u_2) \\ \mu(\partial_1 u_3 + \partial_3 u_1) & \mu(\partial_2 u_3 + \partial_3 u_2) & \lambda\,\mathrm{div}u + 2\mu\partial_3 u_3 \end{pmatrix} \\
&= -\begin{pmatrix} \mu\Delta u_1 + (\lambda+\mu)\partial_1 \mathrm{div}\vec{u} \\ \mu\Delta u_2 + (\lambda+\mu)\partial_2 \mathrm{div}\vec{u} \\ \mu\Delta u_3 + (\lambda+\mu)\partial_3 \mathrm{div}\vec{u} \end{pmatrix} \\
&= -L\vec{u} = -(\mu\Delta\vec{u} + (\lambda+\mu)\,\mathrm{grad}\,\mathrm{div}\,\vec{u})
\end{aligned}
$$

□

Remark 2. *The differential operator L is the so-called Lamé operator:*

$$L\vec{u} = \mu\Delta\vec{u} + (\lambda+\mu)\,grad\,div\,\vec{u} = div\,\sigma \tag{2.20}$$

where

$$\Delta = \nabla^2 = \partial_1^2 + \partial_2^2 + \partial_3^2, \quad grad = (\partial_1, \partial_2, \partial_3)^T, \quad div\,\vec{u} = \partial_1 u_1 + \partial_2 u_2 + \partial_3 u_3 = trace\,\varepsilon(\vec{u}).$$

In matrix form the operator L can be written as:

$$L\vec{u} = \begin{pmatrix} \mu\Delta + (\lambda+\mu)\partial_1^2 & (\lambda+\mu)\partial_1\partial_2 & (\lambda+\mu)\partial_1\partial_3 \\ (\lambda+\mu)\partial_2\partial_1 & \mu\Delta + (\lambda+\mu)\partial_2^2 & (\lambda+\mu)\partial_2\partial_3 \\ (\lambda+\mu)\partial_3\partial_1 & (\lambda+\mu)\partial_2\partial_3 & \mu\Delta + (\lambda+\mu)\partial_3^2 \end{pmatrix} \begin{pmatrix} u_1 \\ u_2 \\ u_3 \end{pmatrix}.$$

The differential equation system:

$$-L\vec{u} = -[\mu\Delta\vec{u} + (\lambda+\mu)\,grad\,div\,\vec{u}] = f \tag{2.21}$$

is called the ***Lamé or stationary Lamé-Navier System for the displacement field*** $\vec{u}$ ***in 3D***.

In terms of the Sommerfeld matrix $\widehat{C}$ (2.9) and of $\mathcal{G}$ (2.12), the Lamé operator (2.20) also takes the form

$$L\vec{u} = \mathcal{G}^\top\vec{\sigma} = \mathcal{G}^\top\widehat{C}\vec{\varepsilon} = \mathcal{G}^\top\widehat{C}\mathcal{G}\vec{u} = \sum_{j,k=1}^{n} \frac{\partial}{\partial y_j}\mathcal{G}_j^\top\widehat{C}\mathcal{G}_k\frac{\partial}{\partial y_k}\vec{u}. \tag{2.22}$$

Lamé or stationary Lamé-Navier System for the displacement field $\vec{u}$ in 2D.
There are cases in which the theory naturally reduces to two dimensions, where most of the analytical results have been obtained.

Also, mathematical investigations of crack problems mainly deal with the 2D case, where the singularities arise near the crack tip, [66], [86], [88], [81].
The equations of the plane theory of linearized elasticity, i.e. the two-dimensional Lamé equations, apply to two cases of equilibrium of elastic bodies which are of considerable interest in practice, namely to the case of *plane strain* and to the case of *plane stress*.

Definition 5. *The plane stress formulation is defined through the condition*

$$\sigma_{13} = \sigma_{23} = \sigma_{33} = 0. \tag{2.23}$$

Under the assumption of plane stress state (2.23) it follows from (2.11) that:

$$\begin{pmatrix} \varepsilon_{11} \\ \varepsilon_{22} \\ \varepsilon_{33} \\ 2\varepsilon_{12} \\ 2\varepsilon_{23} \\ 2\varepsilon_{13} \end{pmatrix} = \frac{1}{E} \begin{pmatrix} 1 & -\nu & -\nu & 0 & 0 & 0 \\ -\nu & 1 & -\nu & 0 & 0 & 0 \\ -\nu & -\nu & 1 & 0 & 0 & 0 \\ 0 & 0 & 0 & 2(1+\nu) & 0 & 0 \\ 0 & 0 & 0 & 0 & 2(1+\nu) & 0 \\ 0 & 0 & 0 & 0 & 0 & 2(1+\nu) \end{pmatrix} \begin{pmatrix} \sigma_{11} \\ \sigma_{22} \\ 0 \\ \sigma_{12} \\ 0 \\ 0 \end{pmatrix}$$

i.e. $\varepsilon_{13} = \varepsilon_{23} = 0$ and the component ε_{33} can be computed from the solution of

$$\varepsilon_{33} = -\frac{\nu}{E}(\sigma_{11} + \sigma_{22}).$$

It follows that the σ-ε relation reduces to:

$$\begin{pmatrix} \varepsilon_{11} \\ \varepsilon_{22} \\ 2\varepsilon_{12} \end{pmatrix} = \frac{1}{E} \begin{pmatrix} 1 & -\nu & 0 \\ -\nu & 1 & 0 \\ 0 & 0 & 2(1+\nu) \end{pmatrix} \begin{pmatrix} \sigma_{11} \\ \sigma_{22} \\ \sigma_{12} \end{pmatrix}. \tag{2.24}$$

The inversion of (2.24) leads to:

$$\begin{pmatrix} \sigma_{11} \\ \sigma_{22} \\ \sigma_{12} \end{pmatrix} = \frac{E}{(1-\nu^2)} \begin{pmatrix} 1 & \nu & 0 \\ \nu & 1 & 0 \\ 0 & 0 & \frac{1-\nu}{2} \end{pmatrix} \begin{pmatrix} \varepsilon_{11} \\ \varepsilon_{22} \\ 2\varepsilon_{12} \end{pmatrix}. \tag{2.25}$$

Then:

$$\sigma_{11} + \sigma_{22} = \frac{E}{(1-\nu^2)}((1+\nu)\varepsilon_{11} + (1+\nu)\varepsilon_{22}) = \frac{E}{(1-\nu)}(\varepsilon_{11} + \varepsilon_{22})$$
$$\varepsilon_{33} = -\frac{\nu}{E}(\sigma_{11} + \sigma_{22}) = -\frac{\nu}{(1-\nu)}(\varepsilon_{11} + \varepsilon_{22}).$$

In the case of the plane stress state, $\varepsilon_{11}, \varepsilon_{22}$ and ε_{33} are dependent.

Remark 3. *Furthermore it is assumed that stress and loadings depend on y_1 and y_2, only. i.e. $\sigma = \sigma(y_1, y_2)$ and $\varepsilon = \varepsilon(y_1, y_2)$ in the plane stress state:*
$-\frac{\nu}{(1-\nu)}(\varepsilon_{11}+\varepsilon_{22}) = \varepsilon_{33} = \varepsilon_{33}(y_1, y_2) = \frac{\partial u_3}{\partial y_3} \Rightarrow \frac{\partial u_3}{\partial y_3} =$ *constant with respect to* y_3.
Therefore $u_3 = \widetilde{u_3}(y_1, y_2)y_3$, along with $u_1 = u_1(y_1, y_2)$, $u_2 = u_2(y_1, y_2)$.
Then

$$0 = \varepsilon_{13}(y_1, y_2) = \frac{1}{2}\left(\frac{\partial u_3}{\partial y_1} + \frac{\partial u_1}{\partial y_3}\right) = \frac{y_3}{2}\frac{\partial \widetilde{u_3}}{\partial y_1} \Rightarrow \frac{\partial \widetilde{u_3}}{\partial y_1} = 0.$$

And correspondingly

$$\varepsilon_{23}(y_1, y_2) = 0 \Rightarrow \frac{\partial \widetilde{u_3}}{\partial y_2} = 0.$$

In a similar manner we define the plane strain state as follows:

Definition 6. *In the plane strain case it is assumed that:*

$$\varepsilon_{13} = \varepsilon_{23} = \varepsilon_{33} = 0. \tag{2.26}$$

Under the assumption of plane strain state (2.26) it follows from (2.10) that:

$$\begin{pmatrix} \sigma_{11} \\ \sigma_{22} \\ \sigma_{33} \\ \sigma_{12} \\ \sigma_{23} \\ \sigma_{13} \end{pmatrix} = \begin{pmatrix} 2\mu+\lambda & \lambda & \lambda & 0 & 0 & 0 \\ \lambda & 2\mu+\lambda & \lambda & 0 & 0 & 0 \\ \lambda & \lambda & 2\mu+\lambda & 0 & 0 & 0 \\ 0 & 0 & 0 & \mu & 0 & 0 \\ 0 & 0 & 0 & 0 & \mu & 0 \\ 0 & 0 & 0 & 0 & 0 & \mu \end{pmatrix} \begin{pmatrix} \varepsilon_{11} \\ \varepsilon_{22} \\ 0 \\ 2\varepsilon_{12} \\ 0 \\ 0 \end{pmatrix}$$

$$= \frac{E}{(1+\nu)(1-2\nu)} \begin{pmatrix} 1-\nu & \nu & \nu & 0 & 0 & 0 \\ \nu & 1-\nu & \nu & 0 & 0 & 0 \\ \nu & \nu & 1-\nu & 0 & 0 & 0 \\ 0 & 0 & 0 & \frac{1-2\nu}{2} & 0 & 0 \\ 0 & 0 & 0 & 0 & \frac{1-2\nu}{2} & 0 \\ 0 & 0 & 0 & 0 & 0 & \frac{1-2\nu}{2} \end{pmatrix} \begin{pmatrix} \varepsilon_{11} \\ \varepsilon_{22} \\ 0 \\ 2\varepsilon_{12} \\ 0 \\ 0 \end{pmatrix},$$

it follows for isotropic materials that $\sigma_{13} = \sigma_{23} = 0$ and

$$\sigma_{33} = \frac{E\ \nu}{(1+\nu)(1-2\nu)}(\varepsilon_{11}+\varepsilon_{22}).$$

In this case, the σ-ε relation is reduced to, (it holds for compressible materials, i.e. $\nu \neq \frac{1}{2}$):

$$\begin{pmatrix} \sigma_{11} \\ \sigma_{22} \\ \sigma_{12} \end{pmatrix} = \frac{E}{(1+\nu)(1-2\nu)} \begin{pmatrix} 1-\nu & \nu & 0 \\ \nu & 1-\nu & 0 \\ 0 & 0 & \frac{1-2\nu}{2} \end{pmatrix} \begin{pmatrix} \varepsilon_{11} \\ \varepsilon_{22} \\ 2\varepsilon_{12} \end{pmatrix}.$$

With the inverse matrix it holds the corresponding relation for the plane strain state

$$\begin{pmatrix} \varepsilon_{11} \\ \varepsilon_{22} \\ 2\varepsilon_{12} \end{pmatrix} = \frac{(1+\nu)}{E} \begin{pmatrix} 1-\nu & -\nu & 0 \\ -\nu & 1-\nu & 0 \\ 0 & 0 & 2 \end{pmatrix} \begin{pmatrix} \sigma_{11} \\ \sigma_{22} \\ \sigma_{12} \end{pmatrix}. \tag{2.27}$$

It follows:

$$\varepsilon_{11}+\varepsilon_{22} = \frac{(1+\nu)}{E}((1-2\nu)\sigma_{11}+(1-2\nu)\sigma_{22}) = \frac{(1+\nu)(1-2\nu)}{E}(\sigma_{11}+\sigma_{22}),$$
$$\sigma_{33} = \frac{E\ \nu}{(1+\nu)(1-2\nu)}(\varepsilon_{11}+\varepsilon_{22}) = \nu\,(\sigma_{11}+\sigma_{22}).$$

In the case of plane strain state, σ_{11}, σ_{22} and σ_{33} are dependent.

Remark 4. *In plane strain state:*

$$0 = \varepsilon_{33} = \frac{\partial u_3}{\partial y_3} \quad \Rightarrow \quad u_3 = \widetilde{u_3}(y_1, y_2)$$

Also it holds

$$0 = \varepsilon_{13} = \frac{1}{2}\left(\frac{\partial u_3}{\partial y_1} + \frac{\partial u_1}{\partial y_3}\right) \Rightarrow \frac{\partial u_1(y_1,y_2,y_3)}{\partial y_3} = -\frac{\partial \widetilde{u_3}(y_1,y_2)}{\partial y_1} \Rightarrow u_1 = y_3\ \widetilde{u_1}(y_1,y_2).$$

In similar way

$$\varepsilon_{23} = 0 \Rightarrow \frac{\partial u_2(y_1,y_2,y_3)}{\partial y_3} = -\frac{\partial \widetilde{u_3}}{\partial y_2} \Rightarrow u_2 = y_3\ \widetilde{u_2}(y_1,y_2).$$

i.e. the displacement is independent of the y_3-coordinate and the u_3-component of the displacement vector vanishes, $\vec{u} = (y_3\ \widetilde{u_1}(y_1,y_2), y_3\ \widetilde{u_2}(y_1,y_2), \widetilde{u_3}(y_1,y_2))$.

From (2.20) can read off for the plane strain state:

$$-div\sigma(\vec{u}) = -\begin{pmatrix} \mu\Delta u_1 + (\lambda+\mu)\partial_1 div\vec{u} \\ \mu\Delta u_2 + (\lambda+\mu)\partial_2 div\vec{u} \\ \mu\Delta u_3 + (\lambda+\mu)\partial_3 div\vec{u} \end{pmatrix}$$
$$= -\begin{pmatrix} \mu y_3\Delta_2\widetilde{u_1} + (\lambda+\mu)y_3\partial_1 div_2\vec{u} \\ \mu y_3\Delta_2\widetilde{u_2} + (\lambda+\mu)y_3\partial_2 div_2\vec{u} \\ \mu\ \Delta_2\widetilde{u_3} \end{pmatrix} = -L\vec{u}.$$

The displacement in the y_1y_2-plane, also independent of y_3, defines a two dimensional in-plane problem. Since the anti-plane and the in-plane elastic problem are uncoupled, one can consider the displacement field $\vec{u}$ as

$$u_1 = u_1(y_1,y_2),\ u_2 = u_2(y_1,y_2) \ \text{ and } \ u_3 = u_3(y_1,y_2).$$

Then (2.21) is:

$$-\begin{pmatrix} \mu\Delta+(\lambda+\mu)\partial_1^2 & (\lambda+\mu)\partial_1\partial_2 & 0 \\ (\lambda+\mu)\partial_2\partial_1 & \mu\Delta+(\lambda+\mu)\partial_2^2 & 0 \\ 0 & 0 & \mu\Delta \end{pmatrix}\begin{pmatrix} u_1 \\ u_2 \\ u_3 \end{pmatrix} = \begin{pmatrix} f_1 \\ f_2 \\ f_3 \end{pmatrix}.$$

Two types of 2D problems can be derived from here:

- ***The in-plane case Lamé equations:*** It is described by:

$$-\begin{pmatrix} \mu\Delta+(\lambda+\mu)\partial_1^2 & (\lambda+\mu)\partial_1\partial_2 \\ (\lambda+\mu)\partial_2\partial_1 & \mu\Delta+(\lambda+\mu)\partial_2^2 \end{pmatrix}\begin{pmatrix} u_1 \\ u_2 \end{pmatrix} = \begin{pmatrix} f_1 \\ f_2 \end{pmatrix}.$$

- ***The out-of plane Lamé equation:*** It is described by:

$$\mu\left(\frac{\partial^2}{\partial y_1^2}+\frac{\partial^2}{\partial y_2^2}\right)u_3 = f_3.$$

  It coincides with the Laplace equation if $f_3 = 0$.

Weak formulation

Given the linearized boundary value problem (2.17), (2.18), (2.19) with $f \in [L^2(\Omega)]^2$, the force density to the body Ω_0 and $g \in [H^{1/2}(\Gamma_N)]^2$.

In order to be able to give the variational formulation of this problem, let us introduce the set of admissible displacement fields. We require that the displacement field belongs to the space $W \subset [H^1(\Omega)]^2$, which is defined by vanishing essential boundary conditions.

$$W := \left\{ \mathrm{u} \in [H^1(\Omega)]^2, \mathrm{u} = 0 \text{ on } \Gamma_0 \right\}.$$

The equilibrium state of the solid defined by the problem, corresponds to the minimum of the potential energy for the body is given by:

$$I(\mathrm{u},\Omega) = \frac{1}{2}\int_\Omega \sigma(\mathrm{u}) : \varepsilon(\mathrm{u}) - \int_\Omega f\cdot\mathrm{u} - \int_{\Gamma_1} g\cdot\mathrm{u}, \quad \forall \mathbf{u} \in W :$$

The equilibrium problem reads: For given load (f, g) we seek $\mathrm{u} \in W$, which minimizes the potential energy functional, i.e.:

$$\inf_{v\in W} I(v,\Omega),$$

and it can be described by the variational equation:

$$\int_\Omega \sigma(\mathrm{u}) : \varepsilon(\mathrm{v}) = \int_\Omega f\cdot\mathrm{v} + \int_{\Gamma_1} g\cdot\mathrm{v}, \quad \forall \mathrm{v} \in W. \tag{2.28}$$

Thanks to the Korn inequality there exists a unique solution $\mathrm{u} \in W$ to the problem (2.28) for meas $\Gamma_0 > 0$.

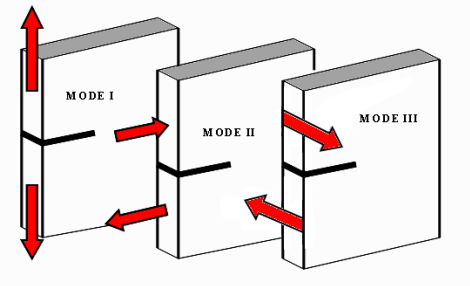

Figure 2.2: Three basic loading modes for cracked body. In plane cases: Mode I, II, Out-of-plane case: Mode III.

2.2 Basics of fracture mechanics

In this section, some formalisms are established using concepts of continuum mechanics in order to provide a framework for discussing both static and dynamic fracture mechanics.

2.2.1 Modes of Fracture

Three distinct modes of fracture may occur, depending on the orientation of the applied loads with respect to the crack, as it is illustrated in Figure 2.2. *The crack-opening mode (MODE I)* occurs when the elastic body is loaded by tensile forces acting perpendicular to the crack front surfaces.
Shear forces parallel to the crack flanks and perpendicular to the crack front result in fracture by *the sliding mode (MODE II)*, while shear forces parallel to the crack front give rise to fracture by *the tearing mode (MODE III)*.
With a coordinate system on the crack front, the three modes may be specified as follows, see Table (2.1) ("horizontal" refers to the y_1 direction, "vertical" to the y_2 direction).

A generic loading situation produced by some combination of forces without any particular symmetry is referred to as *mixed mode fracture*.
One experimental difficulty of Modes II and III is that the crack faces are not pulled away from one another. In two dimensional isotropic materials, Mode II fracture cannot easily be observed, since slowly propagating cracks spontaneously orient themselves so as to make the Mode II component of the loading vanish near the crack tip. Pure Mode III fracture, although experimentally difficult to achieve, is sometimes used as a model system for theoretical study since, in this case, the equations of elasticity simplify considerably. Analytical solutions, obtained in this mode, have provided insight to the fracture process.

MODES	**Description**
The crack-opening mode. It is traditionally referred to as MODE I.	Horizontal displacements are symmetric, vertical ones anti-symmetric. $u_1(y_1,-y_2,y_3) = u_1(y_1,y_2,y_3)$, $u_2(y_1,-y_2,y_3) = -u_2(y_1,y_2,y_3)$. $u_3 = 0$ (plane strain), $\partial_3^2 u_3 = 0$ (plane stress)
The shearing (or sliding) mode. It is traditionally referred to as MODE II.	Horizontal displacements are anti-symmetric, vertical ones are symmetric. $u_1(y_1,-y_2,y_3) = -u_1(y_1,y_2,y_3)$, $u_2(y_1,-y_2,y_3) = u_2(y_1,y_2,y_3)$. $u_3 = 0$ (plane strain), $\partial_3^2 u_3 = 0$ (plane stress)
The anti-plane shearing. (or tearing, or sliding) mode It is traditionally referred to as MODE III	The only non-vanishing displacement, u_3 is anti-symmetric, $u_1 = u_2 = 0$, $u_3(y_1,-y_2,y_3) = -u_3(y_1,y_2,y_3)$ $\partial_3 u_3 = 0$

Table 2.1: The symmetric modes

2.2.2 Stress intensity factors

The most important parameters in 2D linear elastic fracture mechanics are the stress intensity factors, which are associated directly or indirectly with fracture criteria and crack propagation.

The dynamic stress intensity factors are written as a function of the time dependent crack tip position $h(t)$ (reflecting the time evolving geometry), crack tip velocity $h'(t)$ (reflecting dynamic effects) and time t (mirroring the reflection of waves from geometrical boundaries, etc). As a result, we have that $k = k(t,h,h')$.

They are measures of the strength of the stress singularity at a crack tip, and they are useful from a mechanics perspective as they characterize the displacement, stress and strain in the near field around the crack tip.

Its calculation in finite solids under arbitrary loading conditions is difficult and is usually done via numerical approximation. Typically this is performed by using finite element methods, boundary element methods [30], or boundary collocation of crack-tip stress field expansions. Analytical extraction formulas for the dynamic stress intensity factor for the out-of-plane case will be presented in chapter 4, for the in-plane case in chapter 6, whereas we extract stress intensity factors from the finite element solutions quite accurately in chapter 7.

2.2.3 The time-dependent Navier Lamé equations.

The complete formal development of fracture mechanics is very elaborate. For static 2D cracks, there is a formalism developed by N. Muskhelishvili (1891-1976), [61] that allows one to use conformal mapping for obtaining the stress fields around two-dimensional voids in a solid. We will present a variant of this technique in the chapter 5 that allows one to find fields surrounding a moving crack.

Cracks are present essentially in almost of all structural materials. Elastic waves propagating in a solid are modified by the presence of cracks.

Elastic waves are often modeled by the linear Navier-Lamé equation system in a three-dimensional space-domain:

$$\rho \vec{u}_{tt} - (\mu \Delta \vec{u} + (\lambda + \mu)\ \mathrm{grad}(\mathrm{div}\ \vec{u})) = \rho \tilde{f} \tag{2.29}$$

where $\vec{u}(y,t) = \vec{u} = (u_1,u_2,u_3)^T$ is the displacement field, [69], [22], [57]. Here ρ the mass-density, λ, μ the Lamé coefficients. Note that the parameters ρ, λ, μ in general are not really constant; e.g. in seismology they are functions of position r and vary significantly, in particular with depth. $\tilde{f}(y,t) = \tilde{f} = (\tilde{f}_1, \tilde{f}_2, \tilde{f}_3)^T$ is the density of the volume forces.

An alternative form for (2.29), is obtainable by using a well-known result in vector analysis, i.e. the vector identity:

$$\nabla^2\vec{u} = \nabla\nabla\cdot\vec{u} - \nabla\times(\nabla\times\vec{u}).$$

Substituting this result for $\nabla^2\vec{u}$ in (2.29) gives:

$$(\lambda+2\mu)\nabla(\nabla\cdot\vec{u}) - \mu\nabla\times(\nabla\times\vec{u}) + \rho\vec{f} = \rho\ddot{\vec{u}}. \tag{2.30}$$

In (2.30) the term $\nabla(\nabla\cdot\vec{u})$ represents the dilatation and $\nabla\times(\nabla\times\vec{u})$ the rotation. The derivation of (2.29) is given in [32], where it is explained that the term involving λ represents the stress that do work in expansion or compression, whereas the terms in μ represent the shear stress.

To give a more general method of decomposing elastic waves into longitudinal and transverse waves, we write the vector form of Navier-Lamé equations (2.29) under the assumption of small displacement theory and homogeneous, isotropic linear elastic material behaviour:

$$(c_1^2 - c_2^2)\nabla(\nabla\cdot\vec{u}) + c_2^2\nabla^2\vec{u} - \ddot{\vec{u}} = \vec{f} \tag{2.31}$$

where c_1, c_2 are the longitudinal or dilatational wave propagation velocity and the shear or rotational wave propagation speed, respectively. Both wave speeds for an isotropic elastic material can be defined in terms of the mass-density ρ and the Lamé coefficients λ,μ as follows:

$$c_1^2 = \frac{(\lambda+2\mu)}{\rho}, \tag{2.32}$$

$$c_2^2 = \frac{\mu}{\rho}. \tag{2.33}$$

We see that they only depend on the properties of the material through which they propagate. Furthermore, for the isotropic case, the wave speeds c_1 and c_2 do not depend on the propagation direction.

Alternative expressions of c_1 and c_2 in terms of E,ν are given by:

$$\begin{aligned} c_1^2 &= \frac{(\lambda+2\mu)}{\rho} = \frac{\mu(4\mu-E)}{\rho(3\mu-E)} = \frac{E(1-\nu)}{\rho(1+\nu)(1-2\nu)} = \frac{2\mu(1-\nu)}{\rho(1-2u)}, \\ c_2^2 &= \frac{\mu}{\rho} = \frac{E}{2\rho(1+\nu)}. \end{aligned} \tag{2.34}$$

ρ being the density, E and ν are the Young's modulus and Poisson's ratio, respectively, λ and μ are the Lamé constants.
The relationships among these elastic constants are:

$$E = \frac{\mu(3\lambda+2\mu)}{\lambda+\mu}, \quad \lambda = \frac{E\nu}{(1+\nu)(1-2\nu)}, \quad \nu = \frac{\lambda}{2(\lambda+\mu)}, \quad \mu = \frac{E}{2(1+\nu)}.$$

Anoher useful relationship follows from recognizing that the ratio of the two wave speeds $\frac{c_1}{c_2}$ has a form depending only on Poisson's ratio and it may be expressed as:

$$\frac{c_1}{c_2} = \left(\frac{\lambda+2\mu}{\mu}\right)^{\frac{1}{2}} = \left(\frac{2-2\nu}{1-2\nu}\right)^{\frac{1}{2}}.$$

Since we assume $0 \leq \nu < \frac{1}{2}$, we see that $c_1 > c_2$. Nominal values of the propagation velocities for several materials are given in Table (2.2).

Propagation velocities for several materials

Material	$c_1\left[\frac{m}{s}\right] \times 10^{-3}$	$c_2\left[\frac{m}{s}\right] \times 10^{-3}$
Aluminum	6.15	3.10
Gold	3.14	1.17
Lead	2.12	0.74
Magnesium	6.44	3.09
Silver	3.45	1.57
Steel	5.71	3.16
Tin	2.96	1.49
Zinc	3.86	2.56

Table 2.2: Propagation velocities c_1 and c_2 for vaious materials.

In linear elasticity for isotropic material, the governing equations are the dynamic Navier-Lamé- equations. The following situations will be study in detail in Chapters 4, 5:

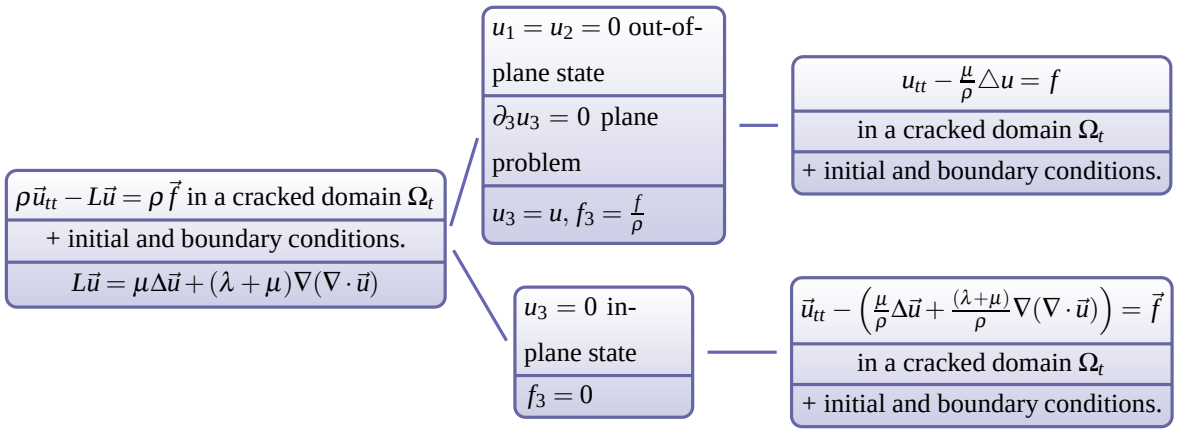

2.3 Griffith and Irwin criteria

For a given arbitrary crack C_0 in a body Ω_0 it is in general unknown in advance which path the crack tip will follow if the crack grows.
The Griffith-criterion is a classical and commonly applied fracture criterion to decide whether or not the crack will propagate under given forces.
The Griffith criterion in the static case reads as follows, [2], [31]:
The crack is stationary for the given forces, if the total potential energy of the actual configuration is minimal compared to the total potential energy of all admissible neighboring configurations.

Due to our assumption that the crack grows straight the set of admissible configurations is relativ small and determined through this condition.
Under suitable assumptions on the crack and the applied forces, this criterion in the static case can be reformulated in terms of the energy release rate which is related to the derivative of the potential deformation energy with respect to the crack length, see e.g. [62], [58]
The total energy is the sum of the deformation energy and a dissipative energy. The deformation energy consists of the stored energy and the work of the external forces.
The total potential energy $\Pi(\Omega,u,F)$ of an elastic body Ω generated by the displacement field u and the exterior loading $F = (f,h)$, is given by

$$\Pi(\Omega,u,F) = I_{elast}(\Omega,u) - W(\Omega,u,F) + D(\Omega).$$

Here, $I_{elast}(\Omega,u)$ denotes the stored elastic strain energy $I_{elast}(\Omega,u) = \int_\Omega W_{elas}(\varepsilon(u))dx$ with the stored energy density W_{elas}. Moreover,

$$W(\Omega,u,F) = \int_\Omega f\,u dx + \int_{\Gamma_N} h\,u ds$$

is the work of the exterior forces $F = (f,h)$ and

$$G(\Omega,u,F) = I_{elast}(\Omega,u) - W(\Omega,u,F)$$

denotes the potential deformation energy. The quantity $D(\Omega)$ describes a dissipative energy which in our case characterises the energy which is spent to create the new crack surface. In the simplest case it is assumed that $D(\Omega)$ is proportional to the macroscopic crack surface.

The Griffith fracture criterion can be reformulated as follows:
A crack in a domain Ω is stationary for a given loading $F = (f,h)$, if the potential deformation energy, which would be released at a crack extension, is less than the energy which is needed to create the new crack surface.
In other words, if for $\delta > 0$

$$G(\Omega_0,u_0,F) - G(\Omega_\delta,u_\delta,F) < D(\Omega_0) - D(\Omega_\delta) = 2\delta\gamma \tag{2.35}$$

or in differential form,

$$\lim_{\delta\to 0} - \left[\frac{G(\Omega_\delta,u_\delta,F) - G(\Omega_0,u_0,F)}{\delta}\right] < 2\gamma. \tag{2.36}$$

where u_0 and u_δ are the corresponding displacement fields, then the crack is **stationary**.
Based on the definition, it is shown that the energy release rate can be expressed via the Griffith formula, and by the J -integral, [16], [74].

Griffith's work was ignored for over twenty years until a group under G.R. Irwin at the U.S. Naval Research Laboratory took it up during World War II. Irwin and his colleagues developed a modified form of Griffith's approach; they reformulated it in terms of stress, rather than energy.
The classical formulations of fracture criteria based on the notions of energy release rate and critical stress intensity factor (SIF) deal with isolated crack tips and do not describe the interaction of cracks.

The Irwin criterion based on the comparision of the stress intensity factor K_I with a critical value, denoted by K_{IC} (a material parameter). A crack will begin to extend when the stress intensity factor has been increasing to a material specific value, K_{IC}. For values of the stress intensity factor smaller than the critical value there is no growth. That means the Irwin criterion in its simplest form says that a crack will grow if:

$$K_I > K_{IC}.$$

In the case in which the crack is dynamically extending through the motion of the crack tip, a generalized Griffith energy balance law is used. At any instant of time t the rate of the total energy is given,

$$\hat{\Pi}(t) = \dot{D}(t) + \dot{E}(t) - \hat{A}(t) + \dot{K}(t) = 0$$

where $\dot{E}$ denotes the rate of the elastic energy,

$$\dot{E}(t) = \frac{1}{2}\frac{d}{dt}\int_{\Omega_t} \sigma(\vec{u}) : \varepsilon(\vec{u})\, dy$$

$\hat{A}$ the external energy

$$\hat{A}(t) = \int_{\Omega_t} \rho\, \vec{f} \cdot \vec{u}_t \; dy + \int_{\Gamma_N} \rho\, \vec{q} \cdot \vec{u}_t \, ds,$$

$\dot{K}$ the rate of the kinetic energy

$$\dot{K}(t) = \frac{d}{dt}\int_{\Omega_t} \frac{1}{2}\rho\, |\vec{u}_t|^2 \, dy.$$

$\dot{D} = \frac{d}{dt}D$ is then the rate of dissipative energy.

The assumption of a nominally linear elastic material response leads to the concept of stress intensity factor or energy release rate as a crack tip field characterizing parameter. In light of experience with rapid crack advance in real materials it was proposed in [8] that the current value of the stress intensity factor or energy release rate during dynamic crack growth can be seen as representation of the resistance of the material to crack advance. This material-specific resistance measure is termed “dynamic fracture toughness”. The fracture toughness is defined as a “generic term for measures of resistance to extension of a crack“ [1]. It is an empirical material property that is determined by conducting tests following standard fracture toughness test procedures, which have been published by national and international standard organizations.
These ideas provide a framework for the prediction of crack advance in a body with known fracture resistance subjected to specified loads, or for the extraction of fracture resistance information from a laboratory experiment in which both, driving force and crack motion are measured or inferred, [8].

It is known that there always exists a region (albeit small) near the crack tip (stationary or growing) where the dynamic stress intensity factor characterizes the amplitude of the local stress and controls the failure process, [46].

On the other hand, the level of resistance to crack advance that is exhibited by a material may depend on the crack tip speed. It was reported [39], [40], [49], [21], etc. that the dynamic fracture toughness depends on the crack tip speed $h'(t)$ in a characteristic way. The most significant feature of this dependence is that the fracture toughness is a monotone increasing function with respect to the crack speed $h'(t)$.

In certain cases, namely small-scale yielding, rate independent behaviour under monotonically increasing stress intensity factor, [92], [8], [5], [25], [85], the generalized Griffith fracture criterion can be assumed:

$$G(h,h') = \Gamma(h,h'). \tag{2.37}$$

$\Gamma(h,h')$ denotes the crack growth resistance for a particular material, which is determined under given environmental conditions by experiments, [8], whereas $G(h,h') = \dfrac{\dot{D}(t)}{h'(t)}$ with $h'(t) \neq 0$, denotes the dynamic energy release rate, and $\dot{D}(t) = \dot{D}(t,h,h')$ is the rate of the dissipative energy.

CHAPTER 3

Linear elastostatics for cracked bodies

3.1 An eigenvalue problem in the vicinity of crack tip

This chapter is concerned with the study of the nature and behavior of two-dimensional (2D) elastic fields near the cracks. It is well known that stress singularities can arise in a neighborhood of the crack tip. The detailed knowledge of the singular terms of the elastic fields is of interest e.g., in crack mechanics. Moreover, in computational mechanics, the lack of regularity near the crack tip demands modified discretization procedures.
As is well known from many classical works, (see [53], [64], [66], [86], [90]) in general the weak solution of boundary value problems may show certain singular behavior near angular conical points, e. g. crack tips.
The solution has there the form of a linear combination of certain singular functions and a regular part, where we understand as singular functions those which have unbounded derivatives near the conical points.
Writing the boundary value problems in polar coordinates (r, ω) centered at the crack tip, we get a parameter-depending boundary value problem. Its eigenvalues α_i (in general in $\mathbb{C}$) and the eigensolutions $u(\alpha_i; \cdot)$ generate the singular terms of the elastic fields near the conical points. They have the form (here written without those angles where logarithmic terms appear)

$$\vec{u} = \sum_i c_{\alpha_i} r^{\alpha_i} \vec{u}(\omega) + \vec{u}_{\text{reg}}.$$

By introducing the corresponding separation ansatz $\vec{u} = r^{\alpha}\vec{g}(\omega)$, the original problem can be rewritten as a quadratic eigenvalue problem (see (3.6)) for α.

3.2 Singularities for the 2D Lamé Equations

This section is devoted to describe how regular are the weak solutions of boundary value problems in the theory of plane linearized elasticity. We consider the 2D elasticity problem for an elastic body with a crack. The singular behavior in the vicinity of conical points can be described with the help of asymptotic singular representations for the solution, which essentially depend on the zeros of certain transcendental functions. We use special ansatzes and spherical coordinates to derive a generalized boundary eigenvalue problem. The resulting eigenvalues and eigensolutions generate the singular terms and they will be computed with PDE2D [27]. The eigensolutions are described by analytical formulas. The regularity of the corresponding weak solutions will be investigated.
We give the singular behavior of the weak solution near the conical points, analogously to [84] and similar to [89]. With these results, it is possible to ensure regularity for the weak solution. As classically, to get this regularity result, it suffices to establish the existence of a strip free of poles.

3.2.1 Formulation of the Problem

We consider a 2D elastic isotropic body occupying the domain Ω with an interior crack and smooth boundary $\partial\Omega$. Let us denote $\vec{u}(x) = (\mathrm{u}_1(x), \mathrm{u}_2(x))^T$ the displacement field and by $\varepsilon(\vec{u})$ the associated linearized strain tensor (2.7) and the linearized stress tensor $\sigma(\vec{u})$, is given by Hooke's law, (2.8).
The regularity of the weak solution can be described by a decomposition of the 2D solution field V into a singular and a regular term:

$$V = V_{sing} + V_{reg}.$$

The singular behavior of the linear elastic field occurs at the tip of a crack. Such singular behavior can be described by means of asymptotic expansions with respect to the distance to the geometrical and structural singularities, see [50].
The main goal of this chapter is the derivation and computation of the singular terms. We use ideas from Kozlov, Mazya and Rossmann, [89] to determine the singular terms.

3.3 Calculation of the Asymptotic Expansion

We discuss in this section when singular terms ocurr near conical points and which structure they have.
First, we localize the boundary value problems near a conical point and consider so-called model problems in an infinite cone. By using special ansatz methods and the transformation in spherical coordinates we get a generalized eigenvalue problem. The singular terms u_{sing} are generated by eigenpairs of a generalized eigenvalue problem.

3.3.1 Localization and the model problem

The calculation of the asymptotic expansion describing the behavior of the weak solution $\mathrm{u} \in W$ of the problem (2.28):

$$\int_\Omega \sigma(\mathrm{u}) : \varepsilon(\mathrm{v}) = \int_\Omega f \cdot \mathrm{v} + \int_{\Gamma_1} g \cdot \mathrm{v}, \quad \forall \mathrm{v} \in W.$$

in the vicinity of the crack tip is a local problem, where

$$W = \left\{ \mathrm{u} \in [H^1(\Omega)]^2, \mathrm{u} = 0 \text{ on } \Gamma_0 \right\}.$$

Therefore we localize our problem by multiplying the weak solution of the Lamé problem **u(x)** with a cut-off function $\eta = \eta(|x|) = \eta(r) \in C^\infty(B_\varepsilon(O_i))$, η_i is defined on an $\varepsilon-$ball $B_\varepsilon(O_i)$ around the conical point O_i, $i \in 1, \ldots, N$ and such that $\eta_i \equiv 1$ on $B_{\varepsilon/2}(O_i)$.
We assume to have N corner points O_i and moreover that the support of η_i contains only one of the corner points, namely O_i.
Inserting $v_i = \eta_i u$ into our problem, we get a new boundary value problem defined in an infinite cone K_i:

$$K_i := \left\{ (x,y) \in \mathbb{R}^2 \,|\, x = r_i \cos\omega_i, y = r_i \sin\omega_i, 0 < r_i < \infty, -\omega_{i_0}/2 < \omega_i < \omega_{i_0}/2 \right\}$$

r_i denotes $r_i = |x - O_i|$.
The solution $V_i = \eta_i U$ of the boundary value problem in K_i can be decomposed into a homogeneous and a particular solution because of the linearity of the operator. So we get:

$$V_i = V_{i_{hom}} + V_{i_{part}}$$

The solution $V_{i_{hom}}$ can be splitt additively into a regular part and a singular part. We shall calculate the singular part and we will note that the particular solution can be chosen regular enough. Therefore it holds:

$$V_i = V_{i_{sing}} + V_{i_{reg}}.$$

3.3.2 The generalized eigenvalue problem

In order to solve the homogeneous boundary value problem for the Lamé equations in K_i we write the operator in polar coordinates and introduce spherical coordinates. Finally, we use separation of variables which leads to a generalized eigenvalue problem. We omit the indexes for simplifications.

For the displacement $(\mathrm{u}_1, \mathrm{u}_2)$, the homogeneous Lamé equations have the form in polar coordinates r, ω, see Appendix A:

$$\begin{aligned} \Delta \mathrm{u}_r - \frac{1}{r^2}\mathrm{u}_r - \frac{2}{r^2}\partial_\omega \mathrm{u}_\omega + (1-2\nu)^{-1}\partial_r\left(\frac{1}{r}\partial_r(r\,\mathrm{u}_r) + \frac{1}{r}\partial_\omega \mathrm{u}_\omega\right) = 0 \\ \Delta \mathrm{u}_\omega - \frac{1}{r^2}u_\omega + \frac{2}{r^2}\partial_\omega \mathrm{u}_r + (1-2\nu)^{-1}\frac{1}{r^2}\partial_\omega\left(\partial_r(r\,\mathrm{u}_r) + \partial_\omega \mathrm{u}_\omega\right) = 0 \end{aligned} \tag{3.1}$$

where

$$\begin{pmatrix} \mathrm{u}_r \\ \mathrm{u}_\omega \end{pmatrix} = \begin{pmatrix} \cos\omega & \sin\omega \\ -\sin\omega & \cos\omega \end{pmatrix} \begin{pmatrix} \mathrm{u}_1 \\ \mathrm{u}_2 \end{pmatrix}. \tag{3.2}$$

Spherical basis

We introduce a spherical basis in $\mathbb{R}^2$ since the resulting generalized eigenvalue problems can be solved elementarily. The spherical basis system is defined by:

$$\vec{e_r} = \begin{pmatrix} \cos\omega \\ \sin\omega \end{pmatrix}, \quad \vec{e_\omega} = \begin{pmatrix} -\sin\omega \\ \cos\omega \end{pmatrix}$$

where ω describes the polar angle.

The Cartesian displacement vector $\vec{u}$ can be written as $\vec{u} = u_1\vec{e_1} + u_2\vec{e_2}$ in the standard basis $\{\vec{e_1}, \vec{e_2}\}$ and also as $\vec{u} = u_r(r,\omega)\vec{e_r} + u_\omega(r,\omega)\vec{e_\omega}$ in the spherical basis $\{\vec{e_r}, \vec{e_\omega}\}$, i.e.:

$$\begin{pmatrix} \mathrm{u}_r \\ \mathrm{u}_\omega \end{pmatrix} = \begin{pmatrix} \cos\omega & \sin\omega \\ -\sin\omega & \cos\omega \end{pmatrix} \begin{pmatrix} \mathrm{u}_1 \\ \mathrm{u}_2 \end{pmatrix}.$$

Vice versa we get the Cartesian description of a spherical vector by the transformation

$$\begin{pmatrix} \mathrm{u}_1 \\ \mathrm{u}_2 \end{pmatrix} = \begin{pmatrix} \cos\omega & -\sin\omega \\ \sin\omega & \cos\omega \end{pmatrix} \begin{pmatrix} \mathrm{u}_r \\ \mathrm{u}_\omega \end{pmatrix}.$$

The expressions for the components of the stress tensor are:

$$\begin{aligned} \sigma_{\omega\omega}(\mathrm{u}) &= (\lambda + 2\mu)\frac{1}{r}\left(\partial_\omega \mathrm{u}_\omega + \mathrm{u}_r\right) + \lambda\,\partial_r \mathrm{u}_r, \\ \sigma_{rr}(\mathrm{u}) &= (\lambda + 2\mu)\,\partial_r \mathrm{u}_r + \lambda\frac{1}{r}\left(\partial_\omega \mathrm{u}_\omega + \mathrm{u}_r\right), \\ \sigma_{r\omega}(\mathrm{u}) &= \mu\left(\frac{1}{r}\partial_\omega \mathrm{u}_r + \partial_r \mathrm{u}_\omega - \frac{1}{r}\mathrm{u}_\omega\right). \end{aligned} \tag{3.3}$$

The Cartesian vectors of the differential equation system (3.1) are transformed into the spherical ones. Singular solutions are sought by means of the separation ansatz:

$$\begin{aligned} \mathrm{u}_r(r,\omega) &= r^\alpha g_1(\omega), \\ \mathrm{u}_\omega(r,\omega) &= r^\alpha g_2(\omega). \end{aligned} \tag{3.4}$$

Inserting (3.4) into the equations (3.1) and into (3.3), if $r > 0$ the radial dependance can be canceled.
The singular solutions of the 2D Lamé equations with corresponding boundary conditions, are given by the solutions of the following generalized boundary eigenvalue problem:
Find parameters α for which eigensolutions g_1, g_2 exist such that:
for all $\omega \in (-\omega_0/2, \omega_0/2)$:

$$\begin{aligned} &\begin{pmatrix} 1-2\nu & 0 \\ 0 & 2-2\nu \end{pmatrix} \begin{pmatrix} g_1'' \\ g_2'' \end{pmatrix} + \begin{pmatrix} 0 & \alpha-3+4\nu \\ \alpha+3-4\nu & 0 \end{pmatrix} \begin{pmatrix} g_1' \\ g_2' \end{pmatrix} + \\ &+ \begin{pmatrix} (2-2\nu)(\alpha^2-1) & 0 \\ 0 & (1-2\nu)(\alpha^2-1) \end{pmatrix} \begin{pmatrix} g_1 \\ g_2 \end{pmatrix} = \begin{pmatrix} 0 \\ 0 \end{pmatrix}, \end{aligned} \tag{3.5}$$

i.e. for $\omega \in (-\omega_0/2, \omega_0/2)$:

$$\begin{aligned} (1-2\nu)g_1'' + (\alpha-(3-4\nu))g_2' + (2-2\nu)(\alpha^2-1)g_1 = 0, \\ (2-2\nu)g_2'' + (\alpha+(3-4\nu))g_1' + (1-2\nu)(\alpha^2-1)g_2 = 0. \end{aligned} \tag{3.6}$$

and the stress given in spherical basis by:

$$\begin{aligned} \sigma_{\omega\omega}(\mathrm{u}) &= r^{\alpha-1}\left((\lambda+2\mu)g_2' + (\lambda+2\mu+\alpha\lambda)g_1\right), \\ \sigma_{rr}(\mathrm{u}) &= r^{\alpha-1}\left(((\lambda+2\mu)\alpha+\lambda)g_1 + \lambda g_2'\right), \\ \sigma_{r\omega}(\mathrm{u}) &= \mu r^{\alpha-1}\left(g_1' - (1-\alpha)g_2\right). \end{aligned} \tag{3.7}$$

3.3.3 Analytic solutions of the eigenvalue problem

In this subsection we solve the generalized eigenvalue problem. First we calculate the fundamental system to the differential equations, after that we consider the boundary conditions. Then we will see the structure of the local solutions and finally we transfer the local solutions into the Cartesian basis.
Fundamental system to the ordinary differential system We repeat the ordinary differential system in ω with parameter α and we need to distinguish between the cases:

- $\alpha \neq \{0\}$
- $\alpha = 0$

The case $\alpha \neq \{0\}$.
From (3.6) we get:

$$\begin{aligned}(\alpha-(3-4\nu))g_2' &= -(1-2\nu)g_1'' - (2-2\nu)(\alpha^2-1)g_1 \\ (1-2\nu)(\alpha^2-1)(\alpha-(3-4\nu))g_2' &= (1-2\nu)(2-2\nu)\,g_1^{(4)} + \\ &\quad \left[(2-2\nu)^2(\alpha^2-1) - (\alpha^2-(3-4\nu)^2)\right] g_1''\end{aligned} \tag{3.8}$$

We can through differentiation and substitution get a linear homogeneous ordinary differential equation (3.9) with constant complex coefficients for g_1:

$$g_1^{(4)}(\omega) + \frac{\left[\left((1-2\nu)^2+(2-2\nu)^2\right)(\alpha^2-1) - (\alpha^2-(3-4\nu)^2)\right]}{(1-2\nu)(2-2\nu)} g_1''(\omega) + (\alpha^2-1)^2 g_1(\omega) = 0 \tag{3.9}$$

with a simple calculation we get for (3.9):

$$g_1^{(4)}(\omega) + 2(1+\alpha^2)g_1''(\omega) + (\alpha^2-1)^2 g_1(\omega) = 0$$

From the theory of linear differential equations with constant complex coefficients (see [35] p.29ff) is known that there are four independent solutions which we can get by the ansatz

$$g_1(\omega) = e^{\beta\omega}. \tag{3.10}$$

The exponents β are the roots of the characteristic polynomial (3.11)

$$\beta^4 + 2(1+\alpha^2)\beta^2 + (\alpha^2-1)^2 = 0 \tag{3.11}$$

We get:

$$\beta_{1,2} = \pm i(\alpha+1) \qquad \beta_{3,4} = \pm i(\alpha-1)$$

We have four solutions of type (3.10)

$$e^{\pm i(\alpha+1)\omega} \qquad e^{\pm i(\alpha-1)\omega}$$

and with Euler's formula we achieve four linearly independent solutions for g_1:

$$\begin{aligned} g_1^1(\omega) &= \cos[(\alpha+1)\omega] & g_1^2(\omega) &= \sin[(\alpha+1)\omega] \\ g_1^3(\omega) &= \cos[(\alpha-1)\omega] & g_1^4(\omega) &= \sin[(\alpha-1)\omega] \end{aligned}$$

With these solutions for g_1 we get the corresponding solutions for g_2.
So we obtain for $\alpha \neq \{0\}$ the fundamental system for $\begin{pmatrix} g_1 \\ g_2 \end{pmatrix}$.

The general solution of the system (3.6) for $\alpha \neq 0$ is a linear combination of the vectores (3.12), (compare with [81]).

$$\begin{pmatrix} \cos[(\alpha+1)\omega] \\ -\sin[(\alpha+1)\omega] \end{pmatrix}, \quad \begin{pmatrix} \sin[(\alpha+1)\omega] \\ \cos[(\alpha+1)\omega] \end{pmatrix}, \\ \begin{pmatrix} (3-4\nu-\alpha)\cos[(1-\alpha)\omega] \\ -(\alpha+3-4\nu)\sin[(1-\alpha)\omega] \end{pmatrix}, \quad \begin{pmatrix} (3-4\nu-\alpha)\sin[(1-\alpha)\omega] \\ (\alpha+3-4\nu)\cos[(1-\alpha)\omega] \end{pmatrix}. \tag{3.12}$$

The case $\alpha = 0$.

For $\alpha = 0$ we get for the characteristic polynomial two roots of multiplicity two,

$$\alpha_1 = i \qquad \alpha_2 = -i.$$

For each root α_k of multiplicity two we know according to ([35], Theorem 2.2, p.31) that $e^{\alpha_k \omega}$ and $\omega e^{\alpha_k \omega}$ both are solutions of the differential equation. So we achieve four independent solutions:

$$g_1^1(\omega) = \cos[\omega] \qquad g_1^2(\omega) = \sin[\omega]$$
$$g_1^3(\omega) = \omega\cos[\omega] \qquad g_1^4(\omega) = \omega\sin[\omega].$$

With the other differential equation of our system (3.6) we get the following fundamental system:

$$\begin{pmatrix} \cos[\omega] \\ -\sin[\omega] \end{pmatrix}, \qquad \begin{pmatrix} \sin[\omega] \\ \cos[\omega] \end{pmatrix}, \\ \begin{pmatrix} \omega\cos[\omega] \\ -\dfrac{1}{3-4\nu}\cos[\omega] - \omega\sin[\omega] \end{pmatrix}, \quad \begin{pmatrix} \omega\sin[\omega] \\ -\dfrac{1}{3-4\nu}\sin[\omega] + \omega\cos[\omega] \end{pmatrix}. \tag{3.13}$$

The general solution of the parameter dependent system of ordinary differential equations (3.6) is given by the following algebraic system for the constants $c_1, \cdots, c_4$:

$$u = \sum_{k=1}^{4} c_k u^{(k)}(\alpha, \omega_0), \qquad u^{(k)} = \begin{pmatrix} u_r^{(k)} \\ u_\omega^{(k)} \end{pmatrix}. \tag{3.14}$$

Note that the components in (3.12) $u_r^{(1)}, u_\omega^{(2)}, u_r^{(3)}, u_\omega^{(4)}$ are even functions of the variable ω and the components $u_\omega^{(1)}, u_r^{(2)}, u_\omega^{(3)}, u_r^{(4)}$ are odd functions.

The characteristic determinants

Inserting the solutions (3.12) into the different boundary conditions we obtain a system of

four homogeneous linear equations for the free coefficients c_j, $j = 1, \cdots, 4$. More precisely we get:

$$A(\alpha) \begin{pmatrix} c_1 \\ c_2 \\ c_3 \\ c_4 \end{pmatrix} = 0 \tag{3.15}$$

where the 4×4-matrix $A(\alpha)$ depends on the chosen boundary conditions. There exist non-trivial solutions, if:

$$\det A(\alpha) = 0. \tag{3.16}$$

Possible parameters α are determined by the eigenvalue condition (3.16).
The condition (3.16) yields a characteristic equation whose zeros are the singular exponents of the singular expansion of u.

Dirichlet Problem

$$u = \begin{pmatrix} u_r \\ u_\omega \end{pmatrix} = 0 \quad \text{on } \partial K \backslash \{0\},$$

is to satisfy the boundary conditions in terms of u_r and u_ω:

$$\begin{aligned} \mathrm{u}_r(r, -\omega_0/2) &= r^\alpha g_1(-\omega_0/2) = 0, \Rightarrow g_1(-\omega_0/2) = 0, \\ \mathrm{u}_\omega(r, -\omega_0/2) &= r^\alpha g_2(-\omega_0/2) = 0 \Rightarrow g_2(-\omega_0/2) = 0, \\ \mathrm{u}_r(r, \omega_0/2) &= r^\alpha g_1(\omega_0/2) = 0, \Rightarrow g_1(\omega_0/2) = 0, \\ \mathrm{u}_\omega(r, \omega_0/2) &= r^\alpha g_2(\omega_0/2) = 0 \Rightarrow g_2(\omega_0/2) = 0. \end{aligned} \tag{3.17}$$

Theorem 2. *Every eigenvalue of the Lamé operator with Dirichlet boundary conditions (3.17) is a solution of one of the following equations:*
For $\alpha \neq 0$

$$\begin{aligned} (3-4\nu)\sin[\alpha\omega_0] - \alpha\sin[\omega_0] = 0, \\ (3-4\nu)\sin[\alpha\omega_0] + \alpha\sin[\omega_0] = 0, \end{aligned} \tag{3.18}$$

and for $\alpha = 0$

$$\begin{aligned} (3-4\nu)\omega_0 - \sin[\omega_0] = 0, \\ (3-4\nu)\omega_0 + \sin[\omega_0] = 0. \end{aligned} \tag{3.19}$$

Proof. **For $\alpha \neq 0$:**

From (3.12) and (3.17) follows that the homogeneous system of linear equations reads, we have called $A := 3 - 4\nu$

$$\begin{pmatrix} \cos[(1+\alpha)w_0/2] & \sin[(1+\alpha)w_0/2] & (A-\alpha])\cos[(1-\alpha)w_0/2] & (A-\alpha)\sin[(1-\alpha)w_0/2] \\ -\sin[(1+\alpha)w_0/2] & \cos[(1+\alpha)w_0/2] & -(A+\alpha)\sin[(1-\alpha)w_0/2] & (A+\alpha)\cos[(1-\alpha)w_0/2] \\ \cos[(1+\alpha)w_0/2] & -\sin[(1+\alpha)w_0/2] & (A-\alpha)\cos[(1-\alpha)w_0/2] & -(A-\alpha)\sin[(1-\alpha)w_0/2] \\ \sin[(1+\alpha)w_0/2] & \cos[(1+\alpha)w_0/2] & (A+\alpha)\sin[(1-\alpha)w_0/2] & (A+\alpha)\cos[(1-\alpha)w_0/2] \end{pmatrix} \begin{pmatrix} c_1 \\ c_2 \\ c_3 \\ c_4 \end{pmatrix} = \begin{pmatrix} 0 \\ 0 \\ 0 \\ 0 \end{pmatrix}$$

The determinant of the system is solved by Wolfram Mathematica 6.0 ®, Fig. 3.1.

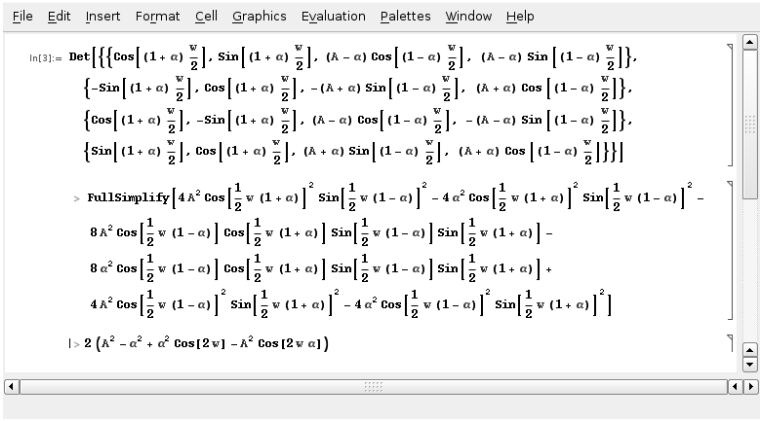

Figure 3.1: Wolfram Mathematica 6.0 ® for the Dirichlet Problem

From trigonometrical formulas we get:
$A^2-\alpha^2+\alpha^2\cos[2w_0]-A^2\cos[2w_0\alpha] = 2A^2(1-\cos^2(\alpha w_0))-2\alpha^2(1-\cos^2(w_0))$.
Nontrivial solutions exist if the determinants of the systems vanish,

$$((3-4\nu)\sin[\alpha\omega_0]-\alpha\sin[\omega_0])=0,$$
$$((3-4\nu)\sin[\alpha\omega_0]+\alpha\sin[\omega_0])=0.$$

For $\alpha = 0$, figure 3.2:

$$\begin{pmatrix} \cos[w_0/2] & \sin[w_0/2] & (w_0/2)\cos[w_0/2] & (w/2)\sin[w/2] \\ -\sin[w_0/2] & \cos[w_0/2] & -(w_0/2)\sin[w_0/2]-1/A\cos[w_0/2] & (w_0/2)\cos[w_0/2]-1/A\sin[w_0/2] \\ \cos[w_0/2] & -\sin[w_0/2] & -(w_0/2)\cos[w_0/2] & (w_0/2)\sin[w_0/2] \\ \sin[w_0/2] & \cos[w_0/2] & -(w_0/2)\sin[w_0/2]-1/A\cos[w_0/2] & -(w_0/2)\cos[w_0/2]+1/A\sin[w_0/2] \end{pmatrix} \begin{pmatrix} c_1 \\ c_2 \\ c_3 \\ c_4 \end{pmatrix} = \begin{pmatrix} 0 \\ 0 \\ 0 \\ 0 \end{pmatrix}$$

We write $-1+2A^2w_0^2+\cos(2w_0) = 2A^2w_0^2+(\cos^2(w_0)-1)-\sin^2(w_0)$ and the results follow. □

Remark 5. *Let us now consider the exceptional value* $\alpha = 0$. *There are nontrivial solutions if and only if the corresponding determinants vanish. i.e*

$$((3-4\nu)\omega_0 \mp \sin[\omega_0])=0$$

and vanish for $\omega_0 = 0$ *only. Therefore* $\alpha = 0$ *is no eigenvalue in the Dirichlet/Dirichlet case because the determinants do not vanish for all* $0 < \omega \leq 2\pi$.

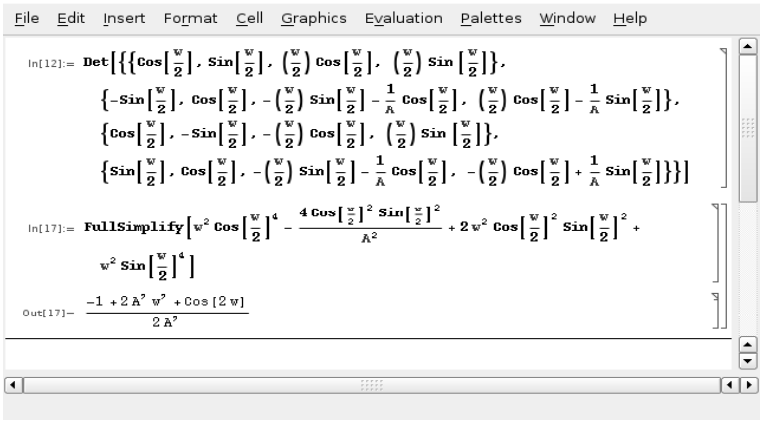

Figure 3.2: Wolfram Mathematica 6.0 ® for the Dirichlet Problem $\alpha = 0$.

Neumann Problem

Now we study the eigenvalues and eigenfunctions for the Lamé system with Neumann boundary condition given by $\sigma \cdot n = 0$ on the crack faces:

$$\sigma_{\omega\omega} = \sigma_{r\,\omega} = 0, \quad \text{for } \omega = -\omega_0/2 \text{ and} \omega = \omega_0/2.$$

i.e. for $\omega \in \{-\omega_0/2, \omega_0/2\}$ holds, $\left(\lambda = \dfrac{2\mu\nu}{1-2\nu}\right)$:

$$\begin{aligned} \frac{(1-\nu)}{\nu}\frac{1}{r}\left(\partial_\omega \mathrm{u}_\omega + u_r\right) + \partial_r \mathrm{u}_r = 0, \\ \left(\frac{1}{r}\partial_\omega \mathrm{u}_r + \partial_r \mathrm{u}_\omega - \frac{1}{r}\mathrm{u}_\omega\right) = 0. \end{aligned} \tag{3.20}$$

Theorem 3. *Every eigenvalue of the Lamé system with Neumann boundary conditions (3.20) is a solution of one of the following equations:*
For $\alpha \neq 0$***:***

$$\begin{aligned} \sin[\alpha\omega_0] + \alpha\sin[\omega_0] = 0, \\ \sin[\alpha\omega_0] - \alpha\sin[\omega_0] = 0. \end{aligned} \tag{3.21}$$

And ***for*** $\alpha = 0$

$$\begin{aligned} \alpha^2\omega_0\lambda - \frac{\alpha[4\mu(\nu-1)+\lambda(\alpha+4(\nu-1))]}{(3-4\nu)}\sin[\omega_0] = 0, \\ \alpha^2\omega_0\lambda + \frac{\alpha[4\mu(\nu-1)+\lambda(\alpha+4(\nu-1))]}{(3-4\nu)}\sin[\omega_0] = 0 \end{aligned} \tag{3.22}$$

Proof. **For $\alpha \neq 0$.**
Putting (3.4) into the Lamé system we get the system given by (3.6), while the boundary conditions take the form (3.7)

$$\begin{aligned}\left((\lambda+2\mu)\,g_2' + (\lambda+2\mu+\alpha\lambda)g_1\right)|_{\omega=-\omega_0/2,\omega_0/2} &= 0,\\ \left(g_1' - (1-\alpha)\,g_2\right)|_{\omega=-\omega_0/2,\omega_0/2} &= 0.\end{aligned}$$

Inserting the general solutions (3.12) of system (3.6) into the boundary conditions (3.20), we obtain the following algebraic system for the coefficients $c_1,\cdots,c_4$:

$$\begin{pmatrix} -2\mu\alpha\cos[(1+\alpha)\omega_0/2] & -2\mu\alpha\sin[(1+\alpha)\omega_0/2] & 2\mu\alpha(1+\alpha)\cos[(1-\alpha)\omega_0/2] & 2\mu\alpha(1+\alpha)\sin[(1-\alpha)\omega_0/2] \\ -2\alpha\sin[(1+\alpha)\omega_0/2] & 2\alpha\cos[(1+\alpha)\omega_0/2] & -2\alpha(\alpha-1)\sin[(1-\alpha)\omega_0/2] & 2\alpha(\alpha-1)\cos[(1-\alpha)\omega_0/2] \\ -2\mu\alpha\cos[(1+\alpha)\omega_0/2] & 2\mu\alpha\sin[(1+\alpha)\omega_0/2] & 2\mu\alpha(1+\alpha)\cos[(1-\alpha)\omega_0/2] & -2\mu\alpha(1+\alpha)\sin[(1-\alpha)\omega_0/2] \\ 2\alpha\sin[(1+\alpha)\omega_0/2] & 2\alpha\cos[(1+\alpha)\omega_0/2] & 2\alpha(\alpha-1)\sin[(1-\alpha)\omega_0/2] & 2\alpha(\alpha-1)\cos[(1-\alpha)\omega_0/2] \end{pmatrix} \begin{pmatrix} c_1 \\ c_2 \\ c_3 \\ c_4 \end{pmatrix} = \begin{pmatrix} 0 \\ 0 \\ 0 \\ 0 \end{pmatrix}$$

With help of Mathematica 6.0 it holds, Figure 3.3

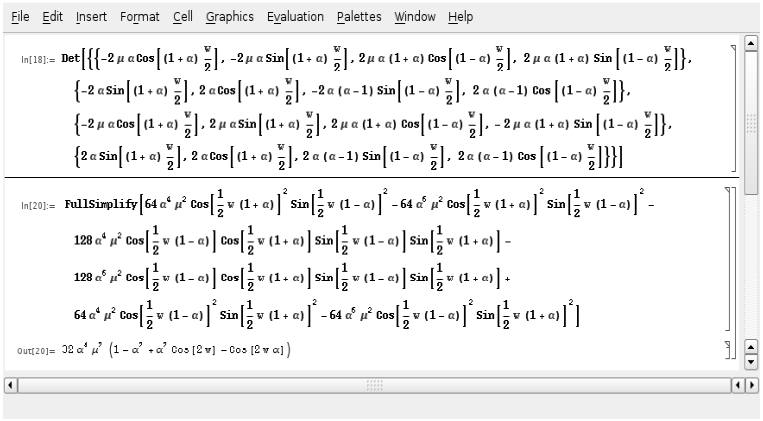

Figure 3.3: Wolfram Mathematica 6.0 ® for the Neumann Problem

$$32\alpha^2\mu\alpha^2\left(1-\alpha^2+\alpha^2\cos(2w_0)-\cos(2w_0\alpha)\right) = 32\alpha^2\mu\alpha^2(2\sin^2(\alpha w_0)-2\alpha^2\sin^2(w_0)).$$

Therefore, nontrivial solutions exist if the determinant of the system vanishs, so we get the eigenvalue conditions.

For $\alpha = 0$, Figure 3.4

□

Remark 6. *The equations (3.21) coincide with (3.18) for $\nu = \frac{1}{2}$. Therefore, the spectra corresponding to the Dirichlet and the Neumann problems have several common properties.*
In contrast to the Dirichlet problem, the spectrum generated by the Neumann problem contains the number $\alpha = 0$. i.e. $\alpha = 0$ is eigenvalue for all $0 < \omega_0 \leq 2\pi$.

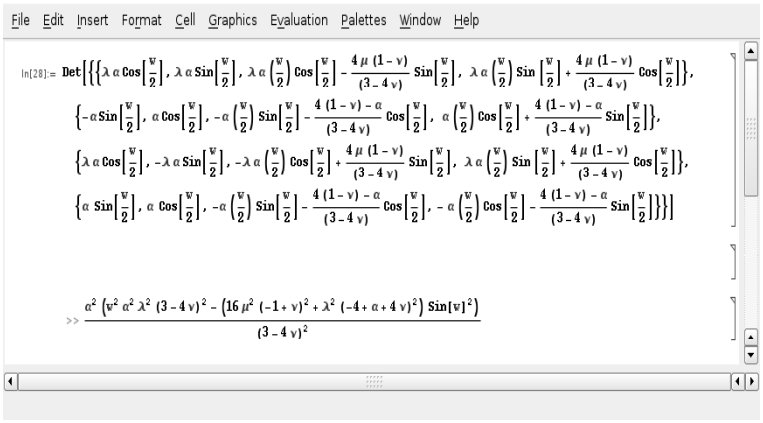

Figure 3.4: Wolfram Mathematica 6.0 ® for the Neumann Problem $\alpha = 0$.

The common roots $\alpha \neq 0$ of (3.21) exist only in the cases $\omega_0 = \pi$ and $\omega_0 = 2\pi$.
The case $\omega_0 = 2\pi$ corresponds to our interest in fracture mechanics and the number $\pm\frac{k}{2}$, $k = 1, \cdots$ are the eigenvalues.

Neumann-Dirichlet Conditions

Let us here also give the characteristic equation in the case in which we have homogeneous Neumann conditions on the crack and homogeneous Dirichlet conditions for $\vec{u}$.

Theorem 4. *Every eigenvalue of the Lamé system with Neumann/Dirichlet boundary conditions is a solution of one of the following equations:*

***For** $\alpha \neq 0$.*

$$\sin^2(\alpha\omega_0) - \frac{(\lambda+2\mu)^2}{(\lambda+\mu)(\lambda+3\mu)} + \alpha^2 \frac{(\lambda+\mu)}{(\lambda+3\mu)} \sin^2\omega_0 = 0. \tag{3.23}$$

Proof. **For** $\alpha \neq 0$, Figure 3.5:

We use trigonometrical formulas to simplify this result, ($A = 3 - 4\nu$):
$-4\mu\alpha^2(1 + A^2 - 2\alpha^2 + 2\alpha^2\cos[2w_0] + 2A\cos[2w_0\alpha])$.
Also we use the following relations between the Lamé coefficients λ, μ and Poisson's ratio $\nu = \frac{\lambda}{2(\lambda+\mu)}$, in the plane strain state, (compare Def. 6):

$$\frac{\lambda+\mu}{\lambda+3\mu} = \frac{1}{3-4\nu} \quad \text{and} \quad \frac{(\lambda+2\mu)^2}{(\lambda+\mu)(\lambda+3\mu)} = \frac{4(1-\nu)^2}{(3-4\nu)}$$

whereas in the case of plane stress, (see Def. 5), λ is to be replaced by $\widetilde{\lambda} = \frac{2\mu\lambda}{\lambda+2\mu}$.
The resulting characteristic equation for this case follows. □

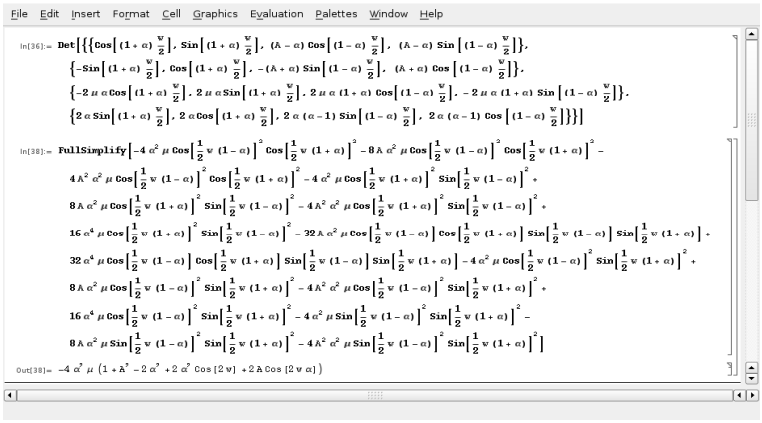

Figure 3.5: Wolfram Mathematica 6.0 ® for the Dirichlet/Neumann Problem.

Remark 7. *If we have* ***Neumann-Dirichlet boundary condition*** *the determinant for the exceptional value* $\alpha = 0$ *is equal to*

$$4\mu^2 \left(\frac{\lambda + 2\mu}{\lambda + 3\mu} \right)^2$$

and $\alpha = 0$ *is no eigenvalue.*
The equations (3.18), (3.21) and (3.23) as well the corresponding singular functions were derived in [65] and [84]. They were also studied in [76].

3.3.4 Regularity of solutions to the Lamé Equations.

We characterize the regularity of the singular terms of the original boundary value problems in the domain Ω starting from a weak solution u $\in [H^1(\Omega)]^2$.
The eigenvalues α are called singularity exponents, since they enter the singular functions as a power of r and they are the roots of the transcendental equations. In [90] there are formulas for the coefficients $c_{\alpha,j}$, which are called stress intensity factors.

Theorem 5. *If $\omega < 2\pi$ then the equations (3.18) have no zeros in the strip $Re(\alpha) \in (0,1/2]$.*

Proof. We proceed as in the proof of ([76], Theorem 2.2.)
Let us now study the roots of:

$$\sin[\alpha\omega] = \frac{1}{(3-4\nu)}\alpha\sin[\omega].$$

Writing $\alpha = \xi + i\zeta$, with $\xi, \zeta \in \mathbb{R}$ and taking the real part and imaginary part of this equation, we obtain the system:

$$\sin[\xi\omega]\cosh[\zeta\omega] = K\xi\sin[\omega],$$
$$\cos[\xi\omega]\sinh[\zeta\omega] = K\zeta\sin[\omega],$$

with $K = \dfrac{1}{(3-4\nu)} \in (0,1]$.
For a fixed $\zeta \in \mathbb{R}$, we consider the two functions:

$$f_1 : \mathbb{R} \to \mathbb{R}: \quad \xi \mapsto \sin[\xi\omega]\cosh[\zeta\omega],$$
$$f_2 : \mathbb{R} \to \mathbb{R}: \quad \xi \mapsto K\xi\sin[\omega].$$

For $0 < \omega < 2\pi$ it is easily verified that:

$$f_1(0) = f_2(0) = 0, \qquad f_1\left(\frac{1}{2}\right) > f_2\left(\frac{1}{2}\right).$$

Since f_1 is concave in the interval $\left[0, \dfrac{\pi}{\omega}\right]$ (notice that $\dfrac{1}{2} < \dfrac{\pi}{\omega}$) we obtain in this case for all $\xi \in \left(0, \dfrac{1}{2}\right]$:

$$f_1(\xi) \geq 2\xi f_1\left(\frac{1}{2}\right) > 2\xi f_2\left(\frac{1}{2}\right) = f_2(\xi).$$

Therefore $\sin[\xi\omega]\cosh[\zeta\omega] = K\xi\sin[\omega]$ has no solution in the interval $\xi \in (0,1/2]$ if $\omega < 2\pi$,

$$\sin[\alpha\omega] = \frac{1}{(3-4\nu)}\alpha\sin[\omega].$$

An analogous argument shows the same results for $\sin[\alpha\omega] = -\dfrac{1}{(3-4\nu)}\alpha\sin[\omega]$. □

Theorem 6 ([3]). *If $\omega < 2\pi$ then the equation (3.21) has no zeros in the strip $Re(\alpha) \in (0,1/2]$.*

Theorem 7 ([3]). *If $\omega < \pi$ then the equation (3.23) has no zeros in the strip $Re(\alpha) \in (0,1/2]$ and if $\omega < 2\pi$ then this equation has no zeros in the strip $Re(\alpha) \in (0,1/4]$.*

Lemma 2. *If for Ω the interior angle ω at the crack tip of $\partial\Omega$ fulfill $\omega < 2\pi$ for the Dirichlet-Dirichlet and Neumann-Neumann conditions and $\omega < \pi$ for the Neumann-Dirichlet conditions. Then a solution $u \in W$ of (2.28) with data data f in$[L^2(\Omega)]^2$ and $g \in [H^{1/2}(\Gamma_N)]^2$ satisfies:*

$$u \in [H^{\frac{3}{2}+\varepsilon}(\Omega)]^2, \quad \text{for some } \varepsilon > 0.$$

Proof. It follows as in the proof of ([76], Theorem 2.3). □

3.4 Computation of the singular exponents

In section 3.3 we have discussed the structure of the singular terms. Now, we compute the eigenvalues and point out the dependence of the exponent on the apex angle. The eigenvalues α are given by the correspondent eigenvalue condition for each boundary value problem.
The problem is simulated computationally by using the software PDE2D [27]. The code is written in Appendix B.
The problem (3.6) is a linear differential equation system where the eigenvalue α appears in a nonlinear form and it does not fit into the standard PDE2D eigenvalue problem format, therefore a different approach will be taken.
Although we want to solve a series of steady-state problems, for convenience we consider our problem as time dependent, where the time variable is used to represent the eigenvalue parameter α.
Some "random" nonhomogeneous terms will be added to each differential equation and the problem will be solved for various values of α in a range (α_0, α_1), with:

$$\alpha = \alpha_0 + \frac{i}{\text{NSTEPS}} * (\alpha_1 - \alpha_0), \quad i = 1, \cdots, \text{NSTEPS},$$

NSTEPS the number of time steps.
The distribution of zeros is considered with $\alpha_0 = 0 \leq \text{Re}\alpha \leq 4 = \alpha_1$ and NSTEPS $= 200$.
A collocation finite element method is used to solve the problem with cubic Hermite basis functions on the subintervals defined by the grid points: xgrid(1),xgrid(2),$\cdots$, xgrid(NXGRID).
The number of xgrid lines, NXGRID, was taken here equal to 100 and 50 the number of points of the uniform grid, xgrid(1)=$-\frac{\omega_0}{2}$ and xgrid(NXGRID)=$\frac{\omega_0}{2}$ for different values of ω_0.

3.4.1 Distribution of the eigenvalues

DIRICHLET PROBLEM

We shall compute at first the roots of the transcedental equations (3.18).
The knowledge of the eigenvalues and associated eigenvectors is decisive for the description of the behavior of the solution u of (2.28) in the vicinity of a crack tip.
The eigenvalues for Dirichlet-Dirichlet boundary conditions satisfy:

$$(3-4\nu)\sin[\alpha\omega_0]-\alpha\sin[\omega_0]=0,$$
$$(3-4\nu)\sin[\alpha\omega_0]+\alpha\sin[\omega_0]=0,$$

with the Dirichlet boundary conditions given for the numerical aspects in $\omega=\pm\frac{\omega_0}{2}$, as in [89] it is made. i.e.

$$u_r(\pm\omega_0/2)=u_\omega(\pm\omega_0/2)=0. \tag{3.24}$$

To find the numerical solution of (3.6) with boundary conditions (3.24), we develop a technique like the one described in [26].
We save the norm of the solution of (3.6) with boundary condition (3.24) and later plot this norm as function of α. When α is close to an eigenvalue, the corresponding solution will be very large, compare with (3.30).
With this search criterion we can obtain the eigenvalues and later on the eigenfunctions are compute, see Table 3.1 where only some values are shown as an example, and the corresponding Figure 3.6(b) for $\omega_0=2\pi$.

Spectral problems for $\omega_0=\pi$ and $\omega_0=2\pi$.

We apply this general theory to special geometries correspond to the case of opening angles π (half-space) and 2π (crack). For understanding conical point singularities, the case of a crack is the most important one. Here the singular exponents are half-integers.

Let α be a solution of the equation (3.18). Then every solution has the form, [89]:
for an eigenvalue satisfying the equality $(3-4\nu)\sin[\alpha\omega_0]-\alpha\sin[\omega_0]=0$, we get the eigenvector:

$$\begin{aligned}\begin{pmatrix}\mathrm{u}_r^-\\ \mathrm{u}_\omega^-\end{pmatrix} &= c_1\mathrm{u}^{(1)}+c_3\mathrm{u}^{(3)}\\ &=[(3-4\nu)\cos[\alpha\omega_0]-\alpha\cos[\omega_0]]\begin{pmatrix}\cos[(1+\alpha)\omega]\\ -\sin[(1+\alpha)\omega]\end{pmatrix}+(-1)\begin{pmatrix}(3-4\nu-\alpha)\cos[(1-\alpha)\omega]\\ -(3-4\nu+\alpha)\sin[(1-\alpha)\omega]\end{pmatrix}.\end{aligned} \tag{3.25}$$

If α satisfies the equality $(3-4\nu)\sin[\alpha\omega_0]+\alpha\sin[\omega_0]=0$, then, in a similar way, we obtain the eigenvector:

$$\begin{aligned}\begin{pmatrix} u_r^+ \\ u_\omega^+ \end{pmatrix} &= c_2 u^{(2)} + c_4 u^{(4)} \\ &= [(3-4\nu)\cos[\alpha\omega_0]+\alpha\cos[\omega_0]]\begin{pmatrix} \sin[(1+\alpha)\omega] \\ \cos[(1+\alpha)\omega] \end{pmatrix} + (-1)\begin{pmatrix} (3-4\nu-\alpha)\sin[(1-\alpha)\omega] \\ (3-4\nu+\alpha)\cos[(1-\alpha)\omega] \end{pmatrix}.\end{aligned} \tag{3.26}$$

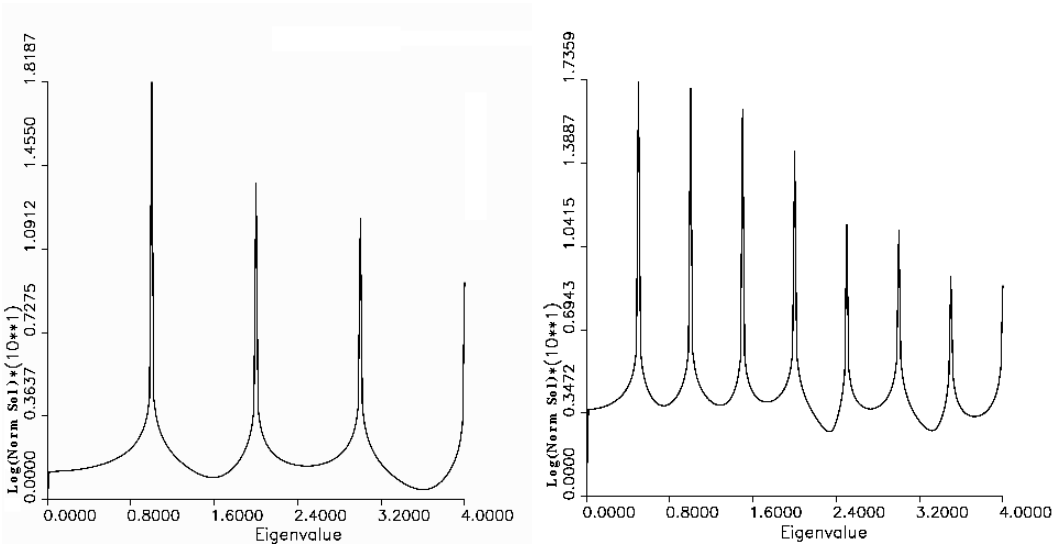

(a) Eingenvalues for $\omega_0=\pi$.

(b) Eingenvalues for $\omega_0=2\pi$.

Figure 3.6: Eigenvalues generated by the Dirichlet problem with $\nu=0.45$. Compare with numerical search criterion shown in table 3.1 for $\omega_0=2\pi$.

We compute now the eigenvectors corresponding to the eigenvalues for the case $\nu=0.45$ and $\omega_0=\pi$. They are showed in plots (3.7(a)), (3.7(b)), (3.7(c)), (3.7(d)).

In similar way for $\omega_0=2\pi$ in plots (3.8(a)), (3.8(b)), (3.8(c)), (3.8(d)), (3.8(e)), (3.8(f)), (3.8(g)), (3.8(h)).

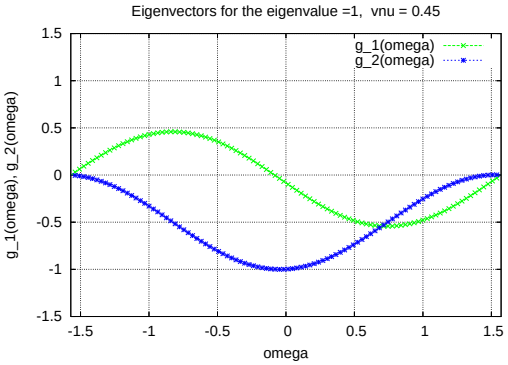

(a) Eigenvector for $\alpha = 1$

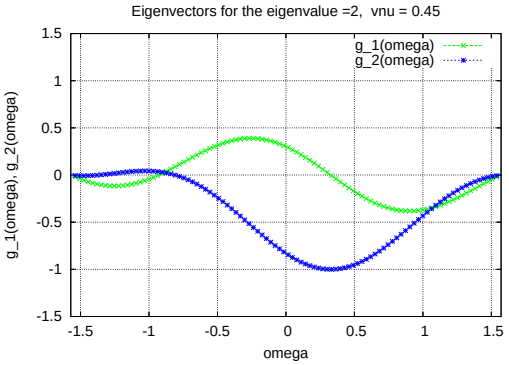

(b) Eigenvector for $\alpha = 2$

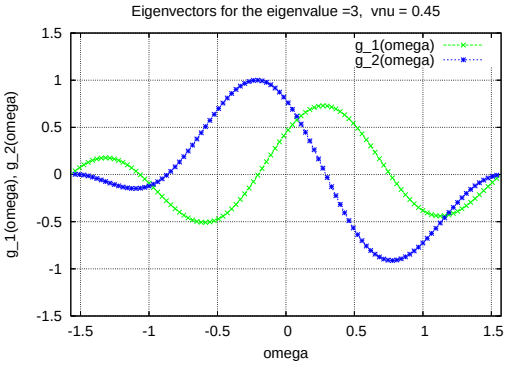

(c) Eigenvector for $\alpha = 3$

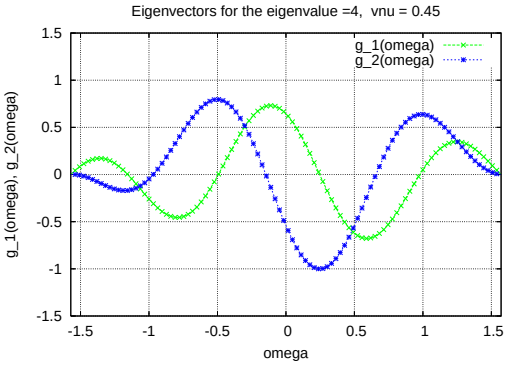

(d) Eigenvector for $\alpha = 4$

Figure 3.7: Eigenvectors for $\omega_0 = \pi$.

α	**sol. norm**			α	**sol.norm**	
0.01	21.686			0.51	396.34	
0.02	21.705			0.52	194.23	
0.03	21.736			0.53	126.85	
...	...			...	...	
0.47	143.32			0.97	121.12	
0.48	210.66			0.98	179.49	
0.49	412.86			0.99	354.37	
0.5	334920000			1	106400000	
$\alpha = 0.5$	is eigenvalue			$\alpha = 1$	is eigenvalue	
ω_0	**g1**	**g2**		ω_0	**g1**	**g2**
-3.14159	0	0		-3.14159	0	0
-3.07813	0.01525	0.01239		-3.07813	0.06356	0.00433
-3.01466	0.03304	0.02306		-3.01466	0.12716	0.00058
-2.95119	0.05319	0.03177		-2.95119	0.18978	-0.01119
-2.88773	0.07548	0.0383		-2.88773	0.2504	-0.03079
-2.82426	0.09968	0.04243		-2.82426	0.30805	-0.05791
...	...	...		-2.76079	0.3618	-0.09211
2.82426	0.03324	0.07795		-2.69733	0.4108	-0.13284
2.88773	0.03264	0.06121		...	...	...
2.95119	0.02895	0.04473				
3.01466	0.02223	0.02884				
3.07813	0.01254	0.01384				
3.14159	0	0				
...	...	...				

Table 3.1: Search criterion of the eigenvalues and computation of the corresponding eigenfunctions with Dirichlet conditions given on $\pm\omega_0/2$ and $\omega_0 = 2\pi$.

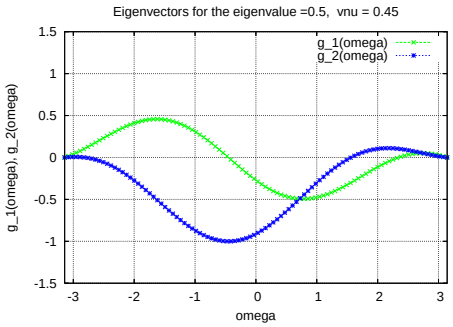

(a) Eigenvector for $\alpha = 0.5$

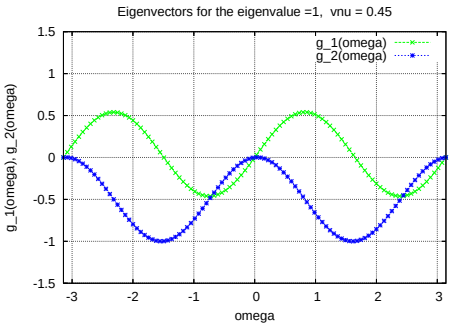

(b) Eigenvector for $\alpha = 1$

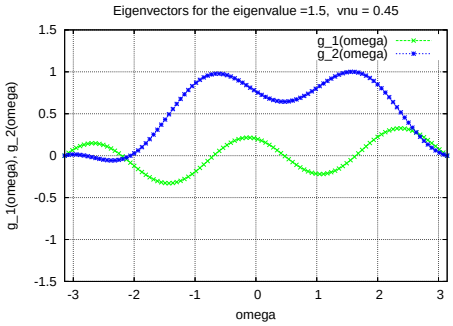

(c) Eigenvector for $\alpha = 1.5$

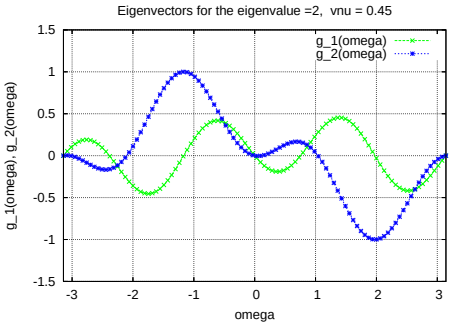

(d) Eigenvector for $\alpha = 2$

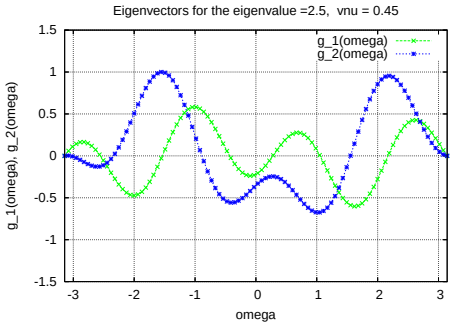

(e) Eigenvector for $\alpha = 2.5$

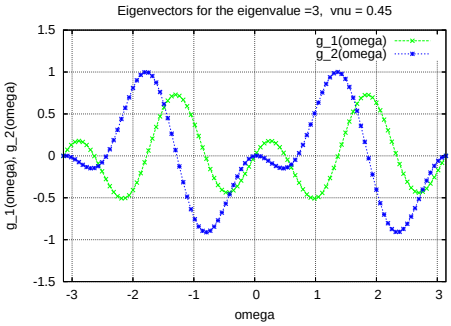

(f) Eigenvector for $\alpha = 3$

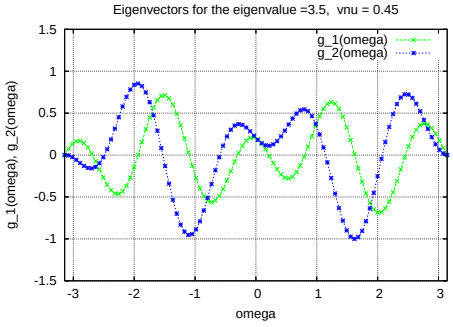

(g) Eigenvector for $\alpha = 3.5$

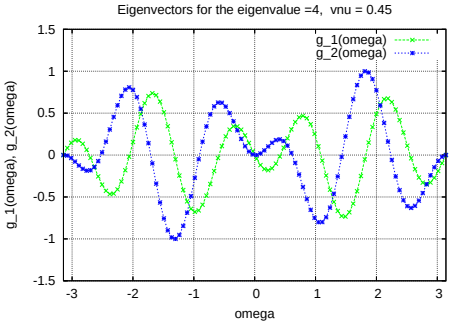

(h) Eigenvector for $\alpha = 4$

Figure 3.8: Eigenvectors for Dirichlet Problem $\omega_0 = 2\pi$ and $\nu = 0.45$

NEUMANN PROBLEM

We consider now (3.21). Analogous to the case of the Dirichlet problem, for an eigenvalue satisfying the equality $\sin[\alpha\omega_0]-\alpha\sin[\omega_0]=0$, the eigenvectors are, [89]:

$$\begin{aligned}\begin{pmatrix}\mathrm{u}_r^-\\ \mathrm{u}_\omega^-\end{pmatrix} &= c_2\mathrm{u}^{(2)}+c_4\mathrm{u}^{(4)}\\ &=(\cos[\alpha\omega_0]-\alpha\cos[\omega_0])\begin{pmatrix}\sin[(1+\alpha)\omega]\\ \cos[(1+\alpha)\omega]\end{pmatrix}+(1)\begin{pmatrix}(3-4\nu-\alpha)\sin[(1-\alpha)\omega]\\ (3-4\nu+\alpha)\cos[(1-\alpha)\omega]\end{pmatrix}.\end{aligned} \tag{3.27}$$

If α satisfies the equality $\sin[\alpha\omega_0]+\alpha\sin[\omega_0]=0$, then, in a similar way, we obtain the eigenvector:

$$\begin{aligned}\begin{pmatrix}\mathrm{u}_r^+\\ \mathrm{u}_\omega^+\end{pmatrix} &= c_1\mathrm{u}^{(1)}+c_3\mathrm{u}^{(3)}\\ &=(\cos[\alpha\omega_0]+\alpha\cos[\omega_0])\begin{pmatrix}\cos[(1+\alpha)\omega]\\ -\sin[(1+\alpha)\omega]\end{pmatrix}+(1)\begin{pmatrix}(3-4\nu-\alpha)\cos[(1-\alpha)\omega]\\ -(3-4\nu+\alpha)\sin[(1-\alpha)\omega]\end{pmatrix}.\end{aligned} \tag{3.28}$$

The condition $\sigma\cdot n=0$ on the crack faces (traction free) implies values of eigenvalues $\alpha=\frac{k}{2}$, $k=1,2,\cdots$, see Figure 3.6(b).
The eigenvalue $\alpha=\frac{1}{2}$ for $\omega_0=2\pi$ (crack) plays an important role in fracture mechanics, [62].

$$\begin{pmatrix}(5-8\nu)\cos(\frac{\omega}{2})-\cos(\frac{3\omega}{2})\\ -(7-8\nu)\sin(\frac{\omega}{2})+\sin(\frac{3\omega}{2})\end{pmatrix},\qquad \begin{pmatrix}(5-8\nu)\sin(\frac{\omega}{2})-3\sin(\frac{3\omega}{2})\\ (7-8\nu)\cos(\frac{\omega}{2})-3\cos(\frac{3\omega}{2})\end{pmatrix} \tag{3.29}$$

The square root singularity $r^{\frac{1}{2}}$ for the displacement corresponds to an unbounded stress with singularity $r^{-\frac{1}{2}}$. $\kappa=3-4\nu$ (plane strain):

$$\begin{pmatrix}(2\kappa-1)\cos\left[\frac{\omega}{2}\right]-\cos\left[\frac{3}{2}\omega\right]\\ -(2\kappa+1)\sin\left[\frac{\omega}{2}\right]+\sin\left[\frac{3}{2}\omega\right]\end{pmatrix},\qquad \begin{pmatrix}(2\kappa-1)\sin\left[\frac{\omega}{2}\right]-3\sin\left[\frac{3}{2}\omega\right]\\ (2\kappa+1)\cos\left[\frac{\omega}{2}\right]-3\cos\left[\frac{3}{2}\omega\right]\end{pmatrix}.$$

After trigonometrical formulas, the cartesian solutions are given by:

$$\begin{pmatrix}\mathrm{u}_1\\ \mathrm{u}_2\end{pmatrix}=\begin{pmatrix}\cos\omega & -\sin\omega\\ \sin\omega & \cos\omega\end{pmatrix}\begin{pmatrix}(2\kappa-1)\cos\left[\frac{\omega}{2}\right]-\cos\left[\frac{3}{2}\omega\right]\\ -(2\kappa+1)\sin\left[\frac{\omega}{2}\right]+\sin\left[\frac{3}{2}\omega\right]\end{pmatrix}=\begin{pmatrix}2\kappa\cos\left[\frac{\omega}{2}\right]-2\cos\left[\frac{\omega}{2}\right]\cos[\omega]\\ 2\kappa\sin\left[\frac{\omega}{2}\right]-2\sin\left[\frac{\omega}{2}\right]\cos[\omega]\end{pmatrix}=2(\kappa-\cos[\omega])\begin{pmatrix}\cos\left[\frac{\omega}{2}\right]\\ \sin\left[\frac{\omega}{2}\right]\end{pmatrix}.$$

and also

$$\begin{pmatrix}\mathrm{u}_1\\ \mathrm{u}_2\end{pmatrix}=\begin{pmatrix}\cos\omega & -\sin\omega\\ \sin\omega & \cos\omega\end{pmatrix}\begin{pmatrix}(2\kappa-1)\sin\left[\frac{\omega}{2}\right]-3\sin\left[\frac{3}{2}\omega\right]\\ (2\kappa+1)\cos\left[\frac{\omega}{2}\right]-3\cos\left[\frac{3}{2}\omega\right]\end{pmatrix}=2\begin{pmatrix}(\kappa+2)\sin\left[\frac{\omega}{2}\right]+\sin\left[\frac{\omega}{2}\right]\cos[\omega]\\ (\kappa-2)\cos\left[\frac{\omega}{2}\right]-\cos\left[\frac{\omega}{2}\right]\cos[\omega]\end{pmatrix}=2\begin{pmatrix}\sin\left[\frac{\omega}{2}\right]((\kappa+2)+\cos[\omega])\\ \cos\left[\frac{\omega}{2}\right]((\kappa-2)-\cos[\omega])\end{pmatrix}.$$

Their linear combination

$$\vec{u} = K_1 r^{\frac{1}{2}}(\kappa - \cos[\omega]) \begin{pmatrix} \cos\left[\frac{\omega}{2}\right] \\ \sin\left[\frac{\omega}{2}\right] \end{pmatrix} + K_2 r^{\frac{1}{2}} \begin{pmatrix} \sin\left[\frac{\omega}{2}\right]((\kappa+2)+\cos[\omega]) \\ \cos\left[\frac{\omega}{2}\right]((\kappa-2)-\cos[\omega]) \end{pmatrix} + \vec{u}_{\text{reg}}$$

satisfies the boundary value problem in a domain with point singularity.

The coefficients K_1 and K_2 are the stress intensity factors. They express the intensity of the singular functions. In particular they can vanish and then the solution u is regular. The coefficients are functions of the external forces, the elastic material parameters and on the geometry of the domain and they can be calculated via so-called coefficient formulae.
The regularity results and coefficient formulae can be applied in different fields, namely sensitivity analysis for linear elastic fields, and derivation of formulas in fracture mechanics for a nonlinear elastic model.

Now we compute the eigenvectors corresponding to the eigenvalues for the case $\nu = 0.3$ and $\omega_0 = 2\pi$. They verify

$$\sin[\alpha\omega_0] - \alpha\sin[\omega_0] = 0$$
$$\sin[\alpha\omega_0] + \alpha\sin[\omega_0] = 0$$

with the Neumann boundary conditions given for the numerical aspects as

$$\sigma n|_{\pm\frac{\omega_0}{2}} = 0,$$

as in [89] it is made.

The eigenvectors are showed in plots (3.9(a)), (3.9(b)), (3.9(c)), (3.9(d)), (3.9(e)), (3.9(f)), (3.9(g)), (3.9(h)).

3.4.2 Extraction of eigenvalues from the discrete solution

A simple method to check the computed eigenvalues is, to extract them from a finite element solution. Here, we use again the fact, that in the neighbourhood on a crack tip, the field $\vec{u}$ can be represented as $\vec{u}(r,\omega) = r^\alpha \vec{g}(\omega)$, where r and ω are again polar coordinates. Then, for a fixed angle ω_0 holds:

$$\frac{|\vec{u}(r_0,\omega_0)|}{|\vec{u}(\frac{r_0}{2},\omega_0)|} = \frac{r_0^\alpha |\vec{g}(\omega_0)|}{\left(\frac{r_0}{2}\right)^\alpha |\vec{g}(\omega_0)|} = 2^\alpha,$$
$$\alpha = \log_2\left(\frac{|\vec{u}(r_0,\omega_0)|}{|\vec{u}(\frac{r_0}{2},\omega_0)|}\right) \tag{3.30}$$

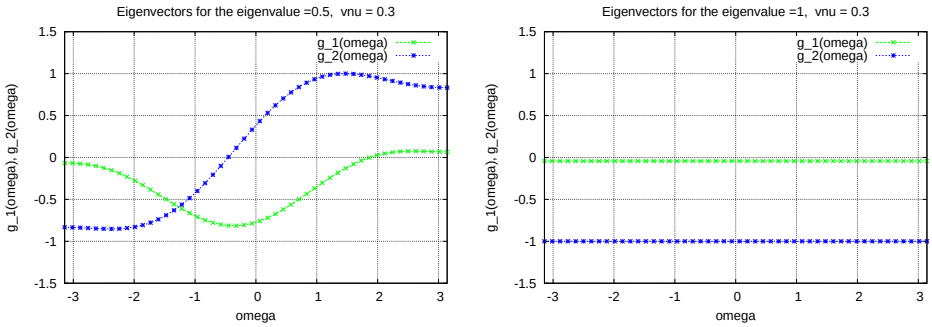

(a) Eigenvector for $\alpha = 0.5$

(b) Eigenvector for $\alpha = 1$

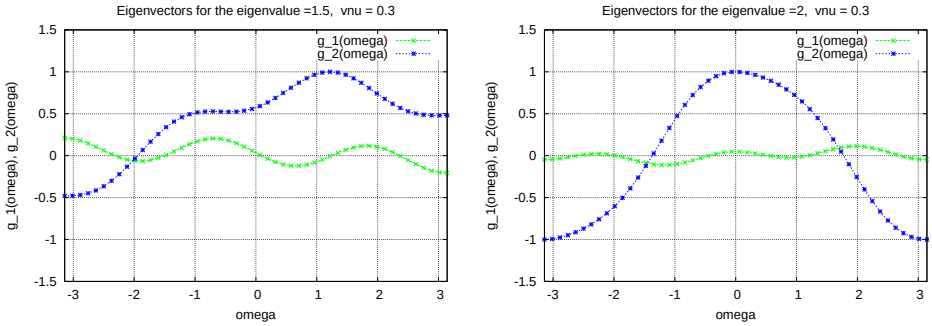

(c) Eigenvector for $\alpha = 1.5$

(d) Eigenvector for $\alpha = 2$

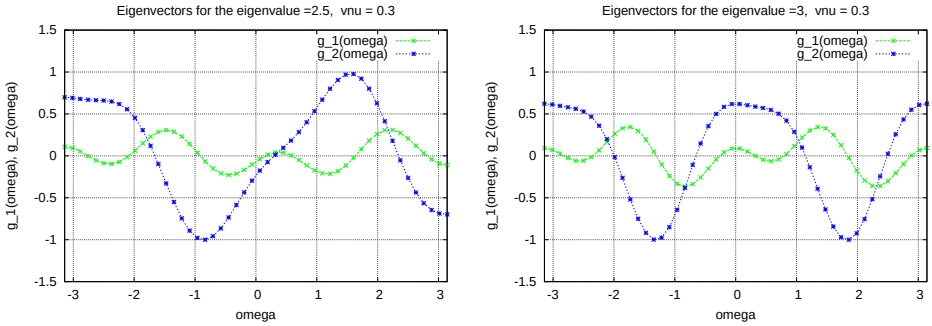

(e) Eigenvector for $\alpha = 2.5$

(f) Eigenvector for $\alpha = 3$

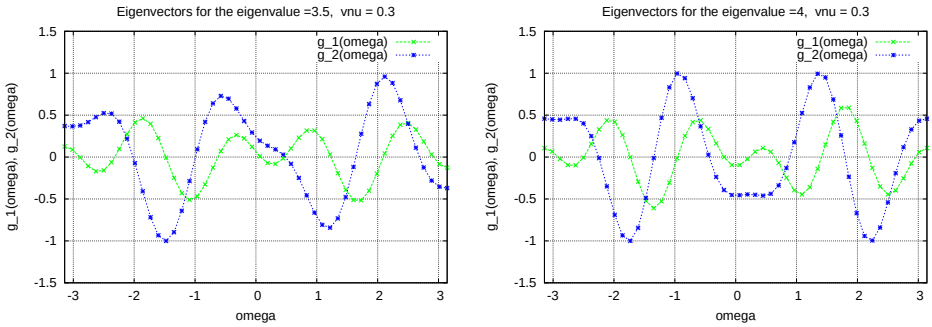

(g) Eigenvector for $\alpha = 3.5$

(h) Eigenvector for $\alpha = 4$

Figure 3.9: Eigenvectors for Neumann Problem with $\omega_0 = 2\pi$ and $\nu = 0.3$.

To compute α by (3.30) from the numerical solution, there are two possibilities:

1. Insert interpolated values of the numerical solution $\vec{u}(\frac{r_0}{2}, \omega_0)$ into (3.30),
2. Calculate α from a fine and a coarse grid.

In the follow we show a part of the FORTRAN CODE used to get the eigenvalues and the corresponding eigenfunctions. Note that the code can be adapted to different boundary conditions, by changing $a(i,j)$ and $b(i,y), i,j = 1,\cdots,4$.

This CODE is written with a velocity function $\alpha_2(t) = \sqrt{1-\left(\frac{h'(t)}{c_2}\right)^2}$ as parameter, (here $\alpha_2(t) = 1$, static case). But we want to remark that this code can be also used for solving the dynamic anisotropic Lamé equations given in Definition 9 numerically, written in spherical coordinates, for $h'(t) \neq 0$. The anisotropic Lamé equations in spherical coordinates are given in Appendix (A.8).

```
C ***********************************************************************
C     INPUT to DBVSUP
C ***********************************************************************
C
C     NXPTS = number of output points.
C
C     NIC = number of boundary conditions at XINITIAL.
C
C     B(NROWB,NCOMP) = boundary condition matrix at XFINAL.
C                      Must be contained in (NFC,NCOMP) sub-matrix.
C
C     NROWB = actual row dimension of B in calling program,
C             NROWB must be .GE. NFC.
c
C     ALPHA(NIC+NEQIVP) = boundary conditions at XINITIAL.
C                         If NEQIVP .GT. 0 (see below), the boundary
C                         conditions at XINITIAL for the initial value
C                         equations must be stored starting in
C                         position (NIC + 1) of ALPHA.
C
C     NIC = number of boundary conditions at XINITIAL.
C
C     BETA(NFC) = boundary conditions at XFINAL.
C
C     NFC = number of boundary conditions at XFINAL.
C
C     IGOFX =0 -- The inhomogeneous term G(X) is identically zero.
C           =1 -- The inhomogeneous term G(X) is not identically zero.
C                 (if IGOFX=1, then Subroutine DGVEC (or DUVEC) must be
C                  supplied).
c
C     IFLAG = a status parameter used principally for output.
C
C     WORK(NDW) = floating point array used for internal storage.
C
```

```
C     NDW = actual dimension of work array allocated by user.
C           An estimate for NDW can be computed from the following
C            NDW = 130 + NCOMP**2 * (6 + NXPTS/2 + expected number of
C                                       orthonormalizations/8)
C
C     IWORK(NDIW) = integer array used for internal storage.
C
C     NDIW = actual dimension of IWORK array allocated by user.
C            An estimate for NDIW can be computed from the following
C            NDIW = 68 + NCOMP * (1 + expected number of
C                                        orthonormalizations)
C
C     NEQIVP = number of auxiliary initial value equations being added
C              to the boundary value problem.
c
      implicit double precision (a-h,o-z)
      parameter (NXPTS=100,NDW=10000,NDIW=10000)
      dimension G(4,NXPTS),xpts(NXPTS),a(2,4),alpha(2),
     & b(2,4),beta(2),work(NDW),iwork(NDIW)
      common /parm2/ ralpha, alpha2
      alpha2 = 1.0
      pi = 4.0*atan(1.d0)
      al = 2*pi
      open (11,file='adr.val')
C  output points
      do 10 i=1,NXPTS
         xpts(i) = -al/2 + (i-1)*al/(NXPTS-1)
   10 continue
      do 15 i=1,15
         iwork(i) = 0
   15 continue
C  g1=0, g2=0 at left end point (-al/2)
      a(1,1) = 1
      a(1,2) = 0
      a(1,3) = 0
      a(1,4) = 0
      alpha(1) = 0
      a(2,1) = 0
      a(2,2) = 1
      a(2,3) = 0
      a(2,4) = 0
      alpha(2) = 0
C  g1=0, g2=0 at right end point (+al/2)
      b(1,1) = 1
      b(1,2) = 0
      b(1,3) = 0
      b(1,4) = 0
      beta(1) = 0
      b(2,1) = 0
      b(2,2) = 1
      b(2,3) = 0
      b(2,4) = 0
      beta(2) = 0
C  DBVSUP input parameters
      IGOFX = 1
      NEQIVP = 0
```

```
      NROWY = 4
      NCOMP = 4
      NROWA = 2
      NIC = 2
      NROWB = 2
      NFC = 2
      RE = 1.d-6
      AE = 0.0
C  solve with different values of ralpha, when solution is large,
C  ralpha is an eigenvalue
      do 100 j=1,400
         ralpha = 0.01*j
         call dbvsup(G,NROWY,NCOMP,xpts,NXPTS,a,NROWA,alpha,NIC,
     &   b,NROWB,beta,NFC,IGOFX,RE,AE,IFLAG,work,NDW,iwork,NDIW,NEQIVP)
         if (IFLAG.NE.0) print *, ' IFLAG = ',IFLAG
         anorm = 0
         do 20 i=1,NXPTS
            anorm = max(anorm,abs(G(1,i)),abs(G(2,i)))
   20    continue
         write(11,7) ralpha,anorm
    7    format (' lambda = ',F12.5,' sol. norm = ',E15.5)
C when norm large print resulting (normalized) g1(phi),g2(phi)
         if (anorm.gt.1000.0) then
            write (11,8) ralpha
    8       format (/,' lambda = ',F12.5,/,5x,'Phi',10x,'G1',10X,'G2',/)
            do 30 i=1,NXPTS
               g1 = G(1,i)/anorm
               g2 = G(2,i)/anorm
               write(11,9) xpts(i),g1,g2
   9          format (3F12.5)
   30       continue
         endif
  100 continue
      stop
      end

      subroutine dfmat(phi,g,gp)
      implicit double precision (a-h,o-z)
      dimension g(4),gp(4)
      common /parm2/ ralpha,alpha2
      rnu = 0.3
      A = 1 + 1/alpha2**2
      B = 1 - 1/alpha2**2
      C = 1./(1-2*rnu)*alpha2**2
      F11 = A/2. - B/2.*cos(2*phi)
      F22 = A/2. - B/2.*cos(2*phi) + C
      D11 = (1-ralpha)*B*sin(2*phi)
      D12 = C*(ralpha-1) - A + B*cos(2*phi)
      D21 = C*(1+ralpha) + A - B*cos(2*phi)
      D22 = (1-ralpha)*B*sin(2*phi)
      E11 = (A/2.+C)*(ralpha**2-1) + B/2.*(ralpha-1)**2*cos(2*phi)
      E12 = -B*(1-ralpha)*sin(2*phi)
      E21 =  B*(1-ralpha)*sin(2*phi)
      E22 =  A/2.*(ralpha**2-1) + B/2.*(ralpha-1)**2*cos(2*phi)
c g1' = g3
      gp(1) = g(3)
```

```
c g2' = g4
      gp(2) = g(4)
c g3' = g1'' = ...
      gp(3) = -(D11*g(3) + D12*g(4) + E11*g(1) + E12*g(2))/F11
c g4' = g2'' = ...
      gp(4) = -(D21*g(3) + D22*g(4) + E21*g(1) + E22*g(2))/F22
      return
      end

      subroutine dgvec(phi,f)
      implicit double precision (a-h,o-z)
      dimension f(4)
c  "random" non-homogeneous terms
      f(1) = 0
      f(2) = 0
      f(3) = exp(phi)
      f(4) = exp(-phi)
      return
      end

      subroutine duivp(x,u,up)
      implicit double precision (a-h,o-z)
      return
      end

      subroutine duvec(x,u,g)
      implicit double precision (a-h,o-z)
      return
      end

      SUBROUTINE DBVSUP (Y, NROWY, NCOMP, XPTS, NXPTS, A, NROWA, ALPHA,
     +   NIC, B, NROWB, BETA, NFC, IGOFX, RE, AE, IFLAG, WORK, NDW,
     +   IWORK, NDIW, NEQIVP)
C***BEGIN PROLOGUE  DBVSUP
C***PURPOSE  Solve a linear two-point boundary value problem using
C            superposition coupled with an orthonormalization procedure
C            and a variable-step integration scheme.
```

3.5 Singularities of the Laplace operator

Because their applications in later chapters, we also need to say a few words about the singular functions generated for the Laplace operator. They depend only on the geometry of the region and boundary conditions of the problem in the neighbourhood of the crack.
As we shown in Appendix A by using the relations (A.2), the two-dimensional Laplace operator has the representation in circular polar coordinates (r,ω):

$$\Delta U = r^{-1}\partial_r\left(r\partial_r U\right) + r^{-2}\partial_\omega^2 U \tag{3.31}$$

We will seek solutions of Laplace's equation associated to (3.31) which have the form

$$U(r,\omega) = r^\alpha g(\omega). \tag{3.32}$$

3.5.1 The Dirichlet problem.

That means, our problem reads

$$-\Delta U = 0, \tag{3.33}$$

$$U(r,-\pi) = U(r,\pi) = 0. \tag{3.34}$$

Since the Laplace operator has the representation (3.31) in polar coordinates, we get the following Dirichlet problem for the function g:

$$-g''(\omega) - \alpha^2 g(\omega) = 0, \quad -\pi < \omega < \pi \tag{3.35}$$

$$g(-\pi) = g(\pi) = 0. \tag{3.36}$$

The operator $-\dfrac{d^2}{d\omega^2} - \alpha^2$ associated to (3.35) is defined on the set of the functions equal to zero at the ends of the interval $(-\pi,\pi)$.
The function (3.32) is a solution of the problem (3.33) if and only if α is an eigenvalue of the operator $-\dfrac{d^2}{d\omega^2} - \alpha^2$ and g is an eigenfunction corresponding to this eigenvalue.
It is easy to show that the eigenvalues are here the number $\alpha_k = \frac{k}{2}, k = 1,2,\cdots$ and

$$g(\omega) = \cos\left(\frac{k\,\omega}{2}\right)$$

are the eigenfunctions corresponding to the eigenvalues α_k.
The solutions for the Dirichlet Laplace problem has the form

$$U_k(r,\omega) = c_k r^{\frac{k}{2}} \cos\left(\frac{k\omega}{2}\right), \quad k = 1,2,\cdots, \tag{3.37}$$

$$\begin{aligned} U(r,\omega) &= c_1 r^{\frac{1}{2}} \cos\left(\frac{\omega}{2}\right) + c_2 r \cos(\omega) + c_3 r^{\frac{3}{2}} \cos\left(\frac{3\omega}{2}\right) + \cdots, \\ &= c_1 r^{\frac{1}{2}} \cos\left(\frac{\omega}{2}\right) + U_R(r,\omega). \end{aligned} \tag{3.38}$$

where $U_R(r,\omega)$ is the regular part and it belongs to $W^{2,4}$.

3.5.2 The Neumann problem.

Next we consider the problem

$$-\Delta U = 0, \tag{3.39}$$

$$\frac{dU}{d\omega}(r,-\pi) = \frac{dU}{d\omega}(r,\pi) = 0. \tag{3.40}$$

As above, we seek solutions of the form (3.32). This leads to the problem

$$-g''(\omega) - \alpha^2 g(\omega) = 0, \quad -\pi < \omega < \pi \tag{3.41}$$

$$g'(-\pi) = g'(\pi) = 0. \tag{3.42}$$

Now the operator $-\dfrac{d^2}{d\omega^2} - \alpha^2$ associated to (3.41) is defined on the set of the functions with derivatives equal to zero at the ends of the interval $(-\pi,\pi)$.
It can be easily verified that the eigenvalues are the number $\alpha_k = \frac{k}{2}, k = 0,1,2,\cdots$ and the corresponding eigenfunctions are

$$g(\omega) = \sin\left(\frac{k\omega}{2}\right).$$

The eigenfunctions associated to the eigenvalue $\alpha_0 = 0$ constitute a particular case. The set of eigenfunctions corresponding to the eigenvalue $\alpha_0 = 0$ consists of the constant functions.
The general solutions for the Neumann Laplace problem has the form

$$U_k(r,\omega) = c_k r^{\frac{k}{2}} \sin\left(\frac{k\omega}{2}\right), \quad k = 1,2,\cdots, \tag{3.43}$$

$$\begin{aligned} U(r,\omega) &= c_1 r^{\frac{1}{2}} \sin\left(\frac{\omega}{2}\right) + c_2 r \sin(\omega) + c_3 r^{\frac{3}{2}} \sin\left(\frac{3\omega}{2}\right) + \cdots, \\ &= c_1 r^{\frac{1}{2}} \sin\left(\frac{\omega}{2}\right) + U_R(r,\omega). \end{aligned} \tag{3.44}$$

where $U_R(r,\omega)$ is the regular part and it is in $W^{2,4}$.

3.5.3 The mixed problem.

Now we are interesed in solutions of the boundary value problem

$$-\Delta U = 0, \tag{3.45}$$

$$U(r,-\pi) = 0, \quad \frac{dU}{d\omega}(r,\pi) = 0. \tag{3.46}$$

This problem is connected with the parameter-depending boundary value problem

$$-g''(\omega) - \alpha^2 g(\omega) = 0, \quad -\pi < \omega < \pi \tag{3.47}$$

$$g(-\pi) = 0, \quad g'(\pi) = 0. \tag{3.48}$$

The espectrum of the Laplace operator corresponding to the problem (3.47)-(3.48) consists of the eigenvalues $\alpha_k = \frac{2k+1}{4}, k = 0,1,2,\cdots$ and the corresponding eigenfunctions are

$$g(\omega) = \cos\left(\frac{2k+1}{4}\omega\right) + (-1)^k \sin\left(\frac{2k+1}{4}\omega\right).$$

The solutions for the Neumann Laplace problem has the form

$$U_k(r,\omega) = c_k r^{\frac{2k+1}{1}} \left(\cos\left(\frac{2k+1}{4}\omega\right) + (-1)^k \sin\left(\frac{2k+1}{4}\omega\right)\right) \quad k = 0,1,2,\cdots.$$

Remark 8. *If we suppose to have a two-dimensional domain containing a crack modeled as a straight segment, then the domain is non-smooth and this yieds strong singularities for the solution along the crack. It is important to know that the asymptotic expansion of the solution contains neither oscillatory terms (i.e. non real exponents) nor logarithmic terms.*
Here (r,ω) are polar coordinates centered at the crack tip. The classical result of the isotropic elasticity theory, which serves as a base of fracture mechanics, and explicit calculations for isotropic materials prove that the singularity exponents are half-integers $\frac{1}{2}, \frac{3}{2}, \cdots$.

CHAPTER 4

Dynamic Fracture near the crack tip: The out-of-plane case.

4.1 The mode III fracture case

Here, we investigate the simpler out-of-plane state, [4], see Table 2.1.
It is known that there always exists a region (albeit small) near the crack tip (stationary or growing) where the dynamic stress intensity factor k_{III} characterizes the amplitude of the local stress and controls the failure process, [46]. On the other hand, the level of resistance to crack advance that is exhibited by a material may depend on the crack tip speed. It was reported [39], [40], [49], [21], etc. that the dynamic fracture toughness depends on the crack tip speed $h'(t)$ in a characteristic way. The most significant feature of this dependence is that the fracture toughness is a monotone increasing function with respect to the crack speed $h'(t)$.
It is essential that we can describe the singular behaviour of the displacement field near the running crack tip and compute the coefficient in front of the leading dynamic crack singularity, the stress intensity factor $k_{III}(t,h,h')$. We get a decomposition of u into a regular term u_R and a singular one (analogously to [52], [64], [86], [80]):

$$u(y,t) = u_R(y,t) + k_{III}\left(t,h,h'\right)\eta(y)\,S_N(y_1 - h(t), y_2) \tag{4.1}$$

with

$$S_N(y_1 - h, y_2, t) = \sqrt{\frac{1}{2\alpha_2(t)}}\sqrt{\sqrt{(R\cos\vartheta - h)^2 + \alpha_2^2(t)R^2\sin^2\vartheta} - (R\cos\vartheta - h)}. \tag{4.2}$$

Here, (R, ϑ) are the current running polar coordinates. We assume that

$$\alpha_2^2(t) = 1 - \frac{h'(t)^2}{c_2^2} \geq \gamma_0^2 > 0. \tag{4.3}$$

Most of the studies on the anti-plane shear crack postulate that the body is infinite in a thickness direction because the mathematical treatment is simple. However this postulate is not pertinent to most practical cases of shearing process. We report here an analytical study on the anti-plane shear crack in a finite configuration. From now on we deal with finite bodies. The mathematical analysis will be done distinguishing between the current configuration (space variables y_1, y_2, noncylindrical domain), a reference configuration (space variables x_1, x_2, cylindrical domain) and a further configuration (space variables z_1, z_2), where the isotropic Laplacian appears. The passage to the different configurations will be described by the corresponding coordinate transformations. We emphasize that this allows us to start from an energy balance equation in the current configuration, to transform it into the reference configuration, to treat the crack singularities there and finally to obtain formula (7.1), [4].

4.2 The mathematical model

The goal is, to describe the time dependent process of an elastic wave within the time interval [0,T]. We consider the noncylindrical domain $Q \subset \mathbb{R}^2$ of the form

$$Q = \bigcup_{t=0}^{T} \Omega_t,$$

where $\Omega_t = \Omega \setminus \sigma_t$, see Figure 4.1. The domain Ω_0 with the pre-crack σ_0 is the reference domain, whereas the domains Ω_t form a family of current configurations, see Fig.4.1.

In linear elasticity for isotropic materials, the governing equations are the dynamic Navier Lamé equations (2.29),

$$\rho \vec{u}_{tt} - (\mu \Delta \vec{u} + (\lambda + \mu) \operatorname{grad}(\operatorname{div} \vec{u})) = \tilde{f}, \text{ in } \Omega_t.$$

We study at first the simpler model for the out-of plane state, that means we assume that $u_1 = u_2 = 0, u_3 = u$ and $\partial_3 u_3 = 0$, see Table (2.1). Then the system (2.29) reduces to a scalar wave equation

$$u_{tt} - c_2^2 \Delta u = f, \tag{4.4}$$

where $f = \frac{\tilde{f}_3}{\rho}$, $c_2^2 = \frac{\mu}{\rho}$. $c_2 = \sqrt{\frac{\mu}{\rho}}$ is the speed of the shear waves which is quite large (for steel $c_2 \approx 3200\ [\frac{m}{s}]$ or for glass $c_2 \approx 3300\ [\frac{m}{s}]$, for more examples see Table 2.2).

We will study an initial-boundary value problem for the wave equation (4.4) in the cracked domain $Q = \bigcup_{t=0}^{T} \Omega_t$, see Fig.4.1.

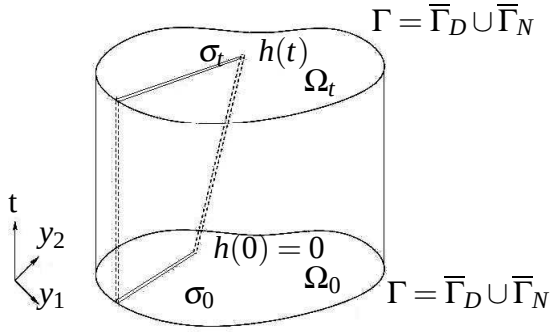

Figure 4.1: Noncylindrical domain Q

Find $u = u(y,t)$ such that

$$\left.\begin{aligned} &\partial_t^2 u - c_2^2 \Delta u = f \text{ in } Q := \cup_{t=0}^{T} \Omega_t, \\ &c_2^2 \partial_n u = 0 \text{ on } \cup_{t=0}^{T} \sigma_t, \\ &c_2^2 \partial_n u = q \text{ on } \Sigma_N := \Gamma_N \times (0,T), \\ &u = 0 \text{ on } \Sigma_D := \Gamma_D \times (0,T), \\ &u(0) = u_0,\ \partial_t u(0) = u_1 \text{ in } \Omega_0, \end{aligned}\right\} \tag{4.5}$$

where $\overline{\Gamma}_D \cup \overline{\Gamma}_N = \Gamma$ and $\Gamma_D \cap \Gamma_N = \emptyset$. On Γ_N, $\partial_n u = \nabla u \cdot n$ means the outward normal derivative while on σ_t it means the normal derivative in one fixed normal direction (therefore $\partial_n u = 0$ on σ_t means that the normal derivative from above and from below are both zero).

The domain Ω_0 with the pre-crack σ_0 is the reference domain, whereas the domains Ω_t form a family of current configurations. We assume, that the motion of Ω_0 to Ω_t is given by a family of mappings

$$y = F_t(x) = x + h(t)\ \theta(x), \quad x \in \Omega_0, \quad y \in \Omega_t. \tag{4.6}$$

This is a standard assumption, see e.g. [51], [63], [9], [87]. The mapping F_t is an element of $C^\infty(\overline{\Omega_0})$, $supp\,\theta \subset U(0)$, $h(0) = 0$, $F_t(\sigma_0) = \sigma_t$.

Here,

$$\theta(x) = \eta(r) \begin{pmatrix} 1 \\ 0 \end{pmatrix}, \tag{4.7}$$

where $\eta = \eta(r)$ is a smooth cut-off function such that $\eta \equiv 1$ in a neighborhood of the crack tip $\{(0,0)\}$ and as usual $r = |x-0| = |x|$ is the distance to the crack tip $\{0\}$.
We assume that F_t is a diffeomorphism from Ω_0 onto Ω_t and moreover that

$$\det \nabla F_t = \det(I + h\nabla\theta) \geq D_0 > 0 \quad \text{for } (x,t) \in \bar{\Omega}_0 \times [0,T] \tag{4.8}$$

for some positive constant D_0 independent of x and t, where

$$\nabla\theta = \begin{pmatrix} \partial_1\theta_1 & \partial_2\theta_1 \\ \partial_1\theta_2 & \partial_2\theta_2 \end{pmatrix}$$

is the Jacobian matrix of θ. If we choose polar coordinates (r,φ), then the Jacobian determinant can be written as $\det \nabla F_t = 1 + h(t)\partial_1\theta_1 = 1 + h(t)\eta'(r)\cos\varphi$. Thus, we have to guarantee that $h(t)$ is small enough. Fix cut-off function η with $C = \max|\eta'(r)|$ we assume

$$|h(t)| < \frac{1}{C}, \tag{4.9}$$

which is realistic for small t. Moreover, F_t is a diffeomorphism and maps the crack σ_0 to σ_t, see e.g [63], [54].
The following mathematical difficulty occurs: problem (4.5) is given in a noncylindrical domain Q. To our knowledge there are no existence, uniqueness and regularity results available. Therefore we transform (4.5) by (4.6) to the cylindrical domain $\Omega_0 \times (0,T)$ setting:

$$\begin{aligned} u(y,t) &= u(F_t(x),t) =: v(x,t), \\ f(y,t) &= f(F_t(x),t) =: \hat{f}(x,t), \\ q(y,t) &= q(F_t(x),t) =: \hat{q}(x,t). \end{aligned} \tag{4.10}$$

Lemma 3. *([4]) The change of variables (4.6) leads to the following transformed problem in the reference configuration Ω_0 :*

$$v_{tt} + \mathcal{A}_0(t)\, v + \mathcal{A}_1(t)\, v + \mathcal{B}(t)\, v_t = \hat{f} \text{ in } \Omega_0 \times (0,T), \tag{4.11}$$

$$c_2^2 (\nabla F_t)^{-\top} \nabla v \cdot (\nabla F_t)^{-\top} n = 0 \text{ on } \sigma_0 \times (0,T), \tag{4.12}$$

$$c_2^2 \partial_n v = \hat{q} \text{ on } \Sigma_N, \tag{4.13}$$

$$v = 0 \text{ on } \Sigma_D, \tag{4.14}$$

$$v(x,0) = u_0(x) \text{ in } \Omega_0, \tag{4.15}$$

$$v_t(x,0) = u_1(x) + h'(0)\ \theta \cdot (\nabla F_t)^{-\top}\ \nabla v(x,0) = v_1(x) \text{ in } \Omega_0, \tag{4.16}$$

where

$$\begin{aligned}
\mathcal{A}_0(t)v &= -\frac{c_2^2}{\det(\nabla F_t)}\, div\left(\det(\nabla F_t)(\nabla F_t)^{-1}(\nabla F_t)^{-\top}\nabla v\right)\\
&\quad + h'^2\ \theta\cdot(\nabla F_t)^{-\top}\nabla\left(\theta\cdot(\nabla F_t)^{-\top}\nabla v\right),\\
\mathcal{A}_1(t)v &= h'^2\ \theta\cdot(\nabla F_t)^{-\top}(\nabla\theta)^{\top}(\nabla F_t)^{-\top}\nabla v\\
&\quad - h''\ \theta\cdot(\nabla F_t)^{-\top}\nabla v,\\
\mathcal{B}(t)v_t &= -2h'\ \theta\cdot(\nabla F_t)^{-\top}\nabla v_t.
\end{aligned}$$

Note that near the crack tip, where $\eta \equiv 1$, the operator $\mathcal{A}_0(t)$ reduces to the anisotropic Laplacian

$$\mathcal{A}_0(t) = -c_2^2(\alpha_2^2(t)\ \partial_1^2 + \partial_2^2),$$

where $\alpha_2^2(t) = 1 - \frac{h'(t)^2}{c_2^2}$.

Lemma 4. *The anisotropic Laplacian $\mathcal{A}_0(t)$ in the reference domain is strongly elliptic with respect to the spatial variables if:*

$$c_2^2 - h'(t)^2 > 0. \tag{4.17}$$

i.e. if the crack tip velocities are bounded.

(4.17) is satisfied if it holds:

$$\exists \alpha_0 > 0 : 1 - \frac{h'(t)^2}{c_2^2} \geq \alpha_0^2 > 0, \forall t \in (0,T). \tag{4.18}$$

This assumption means that the crack velocity is not allowed to be faster than the wave speed, what is practically true. Ravi-Chandar and Knauss (1984) [41] "*all* materials exhibit a limiting crack speed which is on the order of one half of the shear wave speed or less"

In order to get the isotropic Laplacian we transform the space coordinates $x = (x_1, x_2)$ of Ω_0 into

$$\begin{aligned}
z_1 &= q_1(x,t),\\
z_2 &= x_2,
\end{aligned} \tag{4.19}$$

where $z_1 = \frac{x_1}{\alpha_2(t)}$ near the crack tip. For details compare [77].

Lemma 5. *The space-depending principal part in the plane space variable z_1, z_2 is strongly elliptic with respect to the spatial variables if $h''(t)$ is uniformly bounded.*

This last transformation has the following advantages:

- we get an isotropic Laplacian (elliptic operator),
- we can apply the semigroup theory to the transformed initial-boundary value problem to get existence and solvability results,
- description of crack singularities in z-coordinates explicitly:

$$w(z) = w_R(z) + k_{III}\widehat{\eta}S_N(z),$$

$w_R \in H^2(\widetilde{\Omega_0})$ regular part of w, $\widehat{\eta}$ cut-off function ($\widehat{\eta} = 1$ in neighborhood of $h(0)$ and 0 outside), $k_{III} \in \mathbb{R}$, so-called stress intensity factor and S_N Neumann singular function related to the Laplace operator in z coordinates namely, see (3.44) in chapter 3:

$$S_N(z_1, z_2) = \sqrt{r_z}\,\sin\frac{\phi_z}{2}.$$

The inverse transformations from the z-coordinates to the x-coordinates (reference configuration) and finally to the y-coordinates (current configuration) lead the following result:

Fix $t > 0$ and $v = v(x,t)$

$$X_t = \left\{v \in H^2(\Omega_0) : c_2^2\partial_n v = \hat{q} \text{ on } \Gamma_N \cup\ \sigma_0, v = 0 \text{ on } \Gamma_D\right\} \oplus \text{span}\{\eta S_N\}$$

with the singular function

$$S_N\left(\frac{x_1}{\alpha_2(t)}, x_2, t\right) = \sqrt{\frac{r}{2\alpha_2(t)}}\sqrt{\sqrt{\cos^2\phi + \alpha_2^2(t)\sin^2\phi} - \cos\phi} \tag{4.20}$$

defined in the reference configuration.
It follows the main Theorem of this chapter:

Theorem 8. ***H1*** *Assume that (4.18) and (4.9) are satisfied and $h''(t)$ is uniformly bounded.*

H2

$$\hat{f} \in Lip([0,T];\, L^2(\Omega)), \quad \hat{q} \in \tilde{H}^{\frac{1}{2}}(\Gamma_N \times [0,T]),$$
$$u_0 = v(x,0)\ \in X_0, \quad u_1 = \partial_t v(x,0) - h'(0)\ \theta \cdot (\nabla F_t)^{-\top}\ \nabla v(x,0) \in L^2(\Omega)$$

then there exists a unique solution

$$v \in C([0,T];\, X_t) \cap C^1([0,T];\, H^1(\Omega)) \cap C^2([0,T];\, L^2(\Omega))$$

of problem (4.11),$\cdots$,(4.16) in the reference configuration $\Omega_0 \times [0,T]$, with $\partial_t v(x,0) = v_1(x)$. Moreover if

H3

$$u_0 = u_{R0} + k_{III}(0)\ \eta\ S_N(x_1, x_2, 0), \quad k_{III}(0) \in \mathbb{R},\ u_{R0} \in H^2(\Omega_0)$$
$$u_1 \in H_D^1(\Omega_0),$$

then the solution u admits the following decomposition into a regular part and a singular one in the current configuration:

$$u(y,t) = u_R(y,t) + k_{III}(t,h,h')\eta(y)S_N(y_1 - h(t), y_2, t), \tag{4.21}$$

where the regular part u_R is in $C([0,T];H^2(\Omega_t))$, $S_N(y_1 - h(t), y_2, t)$ is given by (4.2) and the stress intensity factor $k_{III}(t,h(t),h'(t))$ belongs to $C([0,T])$.

Furthermore,

$$\tilde{H}^{\frac{1}{2}}(\Gamma_N \times [0,T]) = \{u \in H^{1/2}(\Gamma \times (0,T)) : supp\, u \subset \overline{\Gamma}_N \times (0,T)\},$$
$$H^1_D(\Omega_0) = \{u \in H^1(\Omega_0) : u = 0 \ \ on \ \ \Gamma_D\}.$$

Proof. The theorem is proved in [77]. In order to prove it, concepts from the perturbation theory of T. Kato [82] are used. The succesive change of unknown yields a unique strong solution u of (4.5) for appropiated data. □

Note that we have used the standard notation H^k for Sobolev spaces and C^j for spaces of continously differentiable functions.

In what follows we need explicitly the singular function S_N in the current configuration. We denote both expressions by S_N and write the arguments to mark the regions where we are.

Lemma 6. *The singular function (4.20) in the reference configuration reads in the current configuration*

$$S_N(y_1 - h, y_2, t) = \sqrt{\frac{1}{2\alpha_2(t)}}\sqrt{\sqrt{(R\cos\vartheta - h)^2 + \alpha_2^2(t)R^2\sin^2\vartheta} - (R\cos\vartheta - h)} \tag{4.22}$$

Here, (R,ϑ) are the current polar coordinates with respect to the crack tip $(h(t),0)$.

Proof. Let be $x_1 = r\cos\phi, x_2 = r\sin\phi, r = \sqrt{x_1^2 + x_2^2}$. We consider the (y_1,y_2)-coordinates in that region where the cut-off function $\eta \equiv 1$:

$$\begin{pmatrix} y_1 \\ y_2 \end{pmatrix} = \begin{pmatrix} R\cos\vartheta \\ R\sin\vartheta \end{pmatrix} = \begin{pmatrix} x_1 + h \\ x_2 \end{pmatrix} = \begin{pmatrix} r\cos\phi + h \\ r\sin\phi \end{pmatrix}. \tag{4.23}$$

Let us remark that $R = R(t), \vartheta = \vartheta(t), h = h(t)$. It follows

$$r\cos\phi = R\cos\vartheta - h, \quad r\sin\phi = R\sin\vartheta. \tag{4.24}$$

Inserting (4.24) into $S_N(x_1,x_2,t)$ given by (4.20) we get the relation (4.22). □

4.3 Energy in dynamic fracture

Now we will derive the equation of motion for the running crack tip (7.1) in a mathematically rigorous way.
To this aim we start with the energy balance law in the current configuration Ω_t:

$$\dot{D}(t) = -\dot{E}(t) + \hat{A}(t) - \dot{K}(t). \tag{4.25}$$

Definition 7. *If $u = u(y,t)$ is a solution of problem (4.5), then*

$$\dot{E}(t) = \frac{1}{2}\frac{d}{dt}\int_{\Omega_t} c_2^2 |\nabla_y u(t,y)|^2 \, dy \tag{4.26}$$

is the rate of the elastic energy;

$$\hat{A}(t) = \int_{\Omega_t} f u_t \, dy + \int_{\Gamma_N} q u_t \, ds, \tag{4.27}$$

denotes the external energy and

$$\dot{K}(t) = \frac{d}{dt}\int_{\Omega_t} \frac{1}{2}(u_t)^2 \, dy \tag{4.28}$$

is the rate of the kinetic energy.
D is the dissipative energy and it characterises the energy which is spent for irreversible processes.

Remark 9. *In our case the irreversible process is the breaking of bonds, the nucleation and growth of voids and micro-cracks in the process zone near the crack tip and the formation of a new macroscopic crack surface, Figure 4.2. In the simplest case the dissipative energy is considered in dependence on the fracture toughness and geometry properties. $\dot{D} = \frac{d}{dt}D$ is then the rate of dissipative energy.*

The calculation of the expression $-\dot{E}(t) + \hat{A}(t) - \dot{K}(t)$ will be done by partial integration, the use of the Gauss divergence theorem and the Reynolds transport (Theorem 1). Since the displacement field $u = u(y,t)$ develops crack singularities at the running crack tip we take a family of annular domains Ω_t^δ cutting out the running crack $h(t)$, see Fig.4.3, and consider then the limit for $\delta \to 0$.

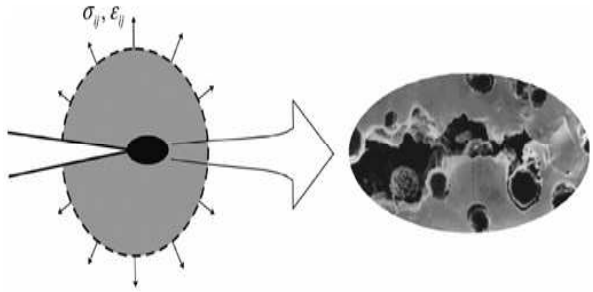

Figure 4.2: The process zone

4.3.1 The energy balance in the annular domain

Let $\Omega_t^\delta = \Omega_t \backslash \overline{M_t^\delta}$ be, where $\{M_t^\delta\}_\delta$ is a family of small neighborhoods of the running crack tip in the current configuration such that $\lim_{\delta\to 0} M_t^\delta = \{(h(t),0)\}$. We denote by C_t^δ the boundary curves of M_t^δ. We consider the energy flux in Ω_t^δ:

$$\dot{D^\delta}(t) = -\dot{E^\delta}(t) + \hat{A^\delta}(t) - \dot{K^\delta}(t), \tag{4.29}$$

where the energies are defined analogously to (4.25),$\cdots$,(4.28) as integrals on Ω_t^δ.
We remark that we use the notations $u_t = \dfrac{\partial u}{\partial t}$, $\dfrac{\partial}{\partial t} = \partial_t$.

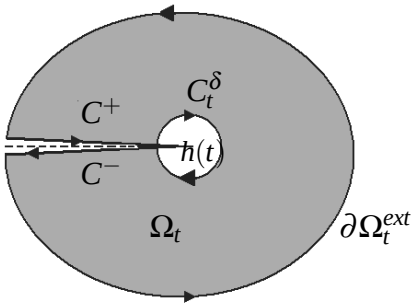

Figure 4.3: A family of annular domains cutting out the running crack $h(t)$.

Lemma 7. *The following identity holds:*

$$\hat{A^\delta}(t) - \dot{E^\delta}(t) - \dot{K^\delta}(t) = -\frac{1}{2}\int_{\Omega_t^\delta} div_y\left[\left(u_t^2 + c_2^2|\nabla u|^2\right)\frac{\partial y(t)}{\partial t}\right] dy - \int_{C_t^\delta} c_2^2 \frac{\partial u}{\partial n}\,\partial_t u\, ds_y, \tag{4.30}$$

where $y(t) = y(x,t) = F_t(x) = x + h(t)\,\theta(x)$ and the scalar field u solves the initial boundary value problem (4.5).

Proof. We start with the wave equation

$$\partial_t^2 u - c_2^2 \Delta u = f \quad \text{in} \quad \Omega_t \tag{4.31}$$

and consider the restriction u^δ of u to Ω_t^δ. We remark that u^δ is smooth enough in Ω_t^δ in order to apply partial integration and the formula of Gauss. Multiplication of (4.31) with $\partial_t u^\delta$ and integration on Ω_t^δ yield

$$\begin{aligned}
&\int_{\Omega_t^\delta} \left(\partial_t^2 u^\delta \, \partial_t u^\delta - c_2^2 \, \Delta u^\delta \, \partial_t u^\delta \right) dy = \\
&\int_{\Omega_t^\delta} \left(\frac{1}{2} \frac{\partial}{\partial t} \left(u_t^{\delta 2} \right) + c_2^2 \, \nabla u^\delta \, \nabla \partial_t u^\delta \right) dy - \int_{\partial \Omega_t^\delta} c_2^2 \, \frac{\partial u^\delta}{\partial n} \, \partial_t u^\delta \, ds_y = \int_{\Omega_t^\delta} f \, \partial_t \, u^\delta \, dy.
\end{aligned}$$

Therefore,

$$\begin{aligned}
&\int_{\Omega_t^\delta} \frac{1}{2} \left(\frac{\partial}{\partial t} \left(u_t^{\delta 2} \right) + c_2^2 \frac{\partial}{\partial t} \left(\nabla u^\delta \right)^2 \right) dy = \\
&\int_{\Omega_t^\delta} f \, \partial_t u^\delta \, dy + \int_{\partial \Omega_t^{ext}} c_2^2 \, \frac{\partial u^\delta}{\partial n} \, \partial_t u^\delta \, ds_y + \int_{C_t^\delta} c_2^2 \, \frac{\partial u^\delta}{\partial n} \, \partial_t u^\delta \, ds_y.
\end{aligned} \tag{4.32}$$

From the Reynolds transport theorem it follows with (4.32) (here we set $u^\delta = u$ in Ω_t^δ):

$$\begin{aligned}
&\dot{E^\delta}(t) + \dot{K}^\delta(t) = \frac{d}{dt} \frac{1}{2} \int_{\Omega_t^\delta} \left[(\partial_t u)^2 + c_2^2 |\nabla u|^2 \right] dy \\
&= \frac{1}{2} \int_{\Omega_t^\delta} \left[\frac{\partial}{\partial t} (\partial_t u)^2 + \frac{\partial}{\partial t} c_2^2 |\nabla u|^2 \right] dy + \frac{1}{2} \int_{\Omega_t^\delta} \operatorname{div} \left[\left((\partial_t u)^2 + c_2^2 |\nabla u|^2 \right) \frac{\partial y}{\partial t} \right] dy \\
&= \int_{\Omega_t^\delta} f \, \partial_t u \, dy + \int_{\Gamma_N} q \, \partial_t u \, ds_y + \int_{C_t^\delta} c_2^2 \, \frac{\partial u}{\partial n} \, \partial_t u \, ds_y + \\
&+ \frac{1}{2} \int_{\Omega_t^\delta} \operatorname{div} \left[\left((\partial_t u)^2 + c_2^2 |\nabla u|^2 \right) \frac{\partial y}{\partial t} \right] dy \\
&= \hat{A^\delta}(t) + \frac{1}{2} \int_{\Omega_t^\delta} \operatorname{div} \left[\left((\partial_t u)^2 + c_2^2 \, |\nabla u|^2 \right) \frac{\partial y}{\partial t} \right] dy + \int_{C_t^\delta} c_2^2 \, \frac{\partial u}{\partial n} \, \partial_t u \, ds_y
\end{aligned}$$

which is (4.30). □

Remark 10. *The family of smooth neighborhoods of $(h(t),0)$, $\{M_t^\delta\}$, in the current configuration is chosen in such a way that their images $\{F_t^{-1}\left(M_t^\delta\right)\}_\delta$ are circles B_δ with radius δ around the crack tip $\{(0,0)\}$ in the reference configuration.*

4.3.2 The limit procedure $\delta \to 0$

We calculate the limit for $\delta \to 0$ of the right hand side of (4.30) transforming both integrals to the reference domain $\Omega_0^\delta = \Omega_0 \backslash \overline{B_\delta}$.

Lemma 8. *For the right hand side of (4.30) holds:*

$$\begin{aligned}
&\lim_{\delta\to 0}\{-\frac{1}{2}\int_{\Omega_t^\delta} div_y\left[\left(u_t^2+c_2^2\,|\nabla u|^2\right)\frac{\partial y(t)}{\partial t}\right]\,dy\}+\lim_{\delta\to 0}\{-\int_{C_t^\delta} c_2^2\,\frac{\partial u}{\partial n}\,\partial_t u\,ds_y\}\\
&=h'(t)\,k_{III}^2(t,h,h')\,c_2^2\,\frac{\pi}{4}\,\frac{(\alpha_2-1)}{\alpha_2}+h'(t)\,k_{III}^2\left(t,h,h'\right)\,c_2^2\,\frac{\pi}{4}\,\frac{1}{\alpha_2}\\
&=h'(t)\,k_{III}^2(t,h,h')\,c_2^2\,\frac{\pi}{4}.
\end{aligned}\tag{4.33}$$

Proof. We start with the integral

$$\begin{aligned}
I_1^\delta&=-\frac{1}{2}\int_{\Omega_t^\delta}\mathrm{div}_y\left(\left(u_t^2+c_2^2|\nabla u|^2\right)\frac{\partial y(t)}{\partial t}\right)dy\\
&=-\frac{1}{2}\int_{\partial\Omega_t^\delta} n_y\cdot\left(u_t^2+c_2^2|\nabla u|^2\right)\,\frac{\partial y(t)}{\partial t}\,ds_y.
\end{aligned}\tag{4.34}$$

We transform the boundary integral (4.34) to the boundary of the reference configuration $\partial\Omega_0^\delta$. We recall that

$$y=\begin{pmatrix}x_1\\x_2\end{pmatrix}+h(t)\begin{pmatrix}\eta(x)\\0\end{pmatrix},$$

where η is a cut-off function with support in a neighborhood of the crack tip $\{(0,0)\}$. After some elementary calculations, see [77], we get

$$\begin{aligned}
I_1^\delta=&-\frac{1}{2}\int_{\partial\Omega^\delta} n_{x_1}\left(\partial_t v-\frac{h'\eta\partial_1 v}{1+h\partial_1\eta}\right)^2 h'(t)\,\eta\,ds_x+\\
&-\frac{1}{2}\int_{\partial\Omega^\delta} n_{x_1}\left(\frac{c_2^2}{(1+h\partial_1\eta)^2}\left((\partial_1 v)^2+(-\partial_1 v h\partial_2\eta+\partial_2 v(1+h\partial_1\eta))^2\right)\right)h'(t)\eta ds_x.
\end{aligned}$$

Note that η vanishes on $\partial\Omega_\delta^{ext}$ and that the first component $n_{x_1}=n_1$ of the normal vector vanishes on the crack $\sigma_0^\pm$. Therefore, we have

$$\begin{aligned}
&I_1=\lim_{\delta\to 0} I_1^\delta=\lim_{\delta\to 0}-\frac{1}{2}\int_{\partial B_\delta} n_1\left([\partial_t v-\frac{h'\eta\partial_1 v}{1+h\partial_1\eta}]^2 h'(t)\,\eta\right)ds_x+\\
&\lim_{\delta\to 0}-\frac{1}{2}\int_{\partial B_\delta} n_1\left(\frac{c_2^2}{(1+h\partial_1\eta)^2}\left((\partial_1 v)^2+(-\partial_1 v h\partial_2\eta+\partial_2 v(1+h\partial_1\eta))^2\right)\right)h'(t)\eta ds_x.
\end{aligned}$$

We assume that δ is so small that $\eta\equiv 1$ on $\overline{B_\delta}$. Furthermore, we use the asymptotic expansion of v on ∂B_δ:

$$v(x,t)=v_R(x,t)+k_{III}\left(t,h,h'\right)S_N(x_1,x_2,t)=v_R+\widehat{v}_S,\tag{4.35}$$

where S_N is given by theorem 8, namely

$$S_N(x_1,x_2,t)=\sqrt{\frac{r}{2\alpha_2(t)}}\sqrt{\sqrt{\cos^2\varphi+\alpha_2(t)^2\sin^2\varphi}-\cos\varphi}=\sqrt{\frac{r}{2\alpha_2(t)}}v_s.$$

Due to the fact that the limit value of the integrals on expressions of v_R vanishes, we get the simplified relation:

$$I_1 = \lim_{\delta\to 0} -\frac{1}{2}\, h'(t)\ \delta \int_{-\pi}^{\pi} \left[n_1 \left(\partial_t \widehat{v}_S - h'\partial_1 \widehat{v}_S\right)^2 + n_1 c_2^2 \left(\partial_1 \widehat{v}_S^2 + \partial_2 \widehat{v}_S^2\right)\right] ds.$$

Since $n_1 = -\cos\phi$ it follows

$$I_1 = \lim_{\delta\to 0} h'(t)\ \delta \int_{0}^{\pi} \left[\cos\phi\ \left(\partial_t \widehat{v}_S - h'\partial_1 \widehat{v}_S\right)^2 + c_2^2 \cos\phi\ \left(\partial_1 \widehat{v}_S^2 + \partial_2 \widehat{v}_S^2\right)\right] ds. \tag{4.36}$$

The singular function S_N behaves with respect to δ as follows:

$$S_N \sim \delta^{\frac{1}{2}}, \quad \partial_t S_N \sim \delta^{\frac{1}{2}}, \quad \partial_1 S_N \sim \delta^{-\frac{1}{2}}, \quad \partial_2 S_N \sim \delta^{-\frac{1}{2}}.$$

It follows from (4.36)

$$\begin{aligned} I_1 &= \lim_{\delta\to 0} h'(t)\ k_{III}^2(t,h,h')\ \delta \int_0^{\pi} \cos\phi \left[\left(h'(t)^2 + c_2^2\right) \left(\partial_1 S_N\right)^2 + c_2^2 \left(\partial_2 S_N\right)^2 \right] d\phi \\ &= c_2^2 \lim_{\delta\to 0} h'(t)\ k_{III}^2(t,h,h')\ c_2^2\ \delta \int_0^{\pi} \cos\phi \left[\left(2-\alpha_2(t)^2\right) \left(\partial_1 S_N\right)^2 + \left(\partial_2 S_N\right)^2 \right] d\phi. \end{aligned} \tag{4.37}$$

Since

$$\begin{aligned} \left(\partial_1 S_N\right)^2 &= \left[\frac{\partial S_N}{\partial r}\cos\phi - \frac{1}{r}\frac{\partial S_N}{\partial \phi}\sin\phi \right]^2 = \frac{1}{2\alpha_2 r}\left[\frac{1}{2} v_s \cos\phi - \frac{\partial v_s}{\partial \phi}\sin\phi \right]^2 \\ \left(\partial_2 S_N\right)^2 &= \left[\frac{\partial S_N}{\partial r}\sin\phi + \frac{1}{r}\frac{\partial S_N}{\partial \phi}\cos\phi \right]^2 = \frac{1}{2\alpha_2 r}\left[\frac{1}{2} v_s \sin\phi + \frac{\partial v_s}{\partial \phi}\cos\phi \right]^2 \end{aligned} \tag{4.38}$$

we have

$$\begin{aligned} &\lim_{\delta\to 0} \delta \int_0^{\pi} \cos\phi \left[\left(2-\alpha_2^2(t)\right) \left(\partial_1 S_N\right)^2 + \left(\partial_2 S_N\right)^2 \right] d\phi \\ &= \frac{1}{2\alpha_2} \int_0^{\pi} \left[\frac{1}{4} v_s^2 \left(1-\alpha_2^2\right)\cos^3\phi + \frac{1}{4} v_s^2 \cos\phi + \left(\frac{\partial v_s}{\partial \phi}\right)^2 \left(\alpha_2^2 - 1\right)\cos^3\phi \right] + \\ &+ \frac{1}{2\alpha_2} \int_0^{\pi} \left[\left(2-\alpha_2^2\right) \left(\frac{\partial v_s}{\partial \phi}\right)^2 \cos\phi + \left(\alpha_2^2 - 1\right)\cos^2\phi \sin\phi\, v_s \frac{\partial v_s}{\partial \phi} \right] d\phi. \end{aligned}$$

Furthermore, we easily check that

$$\begin{aligned} J &= \int_0^{\pi} \cos^2\phi\ \sin\phi\ v_s\ \frac{\partial v_s}{\partial \phi}\, d\phi \\ &= -\int_0^{\pi} \left[-2\ \cos\phi\ \sin^2\phi\ v_s + \cos^3\phi\ v_s + \cos^2\phi\ \sin\phi\ \frac{\partial v_s}{\partial \phi} \right] v_s\, d\phi \\ &= \int_0^{\pi} \left(2\ \cos\phi \left(1-\cos^2\phi\right) v_s^2 - \cos^3\ \phi v_s^2 \right) - J, \end{aligned}$$

or equivalently

$$J = \int_0^\pi \left(\cos\phi \; v_s^2 - \frac{3}{2}\cos^3\phi \; v_s^2 \right) \, d\phi .$$

The expressions of v_s^2 and of $\left(\frac{\partial v_s}{\partial \phi}\right)^2$ read:

$$\begin{aligned}
(v_s)^2 &= \sqrt{\cos^2\phi + \alpha_2^2(t)\sin^2\phi} - \cos\phi = \text{even part} - \cos\phi, \\
\left(\frac{\partial v_s}{\partial \phi}\right)^2 &= \frac{1}{4\left(\cos^2\phi + \alpha_2^2(t)\sin^2\phi\right)} \left[\sqrt{\cos^2\phi + \alpha_2^2(t)\sin^2\phi} \left(\left(\alpha_2^2(t) - 1\right)\cos^2\phi + 1 \right) \right] \\
&\quad + \frac{1}{4}\cos\phi \left(1 + \frac{\alpha_2^2(t) - 1}{\cos^2\phi + \alpha_2^2(t)\sin^2\phi} \right) \\
&= \text{even part} + \frac{1}{4}\cos\phi \left(1 + \frac{\alpha_2^2(t) - 1}{\cos^2\phi + \alpha_2^2(t)\sin^2\phi} \right).
\end{aligned} \tag{4.39}$$

Both terms consist of a even and an odd part with respect to $\frac{\pi}{2}$ and the odd parts contribute to the integral I_1 only.
Inserting these expressions into (4.37) and taking the limit for $\delta \to 0$, we get

$$I_1 = h'(t)\, k_{III}^2(t,h,h')\, c_2^2 \, \frac{\pi}{4} \, \frac{(-1 + \alpha_2(t))}{\alpha_2(t)}$$

Here we have used that

$$\begin{aligned}
\int_0^\pi \frac{\cos^2\phi}{\cos^2\phi + \alpha_2^2(t)\sin^2\phi} d\phi &= \pi \, \frac{1}{1 + \alpha_2(t)}, \\
\int_0^\pi \frac{\cos^4\phi}{\cos^2\phi + \alpha_2^2(t)\sin^2\phi} \, d\phi &= \frac{\pi}{2} \, \frac{1 + 2\alpha_2(t)}{(1 + \alpha_2(t))^2}.
\end{aligned}$$

Now, we consider the second integral of (4.33)

$$I_2^\delta = -\int_{C_t^\delta} c_2^2 \, \frac{\partial u}{\partial n} \, \partial_t u \, ds_y .$$

We transform it to the reference configuration. Since

$$\begin{aligned}
\frac{\partial u}{\partial n_y} &= \nabla_y u \cdot n_y = (\nabla F_t)^{-T} \nabla_x v \cdot \frac{(\nabla F_t)^{-T} n_x}{|(\nabla F_t)^{-T} n_x|}, \\
\partial_t u &= \partial_t v - h'\theta \cdot (\nabla F_t)^{-T} \nabla_x v
\end{aligned}$$

and δ is so small that, $\eta \equiv 1$ on $\overline{B_\delta}$ it follows that

$$I_2^\delta = -c_2^2 \int_{\partial B^\delta} \nabla_x v \cdot \frac{n_x}{|n_x|} \left(\partial_t v - h' \partial_1 v \right) \mathrm{d}s_x \tag{4.40}$$

Since $n_x = -\begin{pmatrix}\cos\phi\\ \sin\phi\end{pmatrix}$, we get from (4.40)

$$I_2 = \lim_{\delta\to 0} I_2^\delta = \lim_{\delta\to 0} c_2^2\,\delta \int_{\partial B^\delta} (\partial_1 v\,\cos\phi + \partial_2 v\,\sin\phi)\,(\partial_t v - h'\,\partial_1 v)\,d\phi. \tag{4.41}$$

As before we split, $v = v_R + \widehat{v}_S$, compare (4.35), and repeat the arguments for the behaviour of the terms v_R and $\widehat{v}_S$ with respect to δ. Furthermore, we use the formulas (4.38).
Then (4.41) can be written as:

$$\begin{aligned} I_2 =& -\frac{c_2^2 h'(t) k_{III}^2(t,h,h')}{\alpha_2(t)} \int_0^\pi \left(\frac{1}{2} v_s \cos\phi - \frac{\partial v_s}{\partial\phi}\sin\phi\right)\left\{\left(\frac{1}{2} v_s\cos\phi - \frac{\partial v_S}{\partial\phi}\sin\phi\right)\cos\phi + \right.\\ &\left. + \left(\frac{1}{2}\,v_s\,\sin\phi + \frac{\partial v_s}{\partial\phi}\,\cos\phi\right)\,\sin\phi\right\} d\phi\\ =& -\frac{c_2^2 h'(t)\,k_{III}^2(t,h,h')}{\alpha_2(t)} \int_0^\pi \left(\frac{1}{2}\,v_s\cos\phi - \frac{\partial v_s}{\partial\phi}\,\sin\phi\right)\frac{1}{2}\,v_s\,d\phi. \end{aligned} \tag{4.42}$$

Since

$$\begin{aligned} (v_s)^2 &= \sqrt{\cos^2\phi + \alpha_2^2(t)\,\sin^2\phi} - \cos\phi,\\ \frac{d}{d\phi}(v_s)^2 &= 2\,v_s\,\frac{\partial v_s}{\partial\phi} = \frac{(\alpha_2^2(t)-1)\cos\phi\,\sin\phi}{\sqrt{\cos^2\phi + \alpha_2^2(t)\sin^2\phi}} + \sin\phi, \end{aligned}$$

it follows that

$$\frac{\partial v_s}{\partial\phi}\,v_s\,\sin\phi = \frac{(\alpha_2^2(t)-1)\cos\phi\,\sin^2\phi}{2\sqrt{\cos^2\phi + \alpha_2^2(t)\,\sin^2\phi}} + \frac{\sin^2\phi}{2}.$$

Again, only the odd terms with respect to $\dfrac{\pi}{2}$ contribute to the integral (4.42). Therefore,

$$\begin{aligned} I_2 &= -\frac{c_2^2\,h'(t)\,k_{III}^2(t,h,h')}{\alpha_2(t)} \int_0^\pi \left(-\frac{1}{4}\,\cos^2\phi - \frac{1}{2}\,\frac{\sin^2\phi}{2}\right) d\phi\\ &= \frac{c_2^2\,h'(t)\,k_{III}^2(t,h,h')}{\alpha_2(t)}\left(\frac{\pi}{8} + \frac{\pi}{8}\right)\\ &= \frac{c_2^2\,h'(t)\,k_{III}^2(t,h,h')}{\alpha_2(t)}\,\frac{\pi}{4} \end{aligned}$$

and the relation (4.33) follows. □

Remark 11. *Lemmata 7 and 8 yield*

$$\lim_{\delta\to 0}\left(-\dot{E}^\delta(t) + \hat{A}^\delta(t) - \dot{K}^\delta(t)\right) = \lim_{\delta\to 0}\dot{D}^\delta(t) = c_2^2\,h'(t)\,k_{III}^2(t,h,h')\,\frac{\pi}{4}.$$

From the other side the energy flux in Ω_t, namely $-\dot{E}(t)+\hat{A}(t)-\dot{K}(t)$, is well defined, at least in the distribution sense (compare Theorem 8). We conclude that

$$\begin{aligned}-\dot{E}(t)+\hat{A}(t)-\dot{K}(t) &= \lim_{\delta\to 0}\left(-\dot{E^{\delta}}(t)+\hat{A^{\delta}}(t)-\dot{K^{\delta}}(t)\right)\\ &= \dot{D}(t) = c_2^2\, h'(t)\, k_{III}^2(t,h,h')\,\frac{\pi}{4}.\end{aligned}$$

4.3.3 Extraction of stress intensity factor for the out-of-plane case

In this subsection we derive some expressions from the analytical results, which are necessary for the numerical computations, (chapter 7). In particular, we prepare the numerical extraction of the dynamical stress intensity factors $k_{III}(t,h,h')$ at time t from the current displacement field decomposition (4.21).

Theorem 9. *Under the assumptions H1-H3 of theorem 8, i.e., the solution $u(y,t)$ of (4.5) can be decomposed as*

$$u(y,t) = u_R(y,t) + k_{III}(t,h,h')\eta(y)S_N(y_1-h(t),y_2,t)$$

where S_N is given by (4.22). Then the stress intensity factor $k_{III}(t,h,h')$ at time t can be found for $R(t)-h(t)>0$ as the limit

$$\lim_{R(t)-h(t)\to 0}\frac{2}{\sqrt{\alpha_2(t)}}\sqrt{(R(t)-h(t))}\frac{\partial u}{\partial y_2}|_{\vartheta=0} = k_{III}(t,h,h'). \tag{4.43}$$

Proof. Since u can be represented as

$$u(y,t) = u_R(y,t) + k_{III}(t,h,h')\eta(y)\sqrt{\frac{1}{2\,\alpha_2\,(t)}}\sqrt{\sqrt{(y_1-h)^2+\alpha_2^2\,(t)y_2^2}-(y_1-h)}$$

we calculate $\frac{\partial u}{\partial y_2}|_{\vartheta=0}$ in a vicinity of the crack tip where $\eta\equiv 1$. We get there

$$\frac{\partial u}{\partial y_2}|_{\vartheta=0} = \frac{\partial u_R}{\partial y_2}|_{\vartheta=0} + k_{III}(t,h,h')\frac{\sqrt{\alpha}_2}{2\sqrt{R-h}} \tag{4.44}$$

Here we have used the fact, compare (4.39), that

$$\frac{\partial S_N}{\partial y_2}|_{\vartheta=0} = \frac{\partial S_N}{\partial x_2}|_{\phi=0} = \frac{1}{\sqrt{2\alpha_2 r}}\frac{\partial v_s}{\partial \phi}|_{\phi=0} = \frac{\sqrt{\alpha}_2}{2\sqrt{r}}.$$

Furthermore, we have $r=R-h$ on the y_1-axis assuming $R>h$. Multiplying (4.44) by $\frac{2\sqrt{R-h}}{\sqrt{\alpha}_2}$ and using the fact that the derivative of the regular part $\frac{\partial u_R}{\partial y_2}$ behaves in a vicinity of the crack tip asymptotically as $\sqrt{R-h}$ the assertion (4.43) follows. □

In books on crack mechanics, [7], [8], [17], one can find the following formula for the dynamic energy release rate for $h'(t) \neq 0$:

$$\frac{\dot{D}(t)}{h'(t)} = \frac{1}{2\mu} \frac{K_{III}^2(t,h,h')}{\alpha_2(t)}, \tag{4.45}$$

where μ is the Lamé coefficient, $\alpha_2(t) = \sqrt{1 - \frac{h'^2(t)}{c_2^2}}$ and $K_{III}(t,h,h')$ represents the stress intensity factor.
Then one finds:

$$\begin{aligned} c_2^2\, k_{III}^2(t,h,h')\, \frac{\pi}{4} &= \frac{1}{2\,\mu}\, \frac{K_{III}^2(t,h,h')}{\alpha_2(t)}, \\ k_{III}^2(t,h,h') &= \frac{2}{\pi}\, \frac{1}{\mu\, c_2^2}\, \frac{K_{III}^2(t,h,h')}{\alpha_2(t)}, \\ k_{III}(t,h,h') &= \sqrt{\frac{2}{\pi\,\mu}}\, \frac{1}{c_2}\, \frac{K_{III}(t,h,h')}{\sqrt{\alpha_2(t)}}. \end{aligned} \tag{4.46}$$

Indeed, the singular function w_{sing} in the z-coordinates, is here written as:

$$w_{sing} = k_{III}(t,h,h')\, \sqrt{r_z}\, \sin\frac{\phi_z}{2} = k_{III}(t,h,h')\, S_N(z,t), \tag{4.47}$$

whereas

$$\widehat{w}_{sing} = \frac{K_{III}(t,h,h')}{\alpha_2(t)\,\mu} \sqrt{\frac{2}{\pi}}\, \sqrt{r_z}\, \sin\frac{\phi_z}{2} = K_{III}(t,h,h')\, \widehat{S}_N(z,t) \tag{4.48}$$

is used in [7], [8], [17], in order to get formula (4.45).

4.3.4 Equation of motion for the running crack tip

In the dynamic fracture problem, the wave propagation couples an energy balance law, which contains the energy release rate due to the crack growth. Now we need to impose a fracture criterion along with the governing field equations and the initial-boundary conditions to describe the crack tip propagation.
It is known, [8], [5], [92], [25], [85], that in certain cases, namely small-scale yielding, rate independent behaviour under monotonically increasing stress intensity factor, it can be assumed that the dynamic energy release rate is controled by some crack growth resistance, denoted by $\Gamma(h,h')$, i.e.:

$$G(h,h') = \Gamma(h,h'). \tag{4.49}$$

The empirical function $\Gamma(h,h')$ for a particular material is determined under given environmental conditions by experiments, [8].
The function $G(h,h')$ is given by

$$G(h,h') = \frac{\dot{D}(t)}{h'(t)}$$

with $h'(t) \neq 0$, and denotes the dynamic energy release rate, and $\dot{D}(t) = \dot{D}(t,h,h')$ is the rate of the dissipative energy.

Assuming that (4.49) holds, i.e. that the dynamic energy release rate $G(h,h')$ can be expressed by the experimentally determined fracture toughness $\Gamma(h,h')$, we use the ordinary differential equation

$$\Gamma(h,h') = k_{III}^2(t,h,h')\, c_2^2\, \frac{\pi}{4} = G(h,h') \tag{4.50}$$

as fracture criterion.

Remark 12. *The quasistatic case, $h'(t) = 0$, therefore $h(t) = 0$, is included in (4.50).*
Moreover, the equation (4.50) in combination with the initial boundary value problem for the wave equation, will be used for the computation of the motion $h(t)$ of the running crack tip, see chapter 7.
Inserting (4.46) into (4.50) we get:

$$\Gamma(h,h') = \frac{1}{2\mu}\frac{K_{III}^2(t,h,h')}{\alpha_2(t)} = G(h,h'),$$

which is the relation in the books e.g. [7], [8], [17].

Finally, the complete formulation for the dynamic coupled problem in mode III reads:

$$\left.\begin{aligned}
&\partial_t^2 u - c_2^2 \Delta u = f \text{ in } Q := \cup_{t=0}^T \Omega_t,\\
&c_2^2 \partial_n u = 0 \text{ on } \cup_{t=0}^T \sigma_t,\\
&c_2^2 \partial_n u = q \text{ on } \Sigma_N := \Gamma_N \times (0,T),\\
&u = 0 \text{ on } \Sigma_D := \Gamma_D \times (0,T),\\
&u(0) = u_0,\ \partial_t u(0) = u_1 \text{ in } \Omega_0,
\end{aligned}\right\} \quad \text{AND} \quad \begin{cases} \Gamma(h,h') = k_{III}^2(t,h,h')\, c_2^2\, \frac{\pi}{4}, \\ h(0) = 0,\ k_{III}(0,h,h') = k_{III}(0). \end{cases}$$

$$u_0 = u_{R0} + k_{III}(0,h_0,h_0')\ \eta\ S_N(y_1,y_2,0),\ u_{R0} \in H^2(\Omega_0), k_{III}(0) \in \mathbb{R},$$
$$S_N(y_1,y_2,0) = \sqrt{\tfrac{1}{2\alpha_2(0)}}\sqrt{\sqrt{(R_0\cos\vartheta_0 - h(0))^2 + \alpha_2^2(0) R_0^2 \sin^2\vartheta_0} - (R_0\cos\vartheta_0 - h(0))},$$
$$\partial_t u(0) = u_1 \in H_D^1(\Omega_0).$$

$$k_{III}(t,h,h') = \lim_{R(t)-h(t)\to 0} \frac{2}{\sqrt{\alpha_2(t)}}\sqrt{(R(t)-h(t))}\frac{\partial u}{\partial y_2}|_{\vartheta=0}.$$

CHAPTER 5

Dynamic Fracture near the crack tip: The in-plane case.

5.1 The in-plane case

In this chapter, local singularity results for the displacement and stress fields of Navier Lamé problem in cracked domains are formulated and proved. The main results of this chapter are presented in Theorem 13 and Theorem 14.

It is natural to try the problem of the interaction of elastic waves in elastic solids with cracks, in the in-plane state, also. The anti-plane shear crack studied in Chapter 4 is an important problem in fracture mechanics and from a mathematical point of view, it has been easier to deal with. For the convenience of the reader we repeat the relevant ideas applied in Chapter 4, although the theoretical treatment for the in-plane state is more complicated and distinct crack velocities occur here. As before the analytical study is considered in a very thin finite body, i.e. we consider a membrane. To our knowledge, in the literature infinite bodies are mostly considered.

The phenomenon of crack-wave interaction is of importance in the exploitation of new and profitable energy resources. Of particular significance are geothermal heat exploitation, oil-shale research and surface and underground mining operations. One of hte interest of getting knowledge of crack-wave interaction is that one may optimize fragmentation and consequently reduce the cost of mining operation. Rock formations found at quarry sites and oil-shale sites form stacks of layered rock with bedding planes and joint are present. Upon detonation of an explosive, the wave pattern generated in layered media is extremely complicated, and running cracks interact with incident and reflected-elastic-wave systems.

Depending on the nature of the wave, the crack may accelerate or decelerate during the interaction phase.

Both wave propagation and fracture play a major role in rock mechanics and mining engineering. Although a large number of scientific results deal with the study of either wave propagation and/or crack propagation, relatively few contributions study the dynamic interaction between elastic waves and cracks.

The present work endeavours to determine the analytical solution in the vicinity of a moving crack located in an isotropic medium. The crack is assumed to be excited by the normally incident plane wave. In particular, we are concerned with the variation of stress intensity factors and displacement fields near the crack tip and we have developed a mathematical model for understanding the process of crack growth, assuming that the crack lies in the interior and it propagates straight along the horizontal axis.

An objective of dynamic fracture mechanics is to predict the motion of a crack tip under given conditions of loading and geometrical configuration. In order to establish an equation of motion for the position $h(t)$ of the crack tip, also here the criterion (4.49) is employed, for a given crack growth resistance $\Gamma(h,h')$ for a given material. We use for the crack growth resistance the same notation as before, but we understand, its expression is different from the one in the out-of plane state. Again this criterion is the requirement that the rate of energy near the tip of a crack is equal to a specific fracture resistance.

With the dynamic stress intensity factor available for non-uniform crack grow, the dynamic energy release rate $G(t,h)$ is also available. Then, if the criterion (4.49) is assumed to hold as discussed in Chapter 4, then an equation of motion for the crack tip is obtained.

In the particular Mode I fracture case ($k_{II}(t,h,h')=0$), the following expression for the crack growth resistance $\Gamma(h,h')$, [93], [8], [55], is valid:

$$\Gamma(h,h') = \left(1-\frac{h'(t)}{c_R}\right)\frac{(1-\nu^2)}{E}k_I(t,h,0)^2, \tag{5.1}$$

where c_R denotes the Rayleigh wave speed, ν and E are the elastic constants, $k_I = k_I(t,h,h')$ the stress intensity factor refers to mode I, more details see Table 5.1.

Remark 13. *The effects of loading and geometry are included in $k_I(t,h,0)$, which denotes the stress intensity factor for the mode I that would have resulted from the applied loading if the crack tip had always been at its instantaneous position represented by $h=h(t)$.*

The dynamic fracture resistance $\Gamma(h,h')$ is an empirical relation and cannot be determined from continuum mechanics theory and is also difficult to be determined by experiments.

Assuming that (4.49) is valid, the particular problem for a pure mode I crack propagation reads:
Find $h = h(t)$ such that the ordinary differential equation holds:

$$\Gamma(h,h') = \left(1 - \frac{h'(t)}{c_R}\right) \frac{(1-\nu^2)}{E} k_I(t,h,0)^2 = G(h,h'), \quad h(0) = 0. \tag{5.2}$$

$G(h,h')$ is derived in chapter 6, on the basis of an overall energy rate balance.

5.2 Problem setting

The propagation of cracks by the influence of elastic waves can be considered as a moving boundary value problem. Recall that we model the elastic structure by the Navier Lamé problem (2.31) in the domain Q:

$$(c_1^2 - c_2^2)\nabla(\nabla \cdot \vec{u}) + c_2^2 \nabla^2 \vec{u} - \ddot{\vec{u}} = \vec{f}, \quad \text{in } Q = \bigcup_{t=0}^{T} \Omega_t,$$

with corresponding boundary Neumann and Dirichlet conditions defined on

$$\Gamma = \overline{\Gamma}_D \cup \overline{\Gamma}_N, \quad \Gamma_D \cap \Gamma_N = \emptyset.$$

The general Neumann boundary conditions defined on $\Gamma_N \times (0,T)$ has the form:

$$\sigma n = \text{prescribed function}, \tag{5.3}$$

They can be written:

$$\lambda \frac{\partial u_k}{\partial y_k} n_i + \mu \left(\frac{\partial u_i}{\partial y_j} + \frac{\partial u_j}{\partial y_i}\right) n_j = \text{prescribed function}, \quad \text{on } \Gamma_N \times (0,T), \tag{5.4}$$

or in terms of displacements,

$$\lambda\, (\mathrm{div}\vec{u})\, n + 2\mu\, \partial_n \vec{u} + \mu\, \vec{n} \times \mathrm{curl}\, \vec{u} = \text{prescribed function}, \quad \text{on } \Gamma_N \times (0,T). \tag{5.5}$$

We assume $u_3 = 0$ and $f_3 = 0$. In vector notation, the boundary-value problem for Navier Lamé equation with prescribed function on the boundary takes the form, [18]:

$$\left.\begin{aligned}
&(\lambda+\mu)\nabla(\nabla\cdot\vec{u}) + \mu\nabla^2\vec{u} + \rho\vec{f} = \rho\vec{u}_{tt} \quad \text{in } Q := \bigcup_{t=0}^{T} \Omega_t,\\
&\lambda\, (\mathrm{div}\vec{u})\, n + 2\mu\, \partial_n\vec{u} + \mu\, \vec{n} \times \mathrm{curl}\, \vec{u} = 0 \quad \text{on } \bigcup_{t=0}^{T} \sigma_t,\\
&\lambda\, (\mathrm{div}\vec{u})\, n + 2\mu\, \partial_n\vec{u} + \mu\, \vec{n} \times \mathrm{curl}\, \vec{u} = \rho\vec{q} \quad \text{on } \Sigma_N := \Gamma_N \times (0,T),\\
&\vec{u}(t,y) = 0 \quad \text{on } \Sigma_D := \Gamma_D \times (0,T),\\
&\vec{u}(0,y) = \vec{u}_0,\ \partial_t\vec{u}(0,y) = \vec{u}_1 \quad \text{in } \Omega_0.
\end{aligned}\right\} \tag{5.6}$$

Here we denote $\nabla\vec{u}$:

$$\nabla\vec{u} = (\mathrm{D}\vec{u})^\top = \begin{pmatrix} \partial_{y_1}u_1 & \partial_{y_2}u_1 \\ \partial_{y_1}u_2 & \partial_{y_2}u_2 \end{pmatrix}^\top.$$

The homogeneous equation $\lambda\,(\mathrm{div}\vec{u})\,n + 2\,\mu\,\partial_n\vec{u} + \mu\,\vec{n}\times\mathrm{curl}\,\vec{u} = 0$, on $\bigcup_{t=0}^{T}\sigma_t$ means that the crack faces are free from stress.

The mathematical analysis is done as before distinguishing between the current configuration; noncylindrical domain; and the reference domain; cylindrical one. We remenber that Ω_0 with a pre-crack represents the reference domain, whereas $\Omega_t = \Omega\setminus\sigma_t$ represents the family of current configurations.

Let us denote as before the space variables y_1, y_2 in the current plane section of Q and x_1, x_2 the space variables in the plane section of the reference domain.

The anisotropic Lamé operator to the problem (5.6) in the reference configuration is given by Definition 9.

We map the Navier-Lamé equations (2.31) from the current configuration to the reference one near the crack tip, where the singularities occur.

Lemma 9. *The change of variables (4.6) along with the assumptions (4.7) $\cdots$ (4.9) leads to the following transformed Navier-Lamé problem near the crack tip in the reference configuration Ω_0:*

$$\partial_t^2\vec{v} - h''\,(\nabla_x\vec{v})^\top - 2\,(h')\,(\nabla_x\partial_t\vec{v})^\top + (h')^2\left(\nabla_x\,(\nabla_x\vec{v})^\top\right)^\top - c_2^2\nabla^2\vec{v} - (c_1^2 - c_2^2)\nabla\,(\nabla\cdot\vec{v}) = \vec{\hat{f}}. \tag{5.7}$$

Proof. We transform (2.31) by (4.6) to the cylindrical domain $\Omega_0\times(0,T)$ by setting:

$$\left.\begin{aligned} \vec{u}(y,t) = \vec{u}(F_t(x),t) = (u_1(F_t(x),t), u_2(F_t(x),t)) =: \vec{v}(x,t) = (v_1(x,t), v_2(x,t)), \\ \vec{f}(y,t) = \vec{f}(F_t(x),t) = (f_1(F_t(x),t), f_2(F_t(x),t)) =: \vec{\hat{f}}(x,t) = (\hat{f}_1(x,t), \hat{f}_2(x,t)). \end{aligned}\right\} \tag{5.8}$$

The derivatives are transformed for $x\in\Omega_0$, $y\in\Omega_t$:

$$\begin{aligned} \nabla_x\vec{v} = (D_x\vec{v})^\top &= \begin{pmatrix} \partial_{x_1}v_1 & \partial_{x_2}v_1 \\ \partial_{x_1}v_2 & \partial_{x_2}v_2 \end{pmatrix}^\top \\ &= \begin{pmatrix} \partial_{x_1}y_1 & \partial_{x_2}y_1 \\ \partial_{x_1}y_2 & \partial_{x_2}y_2 \end{pmatrix}^\top \begin{pmatrix} \partial_{y_1}u_1 & \partial_{y_2}u_1 \\ \partial_{y_1}u_2 & \partial_{y_2}u_2 \end{pmatrix}^\top \\ &= (D_xF_t)^\top\,(D_y\vec{u})^\top \\ &= (\nabla F_t)\,(\nabla_y\vec{u}). \end{aligned}$$

Therefore we get, with help of the Piola transformation [69]

$$\nabla_y \vec{u} = (\nabla_x F_t(\vec{x}))^{-1} \nabla_x \vec{v}, \tag{5.9}$$

$$\begin{aligned} \operatorname{div}(D_y \vec{u}) &= \Delta_y \vec{u} = \operatorname{div}_y (\nabla_y \vec{u})^\top \\ &= \frac{1}{\det \nabla_x (F_t(x))} \operatorname{div}_x \left[(\det \nabla_x F_t) (\nabla_x \vec{v})^\top (\nabla F_t)^{-\top} (\nabla F_t)^{-1} \right], \end{aligned} \tag{5.10}$$

$$\partial_t \vec{u} = \partial_t \vec{v} - h'(t) (\nabla_x \vec{v})^\top (\nabla F_t)^{-\top} \theta \tag{5.11}$$

$$\begin{aligned} \partial_t^2 \vec{u} = {} & \partial_t^2 \vec{v} - h'' (\nabla_x \vec{v})^\top (\nabla F_t)^{-\top} \theta + \left(h'\right)^2 (\nabla_x \vec{v})^\top (\nabla F_t)^{-\top} (\nabla \theta)^\top (\nabla F_t)^{-\top} \theta + \\ & - 2 \left(h'\right) (\nabla_x \partial_t \vec{v})^\top (\nabla F_t)^{-\top} \theta + \left(h'\right)^2 \left(\nabla_x \left[(\nabla_x \vec{v})^\top (\nabla F_t)^{-\top} \theta \right] \right)^\top (\nabla F_t)^{-\top} \theta, \end{aligned} \tag{5.12}$$

$$\nabla_y (\nabla_y \cdot \vec{u}) = \frac{1}{\det \nabla_x (F_t(x))} \left[(\nabla F_t)^{-1} \nabla_x (\nabla \cdot \vec{v}) \right] - \frac{h \nabla \cdot \vec{v}}{\left(\det \nabla_x (F_t(x))\right)^2} (\nabla F_t)^{-1} \nabla_x (\nabla_x \cdot \theta). \tag{5.13}$$

Finally, we consider the transformation (4.6) near the crack tip, where $\eta \equiv 1$, and the result follows. □

(5.7) without second-mixed derivatives, in space-time can be written:

$$\partial_t^2 \vec{v} + \mathcal{A}_p \vec{v}$$

where $\mathcal{A}_p$ is the principal part and contributes to the singular solution.

$$\begin{aligned} \mathcal{A}_p \vec{v} := {} & -c_2^2 \begin{pmatrix} \Delta v_1 \\ \Delta v2 \end{pmatrix} - (c_1^2 - c_2^2) \begin{pmatrix} \partial_1^2 v_1 + \partial_1 \partial_2 v_2 \\ \partial_2^2 v_2 + \partial_1 \partial_2 v_1 \end{pmatrix} + \left(h'\right)^2 \begin{pmatrix} \partial_1^2 v_1 \\ \partial_1^2 v_2 \end{pmatrix} \\ = {} & -(c_2^2 - h'^2) \begin{pmatrix} \partial_1^2 v_1 \\ \partial_1^2 v_2 \end{pmatrix} - c_2^2 \begin{pmatrix} \partial_2^2 v_1 \\ \partial_2^2 v_2 \end{pmatrix} - (c_1^2 - c_2^2) \begin{pmatrix} \partial_1^2 v_1 + \partial_1 \partial_2 v_2 \\ \partial_2^2 v_2 + \partial_1 \partial_2 v_1 \end{pmatrix} \\ = {} & -(c_2^2 - h'^2) \left[\begin{pmatrix} \partial_1^2 v_1 \\ \partial_1^2 v_2 \end{pmatrix} - \frac{1}{\alpha_2^2(t)} \begin{pmatrix} \partial_2^2 v_1 \\ \partial_2^2 v_2 \end{pmatrix} - \frac{(c_1^2 - c_2^2)}{c_2^2 \alpha_2^2(t)} \begin{pmatrix} \partial_1^2 v_1 + \partial_1 \partial_2 v_2 \\ \partial_2^2 v_2 + \partial_1 \partial_2 v_1 \end{pmatrix} \right] \end{aligned} \tag{5.14}$$

In (5.14) was used $c_2^2 \alpha_2^2(t) = c_2^2 - h'^2(t)$.

5.2.1 Ellipticity of the operator

Let us consider an general $p \times p$ matrix differential operator A, such that $A = \left(A_{jk}\right)$.
The elements A_{jk} have the orders $\operatorname{ord} A_{jk} \leq l_j + m_k$ and $\operatorname{ord} A_{jk} = 0$, if $l_j + m_k < 0$, where l_j and m_k are integers and $\sum_{j=1}^{p} (l_j + m_j) = 2q$, $q \in \mathbb{N}$.

Definition 8. *Ellipticity of A in the sense of Douglis-Nirenberg.*
Let be $a_0(y,\xi)$ the matrix consisting of the principal symbols of A_{jk}

$$a_{0,jk}(y,\xi) := \sum_{|\alpha|=l_j+m_k} a_\alpha^{jk}(y)\xi^\alpha.$$

A is elliptic in the sense of Douglis-Nirenberg on Ω, if

$$det\,(a_0(y,\xi)) \neq 0, \quad \forall y \in \Omega, \forall \xi \in \mathbb{R}^n \backslash \{0\}. \tag{5.15}$$

Definition 9. *The anisotropic Lamé operator in the reference domain.*
The anisotropic Lamé operator in the reference domain $\Omega_0 \in \mathbb{R}^2$ can be written as:

$$\mathcal{A}_p\vec{v} = \begin{pmatrix} c_2^2\Delta + (c_1^2-c_2^2)\partial_1^2 - h'(t)^2\partial_1^2 & (c_1^2-c_2^2)\partial_1\partial_2 \\ (c_1^2-c_2^2)\partial_1\partial_2 & c_2^2\Delta + (c_1^2-c_2^2)\partial_2^2 - h'(t)^2\partial_1^2 \end{pmatrix} \begin{pmatrix} v_1 \\ v_2 \end{pmatrix}. \tag{5.16}$$

Then the anisotropic Lamé equations in the reference domain $\Omega_0 \in \mathbb{R}^2$ are given by:

$$\mathcal{A}_p\vec{v} = \begin{pmatrix} -\hat{f}_1 \\ -\hat{f}_2 \end{pmatrix}. \tag{5.17}$$

Theorem 10. *The anisotropic Lamé operator $\mathcal{A}_p$ (5.16) is strongly elliptic in the sense of Douglis-Nirenberg if*

$$\left(c_1^2 - h'^2\right) > 0 \quad \textit{and} \quad \left(c_2^2 - h'^2\right) > 0. \tag{5.18}$$

Proof. The elements of $\mathcal{A}_p$ have the order 2 and $\sum_{j=1}^{2}(l_j+m_j) = 4 = 2q$.
The matrix $a_0(y,\xi)$ reads

$$a_0(y,\xi) = a_0(\xi) = \begin{pmatrix} (c_1^2-h'^2)\xi_1^2 + c_2^2\xi_2^2 & (c_1^2-c_2^2)\xi_1\xi_2 \\ (c_1^2-c_2^2)\xi_1\xi_2 & (c_2^2-h'^2)\xi_1^2 + c_1^2\xi_2^2 \end{pmatrix}.$$

We have then for $\left(c_1^2 - h'^2\right) > 0$ and $\left(c_2^2 - h'^2\right) > 0$,

$$\begin{aligned} \det(a_0(\xi)) &= \left[(c_1^2-h'^2)\xi_1^2 + c_2^2\xi_2^2\right]\left[(c_2^2-h'^2)\xi_1^2 + c_1^2\xi_2^2\right] - (c_1^2-c_2^2)^2\xi_1^2\xi_2^2 \\ &= (c_1^2-h'^2)(c_2^2-h'^2)\xi_1^4 + c_1^2c_2^2\xi_2^4 + \\ &+ \left[(c_1^2-h'^2)c_1^2 + (c_2^2-h'^2)c_2^2\right]\xi_1^2\xi_2^2 - (c_1^2-c_2^2)^2\xi_1^2\xi_2^2 \\ &= (c_1^2-h'^2)(c_2^2-h'^2)\xi_1^4 + c_1^2c_2^2\xi_2^4 + \left[-h'^2c_1^2 - h'^2c_2^2 + 2c_1^2c_2^2\right]\xi_1^2\xi_2^2 \\ &= \left(c_1c_2\xi_2^2 + \sqrt{c_1^2-h'^2}\sqrt{c_2^2-h'^2}\,\xi_1^2\right)^2 + \\ &+ \xi_1^2\xi_2^2\left[c_1^2(c_2^2-h'^2) + c_2^2(c_1^2-h'^2) - 2c_1c_2\sqrt{c_1^2-h'^2}\sqrt{c_2^2-h'^2}\right] \end{aligned}$$

The factor in brackets with $\xi_1^2\xi_2^2$ has the form

$$(a-b)^2 > 0$$

with $a := c_1\sqrt{c_2^2 - h'^2}$ and $b = c_2\sqrt{c_1^2 - h'^2}$.
Therefore, $\det(a_0(\xi)) \neq 0, \forall \xi \in \mathbb{R}^2 \backslash \{0\}$. □

We note that $\left(c_1^2 - h'^2\right) > 0 \Rightarrow \left(c_2^2 - h'^2\right) > 0$ because $c_1 > c_2$.

Theorem 11. *The operator $\mathcal{A}_p$ (5.16) is positive definite if (5.18) is satisfied.*

Proof. We write the system (5.17) in the following form:

$$c_{i1lk}\partial_i\partial_l v_k(x) = -\hat{f}_1 \tag{5.19}$$
$$c_{i2lk}\partial_i\partial_l v_k(x) = -\hat{f}_2 \tag{5.20}$$

where the Einstein summation convention is used.
The tensor $C = \left(c_{ijlk}\right)_{ijlk=1,2}$ of fourth order reads for the anisotropic Lamé operator (5.16):

$$\begin{aligned}
c_{1111} &= (c_1^2 - h'^2) \\
c_{1122} &= c_{2112} = \frac{(c_1^2 - c_2^2)}{2} \\
c_{2121} &= c_2^2 \\
c_{1212} &= (c_2^2 - h'^2) \\
c_{1221} &= c_{2211} = \frac{(c_1^2 - c_2^2)}{2} \\
c_{2222} &= c_1^2 \\
c_{ijlk} &= 0 \quad \text{for all remaining indices.}
\end{aligned}$$

i.e.

$$C = \begin{pmatrix} (c_1^2 - h'^2) & 0 & \frac{(c_1^2 - c_2^2)}{2} \\ 0 & (c_1^2 + c_2^2 - h'^2) & 0 \\ \frac{(c_1^2 - c_2^2)}{2} & 0 & c_1^2 \end{pmatrix}.$$

Note that $c_{ijlk} = c_{lkij}$.
The positive definiteness is given by the condition

$$c_{ijlk}\xi_{ij}\xi_{lk} \geq c\,\xi_{lk}^2, \qquad \xi_{lk} = \xi_{kl} \tag{5.21}$$

Therefore the quadratic form reads:

$$\begin{aligned}&(c_{1111}\,\xi_{11}\,\xi_{11}+c_{1122}\xi_{11}\,\xi_{22}+c_{2112}\xi_{21}\,\xi_{12}+c_{2121}\xi_{21}\,\xi_{21}+c_{1212}\xi_{12}\,\xi_{12}+\\&+c_{1221}\xi_{12}\,\xi_{21}++c_{2211}\xi_{22}\,\xi_{11}+c_{2222}\xi_{22}\,\xi_{22})=\\&(c_1^2-h'^2)\,\xi_{11}^2+(c_1^2-c_2^2)\,\xi_{11}\,\xi_{22}+(c_1^2-c_2^2)\,\xi_{21}\,\xi_{12}+c_2^2\,\xi_{21}^2+(c_2^2-h'^2)\,\xi_{12}^2+c_1^2\,\xi_{22}^2=q(\xi)\end{aligned} \tag{5.22}$$

We estimate (5.22),

$$q(\xi)=(c_1^2-h'^2)\,\xi_{11}^2+c_1^2\,\xi_{22}^2+(c_1^2-c_2^2)\,\xi_{11}\,\xi_{22}+(c_1^2+c_2^2-h'^2)\,\xi_{12}^2$$

From the Young's inequality [1], we get for every $\varepsilon > 0$

$$(c_1^2-c_2^2)\,\xi_{11}\,\xi_{22}\geq-\frac{1}{4\varepsilon}(c_1^2-c_2^2)\,\xi_{11}^2-\varepsilon(c_1^2-c_2^2)\,\xi_{22}^2.$$

Hence,

$$q(\xi)\geq(c_1^2-h'^2-\frac{1}{4\varepsilon}c_1^2+\frac{1}{4\varepsilon}c_2^2)\,\xi_{11}^2+(c_1^2-\varepsilon c_1^2+\varepsilon c_2^2)\,\xi_{22}^2+(c_1^2+c_2^2-h'^2)\,\xi_{12}^2$$

If (5.18) is satisfied, for $\varepsilon=\frac{1}{2}$ the following relations hold:

$$\begin{aligned}\left(c_1^2-h'^2-\frac{1}{4\varepsilon}c_1^2+\frac{1}{4\varepsilon}c_2^2\right)&=\left(1-\frac{1}{4\varepsilon}\right)(c_1^2-h'^2)+\frac{1}{4\varepsilon}(c_2^2-h'^2)\geq 0,\\(c_1^2-\varepsilon c_1^2+\varepsilon c_2^2)&=(1-\varepsilon)\,c_1^2+\varepsilon\,c_2^2\geq 0,\\(c_1^2+c_2^2-h'^2)&\geq 0.\end{aligned}$$

Therefore

$$q(\xi)\geq c(\xi_{11}^2+\xi_{22}^2+\xi_{12}^2).$$

□

Now the following mathematical problem occurs: in comparison with Chapter 4 the method based on ideas [4], [77] is not directly applicable transforming the space variables x_1, x_2, to space variables z_1, z_2, where the singular solution of the Navier-Lamé (2.31) could be obtained in easier way. We remark that this step is just a mathematical tool to start from an isotropic Laplacian near the crack tip and to use the known singular fields.

Typically, one tries to decompose the general Navier-Lamé equation into separate equations that relate to longitudinal waves (P-waves) and transversal waves (S-waves) propagation, Fig 5.1. Some features of both sorts of waves in 3D, are summarized in Table 5.1.

[1] $\forall\varepsilon>0:\ ab\geq-\frac{1}{4\varepsilon}a^2-\varepsilon b^2$

WAVES	Description
Longitudinal waves	They are faster than transversal waves and thus arrive first. The particles oscillate in the direction of spreading of the wave. They are also called compressional waves.
Transversal waves	The particles oscillate in the direction perpendicular to the spreading direction. Shear waves - they do not propagate through solids.
Rayleigh waves	They are surface waves. Their amplitude diminishes with the depth. They have large amplitudes.

Table 5.1: Longitudinal, transversal and Rayleigh 3D waves

Remark 14. *A variety of terminology exists for the two wave-types. Dilatational waves are also called irrotational or primary (P) waves. The rotational waves are also called equivoluminal, distortional, and secondary (S) waves.*
The P and S wave designations have arisen in seismology. Other respective designations frequently used are longitudinal and shear waves.
The existence of Rayleigh surface waves, also called surface waves, was first theoretically demostrated by the English scientist, Lord Rayleigh, in 1885. Rayleigh surface waves are of special importance in seismology, acoustic, geophysics and electronics applications.

5.2.2 Helmholtz decomposition

A more elegant and mathematical way to see that solutions of the wave equation are in fact P and S-waves is by realizing that any vector field can be represented by a combination of the gradient of some scalar potential and the curl of a vector potential. This decomposition is known as *Helmholtz's Theorem* and the potentials are often referred as *Helmholtz Potentials*. The basic idea of Helmholtz decomposition is to separate the coupled terms of longitudinal and shear waves. (Hermann Ludwig Ferdinand von Helmholtz, 1821-1894).

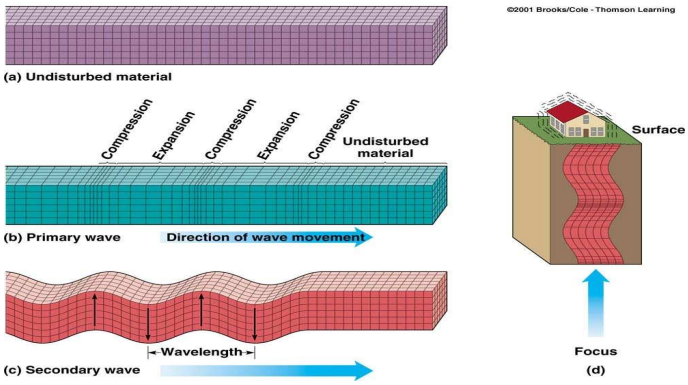

Figure 5.1: Elastic waves-Body Waves

We should note that several of these potentials have been proposed. Some of the most useful are those developed by Lamé, [24], Papkovich, [68] and Neuber [33].

Theorem 12. *Let $\vec{u}$ be a solution of the Navier-Lamé equation (2.29).*

$$\rho\vec{u}_{tt} - (\mu\Delta\vec{u} + (\lambda+\mu)\, grad(div\,\vec{u})) = \rho\,\vec{f}.$$

Then there exists a scalar and a vector potentials ϕ and $\vec{\psi}$ such that:

$$\vec{u} = \nabla\phi + \nabla\times\vec{\psi}, \quad \nabla\cdot\vec{\psi} = 0. \tag{5.23}$$

Also there exist a scalar function f and vector function $\vec{B}$, such that the density vector of the volume forces $\vec{f}(y,t) = \vec{f} = (f_1, f_2, f_3)^T$ can be decomposed as:

$$\vec{f} = \nabla\mathsf{f} + \nabla\times\vec{B}, \quad \nabla\cdot\vec{B} = 0, \tag{5.24}$$

Proof. For details see ([48], pp.52-53). □

Remark 15. *The condition $\nabla\cdot\vec{\psi} = 0$ provides the necessary additional condition to determine uniquely the three components of $\vec{u}$ from the components of ϕ and $\vec{\psi}$.*

Lemma 10. *Assume that Theorem 12 holds. Then the Navier-Lamé equation (2.29) can be decomposed into two scalar elastic wave equations.*

Proof. Substituting (5.23) and (5.24) in (2.29) gives:

$$\rho\left(\nabla\ddot{\phi} + \nabla\times\ddot{\vec{\psi}}\right) - \left(\mu\nabla^2(\nabla\phi + \nabla\times\vec{\psi}) + (\lambda+\mu)\nabla\nabla\cdot(\nabla\phi + \nabla\times\vec{\psi})\right) = \rho\left(\nabla\mathsf{f} + \nabla\times\vec{B}\right)$$

These regroup to

$$\nabla\left[\rho\ddot{\phi} - (\lambda+2\mu)\nabla^2\phi + \rho\mathsf{f}\right] + \nabla\times\left(\rho\ddot{\vec{\psi}} - \mu\nabla^2\vec{\psi} + \rho\vec{B}\right) = 0. \tag{5.25}$$

We have used in (5.25) that:
$\nabla\cdot\nabla\phi = \nabla^2\phi$, $\nabla^2(\nabla\phi) = \nabla\left(\nabla^2\phi\right)$ and the fact that $\nabla\cdot\nabla\times\vec{\psi} = 0$.
The equation (5.25) will be satisfied if each bracketed term vanishes, thus giving

$$(\lambda+2\mu)\nabla^2\phi + \rho \mathsf{f} = \rho\ddot{\phi}, \tag{5.26}$$

and

$$\mu\nabla^2\vec{\psi} + \rho\vec{B} = \rho\ddot{\vec{\psi}}. \tag{5.27}$$

□

If the body forces are zero, we have $\mathsf{f} = 0$ and $\vec{B} = 0$ and the equations (5.26) and (5.27) give the scalar and vector wave equations and they contain the velocities c_1 and c_2, (2.32) and (2.33) respectively.

$$\nabla^2\phi = \frac{1}{c_1^2}\ddot{\phi}, \tag{5.28}$$

$$\nabla^2\vec{\psi} = \frac{1}{c_2^2}\ddot{\vec{\psi}}. \tag{5.29}$$

The significance of the Helmholtz resolution of $\vec{u}$ becomes even more apparent at this stage, (5.28) and (5.29). The scalar potential is seen to be associated with the dilatational part, and the vector potential is associated with the rotational part. Volumetric waves, involving no rotation, propagates with velocity c_1 while rotational waves, involving no volume changes, propagate with velocity c_2.
There are two distinct wave speeds, c_1 and c_2, and we may anticipate that the general solutions of (2.29) will include both types of waves, [34].

A complete representation of the solution $\vec{u}$ of the wave equation was obtained by means of the Helmholtz additive decomposition of the displacement vector into the gradient of a scalar field ϕ and the curl of a divergence vector field $\vec{\psi}$,

$$\left.\begin{aligned} u_1 &= \partial_1\phi + \partial_2\psi_3 - \partial_3\psi_2, \\ u_2 &= \partial_2\phi + \partial_3\psi_2 - \partial_1\psi_3, \\ u_3 &= \partial_3\phi + \partial_1\psi_2 - \partial_2\psi_1. \end{aligned}\right\} \tag{5.30}$$

The relation (5.30) is called the Lamé representation of the displacement vector and it will be used extensively in this chapter.
For the particular case $u_1 = u_1(y_1,y_2)$, $u_2 = u_2(y_1,y_2)$, and $u_3 = 0$, (5.30) is reduced to:

$$\left.\begin{aligned} u_1 &= \partial_1\phi + \partial_2\psi, \\ u_2 &= \partial_2\phi - \partial_1\psi. \end{aligned}\right\} \tag{5.31}$$

with $\psi_3 := \psi$.

Remark 16. *The existence of P and S-waves was first demonstrated by Simon Denis Poisson (1781-1840) in 1828. He also showed that P and S-type waves are, in fact, the only solutions of the wave equations for an unbounded medium, so that (5.30) provides the complete solution for the displacement in an elastic, isotropic and homogeneous medium. If the medium is not unbounded, for instance a half-space with perhaps some stratification, there are more solutions to the general equation of motions. Those solutions are the surface (Rayleigh and Love) waves, Fig. 5.2.*

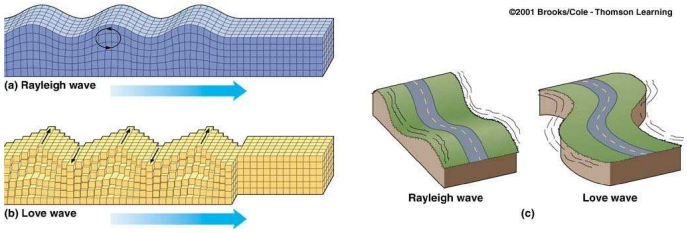

Figure 5.2: Elastic waves-Surface Waves

If (5.31) are substituted into (2.8), i.e. it is considered the particular case $u_1 = u_1(y_1, y_2)$, $u_2 = u_2(y_1, y_2)$, and $u_3 = 0$, then the components of stress in terms of the displacement potentials are

$$\left.\begin{aligned} \sigma_{11} &= \mu\left[\left(\frac{c_1}{c_2}\right)^2 \nabla^2\phi - 2\partial_2^2\phi + 2\partial_{12}^2\psi\right], \\ \sigma_{22} &= \mu\left[\left(\frac{c_1}{c_2}\right)^2 \nabla^2\phi - 2\partial_1^2\phi - 2\partial_{12}^2\psi\right], \\ \sigma_{12} &= \mu\left[2\,\partial_{12}^2\phi + \partial_2^2\psi - \partial_1^2\psi\right]. \end{aligned}\right\} \tag{5.32}$$

Lemma 11. *The components of the stress field can be expressed by the displacement potentials as:*

$$\left.\begin{aligned} \sigma_{11} &= \mu\left\{\left(\frac{1-\alpha_2(t)^2}{1-\alpha_1(t)^2}\right)\frac{\partial^2\phi}{\partial y_1^2} + \left(\frac{2\alpha_1(t)^2 - \alpha_2(t)^2 - 1}{1-\alpha_1(t)^2}\right)\frac{\partial^2\phi}{\partial y_2^2} + 2\frac{\partial^2\psi}{\partial y_1 \partial y_2}\right\}, \\ \sigma_{22} &= \mu\left\{\left(\frac{2\alpha_1(t)^2 - \alpha_2(t)^2 - 1}{1-\alpha_1(t)^2}\right)\frac{\partial^2\phi}{\partial y_1^2} + \left(\frac{1-\alpha_2(t)^2}{1-\alpha_1(t)^2}\right)\frac{\partial^2\phi}{\partial y_2^2} - 2\frac{\partial^2\psi}{\partial y_1 \partial y_2}\right\}, \\ \sigma_{12} &= \mu\left\{2\frac{\partial^2\phi}{\partial y_1 \partial y_2} + \frac{\partial^2\psi}{\partial y_2^2} - \frac{\partial^2\psi}{\partial y_1^2}\right\}. \end{aligned}\right\} \tag{5.33}$$

Proof. We used (5.32) and the relation $\dfrac{c_1^2}{c_2^2} = \dfrac{1-\alpha_2(t)^2}{1-\alpha_1(t)^2}$. □

Due to the general Neumann condition (5.3)

$$\sigma\vec{n} = \text{prescribed function}$$

applied now on the crack faces, where $\vec{n}$ is the unit normal vector of crack faces, i.e., $\vec{n} = \begin{pmatrix} 0 \\ \pm 1 \end{pmatrix}$, the traction free condition on the crack faces implies that

$$\sigma_{22}(y_1, 0, t) = \sigma_{12}(y_1, 0, t) = 0, \quad \text{on } \sigma_t, \tag{5.34}$$

or, in terms of the displacement potentials on σ_t,

$$\left.\begin{aligned} \sigma_{22}|_{y_2=0} &= \mu \left\{ \left(\frac{2\alpha_1^2 - \alpha_2^2 - 1}{1-\alpha_1^2} \right) \frac{\partial^2 \phi}{\partial y_1^2} + \left(\frac{1-\alpha_2^2}{1-\alpha_1^2} \right) \frac{\partial^2 \phi}{\partial y_2^2} - 2\frac{\partial^2 \psi}{\partial y_1 \partial y_2} \right\} |_{y_2=0} = 0, \\ \sigma_{12}|_{y_2=0} &= \mu \left\{ 2\frac{\partial^2 \phi}{\partial y_1 \partial y_2} + \frac{\partial^2 \psi}{\partial y_2^2} - \frac{\partial^2 \psi}{\partial y_1^2} \right\} |_{y_2=0} = 0. \end{aligned} \right\} \tag{5.35}$$

5.2.3 The wave equations for potentials in a 2D cracked domain.

As we have seen (5.23), the displacement field $\vec{u}$ can be generated by the potential fields ϕ and ψ, and they satisfy uncoupled scalar wave equations, (5.28) and (5.29) respectively.
We will describe the crack singularities in the neighborhood of the crack tip for the problem (5.6) following the ideas for Mode III in chapter 4. But now we must introduce two different $\vec{z}$ coordinate systems.
Let us start with the dilatational displacement potential ϕ assuming that no body forces occur. We seek solutions $\phi = \phi(y,t)$ for the wave equation (5.36) in the cracked domain,

$$\ddot{\phi} - c_1^2 \nabla^2 \phi = 0 \text{ in } Q := \bigcup_{t=0}^{T} \Omega_t. \tag{5.36}$$

The distortional displacement potential ψ, (for plane strain), is the solution of (5.37),

$$\ddot{\psi} - c_2^2 \nabla^2 \psi = 0 \text{ in } Q := \bigcup_{t=0}^{T} \Omega_t, \tag{5.37}$$

Suppose that the coordinates (x_1, x_2) in Ω_0 are introduced with its origin at the moving crack tip and oriented with the x_1-axis aligned with the direction of the crack growth.
Mathematically speaking, we fix the x_1-axis of coordinates tangent to the pre-crack σ_0 oriented in the direction of the growing crack. The displacement potentials can then be viewed as functions of the position in the moving coordinate system. The transformed functions are denoted by Φ and Ψ, that means

$$\phi(y,t) = \phi(F_t(x),t) := \Phi(x,t), \tag{5.38}$$

$$\psi(y,t) = \psi(F_t(x),t) := \Psi(x,t). \tag{5.39}$$

Lemma 12. *[4]*
The change of variables (4.6) leads to the following transformed problems in the reference configuration Ω_0 for the corresponding transformed dilatational and distortional displacement potentials:

$$\Phi_{tt} + \mathcal{A}_0^{(1)}(t)\,\Phi + \mathcal{A}_1^{(1)}(t)\,\Phi + \mathcal{B}^{(1)}(t)\,\Phi_t = 0 \text{ in } \Omega_0 \times (0,T). \tag{5.40}$$

The shear wave potential $\Psi(x,t)$ satisfies the same equation with c_2 instead of c_1.

$$\Psi_{tt} + \mathcal{A}_0^{(2)}(t)\,\Psi + \mathcal{A}_1^{(2)}(t)\,\Psi + \mathcal{B}^{(2)}(t)\,\Psi_t = 0 \text{ in } \Omega_0 \times (0,T). \tag{5.41}$$

where

$$\begin{aligned}
\mathcal{A}_0^{(1)}(t)\Phi &= -\frac{c_1^2}{\det(\nabla F_t)}\, div\left(\det(\nabla F_t)(\nabla F_t)^{-1}(\nabla F_t)^{-\top}\nabla\Phi\right)\\
&\quad + h'^2\ \theta\cdot(\nabla F_t)^{-\top}\nabla\left(\theta\cdot(\nabla F_t)^{-\top}\nabla\Phi\right),\\
\mathcal{A}_1^{(1)}(t)\Phi &= h'^2\ \theta\cdot(\nabla F_t)^{-\top}(\nabla\theta)^{\top}(\nabla F_t)^{-\top}\nabla\Phi\\
&\quad - h''\ \theta\cdot(\nabla F_t)^{-\top}\nabla\Phi,\\
\mathcal{B}^{(1)}(t)\Phi_t &= -2h'\ \theta\cdot(\nabla F_t)^{-\top}\nabla\Phi_t.
\end{aligned}$$

and

$$\begin{aligned}
\mathcal{A}_0^{(2)}(t)\Psi &= -\frac{c_2^2}{\det(\nabla F_t)}\, div\left(\det(\nabla F_t)(\nabla F_t)^{-1}(\nabla F_t)^{-\top}\nabla\Psi\right)\\
&\quad + h'^2\ \theta\cdot(\nabla F_t)^{-\top}\nabla\left(\theta\cdot(\nabla F_t)^{-\top}\nabla\Psi\right),\\
\mathcal{A}_1^{(2)}(t)\Psi &= h'^2\ \theta\cdot(\nabla F_t)^{-\top}(\nabla\theta)^{\top}(\nabla F_t)^{-\top}\nabla\Psi\\
&\quad - h''\ \theta\cdot(\nabla F_t)^{-\top}\nabla\Psi,\\
\mathcal{B}^{(2)}(t)\Psi_t &= -2h'\ \theta\cdot(\nabla F_t)^{-\top}\nabla\Psi_t.
\end{aligned}$$

The ellipticity of $\mathcal{A}_0^{(1)}(t)$ and $\mathcal{A}_0^{(2)}(t)$ is guaranteed, that means (5.18) should hold.
The conditions (5.18) are now:

$$\exists\,\gamma_0^{(1)} > 0 : \alpha_1(t)^2 = 1 - \left(\frac{h'(t)}{c_1}\right)^2 \geq \left(\gamma_0^{(1)}\right)^2 > 0, \forall\, t \in (0,T), \tag{5.42}$$

$$\exists\,\gamma_0^{(2)} > 0 : \alpha_2(t)^2 = 1 - \left(\frac{h'(t)}{c_2}\right)^2 \geq \left(\gamma_0^{(2)}\right)^2 > 0, \forall\, t \in (0,T). \tag{5.43}$$

The assumptions (5.42) and (5.43) lead to $h'(t) < c_1$ and $h'(t) < c_2$, which is reasonable, since it is known for non-bounded configurations that, the limit speed of a mode I and II crack is c_R the Rayleigh wave speed, see Table 5.1 and (5.101). Therefore $h'(t) < c_R$.

Without loss of generality we assume that the unit circle $\overline{B}(0,1)$ is included inside Ω_0 and that the set

$$\mathcal{W} := \{x \in \Omega_0 |\, \eta(x) = 1\}$$

contains $\overline{B}(0,1)$ (otherwise we only have to rescale the domain Ω_0).
(5.40) is reduced on $\mathcal{W}$ to:

$$-\frac{\partial^2\Phi}{\partial x_1^2}\left(1-\frac{h'^2}{c_1^2}\right) - \frac{\partial^2\Phi}{\partial x_2^2} - \frac{h''}{c_1^2}\frac{\partial\Phi}{\partial x_1} - 2\frac{h'}{c_1^2}\frac{\partial^2\Phi}{\partial x_1\,\partial t} + \frac{1}{c_1^2}\frac{\partial^2\Phi}{\partial t^2} = 0. \tag{5.44}$$

And the shear wave potential Ψ, (5.41), satisfies the same equation with c_1 replaced by c_2:

$$-\frac{\partial^2\Psi}{\partial x_1^2}\left(1-\frac{h'^2}{c_2^2}\right)-\frac{\partial^2\Psi}{\partial x_2^2}-\frac{h''}{c_2^2}\frac{\partial\Psi}{\partial x_1}-2\frac{h'}{c_2^2}\frac{\partial^2\Psi}{\partial x_1\,\partial t}+\frac{1}{c_2^2}\frac{\partial^2\Psi}{\partial t^2}=0. \tag{5.45}$$

Note that, for the special case of *steady-state* crack growth, $h''=0$ and $\frac{\partial\Phi}{\partial t}=0$, the equations (5.44) and (5.45) reduce to Laplace's equation in the coordinates $x_1,\alpha_1 x_2$ and $x_1,\alpha_2 x_2$, respectively.

The operators $\mathcal{A}_0^{(1)}$ and $\mathcal{A}_0^{(2)}$ are reduced on the set $\mathcal{W}$ to:

$$\mathcal{A}_0^{(1)}=-c_1^2\left(\alpha_1(t)^2\,\partial_1^2+\partial_2^2\right), \tag{5.46}$$
$$\mathcal{A}_0^{(2)}=-c_2^2\left(\alpha_2(t)^2\,\partial_1^2+\partial_2^2\right), \tag{5.47}$$

where

$$\alpha_1(t)^2=1-\left(\frac{h'(t)}{c_1}\right)^2,\quad \alpha_2(t)^2=1-\left(\frac{h'(t)}{c_2}\right)^2.$$

In order to get an isotropic Laplacian for Φ and Ψ and to derive an asymptotic expansion for the stress components as $r=\sqrt{x_1^2+x_2^2}\to 0$, the space coordinates $\vec{x}=(x_1,x_2)\in\Omega_0$ are transformed into appropiate $\vec{z}=(z_1,z_2)$ coordinates for each problem.
This means that two different changes of variables

$$z_1^{(1)}=x_1,\ z_2^{(1)}=\alpha_1(t)\,x_2, \tag{5.48}$$
$$z_1^{(2)}=x_1,\ z_2^{(2)}=\alpha_2(t)\,x_2, \tag{5.49}$$

would transform the operators $\mathcal{A}_0^{(1)}$ and $\mathcal{A}_0^{(2)}$ on $\mathcal{W}$ into the Laplace operator, respectively. But these changes of variables are global and they transform Ω_0 into a time-dependent domain. We handle the wave equations (5.40) and (5.41) similar to [77] and reference therein. That means we should have to make a change of variables near the crack tip and modify it far away, but the new changes of variables are performed different from the one in [77].

$$z_1^{(1)}=x_1,\quad z_2^{(1)}=\rho^{(1)}(x,t)=d^{(1)}(x,t)\,x_2,\quad \text{for } \Phi, \tag{5.50}$$
$$z_1^{(2)}=x_1,\quad z_2^{(2)}=\rho^{(2)}(x,t)=d^{(2)}(x,t)\,x_2,\quad \text{for } \Psi. \tag{5.51}$$

Here we set

$$d^{(1)}(x,t)=\alpha_1(t)\kappa(x)+(1-\kappa(x))\,\gamma_0^{(1)}, \tag{5.52}$$
$$d^{(2)}(x,t)=\alpha_2(t)\kappa(x)+(1-\kappa(x))\,\gamma_0^{(2)}. \tag{5.53}$$

and κ is a cut-off function defined by

$$\kappa(x) = \begin{cases} 1, & \text{if } |x| \leq \frac{1}{2}, \\ (\widehat{r}-1)^2(2\widehat{r}+1)\,(2|x|-1), & \text{if } \frac{1}{2} \leq |x| \leq 1, \\ 0, & \text{if } |x| \geq 1. \end{cases}$$

For any fixed x_1, t, both $\rho^{(1)}(x_1,\cdot,t)$ and $\rho^{(2)}(x_1,\cdot,t)$ are strictly increasing, because $\alpha_1(t) \geq \gamma_0^{(1)}$ and $\alpha_2(t) \geq \gamma_0^{(2)}$, and hence both are injective. Therefore (5.50) and (5.51) induce two diffeomorphisms for any fixed t, between Ω_0 and $\widehat{\Omega}_0^{(1)}$ and $\widehat{\Omega}_0^{(2)}$, respectively

$$\begin{aligned} &\mathcal{G}_t^{(1)} : \Omega_0 \to \widehat{\Omega}_0^{(1)}, && \widehat{\Omega}_0^{(1)} := \left\{ (x_1, \gamma_0^{(1)} x_2) |\, (x_1,x_2) \in \Omega_0 \right\}, \\ &\mathcal{G}_t^{(2)} : \Omega_0 \to \widehat{\Omega}_0^{(2)}, && \widehat{\Omega}_0^{(2)} := \left\{ (x_1, \gamma_0^{(2)} x_2) |\, (x_1,x_2) \in \Omega_0 \right\}. \end{aligned}$$

Also the pre-crack σ_0 is transformed by $\mathcal{G}_t^{(1)}$ and $\mathcal{G}_t^{(2)}$ into $\widehat{\sigma}^{(1)}$ of $\widehat{\Omega}^{(1)}$ and $\widehat{\sigma}_0^{(2)}$ of $\widehat{\Omega}_0^{(2)}$, respectively

$$\begin{aligned} \widehat{\sigma}_0^{(1)} &= \left\{ (x_1, \gamma_0^{(1)} x_2) |\, (x_1,x_2) \in \sigma_0 \right\}, \\ \widehat{\sigma}_0^{(2)} &= \left\{ (x_1, \gamma_0^{(2)} x_2) |\, (x_1,x_2) \in \sigma_0 \right\}. \end{aligned}$$

They are also straight in a neighborhood of $(0,0)$.
Let us note that neither $\widehat{\sigma}^{(i)}$ nor $\widehat{\sigma}_0^{(i)}$, $i = 1,2$ depend on t.
We set now:

$$w^{(1)}(z^{(1)},t) := \Phi(x,t), \quad \text{for } \Phi, \tag{5.54}$$

$$w^{(2)}(z^{(2)},t) := \Psi(x,t), \quad \text{for } \Psi. \tag{5.55}$$

The general singular functions of Φ and Ψ (without explicit boundary conditions) are induced by the crack tip. They are determined by the principal parts of (5.40) and (5.41). We perform the transformations (5.54) and (5.55) on $\mathcal{W}$.

Lemma 13. *The equations (5.44) and (5.45) read in the space variables $z^{(i)}, i = 1,2$, as follows:*

$$-\alpha_1(t)^2 \left(\frac{\partial^2 w^{(1)}}{\partial (z_1^{(1)})^2} + \frac{\partial^2 w^{(1)}}{\partial (z_2^{(1)})^2} \right) - \frac{h''}{c_1^2} \frac{\partial w^{(1)}}{\partial z_1^{(1)}} - 2\frac{h'}{c_1^2} \frac{\partial^2 w^{(1)}}{\partial z_1^{(1)} \partial t} + \frac{1}{c_1^2} \frac{\partial^2 w^{(1)}}{\partial t^2} = 0$$

$$\text{in } \widehat{\Omega}_0^{(1)}, \tag{5.56}$$

$$-\alpha_2(t)^2 \left(\frac{\partial^2 w^{(2)}}{\partial (z_1^{(2)})^2} + \frac{\partial^2 w^{(2)}}{\partial (z_2^{(2)})^2} \right) - \frac{h''}{c_2^2} \frac{\partial w^{(2)}}{\partial z_1^{(2)}} - 2\frac{h'}{c_2^2} \frac{\partial^2 w^{(2)}}{\partial z_1^{(2)} \partial t} + \frac{1}{c_2^2} \frac{\partial^2 w^{(2)}}{\partial t^2} = 0$$

$$\text{in } \widehat{\Omega}_0^{(2)}. \tag{5.57}$$

The corresponding asymptotic expansions near the crack tip can be obtained from those of the Laplacian.

$$\nabla^2 w^{(i)} = \frac{\partial^2 w^{(i)}}{\partial (z_1^{(i)})^2} + \frac{\partial^2 w^{(i)}}{\partial (z_2^{(i)})^2}, \quad i = 1,2. \tag{5.58}$$

The main results of this chapter are presented in theorem 13, where the singular representation of the solutions of Navier Lamé problems on cracked domains is described. As a first application of the obtained results, we improve singularity theorem 14 which describes the behaviour of the displacement and stress fields for the Navier Lamé equations near the crack tip. Furthermore the singularity results of this chapter are essential for chapter 6, where we study the energy related to this problem, which is concerned with generalized Griffith fracture criterion for elastic materials.

Fix $t > 0$ and $\vec{v} = \vec{v}(\vec{x}, t)$

$$X_t = \left\{ \vec{v} \in [H^2(\Omega_0)]^2 : \sigma(\vec{v})\, n = \text{prescribed function on } \Gamma_N \cup \sigma_0, \vec{v} = 0 \text{ on } \Gamma_D \right\} \oplus \text{span}\{S_N^I\} \oplus \text{span}\{S_N^{II}\}$$

in a neighborhood of the crack tip $h = h(t)$, where S_N^1 and S_N^2 are the singular functions defined in the reference configuration:

$$S_N^1(x,t) = \begin{pmatrix} \frac{(1+\alpha_2(t)^2)\, r^{\frac{1}{2}}}{\mu D} \left[\sqrt{\frac{\sqrt{\cos^2\varphi + \alpha_1(t)^2 \sin^2\varphi} + \cos\varphi}{\cos^2\varphi + \alpha_1(t)^2 \sin^2\varphi}} - \frac{2\,\alpha_1(t)\,\alpha_2(t)}{(1+\alpha_2(t)^2)} \sqrt{\frac{\sqrt{\cos^2\varphi + \alpha_2(t)^2 \sin^2\varphi} + \cos\varphi}{\cos^2\varphi + \alpha_2(t)^2 \sin^2\varphi}} \right] \\ \frac{(1+\alpha_2(t)^2)\, r^{\frac{1}{2}}}{\mu D} \left[-\alpha_1(t) \sqrt{\frac{\sqrt{\cos^2\varphi + \alpha_1(t)^2 \sin^2\varphi} - \cos\varphi}{\cos^2\varphi + \alpha_1(t)^2 \sin^2\varphi}} + \frac{2\,\alpha_1(t)}{(1+\alpha_2(t)^2)} \sqrt{\frac{\sqrt{\cos^2\varphi + \alpha_2(t)^2 \sin^2\varphi} - \cos\varphi}{\cos^2\varphi + \alpha_2(t)^2 \sin^2\varphi}} \right] \end{pmatrix},$$

and

$$S_N^2(x,t) = \begin{pmatrix} -\frac{\alpha_2(t)\, r^{\frac{1}{2}}}{\mu D} \left[2 \sqrt{\frac{\sqrt{\cos^2\varphi + \alpha_1(t)^2 \sin^2\varphi} - \cos\varphi}{\cos^2\varphi + \alpha_1(t)^2 \sin^2\varphi}} - (1+\alpha_2(t)^2) \sqrt{\frac{\sqrt{\cos^2\varphi + \alpha_2(t)^2 \sin^2\varphi} - \cos\varphi}{\cos^2\varphi + \alpha_2(t)^2 \sin^2\varphi}} \right] \\ -\frac{r^{\frac{1}{2}}}{\mu D} \left[2\,\alpha_1(t)\,\alpha_2(t) \sqrt{\frac{\sqrt{\cos^2\varphi + \alpha_1(t)^2 \sin^2\varphi} + \cos\varphi}{\cos^2\varphi + \alpha_1(t)^2 \sin^2\varphi}} - (1+\alpha_2(t)^2) \sqrt{\frac{\sqrt{\cos^2\varphi + \alpha_2(t)^2 \sin^2\varphi} + \cos\varphi}{\cos^2\varphi + \alpha_2(t)^2 \sin^2\varphi}} \right]. \end{pmatrix}.$$

with $D := 4\,\alpha_1(t)\,\alpha_2(t) - (1+\alpha_2(t)^2)^2$ and $\alpha_i(t) = \sqrt{1 - \left(\frac{h'(t)}{c_i}\right)^2}$.

The following existence result is a consequence and generalization of the theorem 8.

Theorem 13. ***(Existence)***

H1 *Let h satisfy (4.9) and (5.18), whereas $h''(t)$ is uniformly bounded.*

H2 *Let*

$\vec{\hat{f}}$ *chosen such that the components* $\hat{f}_i \in Lip([0,T]; L^2(\Omega))$,
the given prescribed function on $\Gamma_N \cup \sigma_0$ *is chosen from* $[\tilde{H}^{\frac{1}{2}}(\Gamma_N \times [0,T])]^2$,
the initial data: $\vec{u}_0 = \vec{v}(\vec{x},0) \in X_0$, $\vec{u}_1 = \vec{u}_t(\vec{y},0) \in [L_2(\Omega)]^2$,

then there exists a solution $\vec{v}$ such that

$$v_i \in C([0,T];\, X_t) \cap C^1([0,T];\, H_D^1(\Omega_0)) \cap C^2([0,T];\, L^2(\Omega_0)),\ i=1,2$$

of the formulated problem in the reference configuration $\Omega_0 \times [0,T]$.

Moreover if

H3

$$\begin{aligned}
&\vec{u}_0(x) = \vec{v}_{R_0}(x) + k_I(0,h,h')S_N^1(\vec{x},0) + k_{II}(0,h,h')S_N^2(\vec{x},0),\\
&k_I(0,h,h')\ \text{ and }\ k_{II}(0,h,h') \in \mathbb{R},\\
&\vec{v}_{R_0} \in [H^2(\Omega_0)]^2, \quad \vec{u}_1 \in [H_D^1(\Omega_0)]^2.
\end{aligned}$$

Then there exists a solution $\vec{u}$ of the problem (5.6) in the current configuration and admits the decomposition into a regular part and a singular one:

$$\vec{u}(\vec{y},t) = \vec{u}_R(\vec{y},t) + k_I(t,h,h')S_N^1(\vec{y},t) + k_{II}(t,h,h')S_N^2(\vec{y},t), \tag{5.59}$$

where the singular terms are defined by:

$$S_N^1(\vec{y},t) = \begin{pmatrix} \frac{(1+\alpha_2(t)^2)}{\mu D}\left[\sqrt{\frac{\sqrt{(R\cos\vartheta-h)^2+\alpha_1^2(t)R^2\sin^2\vartheta}+(R\cos\vartheta-h)}{(R\cos\vartheta-h)^2+\alpha_1^2(t)R^2\sin^2\vartheta}} - \frac{2\alpha_1(t)\alpha_2(t)}{(1+\alpha_2(t)^2)}\sqrt{\frac{\sqrt{(R\cos\vartheta-h)^2+\alpha_2^2(t)R^2\sin^2\vartheta}+(R\cos\vartheta-h)}{(R\cos\vartheta-h)^2+\alpha_2^2(t)R^2\sin^2\vartheta}}\right] \\ \frac{(1+\alpha_2(t)^2)}{\mu D}\left[-\alpha_1(t)\sqrt{\frac{\sqrt{(R\cos\vartheta-h)^2+\alpha_1^2(t)R^2\sin^2\vartheta}-(R\cos\vartheta-h)}{(R\cos\vartheta-h)^2+\alpha_1^2(t)R^2\sin^2\vartheta}} + \frac{2\alpha_1(t)}{(1+\alpha_2(t)^2)}\sqrt{\frac{\sqrt{(R\cos\vartheta-h)^2+\alpha_2^2(t)R^2\sin^2\vartheta}-(R\cos\vartheta-h)}{(R\cos\vartheta-h)^2+\alpha_2^2(t)R^2\sin^2\vartheta}}\right] \end{pmatrix}, \tag{5.60}$$

and

$$S_N^2(\vec{y},t) = \begin{pmatrix} -\frac{\alpha_2(t)}{\mu D}\left[2\sqrt{\frac{\sqrt{(R\cos\vartheta-h)^2+\alpha_1^2(t)R^2\sin^2\vartheta}-(R\cos\vartheta-h)}{(R\cos\vartheta-h)^2+\alpha_1^2(t)R^2\sin^2\vartheta}} - (1+\alpha_2(t)^2)\sqrt{\frac{\sqrt{(R\cos\vartheta-h)^2+\alpha_2^2(t)R^2\sin^2\vartheta}-(R\cos\vartheta-h)}{(R\cos\vartheta-h)^2+\alpha_2^2(t)R^2\sin^2\vartheta}}\right] \\ -\frac{1}{\mu D}\left[2\alpha_1(t)\alpha_2(t)\sqrt{\frac{\sqrt{(R\cos\vartheta-h)^2+\alpha_1^2(t)R^2\sin^2\vartheta}+(R\cos\vartheta-h)}{(R\cos\vartheta-h)^2+\alpha_1^2(t)R^2\sin^2\vartheta}} - (1+\alpha_2(t)^2)\sqrt{\frac{\sqrt{(R\cos\vartheta-h)^2+\alpha_2^2(t)R^2\sin^2\vartheta}+(R\cos\vartheta-h)}{(R\cos\vartheta-h)^2+\alpha_2^2(t)R^2\sin^2\vartheta}}\right] \end{pmatrix}, \tag{5.61}$$

$\vec{u}_R$ such that $(u_R)_i$ is in $C([0,T];H^2(\Omega_t)), i=1,2$, $k_I(t,h,h')$ and $k_{II}(t,h,h')$ are the dynamic stress intensity factors and they are in $C([0,T])$.
Also

H5 *(2.8) holds*

then the representation (5.59) may be rewritten for the components $\sigma_{ij}(\vec{u})$ of the stress vector:

$$\begin{aligned}
\sigma_{ij}(\vec{u},\vec{y}) &= \sigma_{ij}(\vec{u}_R,\vec{y}) + k_I(t,h,h')\left[\mu\left(\partial_j\left(S_N^1\right)_i + \partial_i\left(S_N^1\right)_j\right) + \delta_{i,j}\lambda\nabla\cdot S_N^1\right] + \\
&+ k_{II}(t,h,h')\left[\mu\left(\partial_j\left(S_N^2\right)_i + \partial_i\left(S_N^2\right)_j\right) + \delta_{i,j}\lambda\nabla\cdot S_N^2\right] \\
&= \sigma_{ij}(\vec{u}_R,\vec{y}) + k_I(t,h,h')\,\sigma_{ij}(S_N^1,\vec{y}) + k_{II}(t,h,h')\,\sigma_{ij}(S_N^2,\vec{y}).
\end{aligned} \tag{5.62}$$

with $\sigma(\vec{u}_R) \in H^1(\Omega_t)$ for almost all $t > 0$.

Proof of theorem 13

The proof of theorem 13 is long and technical. The arguments for fracture mechanics in mode III in [77] and reference therein, are also transferred to our case.

We want to derive the singular formulas for the solution $\vec{u}$ in (5.59) and for $\vec{\sigma}$ in (5.62). Therefore we shall need the auxiliar problems for the wave potentials ϕ and ψ, or Φ and Ψ, or $w^{(1)}$ and $w^{(2)}$ respectively, according the configuration where we are.

Initial conditions for the wave potentials do not occur explicitly but for data as in the statement of the theorem and by the succesive change of unknows (5.31), (5.38), (5.39), (5.54) and (5.55), it should be realized that they belong to the space where they were extracted at $t = 0$. Consequently they satisfy the assumptions of the existence-theorem given in [77].

There exits solutions related to the Laplace operators (5.58) in the $z^{(i)}$-coordinates, $i = 1,2$ in the slitdomain of the form

$$w^{(i)}(z^{(i)},t) = S_N^{(i)}(z^{(i)},t),\ i = 1,2.$$

Using the change of unknown (5.54) and (5.55),

$$\Phi(\vec{x},t) = S_N^{(1)}(x_1, d^{(1)}(x,t)x_2,t),$$
$$\Psi(\vec{x},t) = S_N^{(2)}(x_1, d^{(2)}(x,t)x_2,t),$$

$d^{(i)}(\vec{x},t)$ are defined by (5.52), (5.53).

As $S_N^{(i)}(x_1, d^{(i)}(x,t)x_2,t),\ i = 1,2$ are regular far from the crack tip, the above expressions are equivalent to:

$$\Phi(\vec{x},t) = \Phi_{\text{sing}}(x_1, \alpha_1(t)x_2,t),$$
$$\Psi(\vec{x},t) = \Psi_{\text{sing}}(x_1, \alpha_2(t)x_2,t),$$

Φ_{sing} and $\Psi_{\text{sing}} \in H^2(\Omega_0)$.

From (5.38), (5.39) follow that

$$\phi(\vec{y},t) = \phi_{\text{sing}}(y_1 - h(t), \alpha_1(t)y_2,t),$$
$$\psi(\vec{y},t) = \psi_{\text{sing}}(y_1 - h(t), \alpha_2(t)y_2,t).$$

The solution $\vec{v}$ of the boundary value problem in the slitdomain can be decomposed in a homogeneous and a particular solution. So we get

$$\vec{v} = \vec{v}_{\text{hom}} + \vec{v}_{\text{part}}.$$

The solution $\vec{v}_{\text{hom}}$ can be split additively into a regular part and a singular part [23].

Note that the particular solution can be chosen regular enough.

In the following we describe how to connect the local solutions $\vec{v}$ given in the slitdomain

with the global solutions in Ω. We call $\vec{V}$ the global solutions, d.h. $\vec{v} = \eta\vec{V}$, with η a cut-off function defined around the crack tip,

$$\begin{aligned}
\vec{V} &= \eta\vec{V} + (1-\eta)\vec{V},\\
\vec{V} &= \vec{v} + (1-\eta)\vec{V},\\
\vec{V} &= \vec{v}_{\text{sing}} + \vec{v}_{\text{reg}} + (1-\eta)\vec{V},\\
\vec{V} &= \vec{v}_{\text{sing}} + \vec{V}_{\text{reg}}.
\end{aligned}$$

These decompositions and the changes of unknown (5.31) and (5.8) yield the first conclusion. Which also implies that $\vec{v}(\cdot,t)$ belongs to $[C([0,T];X_t)]^2$. Note that: the set of initial conditions is expected to coming from (5.34).

The rest of the proof is split into several lemmata: We proceed in the following way:

- In Lemma 14 is described the relationship between the singular fields and the scalar singularities of the potentials ϕ and ψ.
- Lemma 15 provides the singularity results for the wave potentials in the corresponding scaled coordinate plane. And also it states the singularity results for the wave potentials in the current configuration.
- in Lemma 16 some previous computations for the first and second space-derivatives of the singular functions related to the Laplace operator are presented.
- In Lemma 17 we prove that there exists a solution to the dynamic problem for the stress field $\sigma(S_N^{(i)})$, which near the crack tip, has the representation given by (5.62). Here it is written in the spaces variable $z^{(1)}$, $z^{(2)}$.
- In Lemma 18 further singularity results for the stress field in the reference domain are presented.
- Finally, the remaining singularity results for the displacement field $\vec{u}$ are shown in Lemma 19.

Lemma 14. *The singular terms defined in Theorem 13 in the current configuration are related with the singular terms ϕ_{sing}, ψ_{sing} and Φ_{sing}, Ψ_{sing} and $S_N^{(1)}$, $S_N^{(2)}$ through the succesive change of unknowns (5.31), (5.38), (5.39), (5.54) and (5.55).*

Proof. We express u_{sing} by ϕ_{sing}, ψ_{sing} and Φ_{sing}, Ψ_{sing} and $S_N^{(1)}$, $S_N^{(2)}$.
The following results follows:

$$\begin{aligned}(u_{\text{sing}})_1 &= \frac{\partial \phi_{\text{sing}}}{\partial y_1} + \frac{\partial \psi_{\text{sing}}}{\partial y_2} = \frac{\partial \Phi_{\text{sing}}}{\partial x_1} + \frac{\partial \Psi_{\text{sing}}}{\partial x_2} = \frac{\partial S_N^{(1)}}{\partial z_1^{(1)}} + \alpha_2(t)\frac{\partial S_N^{(2)}}{\partial z_2^{(2)}},\\ (u_{\text{sing}})_2 &= \frac{\partial \phi_{\text{sing}}}{\partial y_2} - \frac{\partial \psi_{\text{sing}}}{\partial y_1} = \frac{\partial \Phi_{\text{sing}}}{\partial x_2} - \frac{\partial \Psi_{\text{sing}}}{\partial x_1} = \alpha_1(t)\frac{\partial S_N^{(1)}}{\partial z_2^{(1)}} - \frac{\partial S_N^{(2)}}{\partial z_1^{(2)}},\end{aligned} \tag{5.63}$$

Furthermore

$$\begin{aligned}\sigma_{11}(\vec{u}_{\text{sing}_i}) &= 2\mu\left(\partial_1^2\Phi_{\text{sing}_i} + \partial_{12}^2\Psi_{\text{sing}_i}\right) + \lambda\,\nabla\cdot\begin{pmatrix}\partial_1\Phi_{\text{sing}_i} + \partial_2\Psi_{\text{sing}_i}\\ \partial_2\Phi_{\text{sing}_i} - \partial_1\Psi_{\text{sing}_i}\end{pmatrix},\\ \sigma_{12}(\vec{u}_{\text{sing}_i}) &= \mu\left(2\partial_{12}^2\Phi_{\text{sing}_i} + \partial_2^2\Psi_{\text{sing}_i} - \partial_1^2\Psi_{\text{sing}_i}\right),\\ \sigma_{22}(\vec{u}_{\text{sing}_i}) &= 2\mu\left(\partial_2^2\Phi_{\text{sing}_i} - \partial_{12}^2\Psi_{\text{sing}_i}\right) + \lambda\,\nabla\cdot\begin{pmatrix}\partial_1\Phi_{\text{sing}_i} + \partial_2\Psi_{\text{sing}_i}\\ \partial_2\Phi_{\text{sing}_i} - \partial_1\Psi_{\text{sing}_i}\end{pmatrix}.\end{aligned} \tag{5.64}$$

for $i = I, II$. (5.63) and (5.64) follow from the chain rule. □

Lemma 15. *Let $S_N^{(1)}$ and $S_N^{(2)}$ the general singular functions related to the Laplace operators. Under the succesive transformations (5.38), (5.54) for ϕ and (5.39), (5.55) for ψ, the singular functions for (5.36), (5.37) are:*

$$S_N^{(1)}(z_1^{(1)}, z_2^{(1)}) = A_0^{(1)}(t)\, r_{z^{(1)}}^{\frac{3}{2}} \cos\left(\frac{3}{2}\varphi_{z^{(1)}}\right) + B_0^{(1)}(t)\, r_{z^{(1)}}^{\frac{3}{2}} \sin\left(\frac{3}{2}\varphi_{z^{(1)}}\right), \tag{5.65}$$

$$S_N^{(2)}(z_1^{(2)}, z_2^{(2)}) = A_0^{(2)}(t)\, r_{z^{(2)}}^{\frac{3}{2}} \sin\left(\frac{3}{2}\varphi_{z^{(2)}}\right) + B_0^{(2)}(t)\, r_{z^{(2)}}^{\frac{3}{2}} \cos\left(\frac{3}{2}\varphi_{z^{(2)}}\right), \tag{5.66}$$

whereas in the reference domain:

$$\begin{aligned}S_N^{(1)}(x,t) &= \frac{A_0^{(1)}(t) r^{\frac{3}{2}}}{\sqrt{2}}\left[\cos\varphi\sqrt{\sqrt{\cos^2\varphi + \alpha_1^2\sin^2\varphi} + \cos\varphi} - \alpha_1\sin\varphi\sqrt{\sqrt{\cos^2\varphi + \alpha_1^2\sin^2\varphi} - \cos\varphi}\right] +\\ &+ \frac{B_0^{(1)}(t) r^{\frac{3}{2}}}{\sqrt{2}}\left[\cos\varphi\sqrt{\sqrt{\cos^2\varphi + \alpha_1^2\sin^2\varphi} - \cos\varphi} + \alpha_1\sin\varphi\sqrt{\sqrt{\cos^2\varphi + \alpha_1^2\sin^2\varphi} + \cos\varphi}\right],\\ S_N^{(2)}(x,t) &= \frac{A_0^{(2)}(t) r^{\frac{3}{2}}}{\sqrt{2}}\left[\cos\varphi\sqrt{\sqrt{\cos^2\varphi + \alpha_2^2\sin^2\varphi} - \cos\varphi} + \alpha_2\sin\varphi\sqrt{\sqrt{\cos^2\varphi + \alpha_2^2\sin^2\varphi} + \cos\varphi}\right] +\\ &\frac{B_0^{(2)}(t) r^{\frac{3}{2}}}{\sqrt{2}}\left[\cos\varphi\sqrt{\sqrt{\cos^2\varphi + \alpha_2^2\sin^2\varphi} + \cos\varphi} - \alpha_2\sin\varphi\sqrt{\sqrt{\cos^2\varphi + \alpha_2^2\sin^2\varphi} - \cos\varphi}\right].\end{aligned}$$

Proof. Let $(r_{z^{(i)}}, \varphi_{z^{(i)}})$ be the polar coordinates with center at the crack tip, here 0, and one axis directed along the crack so that $-\pi < \varphi_{z^{(i)}} < \pi$. The general solutions of the Laplace

problem associated to (5.58) have the form, see also section 3.5:

$$\begin{aligned} w^{(1)}(z^{(1)},t) &= A_0^{(1)}(t)\, r_{z^{(1)}}^{q_1} \cos\left(q_1\, \varphi_{z^{(1)}}\right) + B_0^{(1)}(t)\, r_{z^{(1)}}^{q_1} \sin\left(q_1\, \varphi_{z^{(1)}}\right), \\ w^{(2)}(z^{(2)},t) &= A_0^{(2)}(t)\, r_{z^{(2)}}^{q_2} \sin\left(q_2\, \varphi_{z^{(2)}}\right) + B_0^{(2)}(t)\, r_{z^{(2)}}^{q_2} \cos\left(q_2\, \varphi_{z^{(2)}}\right). \end{aligned} \tag{5.67}$$

in general $q_i \in \mathbb{R}, i = 1,2$.

Because of the presence of cracks, it is well-known that the singularity exponents are half-integers $\frac{1}{2}, \frac{3}{2}, \cdots$. We expect to have $r_{z^{(i)}}^{\frac{3}{2}}$ ($q_1 = q_2 = \frac{3}{2}$) for the displacement potential Φ and Ψ corresponding to an unbounded stress (5.33) with singularity $r_{z^{(i)}}^{-\frac{1}{2}}$.

Then there holds (5.65) and (5.66).

In what follows we need explicitly the singular function in the current configuration.

The singular terms $r_{z^{(i)}}^{\frac{3}{2}} \cos\left(\frac{3}{2}\, \varphi_{z^{(i)}}\right)$ given in (5.65) and (5.66) in the $z^{(i)}$-configuration, $i = 1,2$, read in the current configuration

$$\begin{aligned} &\frac{1}{\sqrt{2}} \sqrt{(R\cos\vartheta - h)^2 + R^2 \sin^2\vartheta} \times \\ &\Bigg[(R\cos\vartheta - h) \sqrt{\sqrt{(R\cos\vartheta - h)^2 + \alpha_i(t)^2 R^2 \sin^2\vartheta} + (R\cos\vartheta - h)} + \\ &- \alpha_i(t)\, R \sin\vartheta \sqrt{\sqrt{(R\cos\vartheta - h)^2 + \alpha_i(t)^2 R^2 \sin^2\vartheta} - (R\cos\vartheta - h)} \Bigg] \end{aligned} \tag{5.68}$$

whereas the singular terms $r_{z^{(i)}}^{\frac{3}{2}} \sin\left(\frac{3}{2}\, \varphi_{z^{(i)}}\right)$ given in (5.65) and (5.66) in the $z^{(i)}$-configuration, $i = 1,2$, read in the current configuration

$$\begin{aligned} &\frac{1}{\sqrt{2}} \sqrt{(R\cos\vartheta - h)^2 + R^2 \sin^2\vartheta} \times \\ &\Bigg[(R\cos\vartheta - h) \sqrt{\sqrt{(R\cos\vartheta - h)^2 + \alpha_i(t)^2 R^2 \sin^2\vartheta} - (R\cos\vartheta - h)} + \\ &+ \alpha_i(t)\, R \sin\vartheta \sqrt{\sqrt{(R\cos\vartheta - h)^2 + \alpha_i(t)^2 R^2 \sin^2\vartheta} + (R\cos\vartheta - h)} \Bigg] \end{aligned} \tag{5.69}$$

Here, (R, ϑ) are the current polar coordinates with respect to the crack tip $(h(t), 0)$.

We consider (5.50) and (5.51) in that region where the cut-off function $\kappa \equiv 1$.

$$z_1^{(1)} = x_1, \quad z_2^{(1)} = \alpha_1(t)\, x_2, \quad \text{for } \Phi, \qquad z_1^{(2)} = x_1, \quad z_2^{(2)} = \alpha_2(t)\, x_2, \quad \text{for } \Psi.$$

Let be $x_1 = r\cos\varphi$, $x_2 = r\sin\varphi$, $r = \sqrt{x_1^2 + x_2^2}$, then:

$$\cos\varphi_{z^{(i)}} = \frac{z_1^{(i)}}{r_{z^{(i)}}} = \frac{x_1}{r_{z^{(i)}}} = \frac{\cos\varphi}{\sqrt{\cos^2\varphi + \alpha_i(t)^2\sin^2\varphi}},$$

$$\sin\varphi_{z^{(i)}} = \frac{z_2^{(i)}}{r_{z^{(i)}}} = \frac{\alpha_i(t)\,x_2}{r_{z^{(i)}}} = \frac{\alpha_i(t)\sin\varphi}{\sqrt{\cos^2\varphi + \alpha_i(t)^2\sin^2\varphi}}$$

$$r_{z^{(i)}} = r\sqrt{\cos^2\varphi + \alpha_i(t)^2\sin^2\varphi}.$$

The singular terms $r_{z^{(i)}}^{\frac{3}{2}}\cos\left(\frac{3}{2}\varphi_{z^{(i)}}\right)$ and $r_{z^{(i)}}^{\frac{3}{2}}\sin\left(\frac{3}{2}\varphi_{z^{(i)}}\right)$ in polar coordinates with respect to x-components read (we have used known trigonometrical formulas):

$$\frac{1}{\sqrt{2}}r^{\frac{1}{2}}\left[r\cos\varphi\sqrt{\sqrt{\cos^2\varphi + \alpha_i(t)^2\sin^2\varphi} + \cos\varphi} + \right.$$
$$\left. - \alpha_i(t)\,r\sin\varphi\sqrt{\sqrt{\cos^2\varphi + \alpha_i(t)^2\sin^2\varphi} - \cos\varphi}\right], \tag{5.70}$$

and

$$\frac{1}{\sqrt{2}}r^{\frac{1}{2}}\left[r\cos\varphi\sqrt{\sqrt{\cos^2\varphi + \alpha_i(t)^2\sin^2\varphi} - \cos\varphi} + \right.$$
$$\left. + \alpha_i(t)\,r\sin\varphi\sqrt{\sqrt{\cos^2\varphi + \alpha_i(t)^2\sin^2\varphi} + \cos\varphi}\right]. \tag{5.71}$$

respectively, with:

$$\begin{pmatrix} y_1 \\ y_2 \end{pmatrix} = \begin{pmatrix} R\cos\vartheta \\ R\sin\vartheta \end{pmatrix} = \begin{pmatrix} x_1 + h \\ x_2 \end{pmatrix} = \begin{pmatrix} r\cos\varphi + h \\ r\sin\varphi \end{pmatrix}. \tag{5.72}$$

Let us remark that $R = R(t), \vartheta = \vartheta(t), h = h(t)$. It follows

$$r\cos\varphi = R\cos\vartheta - h, \quad r\sin\varphi = R\sin\vartheta. \tag{5.73}$$

Inserting (5.73) into (5.70) and (5.71) we get the relation (5.68) and (5.69). □

The foregoing analysis of near-tip fields shows that the solutions for the wave potentials can be decomposed into two parts, one of them is given by the homogeneous solution which satisfies the Laplace equation in the corresponding scaled coordinate plane and the other one is the regular part.

The time enters the solution (5.65) and (5.66) through the coefficients:

$$A_0^{(1)}(t), A_0^{(2)}(t), B_0^{(1)}(t), B_0^{(2)}(t).$$

We will see that the set of these singular functions is rich enough in order to realize (5.35). We shall need some previous computations in order to get explicit expressions for (5.60), (5.61) and (5.62). They involve first and second derivatives of the singular functions.

Lemma 16. *The derivatives with respect to $z^{(1)}$ and $z^{(2)}$ of the singular terms $r_{z^{(i)}}^{\frac{3}{2}} \cos\left(\frac{3}{2}\varphi_{z^{(i)}}\right)$ given in (5.65) and (5.66), respectively, are:*

$$\frac{\partial}{\partial z_1^{(i)}} r_{z^{(i)}}^{\frac{3}{2}} \cos\left(\frac{3}{2}\varphi_{z^{(i)}}\right) = \frac{3}{2} r_{z^{(i)}}^{\frac{1}{2}} \cos\left(\frac{\varphi_{z^{(i)}}}{2}\right), \tag{5.74}$$

$$\frac{\partial}{\partial z_2^{(i)}} r_{z^{(i)}}^{\frac{3}{2}} \cos\left(\frac{3}{2}\varphi_{z^{(i)}}\right) = \frac{3}{2} r_{z^{(i)}}^{\frac{1}{2}} \sin\left(\frac{\varphi_{z^{(i)}}}{2}\right), \tag{5.75}$$

$$\frac{\partial^2}{\partial (z_1^{(i)})^2} r_{z^{(i)}}^{\frac{3}{2}} \cos\left(\frac{3}{2}\varphi_{z^{(i)}}\right) = \frac{3}{2}\frac{\partial}{\partial z_1^{(i)}} r_{z^{(i)}}^{\frac{1}{2}} \cos\left(\frac{1}{2}\varphi_{z^{(i)}}\right) = \frac{3}{4} r_{z^{(i)}}^{-\frac{1}{2}} \cos\left(\frac{\varphi_{z^{(i)}}}{2}\right), \tag{5.76}$$

$$\frac{\partial^2}{\partial (z_2^{(i)})^2} r_{z^{(i)}}^{\frac{3}{2}} \cos\left(\frac{3}{2}\varphi_{z^{(i)}}\right) = \frac{3}{2}\frac{\partial}{\partial z_2^{(i)}} r_{z^{(i)}}^{\frac{1}{2}} \sin\left(\frac{1}{2}\varphi_{z^{(i)}}\right) = \frac{3}{4} r_{z^{(i)}}^{-\frac{1}{2}} \cos\left(\frac{\varphi_{z^{(i)}}}{2}\right), \tag{5.77}$$

$$\begin{aligned}\frac{\partial^2}{\partial z_1^{(i)} \partial z_2^{(i)}} r_{z^{(i)}}^{\frac{3}{2}} \cos\left(\frac{3}{2}\varphi_{z^{(i)}}\right) &= \frac{3}{2}\frac{\partial}{\partial z_1^{(i)}} r_{z^{(i)}}^{\frac{1}{2}} \sin\left(\frac{1}{2}\varphi_{z^{(i)}}\right) = \frac{3}{2}\frac{\partial}{\partial z_2^{(i)}} r_{z^{(i)}}^{\frac{1}{2}} \cos\left(\frac{1}{2}\varphi_{z^{(i)}}\right) \\ &= -\frac{3}{4} r_{z^{(i)}}^{-\frac{1}{2}} \sin\left(\frac{\varphi_{z^{(i)}}}{2}\right),\end{aligned} \tag{5.78}$$

and for the singular terms $r_{z^{(i)}}^{\frac{3}{2}} \sin\left(\frac{3}{2}\varphi_{z^{(i)}}\right)$ given in (5.65) and (5.66),

$$\frac{\partial}{\partial z_1^{(i)}} r_{z^{(i)}}^{\frac{3}{2}} \sin\left(\frac{3}{2}\varphi_{z^{(i)}}\right) = \frac{3}{2} r_{z^{(i)}}^{\frac{1}{2}} \sin\left(\frac{\varphi_{z^{(i)}}}{2}\right), \tag{5.79}$$

$$\frac{\partial}{\partial z_2^{(i)}} r_{z^{(i)}}^{\frac{3}{2}} \sin\left(\frac{3}{2}\varphi_{z^{(i)}}\right) = \frac{3}{2} r_{z^{(i)}}^{\frac{1}{2}} \cos\left(\frac{\varphi_{z^{(i)}}}{2}\right), \tag{5.80}$$

$$\frac{\partial^2}{\partial (z_1^{(i)})^2} r_{z^{(i)}}^{\frac{3}{2}} \sin\left(\frac{3}{2}\varphi_{z^{(i)}}\right) = \frac{3}{2}\frac{\partial}{\partial z_1^{(i)}} r_{z^{(i)}}^{\frac{1}{2}} \sin\left(\frac{1}{2}\varphi_{z^{(i)}}\right) = -\frac{3}{4} r_{z^{(i)}}^{-\frac{1}{2}} \sin\left(\frac{\varphi_{z^{(i)}}}{2}\right), \tag{5.81}$$

$$\frac{\partial^2}{\partial (z_2^{(i)})^2} r_{z^{(i)}}^{\frac{3}{2}} \sin\left(\frac{3}{2}\varphi_{z^{(i)}}\right) = \frac{3}{2}\frac{\partial}{\partial z_2^{(i)}} r_{z^{(i)}}^{\frac{1}{2}} \cos\left(\frac{1}{2}\varphi_{z^{(i)}}\right) = -\frac{3}{4} r_{z^{(i)}}^{-\frac{1}{2}} \sin\left(\frac{\varphi_{z^{(i)}}}{2}\right), \tag{5.82}$$

$$\begin{aligned}\frac{\partial^2}{\partial z_1^{(i)} \partial z_2^{(i)}} r_{z^{(i)}}^{\frac{3}{2}} \sin\left(\frac{3}{2}\varphi_{z^{(i)}}\right) &= \frac{3}{2}\frac{\partial}{\partial z_1^{(i)}} r_{z^{(i)}}^{\frac{1}{2}} \cos\left(\frac{1}{2}\varphi_{z^{(i)}}\right) = \frac{3}{2}\frac{\partial}{\partial z_2^{(i)}} r_{z^{(i)}}^{\frac{1}{2}} \sin\left(\frac{1}{2}\varphi_{z^{(i)}}\right) \\ &= \frac{3}{4} r_{z^{(i)}}^{-\frac{1}{2}} \cos\left(\frac{\varphi_{z^{(i)}}}{2}\right).\end{aligned} \tag{5.83}$$

Proof. We use the trigonometrical formulas for cosine and sine of the sum and difference of two angles and the following relations:

$$\partial_1 \varpi = \frac{\partial \varpi}{\partial r}\cos\phi - \frac{1}{r}\frac{\partial \varpi}{\partial \phi}\sin\phi,$$
$$\partial_2 \varpi = \frac{\partial \varpi}{\partial r}\sin\phi + \frac{1}{r}\frac{\partial \varpi}{\partial \phi}\cos\phi.$$

□

The motion field induced by a propagating crack produce asymptotic singularities. The local asymptotic analysis gives solutions which hold exclusively for points close to the crack tip. There exists a solution to the dynamic global problem for the stress field, which near the crack tip, has the representation given by (5.62).

Lemma 17. *The functions representing the angular variation of stress components for any value of instantaneous crack tip speed $h' = h'(t)$ are given in the spaces variable $z^{(1)}$, $z^{(2)}$ by:*

$$\sigma_{11}(z^{(1)},z^{(2)})_{sing} = \mu\left\{\left(1-\alpha_2^2+2\alpha_1^2\right)A_0^{(1)}(t)\,r_{z^{(1)}}^{-\frac{1}{2}}\cos\left(\frac{\varphi_{z^{(1)}}}{2}\right)+2\alpha_2 B_0^{(2)}(t)\,r_{z^{(2)}}^{-\frac{1}{2}}\cos\left(\frac{\varphi_{z^{(2)}}}{2}\right)\right\}+$$
$$+\mu\left\{\left(1-\alpha_2^2+2\alpha_1(t)^2\right)B_0^{(1)}(t)\,r_{z^{(1)}}^{-\frac{1}{2}}\sin\left(\frac{\varphi_{z^{(1)}}}{2}\right)+2\alpha_2\,A_0^{(2)}(t)\,r_{z^{(2)}}^{-\frac{1}{2}}\sin\left(\frac{\varphi_{z^{(2)}}}{2}\right)\right\}, \quad (5.84)$$

$$\sigma_{22}(z^{(1)},z^{(2)})_{sing} = -\mu\left\{\left(1+\alpha_2^2\right)A_0^{(1)}(t)\,r_{z^{(1)}}^{-\frac{1}{2}}\cos\left(\frac{\varphi_{z^{(1)}}}{2}\right)+2\alpha_2\,B_0^{(2)}(t)\,r_{z^{(2)}}^{-\frac{1}{2}}\cos\left(\frac{\varphi_{z^{(2)}}}{2}\right)\right\}+$$
$$-\mu\left\{\left(1+\alpha_2^2\right)B_0^{(1)}(t)\,r_{z^{(1)}}^{-\frac{1}{2}}\sin\left(\frac{\varphi_{z^{(1)}}}{2}\right)+2\alpha_2\,A_0^{(2)}(t)\,r_{z^{(2)}}^{-\frac{1}{2}}\sin\left(\frac{\varphi_{z^{(2)}}}{2}\right)\right\}, \quad (5.85)$$

$$\sigma_{12}(z^{(1)},z^{(2)})_{sing} = -\mu\left\{2\alpha_1\,A_0^{(1)}(t)\,r_{z^{(1)}}^{-\frac{1}{2}}\sin\left(\frac{\varphi_{z^{(1)}}}{2}\right)+(1+\alpha_2^2)B_0^{(2)}(t)\,r_{z^{(2)}}^{-\frac{1}{2}}\sin\left(\frac{\varphi_{z^{(2)}}}{2}\right)\right\}+$$
$$-\mu\left\{2\alpha_1\,B_0^{(1)}(t)\,r_{z^{(1)}}^{-\frac{1}{2}}\cos\left(\frac{\varphi_{z^{(1)}}}{2}\right)+(1+\alpha_2^2)\,A_0^{(2)}(t)\,r_{z^{(2)}}^{-\frac{1}{2}}\cos\left(\frac{\varphi_{z^{(2)}}}{2}\right)\right\}. \quad (5.86)$$

Proof. This lemma can be established by lemmata 14 and 15 and elementary calculation from Lemma 16.
We have also computed the quantities in the following way:

$$\frac{1-\alpha_2^2-(2\alpha_1^2-\alpha_2^2-1)\alpha_1^2}{(1-\alpha_1^2)} = \frac{(1-\alpha_1^2)(1+\alpha_1^2)-\alpha_2^2(1-\alpha_1^2)+\alpha_1^2(1-\alpha_1^2)}{(1-\alpha_1^2)}$$
$$= 1+2\alpha_1^2-\alpha_2^2,$$
$$\frac{2\alpha_1^2-\alpha_2^2-1-\alpha_1^2(1-\alpha_2^2)}{(1-\alpha_1^2)} = \frac{-(1-\alpha_1^2)-\alpha_2^2(1-\alpha_1^2)}{(1-\alpha_1^2)} = -(1+\alpha_2^2).$$

□

Lemma 18. *Under the assumptions of singularity of lemma 17, the following expressions, in the reference space with respect to the polar coordinate* (r,φ)*, hold:*

$$\begin{aligned}\sigma_{11}(r,\varphi) =& \frac{\mu}{\sqrt{2r}}\Bigg\{\left(1-\alpha_2(t)^2+2\alpha_1(t)^2\right)A_0^{(1)}(t)\sqrt{\frac{\sqrt{\cos^2\varphi+\alpha_1(t)^2\sin^2\varphi}+\cos\varphi}{\cos^2\varphi+\alpha_1(t)^2\sin^2\varphi}}+\\ &+2\alpha_2(t)B_0^{(2)}(t)\sqrt{\frac{\sqrt{\cos^2\varphi+\alpha_2(t)^2\sin^2\varphi}+\cos\varphi}{\cos^2\varphi+\alpha_2(t)^2\sin^2\varphi}}\Bigg\}+\\ &+\frac{\mu}{\sqrt{2r}}\Bigg\{\left(1-\alpha_2(t)^2+2\alpha_1(t)^2\right)B_0^{(1)}(t)\sqrt{\frac{\sqrt{\cos^2\varphi+\alpha_1(t)^2\sin^2\varphi}-\cos\varphi}{\cos^2\varphi+\alpha_1(t)^2\sin^2\varphi}}\\ &+2\alpha_2(t)\,A_0^{(2)}(t)\sqrt{\frac{\sqrt{\cos^2\varphi+\alpha_2(t)^2\sin^2\varphi}-\cos\varphi}{\cos^2\varphi+\alpha_2(t)^2\sin^2\varphi}}\Bigg\},\end{aligned}\tag{5.87}$$

$$\begin{aligned}\sigma_{22}(r,\varphi) =& -\frac{\mu}{\sqrt{2r}}\Bigg\{\left(1+\alpha_2(t)^2\right)A_0^{(1)}(t)\sqrt{\frac{\sqrt{\cos^2\varphi+\alpha_1(t)^2\sin^2\varphi}+\cos\varphi}{\cos^2\varphi+\alpha_1(t)^2\sin^2\varphi}}+\\ &+2\alpha_2(t)\,B_0^{(2)}(t)\sqrt{\frac{\sqrt{\cos^2\varphi+\alpha_2(t)^2\sin^2\varphi}+\cos\varphi}{\cos^2\varphi+\alpha_2(t)^2\sin^2\varphi}}\Bigg\}+\\ &-\frac{\mu}{\sqrt{2r}}\Bigg\{\left(1+\alpha_2(t)^2\right)B_0^{(1)}(t)\sqrt{\frac{\sqrt{\cos^2\varphi+\alpha_1(t)^2\sin^2\varphi}-\cos\varphi}{\cos^2\varphi+\alpha_1(t)^2\sin^2\varphi}}+\\ &+2\alpha_2(t)\,A_0^{(2)}(t)\sqrt{\frac{\sqrt{\cos^2\varphi+\alpha_2(t)^2\sin^2\varphi}-\cos\varphi}{\cos^2\varphi+\alpha_2(t)^2\sin^2\varphi}}\Bigg\},\end{aligned}\tag{5.88}$$

$$\begin{aligned}\sigma_{12}(r,\varphi) =& -\frac{\mu}{\sqrt{2r}}\Bigg\{2\alpha_1(t)\,A_0^{(1)}(t)\sqrt{\frac{\sqrt{\cos^2\varphi+\alpha_1(t)^2\sin^2\varphi}-\cos\varphi}{\cos^2\varphi+\alpha_1(t)^2\sin^2\varphi}}+\\ &+(1+\alpha_2(t)^2)B_0^{(2)}(t)\sqrt{\frac{\sqrt{\cos^2\varphi+\alpha_2(t)^2\sin^2\varphi}-\cos\varphi}{\cos^2\varphi+\alpha_2(t)^2\sin^2\varphi}}\Bigg\}+\\ &-\frac{\mu}{\sqrt{2r}}\Bigg\{2\alpha_1(t)\,B_0^{(1)}(t)\sqrt{\frac{\sqrt{\cos^2\varphi+\alpha_1(t)^2\sin^2\varphi}+\cos\varphi}{\cos^2\varphi+\alpha_1(t)^2\sin^2\varphi}}+\\ &+(1+\alpha_2(t)^2)\,A_0^{(2)}(t)\sqrt{\frac{\sqrt{\cos^2\varphi+\alpha_2(t)^2\sin^2\varphi}+\cos\varphi}{\cos^2\varphi+\alpha_2(t)^2\sin^2\varphi}}\Bigg\}.\end{aligned}\tag{5.89}$$

Proof. The transformations of (5.84),$\cdots$, (5.86) in the reference space with respect to the

polar coordinates (r,φ) are now straightforward:

$$\begin{aligned}
\cos^2\left(\frac{\varphi_{z^{(i)}}}{2}\right) &= \frac{1}{2}\left(1+\frac{\cos\varphi}{\sqrt{\cos^2\varphi+\alpha_i(t)^2\sin^2\varphi}}\right),\\
\sin^2\left(\frac{\varphi_{z^{(i)}}}{2}\right) &= \frac{1}{2}\left(1-\frac{\cos\varphi}{\sqrt{\cos^2\varphi+\alpha_i(t)^2\sin^2\varphi}}\right),\\
r_{z^{(i)}} &= r\sqrt{\cos^2\varphi+\alpha_i(t)^2\sin^2\varphi}.
\end{aligned} \tag{5.90}$$

□

Lemma 19. *Under the assumptions of singularity given before for the stress field, then there exists a singular solution for the displacement field $\vec{v}$ in the reference configuration given by:*

$$S_N^1(x,t)=\begin{pmatrix}
\frac{(1+\alpha_2(t)^2)\,r^{\frac{1}{2}}}{\mu D}\left[\sqrt{\frac{\sqrt{\cos^2\varphi+\alpha_1(t)^2\sin^2\varphi}+\cos\varphi}{\cos^2\varphi+\alpha_1(t)^2\sin^2\varphi}}-\frac{2\,\alpha_1(t)\,\alpha_2(t)}{(1+\alpha_2(t)^2)}\sqrt{\frac{\sqrt{\cos^2\varphi+\alpha_2(t)^2\sin^2\varphi}+\cos\varphi}{\cos^2\varphi+\alpha_2(t)^2\sin^2\varphi}}\right]\\
\frac{(1+\alpha_2(t)^2)\,r^{\frac{1}{2}}}{\mu D}\left[-\alpha_1(t)\sqrt{\frac{\sqrt{\cos^2\varphi+\alpha_1(t)^2\sin^2\varphi}-\cos\varphi}{\cos^2\varphi+\alpha_1(t)^2\sin^2\varphi}}+\frac{2\,\alpha_1(t)}{(1+\alpha_2(t)^2)}\sqrt{\frac{\sqrt{\cos^2\varphi+\alpha_2(t)^2\sin^2\varphi}-\cos\varphi}{\cos^2\varphi+\alpha_2(t)^2\sin^2\varphi}}\right]
\end{pmatrix}, \tag{5.91}$$

and

$$S_N^2(x,t)=\begin{pmatrix}
-\frac{\alpha_2(t)\,r^{\frac{1}{2}}}{\mu D}\left[2\sqrt{\frac{\sqrt{\cos^2\varphi+\alpha_1(t)^2\sin^2\varphi}-\cos\varphi}{\cos^2\varphi+\alpha_1(t)^2\sin^2\varphi}}-(1+\alpha_2(t)^2)\sqrt{\frac{\sqrt{\cos^2\varphi+\alpha_2(t)^2\sin^2\varphi}-\cos\varphi}{\cos^2\varphi+\alpha_2(t)^2\sin^2\varphi}}\right]\\
-\frac{r^{\frac{1}{2}}}{\mu D}\left[2\,\alpha_1(t)\,\alpha_2(t)\sqrt{\frac{\sqrt{\cos^2\varphi+\alpha_1(t)^2\sin^2\varphi}+\cos\varphi}{\cos^2\varphi+\alpha_1(t)^2\sin^2\varphi}}-(1+\alpha_2(t)^2)\sqrt{\frac{\sqrt{\cos^2\varphi+\alpha_2(t)^2\sin^2\varphi}+\cos\varphi}{\cos^2\varphi+\alpha_2(t)^2\sin^2\varphi}}\right].
\end{pmatrix} \tag{5.92}$$

with $D:=4\,\alpha_1(t)\,\alpha_2(t)-(1+\alpha_2(t)^2)^2$ *and* $\alpha_i(t)=\sqrt{1-\left(\frac{h'(t)}{c_i}\right)^2}$.

Proof. The boundary conditions (5.34) on the crack faces should be satisfied, i.e. the traction free condition on the cracks faces implies that:

$$\sigma_{12}(r,\pm\pi)=0,\quad \sigma_{22}(r,\pm\pi)=0 \tag{5.93}$$

We get with the specification of the free-traction on σ_0 a homogeneous system of the type

$$A(t)\,X=0,$$

more precisely we get:

$$\begin{pmatrix}
0 & 2\alpha_2(t) & (1+\alpha_2(t)^2) & 0\\
2\alpha_1(t) & 0 & 0 & (1+\alpha_2(t)^2)\\
0 & 2\alpha_2(t) & (1+\alpha_2(t)^2) & 0\\
2\alpha_1(t) & 0 & 0 & (1+\alpha_2(t)^2)
\end{pmatrix}\begin{pmatrix}
A_0^{(1)}(t)\\ A_0^{(2)}(t)\\ B_0^{(1)}(t)\\ B_0^{(2)}(t)
\end{pmatrix}=0. \tag{5.94}$$

The rows of $A(t)$ form a linearly dependent set. For all $A_0^{(1)}(t), A_0^{(2)}(t), B_0^{(1)}(t), B_0^{(2)}(t)$,

$$\det A(t) = 0.$$

Therefore the system has always nontrivial solutions. (5.94) reduces to two linear equations with four unknowns:

$$2\alpha_2(t)A_0^{(2)}(t) + (1+\alpha_2^2)B_0^{(1)}(t) = 0 \tag{5.95}$$

$$2\alpha_1(t)A_0^{(1)}(t) + (1+\alpha_2^2)B_0^{(2)}(t) = 0. \tag{5.96}$$

Here, we have four unknown while we only have two independent relations in (5.95) and (5.96). We can express $A_0^{(1)}(t), A_0^{(2)}(t)$ by $B_0^{(2)}(t), B_0^{(1)}(t)$ respectively.
Then, after the traction free condition on the cracks faces (5.87), (5.88) and (5.89) can be rewritten as (it is assumed $h'(t) \neq c_1, c_2$):

$$\begin{aligned}\sigma_{11}(r,\varphi) = &\frac{\mu}{\sqrt{2r}}\Bigg\{\Bigg(-\left(1-\alpha_2^2+2\alpha_1^2\right)\left(1+\alpha_2^2\right)\sqrt{\frac{\sqrt{\cos^2\varphi+\alpha_1(t)^2\sin^2\varphi}+\cos\varphi}{\cos^2\varphi+\alpha_1(t)^2\sin^2\varphi}}+\\ &+4\alpha_1\alpha_2(t)\sqrt{\frac{\sqrt{\cos^2\varphi+\alpha_2(t)^2\sin^2\varphi}+\cos\varphi}{\cos^2\varphi+\alpha_2(t)^2\sin^2\varphi}}\Bigg)\frac{B_0^{(2)}(t)}{2\alpha_1(t)}\Bigg\}+\\ &+\frac{\mu}{\sqrt{2r}}\Bigg\{\Bigg(\left(1-\alpha_2^2+2\alpha_1(t)^2\right)\sqrt{\frac{\sqrt{\cos^2\varphi+\alpha_1(t)^2\sin^2\varphi}-\cos\varphi}{\cos^2\varphi+\alpha_1(t)^2\sin^2\varphi}}\\ &-\left(1+\alpha_2^2\right)\sqrt{\frac{\sqrt{\cos^2\varphi+\alpha_2(t)^2\sin^2\varphi}-\cos\varphi}{\cos^2\varphi+\alpha_2(t)^2\sin^2\varphi}}\Bigg)B_0^{(1)}(t)\Bigg\},\end{aligned} \tag{5.97}$$

$$\begin{aligned}\sigma_{22}(r,\varphi) = &-\frac{\mu}{\sqrt{2r}}\Bigg\{\Bigg(-\left(1+\alpha_2^2\right)^2\sqrt{\frac{\sqrt{\cos^2\varphi+\alpha_1(t)^2\sin^2\varphi}+\cos\varphi}{\cos^2\varphi+\alpha_1(t)^2\sin^2\varphi}}+\\ &+4\alpha_1\alpha_2(t)\sqrt{\frac{\sqrt{\cos^2\varphi+\alpha_2(t)^2\sin^2\varphi}+\cos\varphi}{\cos^2\varphi+\alpha_2(t)^2\sin^2\varphi}}\Bigg)\frac{B_0^{(2)}(t)}{2\alpha_1(t)}\Bigg\}+\\ &-\frac{\mu}{\sqrt{2r}}\Bigg\{\Bigg(\left(1+\alpha_2^2\right)\sqrt{\frac{\sqrt{\cos^2\varphi+\alpha_1(t)^2\sin^2\varphi}-\cos\varphi}{\cos^2\varphi+\alpha_1(t)^2\sin^2\varphi}}+\\ &-\left(1+\alpha_2^2\right)\sqrt{\frac{\sqrt{\cos^2\varphi+\alpha_2(t)^2\sin^2\varphi}-\cos\varphi}{\cos^2\varphi+\alpha_2(t)^2\sin^2\varphi}}\Bigg)B_0^{(1)}(t)\Bigg\},\end{aligned} \tag{5.98}$$

$$\sigma_{12}(r,\varphi) = -\frac{\mu}{\sqrt{2r}}\Bigg\{\Bigg(-(1+\alpha_2^2)\sqrt{\frac{\sqrt{\cos^2\varphi+\alpha_1(t)^2\sin^2\varphi}-\cos\varphi}{\cos^2\varphi+\alpha_1(t)^2\sin^2\varphi}}+$$
$$+(1+\alpha_2^2)\sqrt{\frac{\sqrt{\cos^2\varphi+\alpha_2(t)^2\sin^2\varphi}-\cos\varphi}{\cos^2\varphi+\alpha_2(t)^2\sin^2\varphi}}\Bigg)B_0^{(2)}(t)\Bigg\}+$$
$$-\frac{\mu}{\sqrt{2r}}\Bigg\{\Bigg(4\alpha_1\alpha_2(t)\sqrt{\frac{\sqrt{\cos^2\varphi+\alpha_1(t)^2\sin^2\varphi}+\cos\varphi}{\cos^2\varphi+\alpha_1(t)^2\sin^2\varphi}}+$$
$$-(1+\alpha_2^2)^2\sqrt{\frac{\sqrt{\cos^2\varphi+\alpha_2(t)^2\sin^2\varphi}+\cos\varphi}{\cos^2\varphi+\alpha_2(t)^2\sin^2\varphi}}\Bigg)\frac{B_0^{(1)}(t)}{2\alpha_2(t)}\Bigg\}. \tag{5.99}$$

The free-traction requirement (5.34) on the crack is already satisfied.
In terms of the time-dependent unknows the singular displacement field reads:

$$\begin{pmatrix}(S_N(r,\varphi))_1\\(S_N(r,\varphi))_2\end{pmatrix} = \sqrt{r}\begin{pmatrix}A_0^{(1)}(t) & \alpha_2(t)B_0^{(2)}(t)\\ \alpha_1(t)B_0^{(1)}(t) & A_0^{(2)}(t)\end{pmatrix}\begin{pmatrix}\sqrt{\frac{\sqrt{\cos^2\varphi+\alpha_1(t)^2\sin^2\varphi}+\cos\varphi}{\cos^2\varphi+\alpha_1(t)^2\sin^2\varphi}}\\ \sqrt{\frac{\sqrt{\cos^2\varphi+\alpha_2(t)^2\sin^2\varphi}+\cos\varphi}{\cos^2\varphi+\alpha_2(t)^2\sin^2\varphi}}\end{pmatrix}+$$
$$+\sqrt{r}\begin{pmatrix}-B_0^{(1)}(t) & -\alpha_2(t)A_0^{(2)}(t)\\ -\alpha_1(t)A_0^{(1)}(t) & B_0^{(2)}(t)\end{pmatrix}\begin{pmatrix}\sqrt{\frac{\sqrt{\cos^2\varphi+\alpha_1(t)^2\sin^2\varphi}-\cos\varphi}{\cos^2\varphi+\alpha_1(t)^2\sin^2\varphi}}\\ \sqrt{\frac{\sqrt{\cos^2\varphi+\alpha_2(t)^2\sin^2\varphi}-\cos\varphi}{\cos^2\varphi+\alpha_2(t)^2\sin^2\varphi}}\end{pmatrix}$$
$$=\sqrt{r}\begin{pmatrix}-\frac{(1+\alpha_2(t)^2)}{2\alpha_1(t)}B_0^{(2)}(t) & \alpha_2(t)B_0^{(2)}(t)\\ \alpha_1(t)B_0^{(1)}(t) & -\frac{(1+\alpha_2(t)^2)}{2\alpha_2(t)}B_0^{(1)}(t)\end{pmatrix}\begin{pmatrix}\sqrt{\frac{\sqrt{\cos^2\varphi+\alpha_1(t)^2\sin^2\varphi}+\cos\varphi}{\cos^2\varphi+\alpha_1(t)^2\sin^2\varphi}}\\ \sqrt{\frac{\sqrt{\cos^2\varphi+\alpha_2(t)^2\sin^2\varphi}+\cos\varphi}{\cos^2\varphi+\alpha_2(t)^2\sin^2\varphi}}\end{pmatrix}+$$
$$+\sqrt{r}\begin{pmatrix}-B_0^{(1)}(t) & \frac{(1+\alpha_2(t)^2)}{2}B_0^{(1)}(t)\\ \frac{(1+\alpha_2(t)^2)}{2}B_0^{(2)}(t) & B_0^{(2)}(t)\end{pmatrix}\begin{pmatrix}\sqrt{\frac{\sqrt{\cos^2\varphi+\alpha_1(t)^2\sin^2\varphi}-\cos\varphi}{\cos^2\varphi+\alpha_1(t)^2\sin^2\varphi}}\\ \sqrt{\frac{\sqrt{\cos^2\varphi+\alpha_2(t)^2\sin^2\varphi}-\cos\varphi}{\cos^2\varphi+\alpha_2(t)^2\sin^2\varphi}}\end{pmatrix}. \tag{5.100}$$

Note that we have actually find how the eigenfunctions look like. They include the eigenfunctions for the both modes, I and II.
We exclude the situation where the crack propagates with the Rayleigh wave speed of the

elastic material. That means, we exclude the nontrivial solution of:

$$D := 4\,\alpha_1(t)\,\alpha_2(t) - (1+\alpha_2(t)^2)^2 = 0. \tag{5.101}$$

The equation (5.101) is called the *Rayleigh wave equation*. The velocity c_R at which Rayleigh waves propagate over an isotropic and elastic surface is the nontrivial root of the equation (5.101). For some other details we refer the reader to (5.118) and Figure 5.3.

The situation $h'(t) = 0$ is included in the continuity conditions.
$B_0^{(1)}(t)$ and $B_0^{(2)}(t)$ are real functions of time t.

Now we can set

$$B_0^{(1)}(t) = 0, \quad B_0^{(2)}(t) = -\frac{2\alpha_1(t)}{\mu\, D} \tag{5.102}$$

we obtain

$$\sigma_{22}(r,\varphi) = -\frac{\left(1+\alpha_2^2\right)^2}{D\,\sqrt{2r}}\left\{\sqrt{\frac{\sqrt{\cos^2\varphi+\alpha_1(t)^2\sin^2\varphi}+\cos\varphi}{\cos^2\varphi+\alpha_1(t)^2\sin^2\varphi}} - \frac{4\,\alpha_1\,\alpha_2}{\left(1+\alpha_2^2\right)^2}\sqrt{\frac{\sqrt{\cos^2\varphi+\alpha_2(t)^2\sin^2\varphi}+\cos\varphi}{\cos^2\varphi+\alpha_2(t)^2\sin^2\varphi}}\right\}. \tag{5.103}$$

$$\sigma_{12}(r,\varphi) = \frac{2\alpha_1\,\left(1+\alpha_2^2\right)}{D\,\sqrt{2r}}\left\{\sqrt{\frac{\sqrt{\cos^2\varphi+\alpha_1(t)^2\sin^2\varphi}-\cos\varphi}{\cos^2\varphi+\alpha_1(t)^2\sin^2\varphi}} - \sqrt{\frac{\sqrt{\cos^2\varphi+\alpha_2(t)^2\sin^2\varphi}-\cos\varphi}{\cos^2\varphi+\alpha_2(t)^2\sin^2\varphi}}\right\}. \tag{5.104}$$

They verify that $\sigma_{12}(r,\pm\pi) = 0$ and $\sigma_{22}(r,\pm\pi) = 0$.

Then we seek the corresponding singular displacement field for the given election (5.102). It has the form:

$$S_N^1(x,t)_1 = \frac{(1+\alpha_2(t)^2)\,\sqrt{2r}}{\mu\, D}\left[\sqrt{\frac{\sqrt{\cos^2\varphi+\alpha_1(t)^2\sin^2\varphi}+\cos\varphi}{\cos^2\varphi+\alpha_1(t)^2\sin^2\varphi}} - \frac{2\,\alpha_1(t)\,\alpha_2(t)}{(1+\alpha_2(t)^2)}\sqrt{\frac{\sqrt{\cos^2\varphi+\alpha_2(t)^2\sin^2\varphi}+\cos\varphi}{\cos^2\varphi+\alpha_2(t)^2\sin^2\varphi}}\right],$$

$$S_N^1(x,t)_2 = \frac{(1+\alpha_2(t)^2)\,\sqrt{2r}}{\mu\, D}\left[-\alpha_1(t)\sqrt{\frac{\sqrt{\cos^2\varphi+\alpha_1(t)^2\sin^2\varphi}-\cos\varphi}{\cos^2\varphi+\alpha_1(t)^2\sin^2\varphi}} + \frac{2\,\alpha_1(t)}{(1+\alpha_2(t)^2)}\sqrt{\frac{\sqrt{\cos^2\varphi+\alpha_2(t)^2\sin^2\varphi}-\cos\varphi}{\cos^2\varphi+\alpha_2(t)^2\sin^2\varphi}}\right].$$

We set now

$$B_0^{(2)}(t) = 0, \quad B_0^{(1)}(t) = -\frac{2\alpha_2(t)}{\mu\, D}. \tag{5.105}$$

We obtain

$$\sigma_{22}(r,\varphi)=\frac{2\alpha_2\ (1+\alpha_2^2)}{D\sqrt{2r}}\left\{\sqrt{\frac{\sqrt{\cos^2\varphi+\alpha_1(t)^2\sin^2\varphi}-\cos\varphi}{\cos^2\varphi+\alpha_1(t)^2\sin^2\varphi}}-\sqrt{\frac{\sqrt{\cos^2\varphi+\alpha_2(t)^2\sin^2\varphi}-\cos\varphi}{\cos^2\varphi+\alpha_2(t)^2\sin^2\varphi}}\right\}. \tag{5.106}$$

$$\sigma_{12}(r,\varphi)=\frac{1}{D\sqrt{2r}}\left\{4\alpha_1\ \alpha_2\sqrt{\frac{\sqrt{\cos^2\varphi+\alpha_1(t)^2\sin^2\varphi}+\cos\varphi}{\cos^2\varphi+\alpha_1(t)^2\sin^2\varphi}}-(1+\alpha_2^2)\sqrt{\frac{\sqrt{\cos^2\varphi+\alpha_2(t)^2\sin^2\varphi}+\cos\varphi}{\cos^2\varphi+\alpha_2(t)^2\sin^2\varphi}}\right\}. \tag{5.107}$$

with the corresponding singular displacement field according to (5.105):

$$S_N^2(x,t)_1=\frac{2\,\alpha_2(t)\,r^{\frac{1}{2}}}{\mu\,D}\left[\sqrt{\frac{\sqrt{\cos^2\varphi+\alpha_1(t)^2\sin^2\varphi}-\cos\varphi}{\cos^2\varphi+\alpha_1(t)^2\sin^2\varphi}}-\frac{(1+\alpha_2(t)^2)}{2}\sqrt{\frac{\sqrt{\cos^2\varphi+\alpha_2(t)^2\sin^2\varphi}-\cos\varphi}{\cos^2\varphi+\alpha_2(t)^2\sin^2\varphi}}\right]$$

$$S_N^2(x,t)_2=\frac{r^{\frac{1}{2}}}{\mu\,D}\left[2\,\alpha_1(t)\,\alpha_2(t)\sqrt{\frac{\sqrt{\cos^2\varphi+\alpha_1(t)^2\sin^2\varphi}+\cos\varphi}{\cos^2\varphi+\alpha_1(t)^2\sin^2\varphi}}-(1+\alpha_2(t)^2)\sqrt{\frac{\sqrt{\cos^2\varphi+\alpha_2(t)^2\sin^2\varphi}+\cos\varphi}{\cos^2\varphi+\alpha_2(t)^2\sin^2\varphi}}\right]$$

The symmetry's properties, (see table 2.1), imply that the singular terms (5.91) correspond to a crack opening mode, i.e. mode I, and (5.92) to a crack shearing mode, i.e. mode II. □

Now, we can write the complete expression for the singular functions in Theorem 13 for the displacement and stress fields in the different configurations, in a neighborhood of the crack tip $h=h(t)$.

Theorem 14. *Given the local transformations (5.48) and (5.49) and let $(r_{z^{(i)}},\varphi_{z^{(i)}}),i=1,2$ be the polar coordinates with center at the crack tip, here 0, and one axis directed along the crack so that $-\pi<\varphi_{z^{(i)}}<\pi$. Let assumptions H1-H3 of Theorem 13 hold. Then the solution of (5.6) admits the decomposition into a regular part and a singular one:*

$$\vec{w}(\vec{z},t)=\vec{w}_R(\vec{z},t)+k_I(t,h,h')S_N^1(\vec{z},t)+k_{II}(t,h,h')S_N^2(\vec{z},t). \tag{5.108}$$

The singular terms are given by:

$$S_N^1(\vec{z},t)=\frac{(1+\alpha_2(t)^2)}{\mu\,D}\sqrt{\frac{2}{\pi}}\begin{pmatrix} r_{z^{(1)}}^{\frac{1}{2}}\cos\left(\frac{\varphi_{z^{(1)}}}{2}\right)-\dfrac{2\,\alpha_1(t)\,\alpha_2(t)}{(1+\alpha_2(t)^2)}r_{z^{(2)}}^{\frac{1}{2}}\cos\left(\frac{\varphi_{z^{(2)}}}{2}\right)\\ -\alpha_1(t)\,r_{z^{(1)}}^{\frac{1}{2}}\sin\left(\frac{\varphi_{z^{(1)}}}{2}\right)+\dfrac{2\,\alpha_1(t)}{(1+\alpha_2(t)^2)}r_{z^{(2)}}^{\frac{1}{2}}\sin\left(\frac{\varphi_{z^{(2)}}}{2}\right)\end{pmatrix}, \tag{5.109}$$

$$S_N^2(\vec{z},t)=\frac{(1+\alpha_2(t)^2)\alpha_2(t)}{\mu\,D}\sqrt{\frac{2}{\pi}}\begin{pmatrix} \dfrac{2}{(1+\alpha_2(t)^2)}r_{z^{(1)}}^{\frac{1}{2}}\sin\left(\frac{\varphi_{z^{(1)}}}{2}\right)-r_{z^{(2)}}^{\frac{1}{2}}\sin\left(\frac{\varphi_{z^{(2)}}}{2}\right)\\ \dfrac{2\alpha_1(t)}{(1+\alpha_2(t)^2)}r_{z^{(1)}}^{\frac{1}{2}}\cos\left(\frac{\varphi_{z^{(1)}}}{2}\right)-\dfrac{1}{\alpha_2(t)}r_{z^{(2)}}^{\frac{1}{2}}\cos\left(\frac{\varphi_{z^{(2)}}}{2}\right)\end{pmatrix}. \tag{5.110}$$

$k_I = k_I(t,h,h')$ *and* $k_{II} = k_{II}(t,h,h')$ *are the dynamic stress intensity factors.*
The regular term $\vec{w}_R$ *is such that each component* $(\vec{u}_i)_R \in C([0,T];H^2(\widetilde{\Omega_0}))$, $i = 1,2$.

Moreover from the decomposition (5.108) for the displacement field follows that there exists a solution for the stress field σ *and admits the decomposition:*

$$\sigma_{ij}(\vec{w},\vec{z}) = \sigma_{ij}(\vec{w}_R,\vec{z}) + k_I(t,h,h')\ \sigma_{ij}(S_N^1(\vec{z},t)) + k_{II}(t,h,h')\ \sigma_{ij}(S_N^2(\vec{z},t)).$$

It is also assumed that the crack does not propagate with the Rayleigh wave speed of the elastic material, then the singular expressions of the stress components around the moving crack tip for any value of instantaneous crack tip speed $h' = h'(t)$ *are given by:*

$$\sigma_{11}(S_N^1(\vec{z},t)) = \frac{1}{\sqrt{2\pi}D}\left[(1-\alpha_2^2+2\alpha_1^2)(1+\alpha_2^2)\, r_{z^{(1)}}^{-\frac{1}{2}}\cos\left(\frac{\varphi_{z^{(1)}}}{2}\right) - 4\alpha_1\,\alpha_2\, r_{z^{(2)}}^{-\frac{1}{2}}\cos\left(\frac{\varphi_{z^{(2)}}}{2}\right)\right], \tag{5.111}$$

$$\sigma_{22}(S_N^1(\vec{z},t)) = -\frac{1}{\sqrt{2\pi}D}\left[(1+\alpha_2^2)^2\, r_{z^{(1)}}^{-\frac{1}{2}}\cos\left(\frac{\varphi_{z^{(1)}}}{2}\right) - 4\,\alpha_1\,\alpha_2\, r_{z^{(2)}}^{-\frac{1}{2}}\cos\left(\frac{\varphi_{z^{(2)}}}{2}\right)\right], \tag{5.112}$$

$$\sigma_{12}(S_N^1(\vec{z},t)) = \frac{1}{\sqrt{2\pi}D}2\alpha_1\ (1+\alpha_2^2)\left[r_{z^{(1)}}^{-\frac{1}{2}}\sin\left(\frac{\varphi_{z^{(1)}}}{2}\right) - r_{z^{(2)}}^{-\frac{1}{2}}\sin\left(\frac{\varphi_{z^{(2)}}}{2}\right)\right]. \tag{5.113}$$

Whereas for the mode II singular field are given by:

$$\sigma_{11}(S_N^2(\vec{z},t)) = -\frac{1}{\sqrt{2\pi}D}2\alpha_2\left[(1-\alpha_2^2+2\alpha_1^2)\, r_{z^{(1)}}^{-\frac{1}{2}}\sin\left(\frac{\varphi_{z^{(1)}}}{2}\right) - (1+\alpha_2^2)\, r_{z^{(2)}}^{-\frac{1}{2}}\sin\left(\frac{\varphi_{z^{(2)}}}{2}\right)\right], \tag{5.114}$$

$$\sigma_{22}(S_N^2(\vec{z},t)) = \frac{1}{\sqrt{2\pi}D}2\alpha_2\ (1+\alpha_2^2)\left[r_{z^{(1)}}^{-\frac{1}{2}}\sin\left(\frac{\varphi_{z^{(1)}}}{2}\right) - r_{z^{(2)}}^{-\frac{1}{2}}\sin\left(\frac{\varphi_{z^{(2)}}}{2}\right)\right], \tag{5.115}$$

$$\sigma_{12}(S_N^2(\vec{z},t)) = \frac{1}{\sqrt{2\pi}D}\left[4\alpha_1\,\alpha_2\, r_{z^{(1)}}^{-\frac{1}{2}}\cos\left(\frac{\varphi_{z^{(1)}}}{2}\right) - (1+\alpha_2^2)\, r_{z^{(2)}}^{-\frac{1}{2}}\cos\left(\frac{\varphi_{z^{(2)}}}{2}\right)\right]. \tag{5.116}$$

$D = 4\,\alpha_1(t)\,\alpha_2(t) - (1+\alpha_2(t)^2)^2$. *The regular term* $\sigma(\vec{w}_R,\vec{z}) \in [H^1(\widetilde{\Omega})]^2$, *for almost all* $t > 0$.

Let us remark that

$$\begin{pmatrix} y_1 \\ y_2 \end{pmatrix} = \begin{pmatrix} R\cos\vartheta \\ R\sin\vartheta \end{pmatrix} = \begin{pmatrix} x_1 + h \\ x_2 \end{pmatrix} = \begin{pmatrix} r\cos\varphi + h \\ r\sin\varphi \end{pmatrix}.$$

with $R = R(t)$, $\vartheta = \vartheta(t)$, $h = h(t)$. It follows

$$r\cos\varphi = R\cos\vartheta - h, \quad r\sin\varphi = R\sin\vartheta. \tag{5.117}$$

Inserting (5.117) into (5.91) and (5.92) we get the singular terms in the current configuration.

Remark 17. *The present expressions for singular stress and displacement fields coincide with those obtained by [73], [20], etc. (in [17], only the expressions for mode I are given). However, to our knowledge, the solutions presented in the literature for stress and*

displacements have been given only in the variable space z, without coming back to the explicit specifications formulated in the current configuration, where the whole mathematical fracture problem is defined.

It should be observed that by simple calculation the terms for dynamic stress and displacement fields given in Theorem 14 indeed reduce to the equivalent well-known results for equilibrium crack tip fields in the same material, at least for the singular term, as the crack speed becomes incrementally small, i.e. $h' \to 0$. *Some care is required in the calculation because both, the term D in the denominator of each expression and each of the quantities in numerator vanish as* $h' \to 0$.

When elastic waves are propagated and transmitted during e.g. blasting or an earthquake phenomenon, they are diffracted at an obstacle or geometric discontinuity and often give rise to a high elevation of local stress. These stress concentrations become extremely severe when the static or moving discontinuity is a crack.
The input waves are diffracted and scattered about the moving crack tip. Regardless of the type of incident waves, whether P- or S-waves, diffraction consists of both P- and S-waves. Hence, the resulting stress field is composed of the stress field of the incident wave and the diffracted P- and S-waves.

For a mathematical description of a propagation of a crack it is most important to reveal the general laws governing the distribution of the stress in a vicinity of the crack tip. We shall make a mathematical idealization for the stress distribution at the crack tip. It is clear that no real material can actually support such a stress distribution.
One of the cornerstone concepts of linear elastic fracture mechanics is the role of the stress intensity factor as a crack tip field characterizing parameter, [71] observed that the elastic stress field near the crack tip has a now familiar form, [30], [8], [67].

The so-called Rayleigh wave equation is given by (5.101). The velocity c_R *at which Rayleigh waves propagate over an isotropic and elastic surface satisfies:*

$$4\sqrt{1-\left(\frac{c_R}{c_1}\right)^2}\sqrt{1-\left(\frac{c_R}{c_2}\right)^2}-\left(2-\left(\frac{c_R}{c_2}\right)^2\right)^2=0 \tag{5.118}$$

The polynomial form of the above equation is

$$\xi^6-8\xi^4+8\left(3-2\frac{\varsigma^2}{\xi^2}\right)\xi^2-16\left(1-\frac{\varsigma^2}{\xi^2}\right)=0$$

where $\xi = \frac{c_R}{c_2}$ *and* $\varsigma = \frac{c_R}{c_1}$, *then* $\frac{\varsigma^2}{\xi^2} = \frac{c_2^2}{c_1^2} = \frac{(1-2\nu)}{2(1-\nu)}$, *(here we used the relation (2.34)).*
It is also possible to write the Rayleigh wave equation in the following way:

$$\left(\frac{c_R}{c_2}\right)^6 - 8\left(\frac{c_R}{c_2}\right)^4 + 8\left(3 - \frac{(1-2\nu)}{(1-\nu)}\right)\left(\frac{c_R}{c_2}\right)^2 - 16\left(1 - \frac{(1-2\nu)}{2(1-\nu)}\right) = 0$$

This equation can be solved numerically for any given isotropic material for $\frac{c_R}{c_2}$. *It has 6 roots, two of them are real, i.e.* $\alpha_1 = \alpha_2 = 1$ *corresponding to* $h' = 0$ *and* c_R. *The other four are complex. For* $0 < \nu < 0.5$ *it follows that* $0.65 < \frac{c_R}{c_2} < 1$.

Matlab Code for the Rayleigh equation.

The Rayleigh velocity has the value $c_R \approx 0.9c_2$, *see [36]*
Here is a MATLAB code, Figure 5.3, that calculates the Rayleigh velocity from the roots of the above

---

```
%Rayleigh-wave characteristic equation for isotropic materials
%
%polycrystalline aluminum
den = 2695;
c11 = 11.1e10;
c44 = 2.5e10;
Cl = sqrt(c11/den);
Ct = sqrt(c44/den);
g = 2*(1-(Ct/Cl)^2);
P = [1 -8 8*g+8 -8*g];%define the characteristic equation
vel = roots(P);% solve
for i = 1:1:3
if(imag(vel(i)) == 0)
velocity = Ct*sqrt(vel(i))%pick the real root, and calculate the velocity
end
end
```

The values for polycrystalline aluminum indicate that the Rayleigh wave velocity is:
velocity =
$2.8499e+03$.

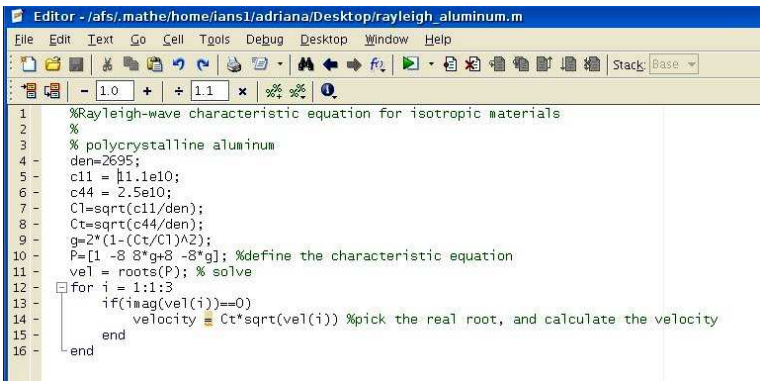

Figure 5.3: Rayleigh-wave characteristic equation for isotropic materials:polycrystalline aluminum

CHAPTER 6

Energy calculations for the in-plane case

6.1 Introduction

In the last section we have dealt with the mechanics of solid bodies containing stationary or propagating cracks, from a mathematical point of view, wherein the effects of inertia are accounted for. In such cases, a knowledge of time-dependent singular stress and displacement fields near the crack tip was essential in understanding the process and nature of fracture.
For getting these fields we have introduced auxiliary potentials ϕ and ψ related to the inplane motion of the crack which are separable into Mode I (opening mode) and Mode II (inplane sliding mode) crack problems.
Once such singular fields near the tip of a propagating crack are determined, other important quantities of relevance in dynamic fracture mechanics, such as dynamic stress intensity factors and dynamic energy release rates can be determined.
In this section we outline the crack tip energy flux in terms of the near tip mechanical fields for the in-plane fracture case.
The importance of the variation of energy measures in the quasistationary crack growth processes was recognized by Griffith and by Irwin in the pioneering discussions of brittle fracture, as outlined in section 2.3. As a first application of the obtained results in chapter 5 about generalized Griffith criterion, we improve here energy Lemmata 20 and 21 for the in-plane fracture case.
We consider now the case in which the crack is dynamically extending through the motion of

the crack tip. Here, generalized Griffith energy balance law is to use. At any instant of time t the rate of the total energy of the problem (5.6) is given by,

$$\hat{\Pi}(t) = \dot{D}(t) + \dot{E}(t) - \hat{A}(t) + \dot{K}(t)$$

with the rate of the elastic energy $\dot{E}$, the external energy $\hat{A}$ and the rate of the kinetic energy $\dot{K}$ defined as (6.2), (6.3), (6.4) for each solution $\vec{u} = \vec{u}(y,t)$ of the problem (5.6), respectively. $\dot{D} = \frac{d}{dt}D$ is then the rate of dissipative energy. The arguments in section 4.3.1, where similar results are proved for linear fracture mechanics in mode III, have to be transferred to our case. This offers a new perspective of the dynamic crack growth problem in elastic materials.

An energy balance law holds if

$$\hat{\Pi}(t) = 0$$

that means, (6.1) holds:

$$\dot{D}(t) = -\dot{E}(t) + \hat{A}(t) - \dot{K}(t). \tag{6.1}$$

First, an expression for crack tip energy flux, defined in the more mathematically convenient reference configuration, is obtained by application of Reynolds's transport Theorem 1 and the divergence theorem. The derived expression for the crack tip energy flux is valid for general material response. Then for the particular case for mode I fracture for which some expression for the fracture toughness is given, (see (4.49)). Assuming small-scale yielding, rate independent behaviour under monotonically increasing stress intensity factors, an equation of motion of the crack tip is written.
We define the energies:

Definition 10. *If $u = u(y,t)$ is a solution of problem (5.6), then*

$$\dot{E}(t) = \frac{1}{2}\frac{d}{dt}\int_{\Omega_t} \sigma(\vec{u}) : \varepsilon(\vec{u})\, dy \tag{6.2}$$

is the rate of the elastic energy;

$$\hat{A}(t) = \int_{\Omega_t} \rho\, \vec{f} \cdot \vec{u}_t \, dy + \int_{\Gamma_N} \rho\, \vec{q} \cdot \vec{u}_t \, ds, \tag{6.3}$$

denotes the external energy and

$$\dot{K}(t) = \frac{d}{dt}\int_{\Omega_t} \frac{1}{2}\rho\, |\vec{u}_t|^2 \, dy \tag{6.4}$$

is the rate of the kinetic energy.
D is the dissipative energy and it characterises the energy which is spent for irreversible processes. There may be a complex process zone at the crack tip, where the material is plastically deformed, voids may be nucleated, there may be chemical reactions. All these processes involve dissipation of energy.

Let be $\Omega_t^\delta = \Omega_t \backslash \overline{M_t^\delta}$, where $\{M_t^\delta\}_\delta$ is a family of small neighborhoods of the running crack tip in the actual configuration such that

$$\lim_{\delta \to 0} M_t^\delta = \{(h(t), 0)\}.$$

We denote by C_t^δ the boundary curves of M_t^δ, see Fig.6.1. Here M_t^δ are so chosen, that $F^{-1}(M_t^\delta) = B_0^\delta$ are circles in the reference configuration.

We consider the energy flux in Ω_t^δ:

$$\dot{D^\delta}(t) = -\dot{E^\delta}(t) + \hat{A^\delta}(t) - \dot{K^\delta}(t), \quad (6.5)$$

where the energies are defined analogously to (6.1), (6.2), $\cdots$,(6.4) as integrals on Ω_t^δ.

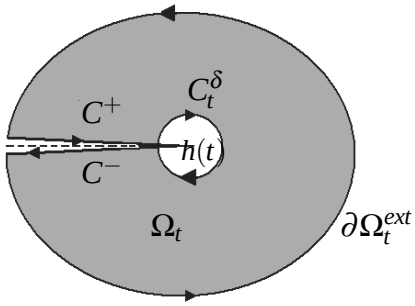

Figure 6.1: A family of annular domains cutting out the running crack $h(t)$.

Lemma 20. *The following identity holds:*

$$\begin{aligned}
\hat{A^\delta}(t) - \dot{E^\delta}(t) - \dot{K^\delta}(t) &= -\frac{1}{2}\int_{\Omega_t^\delta} div\left[\left(\rho\,|\vec{u}_t|^2 + \sigma(\vec{u}) : \varepsilon(\vec{u})\right)\frac{\partial y}{\partial t}\right] dy \\
&\quad - \int_{C_t^\delta}\Big((\lambda+\mu)(\nabla\cdot\vec{u})n + \mu(\nabla\vec{u})n\Big)\cdot\partial_t\vec{u}\,ds_y \\
&= -\frac{1}{2}\int_{\partial\Omega_t^\delta}\left[\left(\rho\,|\vec{u}_t|^2 + \sigma(\vec{u}) : \varepsilon(\vec{u})\right)\frac{\partial y}{\partial t}\right]\cdot n_y\,ds_y + \\
&\quad - \int_{C_t^\delta}\Big((\lambda+\mu)(\nabla\cdot\vec{u})n + \mu(\nabla\vec{u})n\Big)\cdot\partial_t\vec{u}\,ds_y. \qquad (6.6)
\end{aligned}$$

where $y(t) = y(x,t) = F_t(x) = x + h(t)\,\theta(x)$ and the displacement field $\vec{u}$ solves the initial boundary value problem (5.6).

Proof. We start with the Navier Lamé equation

$$\rho\ddot{\vec{u}} - (\lambda+\mu)\nabla(\nabla\cdot\vec{u}) - \mu\nabla^2\vec{u} = \rho\vec{f} \quad \text{in} \quad \Omega_t \qquad (6.7)$$

and consider the restriction u^δ of u to Ω_t^δ. We remark that u^δ is smooth enough in Ω_t^δ in order to apply partial integration and the formula of Gauss.

Multiplication of (6.7) with $\partial_t u^\delta$ and integration on Ω_t^δ yield

$$\int_{\Omega_t^\delta} \left(\rho \ddot{\vec{u}}^\delta \cdot \partial_t \vec{u}^\delta - (\lambda+\mu)\nabla(\nabla\cdot\vec{u}^\delta)\cdot\partial_t\vec{u}^\delta - \mu\nabla^2\vec{u}^\delta\cdot\partial_t\vec{u}^\delta \right) dy = \int_{\Omega_t^\delta} \rho\,\vec{f}\cdot\partial_t\,\vec{u}^\delta\,dy.$$

We have:

$$\int_{\Omega_t^\delta} \left(\frac{1}{2}\frac{\partial}{\partial t}\left(\rho|\vec{u_t}^\delta|^2\right) + (\lambda+\mu)\,(\nabla\cdot\vec{u}^\delta)\cdot(\nabla\cdot\partial_t\vec{u}^\delta) + \mu\,(\nabla\vec{u}^\delta)\cdot(\nabla\partial_t\vec{u}^\delta) \right) dy +$$
$$- \int_{\partial\Omega_t^\delta=\partial\Omega_t^{ext}\cup C_t^\delta\cup C^+\cup C^-} \left((\lambda+\mu)(\nabla\cdot\vec{u}^\delta)n\cdot\partial_t\vec{u}^\delta + \mu(\nabla\vec{u}^\delta)n\cdot\partial_t\vec{u}^\delta \right) ds_y = \int_{\Omega_t^\delta} \rho\,\vec{f}\cdot\partial_t\,\vec{u}^\delta\,dy.$$

Therefore,

$$\int_{\Omega_t^\delta} \frac{1}{2}\left(\frac{\partial}{\partial t}\left(\rho\,|\vec{u_t}^\delta|^2\right) + (\lambda+\mu)\,\frac{\partial}{\partial t}\left(\nabla\cdot\vec{u}^\delta\right)^2 + \mu\frac{\partial}{\partial t}\left(\nabla\vec{u}^\delta\right)^2 \right) dy =$$
$$\int_{\Omega_t^\delta} \rho\,\vec{f}\cdot\partial_t\,\vec{u}^\delta\,dy + \int_{\partial\Omega_t^\delta=\partial\Omega_t^{ext}\cup C_t^\delta\cup C^+\cup C^-} \left((\lambda+\mu)(\nabla\cdot\vec{u}^\delta)n + \mu(\nabla\vec{u}^\delta)n \right)\cdot\partial_t\vec{u}^\delta\,ds_y =$$
$$\int_{\Omega_t^\delta} \rho\,\vec{f}\cdot\partial_t\,\vec{u}^\delta\,dy + \int_{\Gamma_N} \rho\,\vec{q}\cdot\partial_t\vec{u}^\delta\,ds_y + \int_{\Gamma_D} \left((\lambda+\mu)(\nabla\cdot\vec{u}^\delta)n + \mu(\nabla\vec{u}^\delta)n \right)\cdot\partial_t\vec{u}^\delta\,ds_y +$$
$$+ \int_{C_t^\delta} \left((\lambda+\mu)(\nabla\cdot\vec{u}^\delta)n + \mu(\nabla\vec{u}^\delta)n \right)\cdot\partial_t\vec{u}^\delta\,ds_y.$$

We note that:

$$\int_{\Gamma_D} \left((\lambda+\mu)(\nabla\cdot\vec{u}^\delta)n + \mu(\nabla\vec{u}^\delta)n \right)\cdot\partial_t\vec{u}^\delta\,ds_y = 0$$

because $\vec{u}(t,y) = 0$ on Γ_D therefore $\partial_t\vec{u}^\delta|_{\Gamma_D} = 0$ and also

$$\int_{C^+} \left((\lambda+\mu)(\nabla\cdot\vec{u}^\delta)n + \mu(\nabla\vec{u}^\delta)n \right)\cdot\partial_t\vec{u}^\delta\,ds_y = -\int_{C^-} \left((\lambda+\mu)(\nabla\cdot\vec{u}^\delta)n + \mu(\nabla\vec{u}^\delta)n \right)\cdot\partial_t\vec{u}^\delta\,ds_y.$$

It follows:

$$\begin{aligned} &\frac{1}{2}\int_{\Omega_t^\delta} \frac{\partial}{\partial t}\left(\rho\,|\vec{u_t}^\delta|^2 + \sigma(\vec{u}^\delta) : \varepsilon(\vec{u}^\delta) \right) dy = \\ &\hat{A}^\delta(t) + \int_{C_t^\delta} \left((\lambda+\mu)(\nabla\cdot\vec{u}^\delta)n + \mu(\nabla\vec{u}^\delta)n \right)\cdot\partial_t\vec{u}^\delta\,ds_y. \end{aligned} \tag{6.8}$$

From Reynolds' transport theorem we get (here we set $\vec{u}^\delta = \vec{u}$ in Ω_t^δ):

$$
\begin{aligned}
&\dot{E}^\delta(t) + \dot{K}^\delta(t) = \frac{1}{2}\frac{\partial}{\partial t}\int_{\Omega_t^\delta} \left(\rho\,|\vec{u}_t|^2 + \sigma(\vec{u}) : \varepsilon(\vec{u})\right) dy \\
&= \frac{1}{2}\int_{\Omega_t^\delta} \frac{\partial}{\partial t}\left[\left(\rho\,|\vec{u}_t|^2\right) + \sigma(\vec{u}) : \varepsilon(\vec{u})\right] dy + \frac{1}{2}\int_{\Omega_t^\delta} \operatorname{div}\left[\left(\rho\,|\vec{u}_t|^2 + \sigma(\vec{u}) : \varepsilon(\vec{u})\right)\frac{\partial y}{\partial t}\right] dy \\
&= \hat{A}^\delta(t) + \int_{C_t^\delta}\Big((\lambda+\mu)(\nabla\cdot\vec{u})n + \mu(\nabla\vec{u})n\Big)\cdot\partial_t\vec{u}\,ds_y + \\
&+ \frac{1}{2}\int_{\Omega_t^\delta} \operatorname{div}\left[\left(\rho\,|\vec{u}_t|^2 + \sigma(\vec{u}) : \varepsilon(\vec{u})\right)\frac{\partial y}{\partial t}\right] dy \\
&= \hat{A}^\delta(t) + \int_{C_t^\delta}\Big((\lambda+\mu)(\nabla\cdot\vec{u})n + \mu(\nabla\vec{u})n\Big)\cdot\partial_t\vec{u}\,ds_y + \\
&+ \frac{1}{2}\int_{\partial\Omega_t^\delta} \left[\left(\rho\,|\vec{u}_t|^2 + \sigma(\vec{u}) : \varepsilon(\vec{u})\right)\frac{\partial y}{\partial t}\right]\cdot n_y\,ds_y.
\end{aligned}
$$

Here we have used (6.8). It follows (6.6). □

6.1.1 The limit procedure $\delta \to 0$

We calculate the limit for $\delta \to 0$ of the right hand side of (6.6) transforming both integrals to the reference domain $\Omega_0^\delta = \Omega_0 \backslash \overline{B_\delta}$ in space coordinate $\vec{x}$ and then in the $\vec{z}$ space, where the calculations and computations are easier.

Lemma 21. *For the right hand side of (6.6) there holds:*

$$
\begin{aligned}
&\lim_{\delta\to 0}\{-\frac{1}{2}\int_{\partial\Omega_t^\delta}\left[\left(\rho\,|\vec{u}_t|^2 + \sigma(\vec{u}) : \varepsilon(\vec{u})\right)\frac{\partial y}{\partial t}\right]\cdot n_y\,ds_y\} + \\
&+ \lim_{\delta\to 0}\{-\int_{C_t^\delta}\Big((\lambda+\mu)(\nabla\cdot\vec{u})n + \mu(\nabla\vec{u})n\Big)\cdot\partial_t\vec{u}\,ds_y\} \\
&= \frac{h'(t)}{2\mu}\left[\frac{\left(1-\alpha_2(t)^2\right)\left(\alpha_1(t)\,k_1^2(t,h,h') + \alpha_2(t)\,k_2^2(t,h,h')\right)}{4\,\alpha_1(t)\,\alpha_2(t) - (1+\alpha_2(t)^2)^2}\right]
\end{aligned}
\tag{6.9}
$$

Proof. We start with the integral

$$
\begin{aligned}
I_1^\delta &= -\frac{1}{2}\int_{\Omega_t^\delta} \operatorname{div}\left[\left(\rho\,|\vec{u}_t|^2 + \sigma(\vec{u}) : \varepsilon(\vec{u})\right)\frac{\partial y}{\partial t}\right] dy \\
&= -\frac{1}{2}\int_{\partial\Omega_t^\delta}\left[\left(\rho\,|\vec{u}_t|^2 + \sigma(\vec{u}) : \varepsilon(\vec{u})\right)\frac{\partial y}{\partial t}\right]\cdot n_y\,ds_y \\
&= -\frac{1}{2}\int_{\partial\Omega_t^\delta}\left[\left(\rho\,|\vec{u}_t|^2 + (\lambda+\mu)\,(\nabla\cdot\vec{u})^2 + \mu\,(\nabla\vec{u})^2\right)\frac{\partial y}{\partial t}\right]\cdot n_y\,ds_y.
\end{aligned}
\tag{6.10}
$$

We transform the boundary integral (6.10) to the boundary of the reference configuration $\partial\Omega_0^\delta$. We recall that

$$y = \begin{pmatrix} x_1 \\ x_2 \end{pmatrix} + h(t) \begin{pmatrix} \eta\,(x) \\ 0 \end{pmatrix}$$

where η is a cut-off function with support in a neighborhood of the crack tip $\{(0,0)\}$.
After some calculations, we get

$$\begin{aligned} I_1^\delta = &- \frac{h'(t)}{2} \int_{\partial\Omega^\delta} \rho\, |\partial_t \vec{v} - \frac{h'(t)\,\eta\,\partial_1 \vec{v}}{1+h(t)\,\partial_1 \eta}|^2 \begin{pmatrix} \eta\,(x) \\ 0 \end{pmatrix} \cdot n_x\, ds_x + \\ &- \frac{h'(t)}{2} \int_{\partial\Omega^\delta} \left[\frac{(\lambda+\mu)}{(\det \nabla_x (F_t(x)))^2} \left(\nabla \cdot \vec{v}\right)^2 + \mu \left(\left(\nabla_x F_t(\vec{x})\right)^{-1} \right)^2 \left(\nabla_x \vec{v}\right)^2 \right] \begin{pmatrix} \eta\,(x) \\ 0 \end{pmatrix} \cdot n_x\, ds_x. \end{aligned}$$

Note that η vanishes on $\partial\Omega_\delta^{ext}$ and that the first component $n_{x_1} = n_1$ of the normal vector vanishes on the crack $\sigma_0^\pm$. Therefore, we have

$$\begin{aligned} I_1 = \lim_{\delta\to 0} I_1^\delta = \lim_{\delta\to 0} &- \frac{h'(t)}{2} \int_{\partial B_\delta} \rho\, |\partial_t \vec{v} - \frac{h'(t)\,\eta\,\partial_1 \vec{v}}{1+h(t)\,\partial_1 \eta}|^2\, \eta\, n_1\, ds_x + \\ &+ \lim_{\delta\to 0} - \frac{h'(t)}{2} \int_{\partial B_\delta} \left[(\lambda+\mu) \left(\nabla \cdot \vec{v}\right)^2 + \mu \left(\nabla_x \vec{v}\right)^2 \right] \eta\, n_1\, ds_x. \end{aligned}$$

Therefore

$$I_1 = - \frac{h'(t)}{2} \lim_{\delta\to 0} \int_{\partial B_\delta} \left[\rho\, |\partial_t \vec{v} - \frac{h'(t)\,\eta\,\partial_1 \vec{v}}{1+h(t)\,\partial_1 \eta}|^2 + \sigma(\vec{v}) : \varepsilon(\vec{v}) \right] \eta\, n_1\, ds_x.$$

where n_x are the components of the unit outward normal, i.e. $n_x = \begin{pmatrix} n_1 \\ n_2 \end{pmatrix} = - \begin{pmatrix} \cos\varphi \\ \sin\varphi \end{pmatrix}$.
Now we transform the boundary integral to one with respect to the space variable $\vec{z}$.
We recall that

$$\begin{pmatrix} x_1 \\ x_2 \end{pmatrix} = \begin{pmatrix} z_1^{(1)} \\ \frac{z_2^{(1)}}{\alpha_1(t)} \end{pmatrix} = \begin{pmatrix} z_1^{(2)} \\ \frac{z_2^{(2)}}{\alpha_2(t)} \end{pmatrix}.$$

Furthermore, we use (5.108), i.e.:

$$\vec{w}(\vec{z},t) = \vec{w}_R(\vec{z},t) + k_I(t,h,h') S_N^1(\vec{z},t) + k_{II}(t,h,h') S_N^2(\vec{z},t) := \vec{w}_R + \widehat{w}_S,$$

where $S_N^1(\vec{z},t)$ and $S_N^2(\vec{z},t)$ are given by Theorem 14, i.e.:

$$S_N^1(\vec{z},t) = \frac{(1+\alpha_2(t)^2)}{\mu D}\sqrt{\frac{2}{\pi}}\begin{pmatrix} r_{z^{(1)}}^{\frac{1}{2}}\cos\left(\frac{\varphi_{z^{(1)}}}{2}\right) - \dfrac{2\,\alpha_1(t)\,\alpha_2(t)}{(1+\alpha_2(t)^2)}\, r_{z^{(2)}}^{\frac{1}{2}}\cos\left(\frac{\varphi_{z^{(2)}}}{2}\right) \\ -\alpha_1(t)\, r_{z^{(1)}}^{\frac{1}{2}}\sin\left(\frac{\varphi_{z^{(1)}}}{2}\right) + \dfrac{2\,\alpha_1(t)}{(1+\alpha_2(t)^2)}\, r_{z^{(2)}}^{\frac{1}{2}}\sin\left(\frac{\varphi_{z^{(2)}}}{2}\right)\end{pmatrix},$$

$$S_N^2(\vec{z},t) = \frac{(1+\alpha_2(t)^2)\alpha_2(t)}{\mu D}\sqrt{\frac{2}{\pi}}\begin{pmatrix} \dfrac{2}{(1+\alpha_2(t)^2)}\, r_{z^{(1)}}^{\frac{1}{2}}\sin\left(\frac{\varphi_{z^{(1)}}}{2}\right) - r_{z^{(2)}}^{\frac{1}{2}}\sin\left(\frac{\varphi_{z^{(2)}}}{2}\right) \\ \dfrac{2\alpha_1(t)}{(1+\alpha_2(t)^2)}\, r_{z^{(1)}}^{\frac{1}{2}}\cos\left(\frac{\varphi_{z^{(1)}}}{2}\right) - \dfrac{1}{\alpha_2(t)} r_{z^{(2)}}^{\frac{1}{2}}\cos\left(\frac{\varphi_{z^{(2)}}}{2}\right)\end{pmatrix}.$$

It is worthwhile to study the limits of the integrals as $\delta \to 0$ due to the fact that the limit value of the integrals on expressions of $\vec{w}_R$ vanishes and the singular functions S_N^1 and S_N^2 behave with respect to δ as follows:

$$S_N^i \sim \delta^{\frac{1}{2}}, \quad \partial_t S_N^i \sim \delta^{\frac{1}{2}}, \quad \partial_1 S_N^i \sim \delta^{-\frac{1}{2}}, \quad \partial_2 S_N^i \sim \delta^{-\frac{1}{2}}, \quad i = 1,2.$$

Thus the limit of this integral is seen to exist if one considers ∂B_δ to be a circle of radius δ. We assume that δ is small enough that $\eta \equiv 1$ on $\overline{B_\delta}$, then we get the following relation:

$$I_1 = -\frac{h'(t)}{2}\lim_{\delta\to 0}\ \delta\int_{-\pi}^{\pi}\left[\rho\ |\partial_t \widehat{w_S} - h'\partial_1\widehat{w_S}|^2 + \sigma(\widehat{w_S}) : \varepsilon(\widehat{w_S})\right]\ n_1\, ds.$$

Therefore,

$$\begin{aligned} I_1 = \lim_{\delta\to 0} I_1^\delta &= -\frac{h'(t)}{2}\ \int_{-\pi}^{\pi}\left[\rho\ h'(t)^2\ |\partial_1\widehat{w_S}|^2\ +\ \sigma(\widehat{w_S}) : \varepsilon(\widehat{w_S})\right]\ n_1\, ds \\ &= \frac{h'(t)}{2}\ \int_{-\pi}^{\pi}\left[\rho\ h'(t)^2\ |\partial_1\widehat{w_S}|^2\ +\ \sigma(\widehat{w_S}) : \varepsilon(\widehat{w_S})\right]\cos\varphi\, d\varphi \\ &= h'(t)\ \int_{0}^{\pi}\left[\rho\ h'(t)^2\ |\partial_1\widehat{w_S}|^2\ +\ \sigma(\widehat{w_S}) : \varepsilon(\widehat{w_S})\right]\cos\varphi\, d\varphi \end{aligned}$$

Now, we consider the second integral of (6.9)

$$\begin{aligned} I_2^\delta &= -\int_{C_t^\delta}\Big((\lambda+\mu)(\nabla\cdot\vec{u})n + \mu(\nabla\vec{u})n\Big)\cdot\partial_t\vec{u}\, ds_y, \\ &= -\int_{C_t^\delta}\sigma(\vec{u})n_y\ \cdot\partial_t\ \vec{u}\, ds_y \end{aligned}$$

We transform it to the reference configuration and consider δ so small that $\eta \equiv 1$ on $\overline{B_\delta}$, then it follows

$$I_2^\delta = -\int_{\partial B^\delta}\sigma(\vec{v})\frac{n_x}{|n_x|}\cdot\left(\partial_t\vec{v} - h'\partial_1\vec{v}\right)\mathrm{d}s_x. \tag{6.11}$$

As before, we transform it into space variables $\vec{z}$, where we split $\vec{w}$, as

$$\vec{w} = \vec{w}_R + \widehat{w_S},$$

and repeat the arguments for the behaviour of the terms $\vec{w}_R$ and $\widehat{w_S}$ with respect to δ.
Then (6.11) can be written as:

$$I_2 = \lim_{\delta \to 0} I_2^\delta = h' \int_{\partial B^\delta} \sigma(\widehat{w_S}) n \cdot \partial_1 \widehat{w_S} \mathrm{d}s_x, \tag{6.12}$$

$\sigma_{ij}\, n_j$ is the surface traction.
Since $\begin{pmatrix} n_1 \\ n_2 \end{pmatrix} = - \begin{pmatrix} \cos\varphi \\ \sin\varphi \end{pmatrix}$, we get from (6.12)

$$I_2 = \lim_{\delta \to 0} I_2^\delta = -h'(t) \int_{-\pi}^{\pi} (\sigma_{i1} \cos\varphi + \sigma_{i2} \sin\varphi) \cdot \partial_1 \widehat{w_S}\, d\varphi. \tag{6.13}$$

The necessary calculations for integrations can be summarized as follows.
For the given expressions for $\vec{w}_{\text{sing}}$ the first derivatives are obtained as:

$$\partial_1 S_N^1 = \frac{(1+\alpha_2(t)^2)}{\mu D \sqrt{2\pi}} \begin{pmatrix} r_{z^{(1)}}^{-\frac{1}{2}} \cos\left(\frac{\varphi_{z^{(1)}}}{2}\right) - \frac{2\,\alpha_1(t)\,\alpha_2(t)}{(1+\alpha_2(t)^2)} r_{z^{(2)}}^{-\frac{1}{2}} \cos\left(\frac{\varphi_{z^{(2)}}}{2}\right) \\ \alpha_1(t)\, r_{z^{(1)}}^{-\frac{1}{2}} \sin\left(\frac{\varphi_{z^{(1)}}}{2}\right) - \frac{2\,\alpha_1(t)}{(1+\alpha_2(t)^2)} r_{z^{(2)}}^{-\frac{1}{2}} \sin\left(\frac{\varphi_{z^{(2)}}}{2}\right) \end{pmatrix}, \tag{6.14}$$

$$\partial_1 S_N^2 = \frac{(1+\alpha_2(t)^2)\alpha_2(t)}{\mu D \sqrt{2\pi}} \begin{pmatrix} -\frac{2}{(1+\alpha_2(t)^2)} r_{z^{(1)}}^{-\frac{1}{2}} \sin\left(\frac{\varphi_{z^{(1)}}}{2}\right) + r_{z^{(2)}}^{-\frac{1}{2}} \sin\left(\frac{\varphi_{z^{(2)}}}{2}\right) \\ \frac{2\alpha_1(t)}{(1+\alpha_2(t)^2)} r_{z^{(1)}}^{-\frac{1}{2}} \cos\left(\frac{\varphi_{z^{(1)}}}{2}\right) - \frac{1}{\alpha_2(t)} r_{z^{(2)}}^{-\frac{1}{2}} \cos\left(\frac{\varphi_{z^{(2)}}}{2}\right) \end{pmatrix}, \tag{6.15}$$

and moreover

$$\partial_2 S_N^1 = \frac{(1+\alpha_2(t)^2)}{\mu D \sqrt{2\pi}} \begin{pmatrix} \alpha_1(t)\, r_{z^{(1)}}^{-\frac{1}{2}} \sin\left(\frac{\varphi_{z^{(1)}}}{2}\right) - \frac{2\,\alpha_1(t)\,\alpha_2(t)^2}{(1+\alpha_2(t)^2)} r_{z^{(2)}}^{-\frac{1}{2}} \sin\left(\frac{\varphi_{z^{(2)}}}{2}\right) \\ -\alpha_1(t)^2 r_{z^{(1)}}^{-\frac{1}{2}} \cos\left(\frac{\varphi_{z^{(1)}}}{2}\right) + \frac{2\,\alpha_1(t)\,\alpha_2(t)}{(1+\alpha_2(t)^2)} r_{z^{(2)}}^{-\frac{1}{2}} \cos\left(\frac{\varphi_{z^{(2)}}}{2}\right) \end{pmatrix}, \tag{6.16}$$

$$\partial_2 S_N^2 = \frac{(1+\alpha_2(t)^2)\alpha_2(t)}{\mu D \sqrt{2\pi}} \begin{pmatrix} \frac{2\,\alpha_1(t)}{(1+\alpha_2(t)^2)} r_{z^{(1)}}^{-\frac{1}{2}} \cos\left(\frac{\varphi_{z^{(1)}}}{2}\right) - \alpha_2(t) r_{z^{(2)}}^{-\frac{1}{2}} \cos\left(\frac{\varphi_{z^{(2)}}}{2}\right) \\ \frac{2\alpha_1(t)^2}{(1+\alpha_2(t)^2)} r_{z^{(1)}}^{-\frac{1}{2}} \sin\left(\frac{\varphi_{z^{(1)}}}{2}\right) - r_{z^{(2)}}^{-\frac{1}{2}} \sin\left(\frac{\varphi_{z^{(2)}}}{2}\right) \end{pmatrix}. \tag{6.17}$$

We make also the following transformations:

$$h_1 := \frac{1}{r_{z^{(1)}}}\,\cos^2\left(\frac{\varphi_{z^{(1)}}}{2}\right) = \frac{1}{2r}\left(\frac{\sqrt{\cos^2\varphi+\alpha_1(t)^2\sin^2\varphi}+\cos\varphi}{\cos^2\varphi+\alpha_1(t)^2\sin^2\varphi}\right) = \frac{1}{2r}\,(\text{even part}+\text{odd part})$$

$$h_2 := \frac{1}{r_{z^{(2)}}}\,\cos^2\left(\frac{\varphi_{z^{(2)}}}{2}\right) = \frac{1}{2r}\left(\frac{\sqrt{\cos^2\varphi+\alpha_2(t)^2\sin^2\varphi}+\cos\varphi}{\cos^2\varphi+\alpha_2(t)^2\sin^2\varphi}\right) = \frac{1}{2r}\,(\text{even part}+\text{odd part})$$

$$h_3 := \frac{1}{r_{z^{(1)}}}\,\sin^2\left(\frac{\varphi_{z^{(1)}}}{2}\right) = \frac{1}{2r}\left(\frac{\sqrt{\cos^2\varphi+\alpha_1(t)^2\sin^2\varphi}-\cos\varphi}{\cos^2\varphi+\alpha_1(t)^2\sin^2\varphi}\right) = \frac{1}{2r}\,(\text{even part}-\text{odd part})$$

$$h_4 := \frac{1}{r_{z^{(2)}}}\,\sin^2\left(\frac{\varphi_{z^{(2)}}}{2}\right) = \frac{1}{2r}\left(\frac{\sqrt{\cos^2\varphi+\alpha_2(t)^2\sin^2\varphi}-\cos\varphi}{\cos^2\varphi+\alpha_2(t)^2\sin^2\varphi}\right) = \frac{1}{2r}\,(\text{even part}-\text{odd part})$$

$$h_5 := \frac{1}{\sqrt{r_{z^{(1)}}\,r_{z^{(2)}}}}\,\cos\left(\frac{\varphi_{z^{(1)}}}{2}\right)\cos\left(\frac{\varphi_{z^{(2)}}}{2}\right) = \frac{1}{2r}\frac{1}{\sqrt{\cos^2\varphi+\alpha_1(t)^2\sin^2\varphi}\,\sqrt{\cos^2\varphi+\alpha_2(t)^2\sin^2\varphi}}\times$$
$$\left(\frac{\sqrt{\cos^2\varphi+\alpha_1(t)^2\sin^2\varphi}+\cos\varphi}{\cos^2\varphi+\alpha_1(t)^2\sin^2\varphi}\right)\left(\frac{\sqrt{\cos^2\varphi+\alpha_2(t)^2\sin^2\varphi}+\cos\varphi}{\cos^2\varphi+\alpha_2(t)^2\sin^2\varphi}\right)$$

$$h_6 := \frac{1}{\sqrt{r_{z^{(1)}}\,r_{z^{(2)}}}}\,\sin\left(\frac{\varphi_{z^{(1)}}}{2}\right)\sin\left(\frac{\varphi_{z^{(2)}}}{2}\right) = \frac{1}{2r}\frac{1}{\sqrt{\cos^2\varphi+\alpha_1(t)^2\sin^2\varphi}\,\sqrt{\cos^2\varphi+\alpha_2(t)^2\sin^2\varphi}}\times$$
$$\left(\frac{\sqrt{\cos^2\varphi+\alpha_1(t)^2\sin^2\varphi}-\cos\varphi}{\cos^2\varphi+\alpha_1(t)^2\sin^2\varphi}\right)\left(\frac{\sqrt{\cos^2\varphi+\alpha_2(t)^2\sin^2\varphi}-\cos\varphi}{\cos^2\varphi+\alpha_2(t)^2\sin^2\varphi}\right)$$

$$h_7 := \frac{1}{r_{z^{(1)}}}\,\cos\left(\frac{\varphi_{z^{(1)}}}{2}\right)\sin\left(\frac{\varphi_{z^{(1)}}}{2}\right) = \frac{1}{2r}\frac{\alpha_1(t)\,\sin\varphi}{(\cos^2\varphi+\alpha_1(t)^2\sin^2\varphi)}$$

$$h_8 := \frac{1}{\sqrt{r_{z^{(1)}}\,r_{z^{(2)}}}}\,\cos\left(\frac{\varphi_{z^{(1)}}}{2}\right)\sin\left(\frac{\varphi_{z^{(2)}}}{2}\right)$$
$$= \frac{1}{2r}\frac{\sqrt{\sqrt{\cos^2\varphi+\alpha_1(t)^2\sin^2\varphi}+\cos\varphi}\,\sqrt{\sqrt{\cos^2\varphi+\alpha_2(t)^2\sin^2\varphi}-\cos\varphi}}{\left(\cos^2\varphi+\alpha_1(t)^2\sin^2\varphi\right)\left(\cos^2\varphi+\alpha_2(t)^2\sin^2\varphi\right)} = \frac{1}{2r}\,\text{even part}$$

$$h_9 := \frac{1}{\sqrt{r_{z^{(1)}}\,r_{z^{(2)}}}}\,\sin\left(\frac{\varphi_{z^{(1)}}}{2}\right)\cos\left(\frac{\varphi_{z^{(2)}}}{2}\right)$$
$$= \frac{1}{2r}\frac{\sqrt{\sqrt{\cos^2\varphi+\alpha_1(t)^2\sin^2\varphi}-\cos\varphi}\,\sqrt{\sqrt{\cos^2\varphi+\alpha_2(t)^2\sin^2\varphi}+\cos\varphi}}{\left(\cos^2\varphi+\alpha_1(t)^2\sin^2\varphi\right)\left(\cos^2\varphi+\alpha_2(t)^2\sin^2\varphi\right)} = \frac{1}{2r}\,\text{even part}$$

$$h_{10} := \frac{1}{r_{z^{(2)}}}\,\cos\left(\frac{\varphi_{z^{(2)}}}{2}\right)\sin\left(\frac{\varphi_{z^{(2)}}}{2}\right) = \frac{1}{2r}\frac{\alpha_2(t)\,\sin\varphi}{(\cos^2\varphi+\alpha_2(t)^2\sin^2\varphi)}.$$

Here we have used:

$$\int_{-\pi}^{\pi} h_1(r,\varphi)\,\cos\varphi\, r\, d\varphi = -\int_{-\pi}^{\pi} h_3(r,\varphi)\,\cos\varphi\, r\, d\varphi = \frac{1}{\alpha_1(t)}\int_{-\pi}^{\pi} h_7(r,\varphi)\,\sin\varphi\, r\, d\varphi = \frac{\pi}{1+\alpha_1(t)},$$
$$\int_{-\pi}^{\pi} h_2(r,\varphi)\,\cos\varphi\, r\, d\varphi = -\int_{-\pi}^{\pi} h_4(r,\varphi)\,\cos\varphi\, r\, d\varphi = \frac{1}{\alpha_2(t)}\int_{-\pi}^{\pi} h_{10}(r,\varphi)\,\sin\varphi\, r\, d\varphi = \frac{\pi}{1+\alpha_2(t)},$$
$$\int_{-\pi}^{\pi} h_5(r,\varphi)\,\cos\varphi\, r\, d\varphi = -\int_{-\pi}^{\pi} h_6(r,\varphi)\,\cos\varphi\, r\, d\varphi = \int_{-\pi}^{\pi} h_8(r,\varphi)\,\sin\varphi\, r\, d\varphi = \int_{-\pi}^{\pi} h_9(r,\varphi)\,\sin\varphi\, r\, d\varphi = \frac{\pi}{\sqrt{(1+\alpha_1(t))\,(1+\alpha_2(t))}}.$$
$$\int_{-\pi}^{\pi} h_j(r,\varphi)\,\cos\varphi\, r\, d\varphi = 0,\ j = 7,8,\cdots,10,$$
$$\int_{-\pi}^{\pi} h_j(r,\varphi)\,\sin\varphi\, r\, d\varphi = 0,\ j = 1,2,\cdots,6.$$

After long and technical calculations we get:

$$\begin{aligned} I_1+I_2 &= (1-\alpha_2^2)\frac{h'(t)}{2\mu\pi D^2}\left(-(1+\alpha_2^2)^2(1+\alpha_1)\frac{\pi}{1+\alpha_1(t)} + 4\alpha_1\alpha_2(1+\alpha_2)\frac{\pi}{1+\alpha_2(t)}\right)\left(\alpha_1 k_I^2+\alpha_2 k_{II}^2\right) \\ &= (1-\alpha_2^2)\frac{h'(t)}{2\mu D^2}\left(-(1+\alpha_2^2)^2+4\alpha_1\alpha_2\right)\left(\alpha_1 k_I(t,h,h')^2+\alpha_2 k_{II}(t,h,h')^2\right) \\ &= (1-\alpha_2^2)\frac{h'(t)}{2\mu D}\left(\alpha_1 k_I(t,h,h')^2+\alpha_2 k_{II}(t,h,h')^2\right) \end{aligned}$$

We have used the expressions for σ given by Theorem 14.
We have written $\dfrac{\rho}{\mu}h'^2 = \dfrac{1}{c_2^2}h'^2 = (1-\alpha_2^2)$.
Since all the integrals which contain the product $k_I(t,h,h')\,k_{II}(t,h,h')$ vanish, (6.9) does not incluye mixed terms in $k_I(t,h,h')$ and $k_{II}(t,h,h')$. □

Remark 18. *Lemmata 20 and 21 yield*

$$\lim_{\delta\to 0}\left(-\dot{E^\delta}(t)+\hat{A^\delta}(t)-\dot{K^\delta}(t)\right) = \lim_{\delta\to 0}\dot{D^\delta}(t). \tag{6.18}$$

On the other hand the energy flux in Ω_t, namely $-\dot{E}(t)+\hat{A}(t)-\dot{K}(t)$, is well defined, at least in the distribution sense.

Lemma 22. *Let assumptions H1-H3 of Theorem 13 hold. Then the dynamic energy release rate is well defined which means that the limit in (6.18) exists and is finite. The dynamic energy release rate for the initial-boundary problem (5.6) is given by:*

$$G(h,h') = \frac{1}{2\mu}\left[\frac{\left(1-\alpha_2(t)^2\right)\left(\alpha_1(t)\,k_1^2(t,h,h')+\alpha_2(t)\,k_2^2(t,h,h')\right)}{4\,\alpha_1(t)\,\alpha_2(t)-\left(1+\alpha_2(t)^2\right)^2}\right]. \tag{6.19}$$

Proof.

$$\begin{aligned} -\dot{E}(t)+\hat{A}(t)-\dot{K}(t) &= \lim_{\delta\to 0}\left(-\dot{E^\delta}(t)+\hat{A^\delta}(t)-\dot{K^\delta}(t)\right) \\ &= \dot{D}(t) = \frac{h'(t)}{2\mu}\left[\frac{\left(1-\alpha_2(t)^2\right)\left(\alpha_1(t)\,k_1^2(t,h,h')+\alpha_2(t)\,k_2^2(t,h,h')\right)}{4\,\alpha_1(t)\,\alpha_2(t)-\left(1+\alpha_2(t)^2\right)^2}\right]. \end{aligned}$$

The dynamic energy release rate $G(h,h') = \dfrac{\dot{D}(t)}{h'(t)}$, with $h'(t) \neq 0$ is obtaining by refering the instantaneous energy flux $\dot{D}(t)$. □

It should be noted that proceeding to the limit as $h'(t) \to 0$ in relation (6.19), we arrive at the familiar static energy release rate formula (plane strain):

$$G = \frac{1-\nu}{2\mu}\ \left[\, k_1^2 + k_2^2 \,\right] = \frac{1-\nu^2}{E}\ \left[\, k_1^2 + k_2^2 \,\right].$$

In fact it is so because:

$$\frac{\left(1-\alpha_2(t)^2\right)}{4\,\alpha_1(t)\,\alpha_2(t) - \left(1+\alpha_2(t)^2\right)^2} = \frac{h'(t)^2/c_2^2}{4\sqrt{1-\left(\dfrac{h'(t)}{c_1}\right)^2}\sqrt{1-\left(\dfrac{h'(t)}{c_2}\right)^2} - \left(2-\left(\dfrac{h'(t)}{c_2}\right)^2\right)}$$

go

$$\frac{c_1^2}{2(c_1^2-c_2^2)} = (1-\nu) \text{ as } h'(t) \to 0.$$

6.1.2 Extraction of the dynamical stress intensity factors in the in-plane case

Our next target is to derive some expressions for the stress intensity factors from the analytical results. For that we formulate the following auxiliary lemma.

Lemma 23. *If we denote*

$$(v_S^+)^2 := \sqrt{\cos^2\varphi + \alpha_1^2 \sin^2\varphi} + \cos\varphi$$

and

$$(v_S^-)^2 := \sqrt{\cos^2\varphi + \alpha_1^2 \sin^2\varphi} - \cos\varphi$$

then the derivatives are given by:

$$\begin{aligned}\left(\frac{\partial v_S^+}{\partial \varphi}\right)^2 &= \frac{1}{4(\cos^2\varphi + \alpha_1(t)^2\sin^2\varphi)}\left[\sqrt{\cos^2\varphi + \alpha_1^2\sin^2\varphi}\left((\alpha_1(t)^2-1)\cos^2\varphi + 1\right)\right] + \\ &\quad - \frac{\cos\varphi}{4}\left[1 + \frac{\alpha_1(t)^2-1}{\cos^2\varphi + \alpha_1^2\sin^2\varphi}\right], \\ &= \textit{even part} - \frac{\cos\varphi}{4}\left[1 + \frac{\alpha_1(t)^2-1}{\cos^2\varphi + \alpha_1^2\sin^2\varphi}\right], \qquad (6.20)\end{aligned}$$

$$\begin{aligned}\left(\frac{\partial v_S^-}{\partial \varphi}\right)^2 &= \frac{1}{4(\cos^2\varphi + \alpha_1(t)^2\sin^2\varphi)}\left[\sqrt{\cos^2\varphi + \alpha_1^2\sin^2\varphi}\left((\alpha_1(t)^2-1)\cos^2\varphi + 1\right)\right] + \\ &\quad + \frac{\cos\varphi}{4}\left[1 + \frac{\alpha_1(t)^2-1}{\cos^2\varphi + \alpha_1^2\sin^2\varphi}\right], \\ &= \textit{even part} + \frac{\cos\varphi}{4}\left[1 + \frac{\alpha_1(t)^2-1}{\cos^2\varphi + \alpha_1^2\sin^2\varphi}\right], \qquad (6.21)\end{aligned}$$

Proof. If we consider

$$\frac{\partial (v_S^-)^2}{\partial \varphi} = 2\, v_S^- \frac{\partial v_S^-}{\partial \varphi} \Rightarrow \frac{\partial v_S^-}{\partial \varphi} = \frac{\dfrac{\partial (v_S^-)^2}{\partial \varphi}}{2\, v_S^-}$$

Then

$$\begin{aligned}\left(\frac{\partial v_S^-}{\partial \varphi}\right)^2 &= \frac{\left(\dfrac{-\cos\varphi\sin\varphi + \alpha_1(t)^2\sin\varphi\cos\varphi}{\sqrt{\cos^2\varphi + \alpha_1^2\sin^2\varphi}} - \sin\varphi\right)^2}{4\,(v_S^+)^2} \\ &= \frac{1}{4(\cos^2\varphi + \alpha_1(t)^2\sin^2\varphi)} \frac{\left((\alpha_1(t)^2-1)\cos\varphi\sin\varphi - \sin\varphi\sqrt{\cos^2\varphi + \alpha_1^2\sin^2\varphi}\right)^2}{(v_S^+)^2}\end{aligned}$$

With some calculations the results follows.
Note that the terms consist of a even and an odd part with respect to $\frac{\pi}{2}$. □

The novelty of the present chapter is that we use the strong solutions for the displacement field $\vec{u}$ given in the different configurations, Theorems 13 and 14, for determining the stress intensity factors in terms of displacement field (6.22), (6.23), instead of the stress field as usual in the literature.

Theorem 15. *Under the assumptions of Theorem 14.*
Then the dynamic stress intensity factors $k_I = k_I(t,h,h')$ and $k_{II} = k_{II}(t,h,h')$ at time t in the current configuration for $R(t)-h(t) > 0$ are given as the following limits:

$$\lim_{R(t)-h(t)\to 0} \frac{\mu D\sqrt{2\pi(R(t)-h(t))}}{1+\alpha_2(t)^2-2\alpha_1(t)\alpha_2(t)} \frac{du_1(y,t)}{dy_1}|_{y_2=0} = k_I(t,h,h') \tag{6.22}$$

$$\lim_{R(t)-h(t)\to 0} \frac{\mu D\sqrt{2\pi(R(t)-h(t))}}{2\alpha_1(t)\alpha_2(t)-(1+\alpha_2(t)^2)} \frac{du_2(y,t)}{dy_1}|_{y_2=0} = k_{II}(t,h,h'), \tag{6.23}$$

with $D = 4\alpha_1(t)\alpha_2(t)-(1+\alpha_2(t)^2)^2$.

Proof. Since $\vec{u}$ can be represented in $\vec{z}$-coordinate spaces according to (5.108) as

$$\vec{w}(\vec{z},t) = \vec{w}_R(\vec{z},t) + k_I(t,h,h')S_N^1(\vec{z},t) + k_{II}(t,h,h')S_N^2(\vec{z},t).$$

We denote

$$S_N^1(\vec{z},t) = \begin{pmatrix} (S_N^1)_1 \\ (S_N^1)_2 \end{pmatrix}.$$

We get there, compare (6.14):

$$\frac{\partial (S_N^1)_1}{\partial z_1^{(1)}} = \frac{(1+\alpha_2(t)^2)}{\mu D\sqrt{2\pi}} \left(r_{z^{(1)}}^{-\frac{1}{2}} \cos\left(\frac{\varphi_{z^{(1)}}}{2}\right) - \frac{2\alpha_1(t)\alpha_2(t)}{(1+\alpha_2(t)^2)} r_{z^{(2)}}^{-\frac{1}{2}} \cos\left(\frac{\varphi_{z^{(2)}}}{2}\right)\right)$$

$$= \frac{(1+\alpha_2(t)^2)}{\mu D\sqrt{2\pi r}} \left(\frac{1}{\sqrt{2}} \sqrt{\frac{\sqrt{\cos^2\varphi+\alpha_1(t)^2\sin^2\varphi}+\cos\varphi}{\cos^2\varphi+\alpha_1(t)^2\sin^2\varphi}} + \right.$$

$$\left. - \frac{2\alpha_1(t)\alpha_2(t)}{(1+\alpha_2(t)^2)} \frac{1}{\sqrt{2}} \sqrt{\frac{\sqrt{\cos^2\varphi+\alpha_2(t)^2\sin^2\varphi}+\cos\varphi}{\cos^2\varphi+\alpha_2(t)^2\sin^2\varphi}} \right)$$

$$= \frac{(1+\alpha_2(t)^2)}{\mu D\sqrt{2\pi r}} \left(\frac{1}{\sqrt{2}} \sqrt{\frac{\sqrt{x_1^2+\alpha_1(t)^2 x_2^2}+x_1}{\sqrt{x_1^2+\alpha_1(t)^2 x_2^2}}} - \frac{2\alpha_1(t)\alpha_2(t)}{(1+\alpha_2(t)^2)} \frac{1}{\sqrt{2}} \sqrt{\frac{\sqrt{x_1^2+\alpha_2(t)^2 x_2^2}+x_1}{\sqrt{x_1^2+\alpha_2(t)^2 x_2^2}}} \right).$$

We calculate $\frac{\partial (S_N^1)_1}{\partial z_1^{(1)}}|_{z_2^{(1)}=0}$. Note that $\frac{\partial (S_N^2)_1}{\partial z_1^{(1)}}|_{z_2^{(1)}=0} = 0$,

$$\begin{aligned} \frac{\partial (S_N^1)_1}{\partial z_1^{(1)}}|_{z_2^{(1)}=0} &= \frac{\partial (S_N^1)_1}{\partial x_1}|_{x_2=0} = \frac{\partial (S_N^1)_1}{\partial y_1}|_{y_2=0} \\ &= \frac{1+\alpha_2(t)^2 - 2\,\alpha_1(t)\,\alpha_2(t)}{\mu\, D\, \sqrt{2\,\pi\, r}|_{x_2=0}} \end{aligned} \tag{6.24}$$

Multipling (6.24) by $\frac{\sqrt{2\pi r}|_{x_2=0}\,\mu\, D}{(1+\alpha_2(t)^2)-2\,\alpha_1(t)\,\alpha_2(t)}$ and next using the fact that the derivative of the regular part $\partial_1 (w_1)_R$ behaves in a vicinity of the crack tip asymptotically as $\sqrt{r_z}$, the result follows for the stress intensity factor for the mode I in the reference configuration.
Similarly we can do with $\partial_1 (w_2)|_{z_2=0}$ to get $k_{II}(t,h,h')$.

Furthermore, we use the results from lemma 23 and we have $r = R-h$ on the y_1-axis assuming $R > h$. Using the fact that the derivative of the regular part behaves in a vicinity of the crack tip asymptotically as $\sqrt{R-h}$ the assertion in the current configuration follows. □

The expressions for the stress intensity factors in the current configuration (6.22), (6.23) are also very useful for numerical purposes, see Chap. 7.

6.1.3 Equation of motion for the running crack tip

A differential equation for crack tip motion is obtained by imposing a fracture criterion along with the governing field equations and the initial-boundary conditions. We assume to be in the situation that (4.49) holds:

$$G(h,h') = \Gamma(h,h').$$

and then we can equalize the crack growth resistance $\Gamma(h,h')$ for a particular material and the dynamic energy flux $G(h,h')$. This is the natural extension of the Griffith approach.

The formulation of the dynamic fracture problem given by (5.6) is then coupled with an energy balance law assuming that (4.49) holds, i.e. that the dynamic energy release rate $G(h,h')$, (6.19) can be expressed by the experimentally determined fracture toughness $\Gamma(h,h')$, we use the ordinary differential equation

$$\Gamma(h,h') = \frac{1}{2\mu}\left[\frac{\left(1-\alpha_2(t)^2\right)\left(\alpha_1(t)\,k_1^2(t,h,h') + \alpha_2(t)\,k_2^2(t,h,h')\right)}{4\,\alpha_1(t)\,\alpha_2(t) - \left(1+\alpha_2(t)^2\right)^2}\right] \tag{6.25}$$

as fracture criterion.

In a particular case of an opening mode crack ($k_{II} = k_{III} = 0$) the crack growth resistance $\Gamma(h,h')$, [93], [8], [55] is given by (5.1):

$$\Gamma(h,h') = \left(1 - \frac{h'(t)}{c_R}\right) \frac{(1-\nu^2)}{E} k_I(t,h,0)^2,$$

where c_R denotes the Rayleigh wave speed, ν and E are the Poisson and modulus of elasticity. $k_I(t,h,0)$ denotes the stress intensity factor for the mode I that would have resulted from the applied loading if the crack tip had always been at its instantaneous position represented by $h = h(t)$.
In light of (6.25), the crack tip equation of motion for mode I can be rewritten as (6.26):
Find $h = h(t)$ as the solution of the ordinary differential equation:

$$\Gamma(h,h') = \left(1 - \frac{h'(t)}{c_R}\right) \frac{(1-\nu^2)}{E} k_I(t,h,0)^2 = \frac{h'(t)^2}{2\,\mu\, c_2^2} \frac{\alpha_1(t)\, k_1^2(t,h,h')}{D} = G(h,h'), \;\; h(0) = 0. \tag{6.26}$$

with $D = 4\,\alpha_1(t)\,\alpha_2(t) - \left(1+\alpha_2(t)^2\right)^2$.
$\Gamma = \Gamma(h,h')$ depends on crack speed h' and possibly on the crack tip position h. The ordinary differential equation for $h(t)$, (6.26), is a first-order equation, i.e., it does not involve second and higher derivatives of $h(t)$.
The complete formulation for the dynamic coupled problem for in-plane fracture case reads:

$$\left.\begin{aligned}
&(\lambda+\mu)\nabla(\nabla\cdot\vec{u}) + \mu\nabla^2\vec{u} = \rho\vec{u}_{tt} \quad \text{in } Q := \bigcup_{t=0}^{T} \Omega_t,\\
&\lambda\,(\mathrm{div}\vec{u})\,n + 2\,\mu\,\partial_n\vec{u} + \mu\,\vec{n}\times\mathrm{curl}\,\vec{u} = 0 \quad \text{on } \bigcup_{t=0}^{T} \sigma_t,\\
&\lambda\,(\mathrm{div}\vec{u})\,n + 2\,\mu\,\partial_n\vec{u} + \mu\,\vec{n}\times\mathrm{curl}\,\vec{u} = \rho\vec{q} \quad \text{on } \Sigma_N := \Gamma_N\times(0,T),\\
&\vec{u}(t,y) = 0 \quad \text{on } \Sigma_D := \Gamma_D\times(0,T),\\
&\vec{u}(0,y) = \vec{u_0},\ \partial_t\vec{u}(0,y) = \vec{u_1} \quad \text{in } \Omega_0.
\end{aligned}\right\}$$

AND

$$\left\{\begin{aligned}
&\Gamma(h,h') = \frac{1}{2\mu}\left[\frac{\left(1-\alpha_2(t)^2\right)\left(\alpha_1(t)k_1^2(t,h,h') + \alpha_2(t)k_2^2(t,h,h')\right)}{4\,\alpha_1(t)\,\alpha_2(t) - \left(1+\alpha_2(t)^2\right)^2}\right],\\
&h(0) = 0,\ k_I(0,h,h') = k_I(0),\ k_{II}(0,h,h') = k_{II}(0).
\end{aligned}\right.$$

$$\vec{u}_0(x) = \vec{v}_{R_0}(x) + k_I(0,h,h')\eta_1 S_N^{(1)}(x,0) + k_{II}(0,h,h')\eta_2 S_N^{(2)}(x,0),$$

$$k_I(t,h,h') = \lim_{R(t)-h(t)\to 0} \frac{\mu\, D\sqrt{2\,\pi\,(R(t)-h(t))}}{1+\alpha_2(t)^2 - 2\,\alpha_1(t)\,\alpha_2(t)} \frac{du_1(y,t)}{dy_1}|_{y_2=0},$$

$$k_{II}(t,h,h') = \lim_{R(t)-h(t)\to 0} \frac{\mu\, D\sqrt{2\,\pi\,(R(t)-h(t))}}{2\,\alpha_1(t)\,\alpha_2(t) - (1+\alpha_2(t)^2)} \frac{du_2(y,t)}{dy_1}|_{y_2=0}.$$

CHAPTER 7

Numerical results

In this chapter we shall show the numerical results of the model problem examples that we introduced in Chapters 4 and 6.

Numerical simulation plays a crucial role in engineering and science. Many systems or components behavior are mathematically modeled by a set of partial differential equations (PDE) and related boundary conditions, followed with a discrete form of the mathematical problem and a solution given by numerical methods. However, the main and important quantity of interest is not the full field variable, but rather certain outputs that describe the characteristics of a system. Typical outputs are energies, forces, temperatures, fluxes or critical stress/strains. These outputs are controlled by certain system parameters, or inputs, that describe the configuration of the system or component, such as geometry, properties, loads or environment settings. The relevant system behavior is thus described by an implicit input-output relationship, or a mathematical description of the physical problem.

In the field of Fracture Mechanics, many practical applications require the computation of the stress intensity factors. Because of its importance, stress intensity factor values are usually computed and stored in many handbooks, mostly in tabular and graphical form. In general, the calculation of the stress intensity factor requires the knowledge of the solution field of a PDE, and usually, cannot be determined analytically, thus numerical procedures have to be used. The goal of this chapter is the development of numerical methods that provide fast and reliable evaluation of the PDE input-output relationship, in particular, the evaluation of the stress intensity factor from a linear elasticity fracture mechanic model.

7.1 Dynamical crack propagation for Mode III

We now define our scenario. We consider the evolution of a crack in a finite configuration on the time interval [0, T].
More precisely, we assume that the 2D solid contains exactly one finite, straight pre-crack σ_0, which may expand in a straight line along the horizontal axis y_1. Starting from a crack with length l, the crack tip position at time t is given by $h = h(t)$. Besides this unknown quantity h the displacement field $u = u(y_1, y_2, t)$ is the unknown solution of the wave equation in the cracked domain. The unknowns h and u are coupled, through a system of an initial-boundary value problem for the wave equation (4.5) and an initial value problem for an ordinary differential equation (7.1) derived from an energy balance law. Assuming that (4.49) is valid, the latter problem reads:
Find $h = h(t)$ such that, [4]:

$$\Gamma(h, h') = k_{III}^2(t, h, h') c_2^2 \frac{\pi}{4} = G(h, h'), \quad h(0) = 0. \tag{7.1}$$

The constant c_2 is the shear wave speed, $k_{III}(t, h, h')$ the dynamic stress intensity factor, which responds instantaneously to a change in crack propagation velocity $h'(t)$ and it includes the effects of loading and geometry.
The mathematical analysis of the full coupled nonlinear problem (4.5) with (7.1) seems to be difficult and an iterative approach starting from a given pre-crack position is then considered. Computing the wave-displacement and the dynamic stress intensity factor $k_{III}(t, h, h')$ at a certain time $t = t_i$ we use the solution of the ordinary differential equation (7.1) to pass to the next time step $t = t_{i+1}$ and repeat the procedure.

Remark 19. *We have no need for the assumption (4.9) during the numerical computations, since at every time step, when the crack grows, the problem is restarted with the new region and a new triangulation in the current configuration.*

7.1.1 Basic concepts and remarks on the implementation

We discuss some basic concepts of the numerical simulation, namely the software components and environments which are used in the following.
We present simulations in two space dimensions only. For that reason we deal with meshes consisting of triangles using the software package PDE2D [27].
PDE2D approximates the solution using a linear combination of piecewise polynomial basis functions, where the unknown coefficients are functions of time. A Galerkin finite element method with respect to the space variables is here used, which results in a system of ordinary

time dependent differential equations for the unknown coefficient functions; this differential equation system is solved using a finite difference method.
First of all we introduce the decomposition of the domain into a finite number of simplices. The properties assumed for the triangulation are taken from classical textbooks.
For a general region, an initial triangulation is constructed which generally consists of only as many triangles as needed to define the region and to satisfy the following rules (triangles adjacent to a curved boundary may be considered to have one curved edge):

1. The end points of each arc are included as vertices in the triangulation.
2. No vertex of any triangle may touch another in a point which is not a vertex of the other triangle.
3. No triangle may have all three vertices on the boundary.

The last task of the simulation process is the visualization of the computed data. PDE2D generates its own graphics, in PostScript format, and also generates a MATLAB program which can be used to create further plots.
Finally, we apply GNUPlot in order to visualise scalar valued data like the components of the displacement field, dynamic stress intensity factor and energy. GNUPlot is free software, which can be downloaded from [29].

7.1.2 General setting of the simulations

The following simulations are performed in a situation where a square with side length of $2\,m$ with an interior crack on the right side is considered, [4]. The boundary loads are described later for the individual examples. An initial triangulation is shown in Fig.7.1(a), the final triangulation with 4000 elements in Fig.7.1(b) and the corresponding zoom of the cracked zone in Fig.7.1(c).
We focus on the numerical simulation of the coupled problem (4.5) and (7.1). The material parameters used in the following computations and the different pre-conditions on the equation of motion are presented here.
To predict the crack path $h = h(t)$ by numerical calculation, one has to calculate the displacement field at the points around the crack tip, from which the corresponding dynamic stress intensity factor is subsequently extracted. One then repeats this process incrementally.

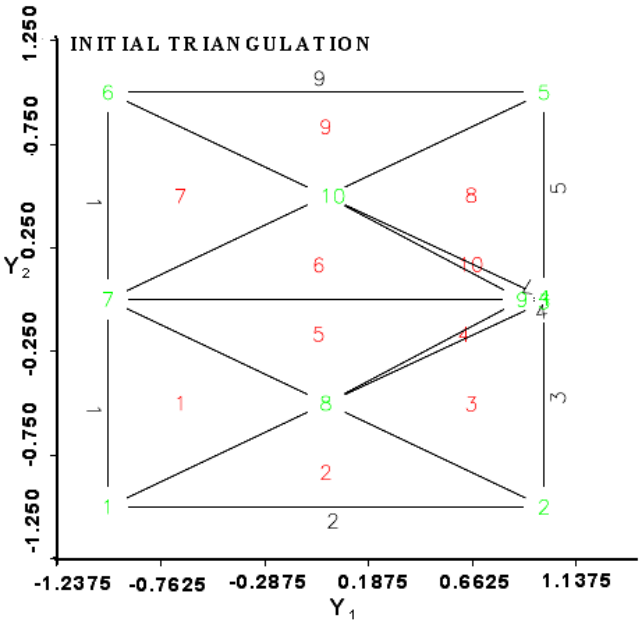

(a) Initial triangulation

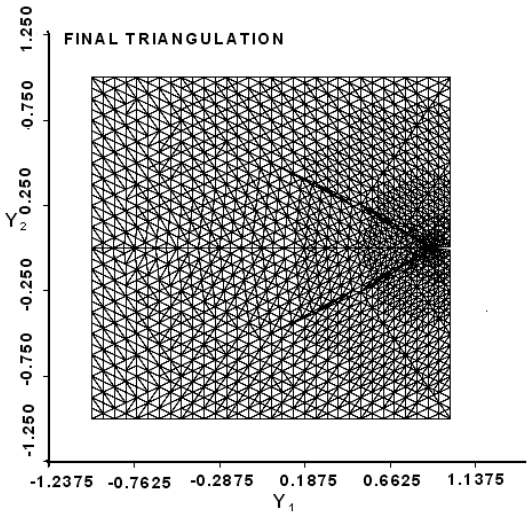

(b) Mesh used in the FE model

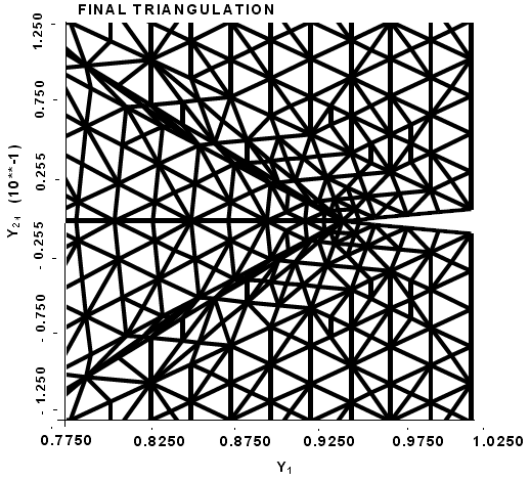

(c) Mesh surrounding the crack tip

Figure 7.1: Computational domains

7.1.3 Iterative solution strategy

The strategy for solving dynamic fracture problems is to obtain the dynamically admissible displacement fields from the governing equation (4.5) subjected to the boundary and initial conditions and then to use the energy rate balance equation (7.1) at the crack tip equation to determine the crack speed. In other words, the following iterative procedure to solve the nonlinear coupled problem is proposed here:

1. Fix $t_0 > 0$ and a time step τ, and set $t_{-1} = 0$, and assume $h(t) = h_0(t)$ is known for $t_{-1} < t < t_0$.

2. Solve the initial boundary value problem (4.5) for the wave equation for $t_{-1} < t < t_0$ in the cracked domain with the given straight crack-path h_0.

3. Extract the corresponding dynamical stress intensity factor $k_{III}(t_0, h_0, h_0')$ by the formula (4.43).

4. Insert $k_{III}(t_0, h_0, h_0')$ into (7.1), use an experimentally chosen formula for $\Gamma(h, h')$ and solve the resulting ordinary differential equation for $h(t)$ with the initial datum $h(t_0) = h_0(t_0)$. Denote the solution by $h_1(t), t \in (t_0, t_0 + \tau)$.

5. Go to step 2 and replace $h_0(t), t_{-1}, t_0$ respectively by $h_1(t), t_0, t_0 + \tau$.

The computational domain consists of a cracked, finite, homogeneous, isotropic and linearly elastic solid, which is described by the square R with vertices (-1,-1),(1,-1),(1,1) and (-1,1) and an interior crack σ_{t_0} from $(h(t_0), 0)$ to (1,0) along the y_1-axis. The crack σ_{t_0} interacts with an incident transient elastic wave, whose front is assumed to be planar. The interaction between the incident wave and the crack forms an initial boundary value problem, which is described by equations (4.5). Its solution is performed numerically by using the software PDE2D to describe the local behaviour of the displacement fields near the crack tip $h(t)$.
The material properties of the square plate are assumed to include:
elastic modulus $E = 68.9GPa$, Poisson's ratio $\nu = 0.3$, mass density $\rho = 2.77(10)^3 Kg/m^3$, Lamé parameter $\mu = 2.7(10)^{10} N/m^2$ and shear wave speed $c_2 = \sqrt{\dfrac{E}{2\rho(1+\nu)}} = 3093 m/s$, [75].

Typical finite element analysis in dynamic fracture mechanics problems for crack propagation involves as a first step, the construction of a mesh appropriate for the crack geometry. Moreover, when the crack evolves, we require that the mesh evolves also and must conform

to the crack geometry. As the crack is part of the mesh, this involves the update of the mesh, as well as the data structure associated with the crack geometry. One must treat a moving-singularity-boundary-value-problem.

Therefore the dump/restart option from PDE2D [26] has been used. This option in PDE2D is useful for this problem because it makes it easy to stop at some value of the time t, adjust the mesh or even the boundary appropriately, and restart. The grids are generated automatically and moved with the solution, by putting a "DO loop" around the main program to vary the initial and final time values each pass, and requesting a restart with a graded mesh.

The initial conditions have been read from the restart file each time and then PDE2D dumps the final solution at the end of each run back into the restart file, [26]. 4000 elements of degree 3 have been used for the final triangulation and the grids are most dense near the crack tip. The corresponding spatial discretization error is $O(h^4)$, where h is the maximum triangle diameter. The number of unknowns is 36596.
The time increment Δt has been chosen as $\Delta t = 0.00003$ s. The time discretization used is the Crank-Nicolson scheme, [26].

The iterative numerical technique proposed here was used in the numerical simulation to find the unknowns (u,h). This technique requires considerable computing time because of the nature of the iteration. Because of that, the MPI-based parallel band solver implemented in PDE2D [27] was used. This is a parallel solver which runs efficiently on multiple processor machines, in our cases 6 processors were used, with the matrix distributed over the available processors. The CPU time required for these computations with 6 processors is: real time = 178m 6s with the mesh refinement at the crack tip.

7.1.4 Order reduction for the time-dependent problem.

There are no body forces, $f = 0$, and the problem (4.5) is broken into two first order equations [26] before it can be solved by PDE2D [27]. The form of the 2D time-dependent system solved by PDE2D [27] is:

$$\begin{aligned} C_{11} * \frac{\partial U}{\partial T} + C_{12} * \frac{\partial V}{\partial T} &= \frac{\partial A_1}{\partial y_1} + \frac{\partial B_1}{\partial y_2} - F_1 \\ C_{21} * \frac{\partial U}{\partial T} + C_{22} * \frac{\partial V}{\partial T} &= \frac{\partial A_2}{\partial y_1} + \frac{\partial B_2}{\partial y_2} - F_2 \end{aligned} \tag{7.2}$$

where all coefficients can be functions of y_1, y_2, T, U, V and the derivatives of U and V.
We set the following functions in (7.2):

$$C_{11} = 1; \quad C_{12} = 0; \quad F1 = -V; \quad A_1 = 0; \quad B_1 = 0$$
$$C_{21} = 0; \quad C_{22} = 1; \quad F2 = 0; \quad A_2 = c_2^2 * Uy_1; \quad B_1 = c_2^2 * Uy_2$$

and the order reduction of (4.5) results.

7.1.5 Simulation of dynamic stress intensity factor

As we pointed out, the crack propagation is simulated by remeshing the whole spatial domain each time increment so that the mesh is always highly refined near the crack-tip.

The computation of stress intensity factors must be carefully done since the evolution of the crack depends on that. Numerical calculations for $k_{III}(t, h, h')$ have been carried out in the following way:

- A regular $(N_{y_1} + 1)$ by $(N_{y_2} + 1)$ rectangular output mesh is used for the discretization of the square configuration, consisting of the points:
  $\left(Y_{1_A} + i * \frac{(Y_{1_B} - Y_{1_A})}{N_{y_1}}, Y_{2_A} + j * \frac{(Y_{2_B} - Y_{2_A})}{N_{y_2}} \right)$, where $i = 0, \ldots, N_{y_1}$ and $j = 0, \ldots, N_{y_2}$ and $Y_{1_A} = -1$, $Y_{1_B} = h(t)$, $Y_{2_A} = -1$ and $Y_{2_B} = 1$.
- The function $\frac{2}{\sqrt{\alpha_2(t)}} \sqrt{(R - h_0(t_0))} \frac{\partial u}{\partial y_2}$ is output at all mesh points.
- To estimate the limit in formula (4.43) we simply use the value of this function at the last output mesh point in front of the crack tip, $(Y_{1_B} - 1, \frac{N_{y_2}}{2})$.

Thus the point where the dynamic stress intensity is evaluated is $(N_{y_1} = N_{y_2} = 60)$:
$(-1 + (N_{y_1} - 1) * \frac{(h(t) + 1)}{N_{y_1}}, -1 + \frac{N_{y_2}}{2} * \frac{2}{N_{y_2}}) = (h(t) - \frac{1}{60} * (h(t) + 1), 0)$.

This is the output mesh point closest to, and in front of the crack tip. The finite element mesh is refined locally in such a way as to ensure that there are several triangles between this point and the crack tip, so that reasonable accuracy can be expected at this point.

The values of $\frac{\partial u}{\partial y_2}$ at the mesh points, from which the dynamic stress intensity factors are subsequently extracted, are computed by PDE2D using exact differentiation of its piecewise polynomial approximation to u.

7.1.6 The fracture toughness

Using the equation of motion of the crack tip (7.1), the crack propagation behaviour is given if the fracture toughness is provided. The fracture toughness $\Gamma = \Gamma(t,h,h')$ is a material parameter which can only be obtained through experimental measurements [6], [39], and it represents the resistance of the material to the advance of the crack. It is determined for various purposes, among others, characterization of a material; characterization of a production process, for example, welding; assessment of the severity of a crack in a structural component. No matter what application is intended for the fracture toughness value, it is an empirical material property that is determined by test with standard rules, [1]. Unfortunately, the fracture process depends on numerous parameters, given by material, test temperature, loading rate, environment, as well as constraint condition in the specimen or component. The latter in turn depends on size and geometry of the specimen or structural component and the proximity of the applied force, to name only the most important factors, [40].
The time history of the dynamic stress intensity factor was obtained for different situations and $h(t)$ was calculated using the generalised equation of motion, the formula (7.1) which includes the situation where the crack propagates with non-uniform speed.

$$\Gamma(h,h') = k_{III}^2(t,h,h')c_2^2\frac{\pi}{4}, \quad h(0) = 0.$$

The quantity Γ appearing on the left-hand side of the equation of motion (7.1) is the fracture toughness. On the right-hand side appears the dynamic stress intensity factor $k_{III}(t,h,h')$, which is entirely determined through an analysis of the boundary/initial value problem, see (4.43).

Dynamic crack propagation is devoted to the study of solid bodies containing cracks that propagate under loading conditions. A number of analytical solutions for crack propagation problems exist. However, these solutions are limited to simple loading conditions, unbounded domains, constant speed or semi-infinite cracks, [8], [67].

Some empirical or experimental expressions for the fracture toughness are found in the literature and are used mostly for the case of semi-infinite crack in an unbounded media or constant speed:

- $\Gamma(h,h') = Constant$, [38], [11]. The results show that the crack propagates with constant speed and the model is not realistic.

- $\Gamma(h,h') = \Gamma_0\, ln\left(\dfrac{v_L}{v_L - h'(t)}\right)$, [21]. Empirical expression from experiments performed at University of Tokyo. Γ_0, v_L are material constants

- $\Gamma(h,h') = \int_{x_{te}(t)-x_{le}(t)}^{0} 2\,\tau_{layer}\dfrac{\partial u(\xi,0,t)}{\partial t}\,d\xi \;+\; h'(t)\int_0^{\gamma_f} 2\,\tau_{layer}(\gamma)\,d\gamma$, [10]. For a cohesive zone model, $\xi = x - x_{le}(t)$, x_{le}=leading edge, x_{te}=trailing edge = the physical crack tip, τ_{layer} layer behaviour.

  It is supposed that the fracture toughness is not a unique function of the crack velocity $h'(t)$. It can also depend on the acceleration behaviour of the crack, i.e., at the same crack velocity. The toughness at the deceleration stage ($dh'/dt < 0$) is greater than the toughness at the acceleration stage ($dh'/dt > 0$). This difference is expressed by using two materials constants v_{L_1} and v_{L_2} ($v_{L_1} > v_{L_2}$), [42], [21]:

- $$\Gamma(h,h') = \begin{cases} \Gamma_0\, ln\left(\dfrac{v_{L_1}}{v_{L_1} - h'(t)}\right), & dh'/dt > 0, \\ \Gamma_0\, ln\left(\dfrac{v_{L_2}}{v_{L_2} - h'(t)}\right), & dh'/dt < 0. \end{cases}$$

Apart from experimental studies, numerical methods are today an alternative for the investigation of cracks propagating in finite bodies under general loading conditions. For the numerical simulations, we assume that Γ depends monotonically on the crack speed h'. We tried two formulas for the fracture toughness. One was:

$$\Gamma_1(h,h') = \beta\frac{1-\alpha_2(t)}{\alpha_2(t)} \tag{7.3}$$

with $\alpha_2(t)$ defined as in (4.3), and $\beta = 36\ \mathrm{MPa}/m^{\frac{1}{2}}$. For more details about β, see e.g. [79]. The other was the empirical expression for fracture toughness proposed in [21],

$$\Gamma_2(h,h') = \Gamma_0\, ln\left(\frac{v_L}{v_L - h'(t)}\right), \tag{7.4}$$

here the material parameters are $\Gamma_0 = 75\ \mathrm{MPa}/m^{\frac{1}{2}}$ and $v_L/c_2 = 0.3$.

We have no experimental justification for $\Gamma_1(h,h')$, as we do for $\Gamma_2(h,h')$. This formula was chosen because it produces qualitatively reasonable results, in particular, when:

- $k_{III} = 0$, then $h'(t) = 0$ and when
- k_{III}^2 is large, then $h'(t)$ approaches c_2.

From (7.1) and (7.3) we get:

$$\frac{1-\alpha_2}{\alpha_2} = k_{III}^2(t,h,h') \left(\frac{c_2^2}{\beta}\right) \frac{\pi}{4}.$$

Simple calculations lead to:

$$h'(t) = c_2 \sqrt{1 - \left(\frac{1}{1+TMP}\right)^2} \tag{7.5}$$

where $TMP(t,h,h') = k_{III}^2(t,h,h') \left(\frac{c_2^2}{\beta}\right) \frac{\pi}{4}$, and c_2^2 and β have the same order of magnitude. Using the second experimentally justified fracture toughness formula (7.4), we get from (7.1):

$$ln\left(\frac{v_L}{v_L - h'(t)}\right) = \left(\frac{c_2^2}{\Gamma_0}\right) \frac{\pi}{4} k_{III}^2(t,h,h') = q\, k_{III}^2(t,h,h')$$

with $q = \left(\frac{c_2^2}{\Gamma_0}\right) \frac{\pi}{4}$. Note that $\left(c_2^2 \frac{\pi}{4}\right)$ and Γ_0 are of the same order.
Simple calculations lead to:

$$h'(t) = v_L \left(1 - exp\left(-q\, k_{III}^2(t,h,h')\right)\right). \tag{7.6}$$

Results of experimental investigations, [47], [8], [38], [5], [39], show that for a dynamically growing crack in specific materials, the fracture toughness depends on the crack tip velocity in a very strong way. For most materials, the fracture toughness is an increasing function of the crack velocity (cf. Fig. 7.2). The data shown in Fig. 7.2 include values of the crack tip speed presented in Subsection 7.2.1.

7.2 Setting

Two examples for the dynamical propagation of a mode III crack under the action of shear waves will be analysed. The first example is related to constant opposed loading concentrated on the top and bottom of the configuration. The second example treats the action of a crack face loading that appears behind its moving tip. For both examples, we take into account the functions $\Gamma_1(h,h')$, (7.3) and $\Gamma_2(h,h')$, (7.4).

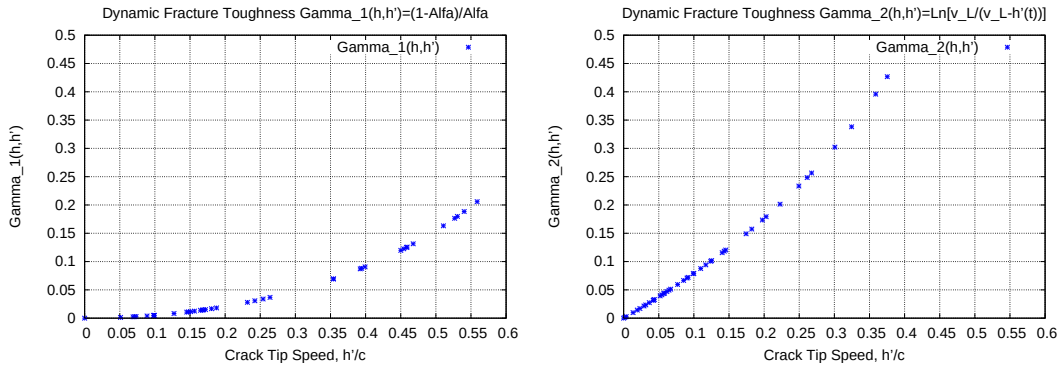

(a) $\Gamma(h,h') = \dfrac{1-\alpha_2}{\alpha_2}$ (b) $\Gamma(h,h') = ln\left(\dfrac{v_L}{v_L - h'(t)}\right)$

Figure 7.2: The dynamic fracture toughness versus normalized crack tip speed

7.2.1 The crack tip propagation with constant load

The out-of-plane displacement $u = u(y_1, y_2, t)$ is obtained by the above 2D finite element analysis for the elastic wave equation under the above conditions, namely the problem is formulated as the following initial-boundary value problem: find a solution $u(y,t)$ which satisfies:

$$\begin{aligned}
&\partial_t^2 u - c_2^2 \Delta u = 0 \quad \text{in } Q = \cup_{t=0}^{T} \Omega_t, \\
&c_2^2 \partial_n u = 0 \quad \text{on } \sigma_t, \\
&c_2^2 \partial_n u = q \quad \text{on } \Gamma_N \times (0,T), \\
&u(y,t_0) = k_{III}(t_0)\, S_N(y_1 - h, y_2, t_0) \quad \text{in } \Omega_{t_0}, \\
&\partial_t u(y,t_0) = 0 \quad \text{in } \Omega_{t_0},
\end{aligned} \tag{7.7}$$

In the first example we deal with the coupled problem (7.7) and (7.1) with a constant load $q = \pm c_2^2 * 10^{-4}$ on the top and bottom, and with $q = 0$ on the rest of the boundary (see Fig.7.3).

7.2.1.1 Displacement field

We consider the elastic displacement field $u(y_1, y_2, t)$ along lines parallel to the crack line but in the immediate vicinity of the crack zone, e.g. $y_2 = 0.1$ and $y_2 = -0.1$. It is obtained numerically in the elastic plate, which is assumed to contain one single crack in its interior, i.e. $h_0 = 0.9$. A Galerkin method with graded mesh with respect to the growing crack is applied for solving (7.7). Figure 7.4 shows the elastic displacement fields $u(y_1, y_2, t)$, for given symmetric y_2 values and for a time t very close to the crack initiation, e.g. $t = 3 * 10^{-5}$ s, produced by the interaction of the crack and the incident wave.

It is to be remembered that the pre-crack in the configuration with length $0.1m$ ($h_0 = 0.9m$) is situated at the mid-plane of the square and on the right side (Fig.7.3). The out-of-plane dis-

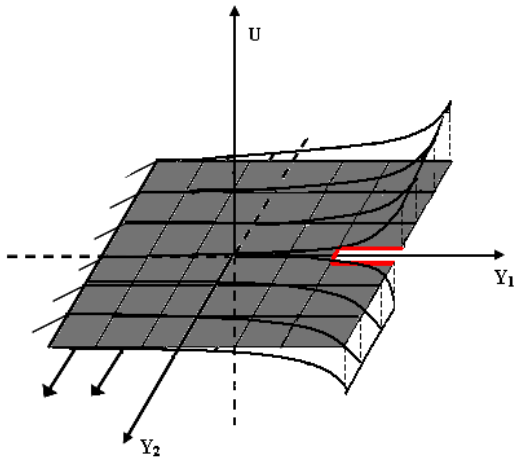

Figure 7.3: A cracked elastic plate under Mode III

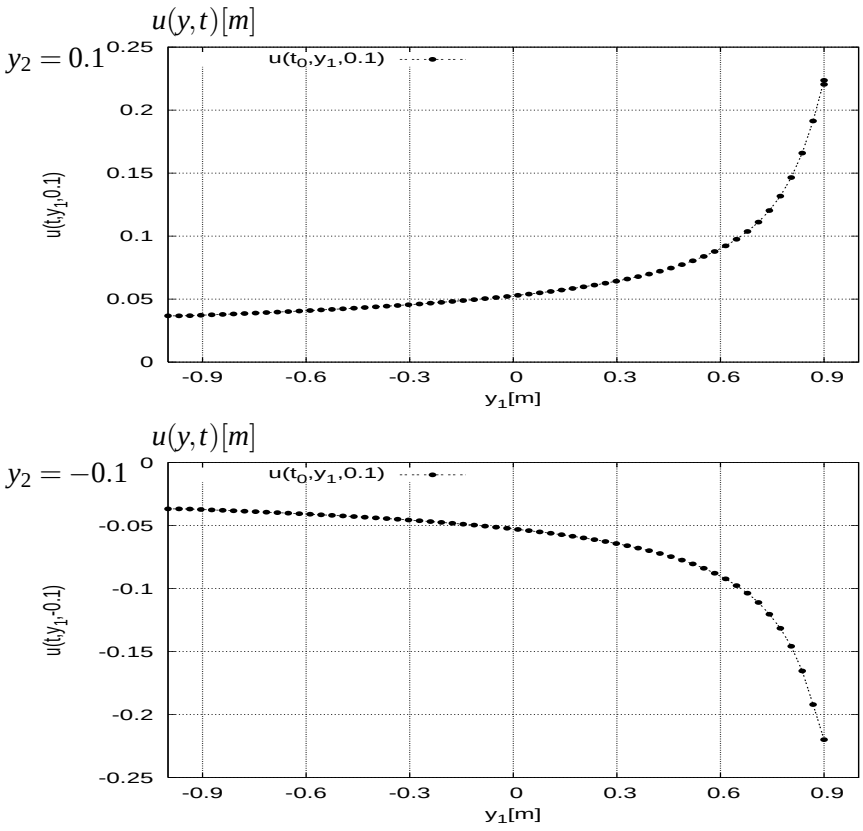

Figure 7.4: Distribution of the displacement fields $u(y,t)$ along lines parallel to the crack surface for the cracked elastic plate, with constant load ($y_2 = 0.1$, $y_2 = -0.1$, $-1 < y_1 < 1$).

placement $u(y,t)$ is obtained by finite element analysis with the PDE2D software program. The displacement field is anti-symmetric with respect to horizontal axis, i.e. u has the property that $u(y_1,-y_2,t) = -u(y_1,y_2,t)$. A finite spike at the time close to the crack initiation is observed, in Fig.7.4. Results for different instants of time $t_1 < t_2 < t_3$... after the crack initiation $t = t_0$ can be also analysed as shown in Figure 7.5. The results show that even for a point which is relatively close to the crack zone or for times very close to crack initiation time the diffracted stress waves radiate from the crack-tip and propagate into the body. The crack started to grow at some later time. It should be remarked that the Figures 7.4 and 7.5

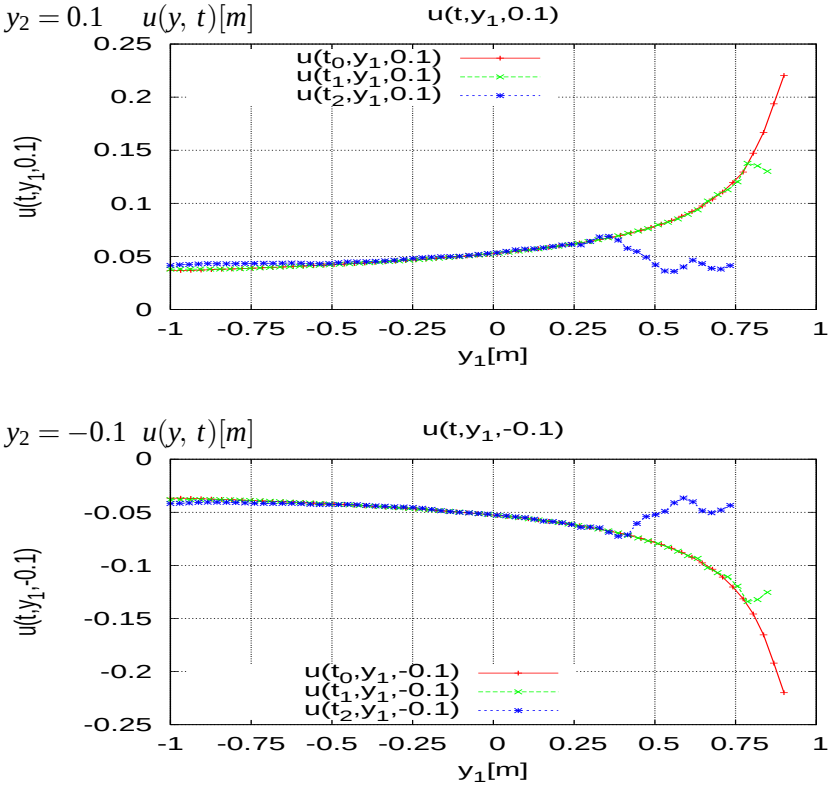

Figure 7.5: Distribution of the dynamic displacement fields along lines parallel to the crack surface ($y_2 = 0.1, y_2 = -0.1, -1 < y_1 < h(t)$) as wave propagates with constant load.

are to be read from right to left.

7.2.1.2 Dynamical stress intensity factor

The dynamic stress intensity factor characterizes the stress field in the vicinity of the crack and controls the crack growth, [47], therefore our attention is focused on the time-dependent

stress intensity factor. In the present approach $k_{III}(t,h,h')$ it is extracted from the displacement field decomposition.

The influence of the waves on the stress intensity factor values at the crack tip is described in the following. We calculate the leading stress intensity factor $k_{III}(t,h,h')$ in (7.7) using formula (4.43):

$$\lim_{R(t)-h_0(t_0)\to 0} \frac{2}{\sqrt{\alpha_2(t)}} \sqrt{(R(t)-h_0(t_0))}\frac{\partial u}{\partial y_2}|_{\vartheta=0} = k_{III}(t_0,h_0,h_0').$$

According to this formula to extract the values of stress intensity factor, positive and negative results for $k_{III}(t,h,h')$ are admissible because positive and negative results for $\frac{\partial u}{\partial y_2}$ are allowed. The change from positive to negative values and back occur as the position of both sides of the crack is changing with the time from up to down because of the influence of the shear wave. This implies that the crack face alters its tearing direction during the crack growth and that induces therefore positive or negative values of $k_{III}(t,h,h')$ with respect to the y_1y_2 coordinate system.

An initial value of $k_{III}(t_0,h_0,h_0') = 1$ was assigned with the numerical intent that the initial data for $u(y,t_0)$ in (7.7) and the unknown h' solved by (7.5) be well-defined. The variation of the estimated dynamic stress intensity factor normalized with respect to their static values versus time is plotted in Figure 7.6, where an initial crack tip position $h_0 = 0.9m$ is supposed.

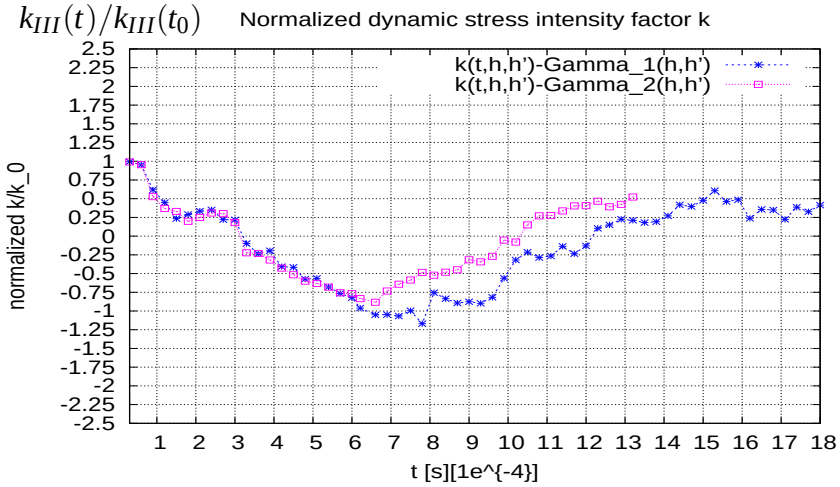

Figure 7.6: The normalized dynamic stress intensity factor history at the running crack-tip under stress wave loading conditions for initial crack length $0.1m$.

The interaction of elastic waves within the crack tip zone provides an appropiate mechanism for the growth of the fracture. This interaction between the shear wave with the growing crack

Table 7.1: Data for the time, the stress intensity factor and the crack tip position in Fig. 7.7

T	$k_{III}(t,h,h')$ for $\Gamma_1(h,h')$	$h(t)$ for $\Gamma_1(h,h')$	$h'(t)$ for $\Gamma_1(h,h')$
$t_1 = 2.70\text{E-}04$	0.2206	0.6656	685.81
$t_2 = 3.60\text{E-}04$	-0.2370	0.6336	196.71
$t_3 = 5.40\text{E-}04$	-0.6793	0.4948	1073.00
$t_4 = 7.20\text{E-}04$	-1.0678	0.1046	1799.67
$t_5 = 8.40\text{E-}04$	-0.8358	0.0047	1387.72
$t_6 = 1.11\text{E-}03$	-0.2655	-0.3085	565.16
$t_7 = 1.26\text{E-}03$	0.1498	-0.3603	206.89
$t_8 = 1.41\text{E-}03$	0.2703	-0.4174	382.96
$t_9 = 1.44\text{E-}03$	0.4179	-0.4335	534.09

influences the behaviour of the displacement fields on the crack lips and generates differents tracks. The stress pulse causes a temporary decrease in the stress intensity factor, which is illustrated in Fig. 7.6. The values of $k_{III}(t,h,h')$ calculated using (7.3) agree quite well with the ones by using (7.4).
The differences reflect the coupling of the different energy balance equations using $\Gamma_1(h,h')$ and $\Gamma_2(h,h')$ with the wave equation.
From (4.43), it is noted that the stress intensity factor significantly depends on the values of $\frac{\partial u}{\partial y_2}$. The stress intensity factor $k_{III}(t,h,h')$ changes sign from positive to negative and again to positive, thereby indicating that the crack faces alter their tearing direction during crack growth as interact with the 2D linear elastic shear wave. These altered tearing directions of the crack faces are rendered visible in Fig. 7.7, where the corresponding tracks running along the crack surfaces are represented through the $u(t,y_1,y_2)$ solutions of (7.7) along the horizontal axis from $y_1 = -1$ to $y_1 = h(t_i)$, $i = 1,..,9$, with y_2 and t fixed each time. The values of considered times t and the corresponding values of $k_{III}(t,h,h')$ for the profile of the surface perturbations are listed in Table 7.1.

The stress intensity factor $k_{III}(t,h,h')$ from the initial values is: $k_{III}(t_0,h_0,h'_0) = 1$. Finally the approximate values of $k_{III}(t,h,h')$ were calculated via (4.43) after computing $h(t)$ via (7.5) and (7.6). In Table 7.2 the approximations of this initial value using increasing number of triangles N in the mesh are shown when one considers $\Gamma_1(h,h')$. Also the relative error is here computed.

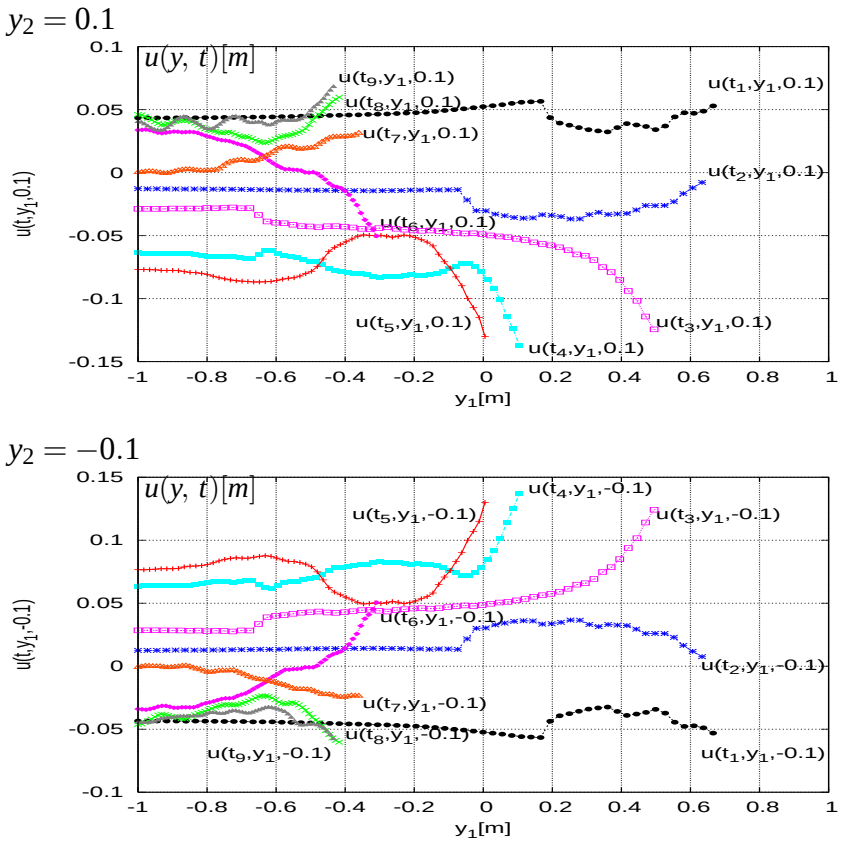

Figure 7.7: Distribution of the dynamic displacement fields along lines parallel to the crack surface ($y_2 = 0.1, y_2 = -0.1, -1 < y_1 < h(t)$) as wave propagates with constant load.

Table 7.2: Relative error of initial data for the stress intensity factor

N	computed $k_{III}(t_0)$ for Γ_1	relative error
40	0.6545	3.4546E-01
96	0.8101	1.8991E-01
192	0.9829	1.7068E-02
500	1.0494	4.9498E-02
1000	0.8368	1.6316E-01
1500	1.0311	3.1045E-02
2500	0.9342	6.5731E-02
3000	1.0325	3.2541E-02
4000	0.9932	6.7412E-03

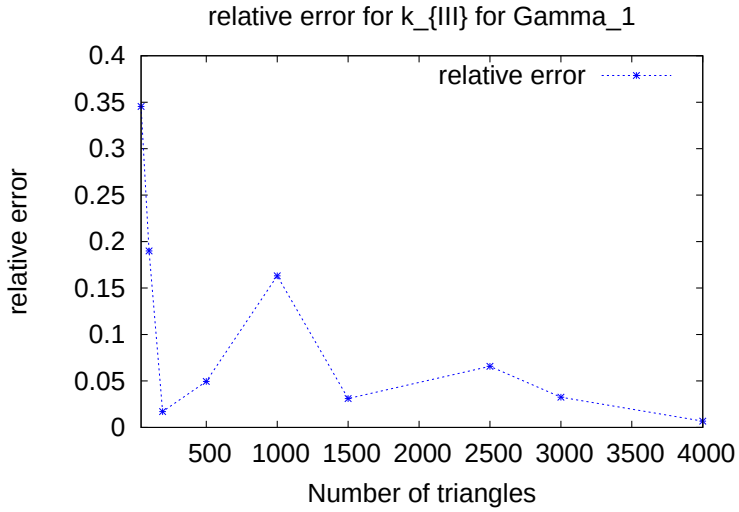

Figure 7.8: Relative error for the calculated values of $k_{III}(t,h,h')$ with Γ_1.

The plane wave, mathematically defined in (7.7), loads the crack and causes dynamic initiation and propagation of the crack-tip $h(t)$. By solving now the equation of motion (7.1) with the afore extracted dynamic stress intensity factor $k_{III}(t,h,h')$, the instantaneous time-dependent crack-tip speed $h'(t)$ can be determined (see iterative procedure).

7.2.1.3 Crack tip speed and crack tip position

For non-constant crack tip velocity, analytical or numerical solutions of dynamic crack propagation problems on the anti-plane shear crack from the viewpoint of the fracture mechanics have only been found for simple configurations such as that of a semi-infinite crack in an unbounded body. However, most practical cases are modeled in finite domains with different boundary conditions. Here we present discussions of the effects of wave interactions on the dynamic stress-intensity factors numerically for finite domains.
Figure 7.9 shows the numerical predictions in which we have used the equation of motion (7.1) to simulate the crack non-uniform velocity $h'(t)$, (7.5) and (7.6) for the considered pre-crack and functions $\Gamma_1(h,h')$, (7.3) and $\Gamma_2(h,h')$, (7.4).
The crack tip speed for $\Gamma_1(h,h')$ corresponding to constant loading described in subsection 7.2.1 behaves similar to the one for time-depending loading, described in subsection 7.2.2, but it is smaller in magnitude.
The non-uniform velocity motion of the crack tip for both $\Gamma_1(h,h')$ and $\Gamma_2(h,h')$ (7.3), (7.4) during which the crack is influenced by incoming waves, starts from an equilibrium state and

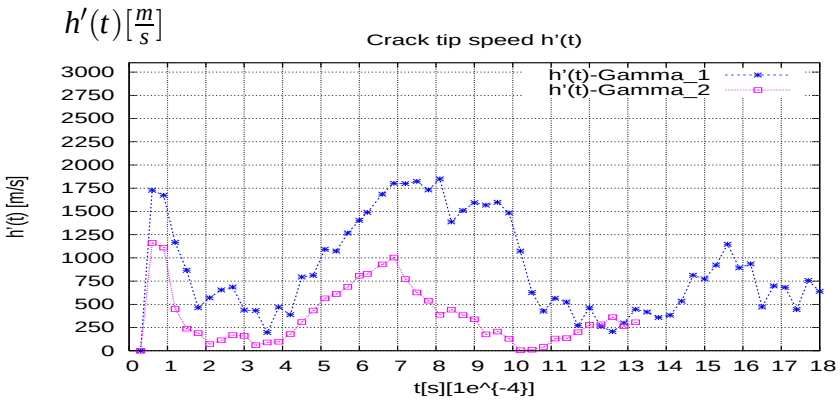

Figure 7.9: Numerical crack-tip speed for initial crack length $0.1m$.

changes more or less abruptly in comparison to the propagation of crack tip subject to crack face loading.

If the crack grows, the stress intensity factor immediately takes on the value associated with this velocity field. The relation between $k_{III}(t,h,h')$ and $h'(t)$ is observed in Figures 7.6 and 7.9, when $k_{III}(t,h,h') \to 0$ then $h'(t) \to 0$ and when $k^2_{III}(t,h,h')$ grows, $h'(t)$ grows, too.

Figure 7.9 implies the presence of a limiting velocity for crack propagation in a short time interval. In the first case for $\Gamma_1(h,h')$ it is concluded that $h'_{max} \sim 0.56c_2$ whereas in the second one for $\Gamma_2(h,h')$, $h'_{max} \sim 0.38c_2$. It seems that because of these maximum of the observed crack tip speed values $h'(t)$, the coefficients β in (7.5) and Γ_0 in (7.6), play the role of stabilisation parameters.

In Figure 7.10, the profile of the crack-tip position is plotted.

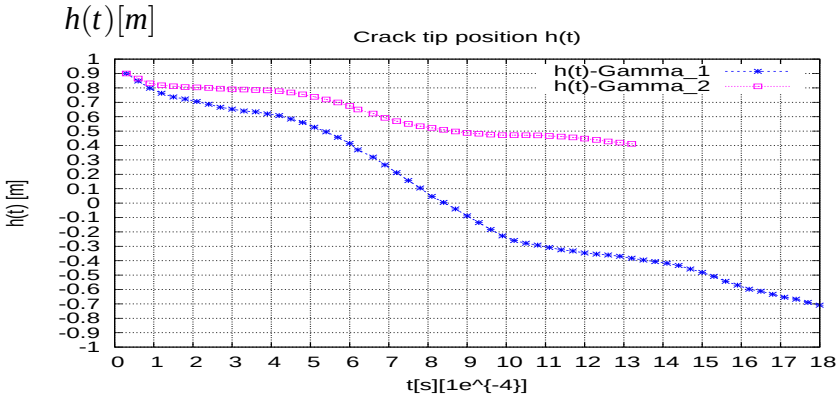

Figure 7.10: Numerical crack-tip position for initial crack length $0.1m$.

7.2.1.4 Effects of triangulation

In this subsection we examine how sensitive are the results with respect to different triangulations. By changing the position of vertex 8 and 10 in Fig. 7.1(a) we get a new initial triangulation Fig. 7.11(a); a new final triangulation with 4000 elements Fig. 7.11(b) and the corresponding zoom of the cracked zone Fig. 7.11(c). Usage of a second triangulation does not significantly affect the computational results. The ability of the FEM model by using PDE2D [27] to solve the dynamic problem was also checked by comparing computational results for the stress intensity factor and the crack tip speed, see Fig. 7.12.

7.2.2 Time-dependent crack face loads

In this section we carry out numerical simulations of the coupled problem with a pair of opposed concentrated time-dependent forces on the crack surfaces. To check the ability of the equation (7.1) to describe dynamic crack development, a rectangular sample with a cut simulating a crack is loaded by applying an intense load to the crack faces. The problem is solved numerically in the same manner as the one for the constant load and it is formulated as the following initial-boundary value problem: find a solution $u(y,t)$ which satisfies

$$\begin{aligned}
&\partial_t^2 u - c_2^2 \Delta u = 0 \quad \text{in } Q = \cup_{t=0}^{T} \Omega_t, \\
&c_2^2 \partial_n u = c_2^2 k_{III}(t_0)\, \partial_{y_2} S_N(y_1 - h, y_2, t_0) \quad \text{on } \sigma_t, \\
&c_2^2 \partial_n u = 0 \quad \text{on } \Gamma_N \times (0,T), \\
&u(y,t_0) = k_{III}(t_0)\, S_N(y_1 - h, y_2, t_0) \quad \text{in } \Omega_{t_0}, \\
&\partial_t u(y,t_0) = 0 \quad \text{in } \Omega_{t_0},
\end{aligned} \tag{7.8}$$

Numerical calculations have been carried out for a cracked square configuration of side-length 2 m. The configuration contains a pre-crack of length 0.1 m and the crack is assumed to grow straight along the horizontal axis to the left due to the stress distributions on the crack lips. On $\{(y_1,y_2) : h(t) \leqslant y_1 \leqslant 1, y_2 = 0\} = \{(y_1,y_2) \in \sigma_t\}$ a time-dependent load is applied which induces a Mode III-loading on the configuration. The load is thus applied on the newly created crack surface of σ_t. On the rest of the boundary we impose homogeneous Neumann boundary conditions.

7.2.2.1 Displacement field

The faces of the crack are subjected to applied, equal but opposite concentrated normal forces which tend to separate the crack faces. For the problem at hand, the full field analytical solution for the elastodynamic field surrounding the crack tip was obtained by formula (4.1).

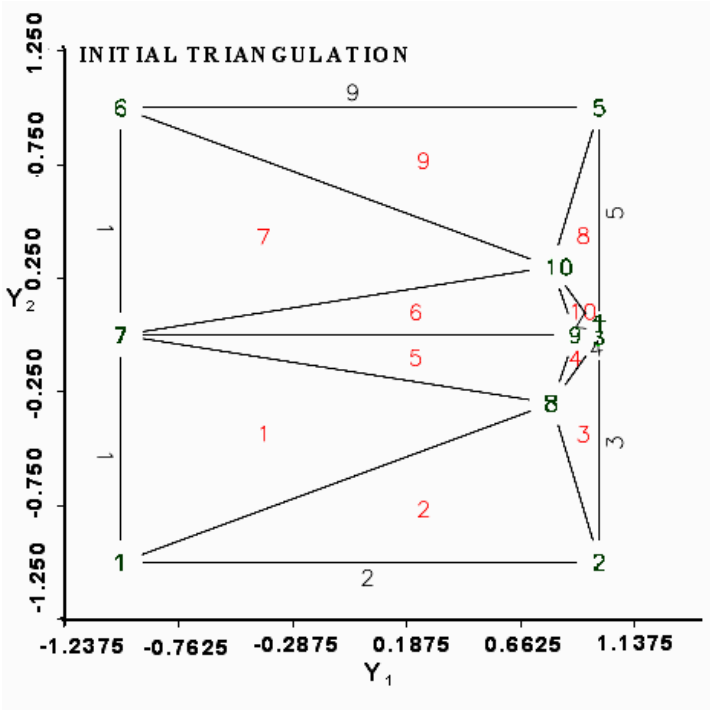

(a) Initial triangulation

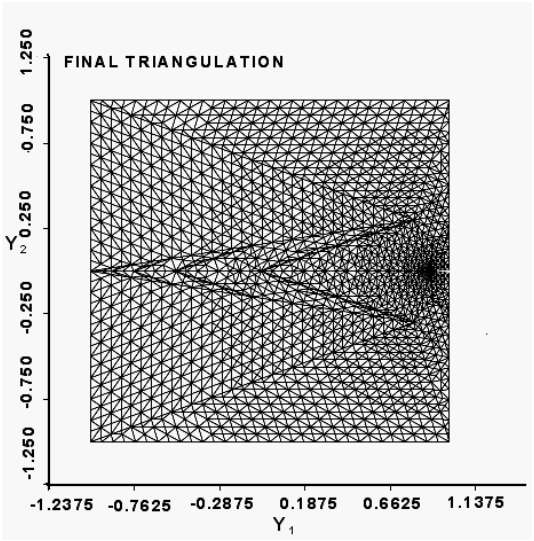

(b) Mesh used in the FE model

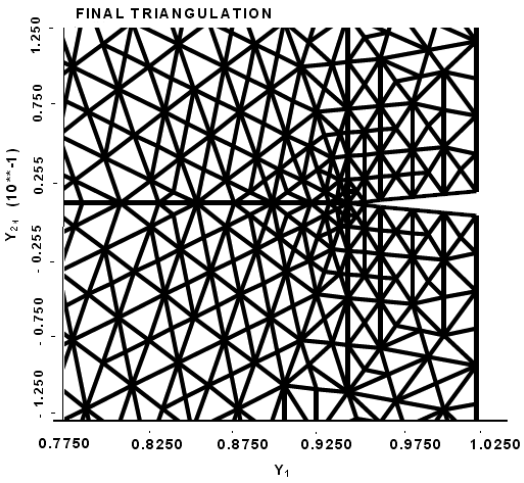

(c) Mesh surrounding the crack tip

Figure 7.11: Computational domains

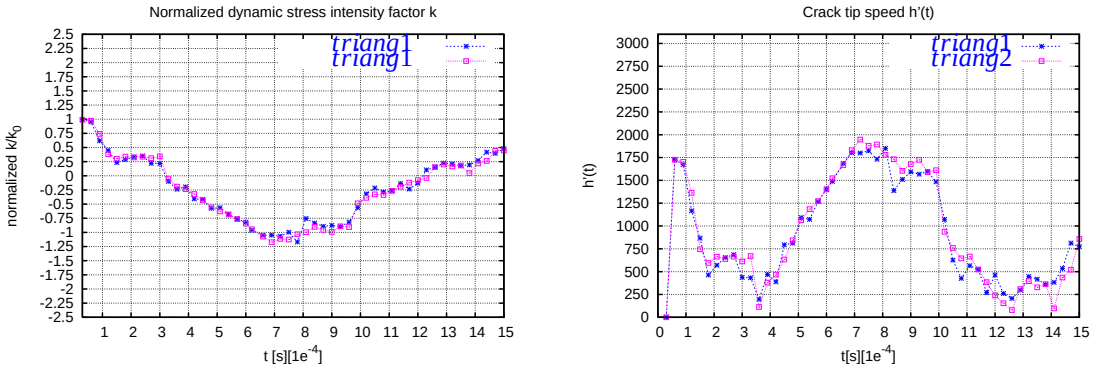

(a) $k_{III}(t,h,h')$ (b) $h'(t)$

Figure 7.12: Computational results for different configurations

Also, the corresponding dynamic Neumann singular functions in the actual configuration are given by formula (4.2). The elastic displacement field $u(y_1,y_2,t)$ is considered along lines parallel to the crack line but in the immediate vicinity of the crack zone, e.g. $y_2 = 0.1$ and $y_2 = -0.1$. It is numerically obtained in the elastic plate, which is assumed to contain one single crack in its interior, i.e. $h_0 = 0.9m$. A Galerkin method with graded mesh with respect to the growing crack is applied for solving (7.8).
The interaction of the crack and the incident wave is shown in Figure 7.13 for the elastic displacement field $u(y_1,y_2,t)$, for given symmetric y_2 values and for a time t very close to the crack initiation time, e.g. $t = 3*10^{-5}$ s. It is to be remembered that the pre-crack in the configuration with length $0.1m$ ($h_0 = 0.9m$) is situated at the mid-plane of the square and on the right side. The out-of-plane displacement $u(y,t)$ is obtained by finite element analysis with the PDE2D software program. The displacement field is anti-symmetric with respect to horizontal axis, i.e. u has the property that $u(y_1,-y_2,t) = -u(y_1,y_2,t)$.
In Figure 7.14 results are shown for different instants of time $t_1 < t_2 < t_3...$ after the crack initiation time $t = t_0$.

7.2.2.2 Dynamical stress intensity factor

We notice that the dynamical stress intensity factor $k_{III} = k_{III}(t,h,h')$ plays a key rule in the above problem (7.8), since the coupling of the wave with the motion of the crack is expressed by nonlinear relations between the motion $h(t)$, its velocity $h'(t)$, the dynamic stress intensity factor $k_{III}(t) = k_{III}(t,h,h')$ and the fracture toughness $\Gamma_1(h,h')$ given by (7.3). The dynamic stress intensity factor characterizes the stress field in the vicinity of the crack, and controls the crack growth. Here, $k_{III}(t,h,h')$ belongs to (7.8) and is extracted by formula (4.43)

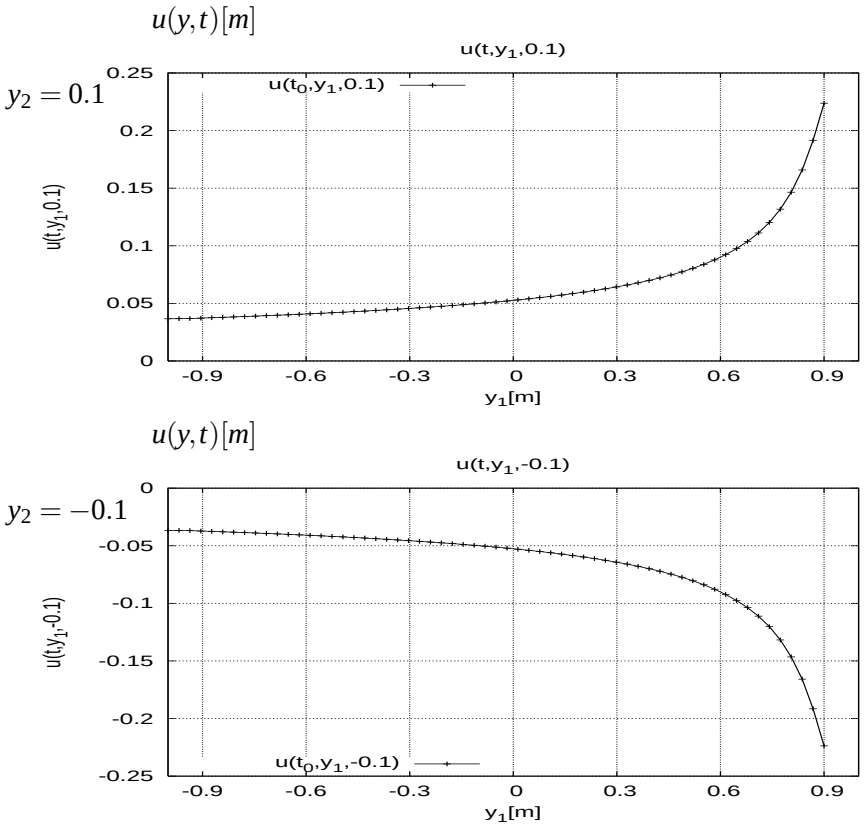

Figure 7.13: Distribution of the displacement fields $u(y,t)$ along lines parallel to the crack surface for the cracked elastic plate ($y_2 = 0.1$, $y_2 = -0.1$, $-1 < y_1 < 1$).

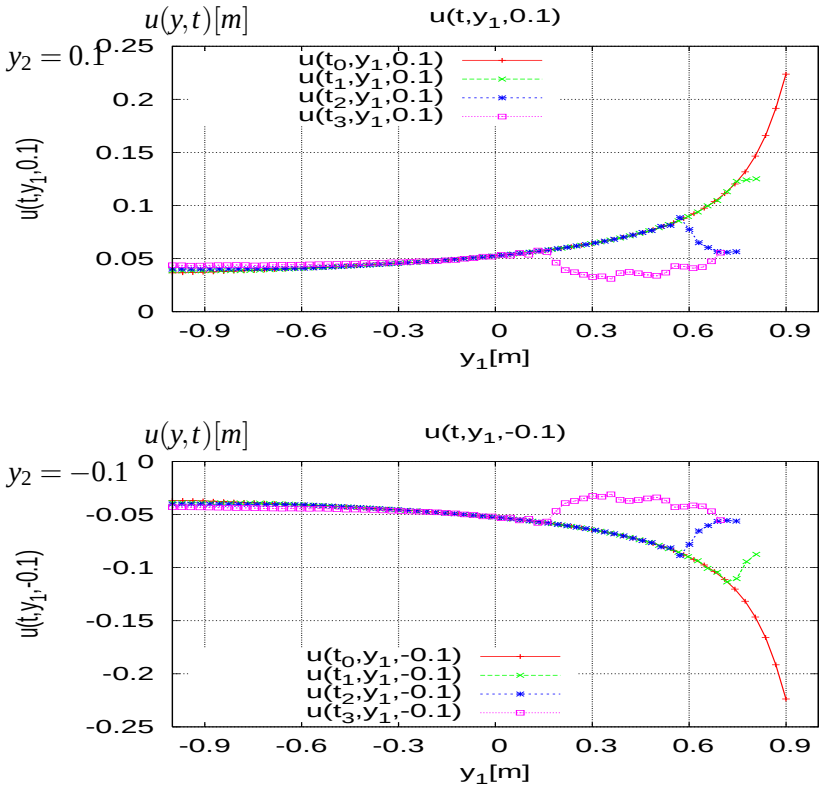

Figure 7.14: Distribution of the dynamic displacement fields along lines parallel to the crack surface ($y_2 = 0.1$, $y_2 = -0.1$, $-1 < y_1 < 1$) as the wave propagates.

Also here an initial value of $k_{III}(t_0, h_0, h_0') = 1$ is used, so that the initial data for $u(y, t_0)$ in (7.8) and (7.5) are well-defined. In Figure 7.15 the normalized estimated dynamic stress intensity factor versus time is plotted, with an initial crack tip position supposed to be $h_0 = 0.9m$ for different functions $\Gamma_1(h, h')$ (7.3) and $\Gamma_2(h, h')$ (7.4).

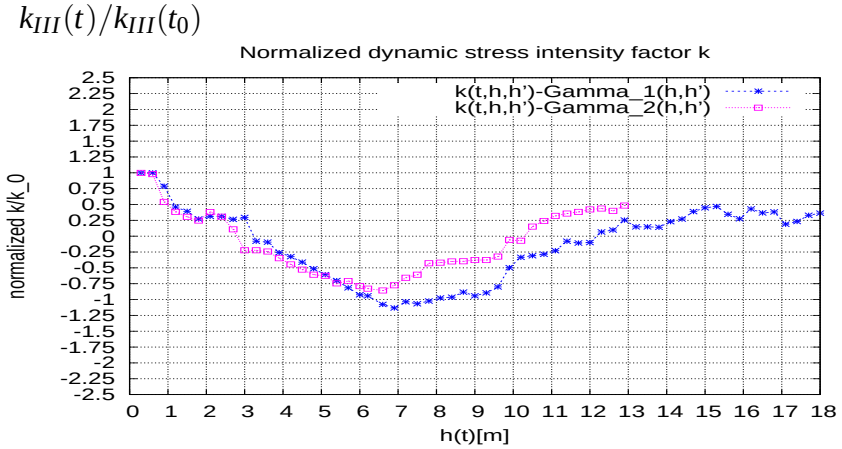

Figure 7.15: The normalized dynamic stress intensity factor history at the running crack-tip under stress wave loading conditions for initial crack length $0.1m$.

From Fig. 7.15 it observed that the stress intensity factor pattern shown for this particular load is quite similar to that of the previously analysed case, Fig. 7.6, thus indicating that the stress waves are interacting similary in both cases.

The interaction of the stress wave with the cracked square configuration gives rise to a dynamic stress intensity factor. Once the wave reaches the crack-tip, $k_{III}(t, h, h')$ decreaces rapidly to a minimum and it increases thereafter until a peak is reached as t increases further. Subsequent wave interactions lead to an oscillation of $k_{III}(t, h, h')$ as Figure 7.15 reveals. The dynamic of the stress intensity factor depends on many factors, such as the loading rate and other loading conditions, the material characteristics, the geometrical configuration.

The stress intensity factor $k_{III}(t, h, h')$ from the initial values is: $k_{III}(t_0, h_0, h_0') = 1$ and the approximate values were calculated via (4.43). In Table 7.3 the approximations of this initial value using increasing number of triangles N in the mesh are shown. Also the relative error is here computed.

The plane wave, mathematically defined in (7.8), loads the crack and causes dynamic initiation and propagation of the crack-tip $h(t)$. By solving now the equation of motion (7.1) with the afore-extracted dynamic stress intensity factor $k_{III}(t, h, h')$, the instantaneous time-dependent crack-tip speed $h'(t)$ (7.5) and (7.6) can be determined (see iterative procedure).

Table 7.3: Relative error of initial data for the stress intensity factor

N	computed $k_{III}(t_0)$	relative error
40	0.6233	3.7665E-01
96	0.8153	1.8468E-01
192	1.0216	2.1625E-02
500	1.0418	4.1806E-02
1000	0.8164	1.8360E-01
1500	1.0442	4.4205E-02
2500	0.9194	8.0555E-02
3000	1.0246	2.4603E-02
4000	1.0119	1.1902E-02

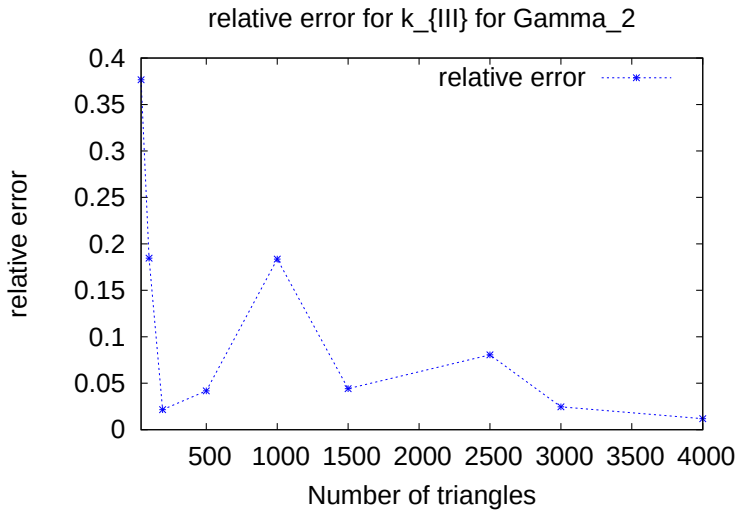

Figure 7.16: Relative error for the calculated values of $k_{III}(t,h,h')$ with Γ_2.

The iterative solution of these two coupled problems provides the solution of the problem of dynamic crack propagation in a 2D-elastic body under Mode III load.

7.2.2.3 Crack tip speed and crack tip position

Figure 7.17 shows the numerical predictions in which we have used the equation of motion (7.1), to simulate the crack non-uniform velocity $h'(t)$ (7.5) and (7.6) for the considered pre-crack.

A general belief seems to prevail that crack propagation velocities cannot exceed elastic wave velocities in a material. There are two important reasons for this: first, classical crack propagation theories are very definite in predicting an upper limit for crack velocity which is never greater than some wave velocity (for a review see reference [19]), and secondly, despite an extensive body of crack velocity data, a measurement exceeding the speed of the pertinent wave has not been reported.

From an experimental point of view, Ravi-Chandar and Knauss (1984) [41] studied dynamic fracture propagation. Based on their observations, the maximum speed of a Mode-III crack in homogeneous material is about $\approx 0.6 * c_2$

When the wave hits the crack, the crack begins to grow with non-uniform speed, [13]. At the instant of crack initiation, the crack first jumps from stationary ($h'(t) = 0$) to a velocity about $0.52 * c_2$ for $\Gamma_1(h, h')$, after that the crack-tip speed decreases and increases again and approaches the maximum observed value of $0.63 * c_2$. Whereas for $\Gamma_2(h, h')$ $h'_{max} \sim 0.38 c_2$.

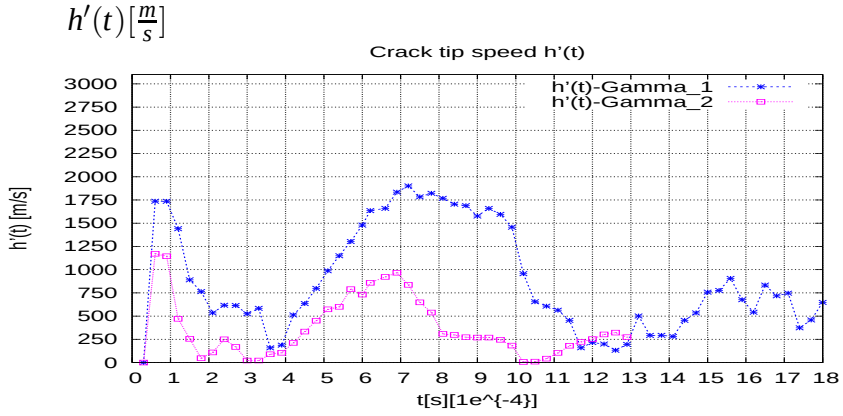

Figure 7.17: Numerical crack-tip speed for initial crack length $0.1m$ and for $\Gamma_1(h, h')$ and $\Gamma_2(h, h')$.

We conclude that at least qualitatively this numerical simulation fits with the experimental investigations.

Once the crack-tip speed history $h'(t)$ is known, the time history $h(t)$ of the crack-tip position

can be also obtained by integrating the crack-tip speed profile. By applying the equation of motion (7.1), which is coupled with the wave equation (7.8), we have been able to determine the time history of the non-uniform crack-tip speed and the crack-tip position.
In Figure 7.18, the profile of the crack-tip position is plotted.

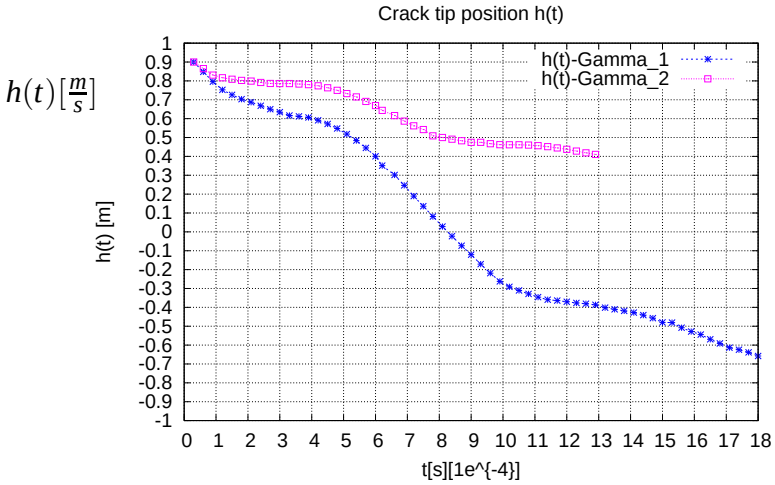

Figure 7.18: Numerical crack-tip position for initial h (crack length $0.1m$).

7.2.2.4 Energetic investigations

We carry out an energetic investigation for the elastic medium with a single crack. It was found above that in formulating the theory of crack propagation the problem of energy dissipation must be examined.
The analysis in this problem for a configuration containing a moving crack can be defined by local and global approaches. The local approach considers the singular elastic displacement field in the vicinity of the crack-tip, see (4.1). The singularity associated with this field is characterised by a parameter called the stress intensity factor $k_{III}(t,h,h')$, see (4.43). On the other hand, the global approach is concerned with the total energy balance in the body and describes the crack growth in terms of the energy release rate G, and the fact that $\dot{D}(t) = G(h,h')h'(t) = \Gamma(h,h')h'(t)$, see (4.25).
The problem of the energy dissipation in the process of crack propagation has been completely settled by the corresponding energy definitions (4.26), (4.27) and (4.28), as well as the energy balance law (4.25).
An annular domain cutting out the running crack tip $h(t)$ is considered as before, see Fig. 4.3 and the kinetic and elastic energies of the system are evaluated by direct computation of the integral (4.28), (4.26) using the solution of displacement u of (7.8) and it is shown in Figure

7.19.

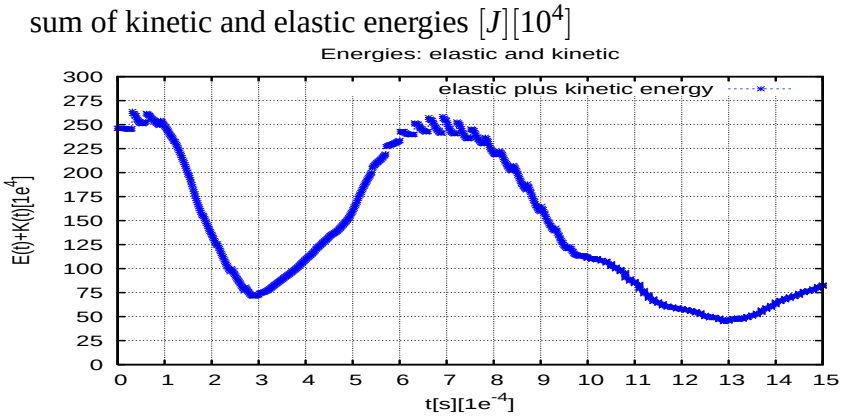

Figure 7.19: Sum of Kinetic and Elastic energies vs. time for the cracked-specimen.

The subsequent decrease in Figure 7.19 after the maximum peak seems to indicate the reflexion of waves from the boundaries.

The Figure 7.20 shows a surface plot for the cracked region, whose boundary was defined by the problem (7.8).

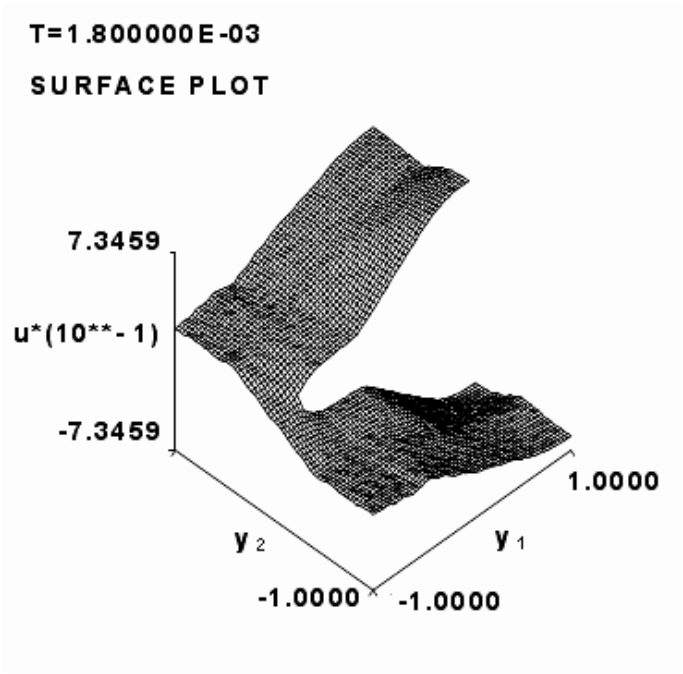

Figure 7.20: Surface Plot

The secuence of figures (7.21), (7.22), (7.23), (7.24), (7.25) and (7.26) shown the interaction of the stress wave with the cracked finite domain. The effect of the applied loading and the reflections of waves is also very important. The waves play with the boundaries of the body also, i.e. our assumption made for 7.19 agrees with these observations, the reflexion of waves from the boundaries is present.
Moreover one notes the alterations of the tearing directions of the crack surface with respect to the other one during the crack growth. That evidences the change from positive to negative values for the calculated stress intensity factor.

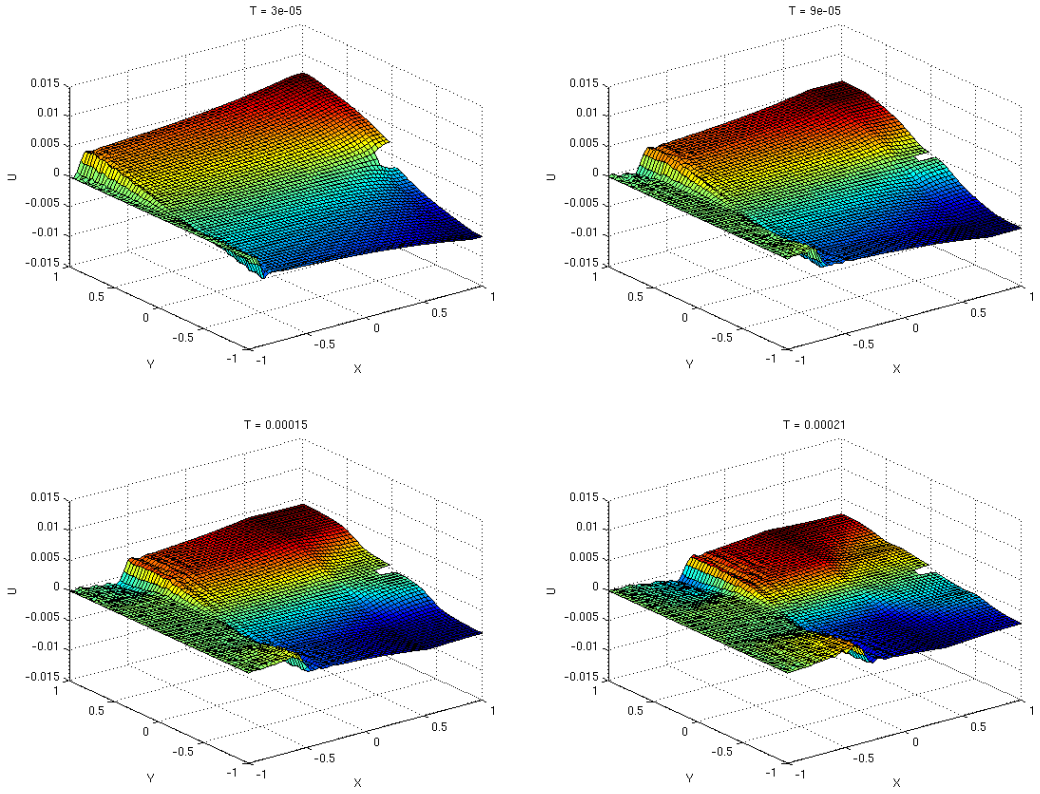

Figure 7.21: Interaction of elastic waves with a crack in the interval $[3e-05,\ 2.1e-04]$ for out-of-plane case.

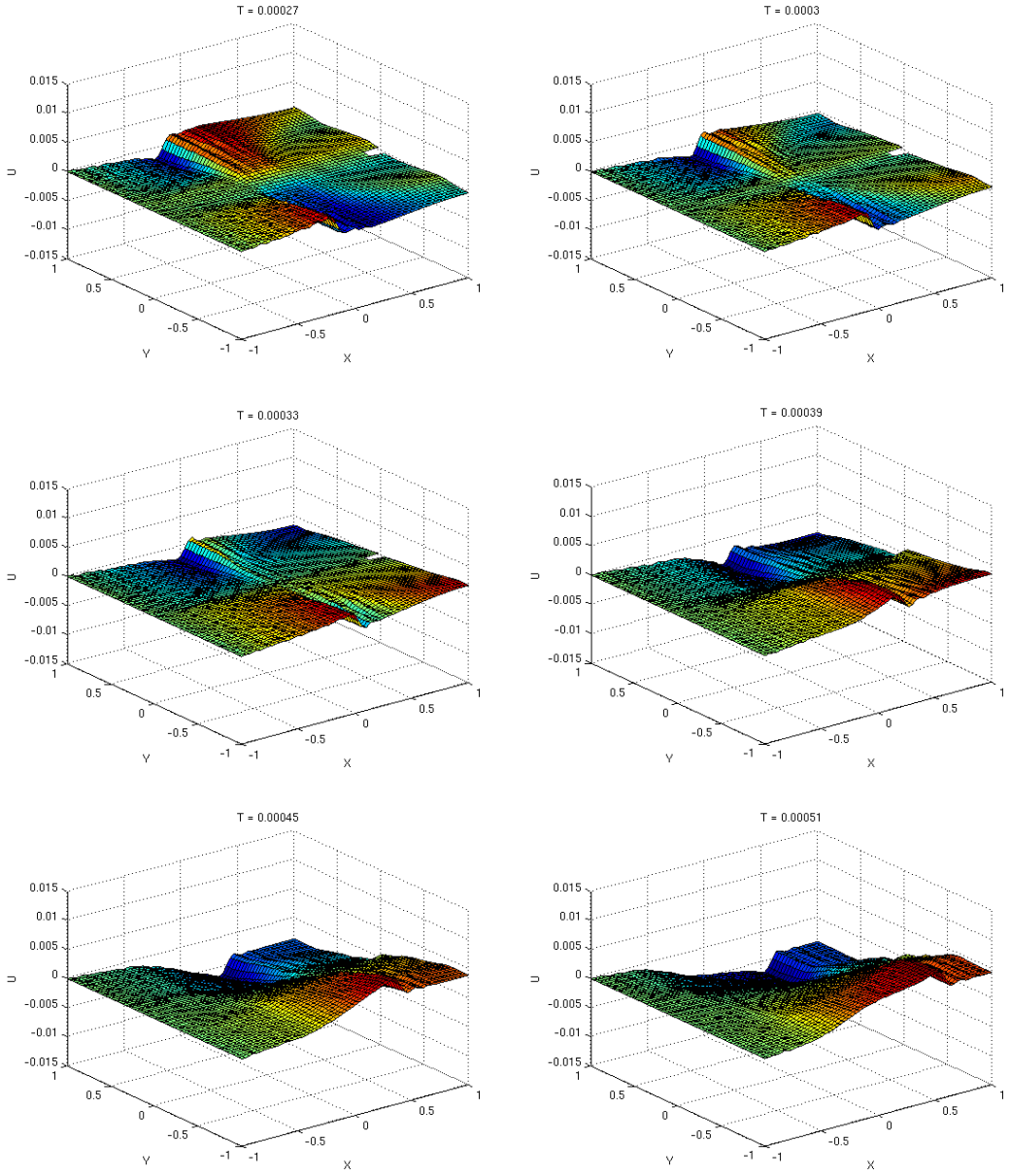

Figure 7.22: Interaction of elastic waves with a crack in the interval $[2.7e-04,\ 5.1e-04]$ for out-of-plane case.

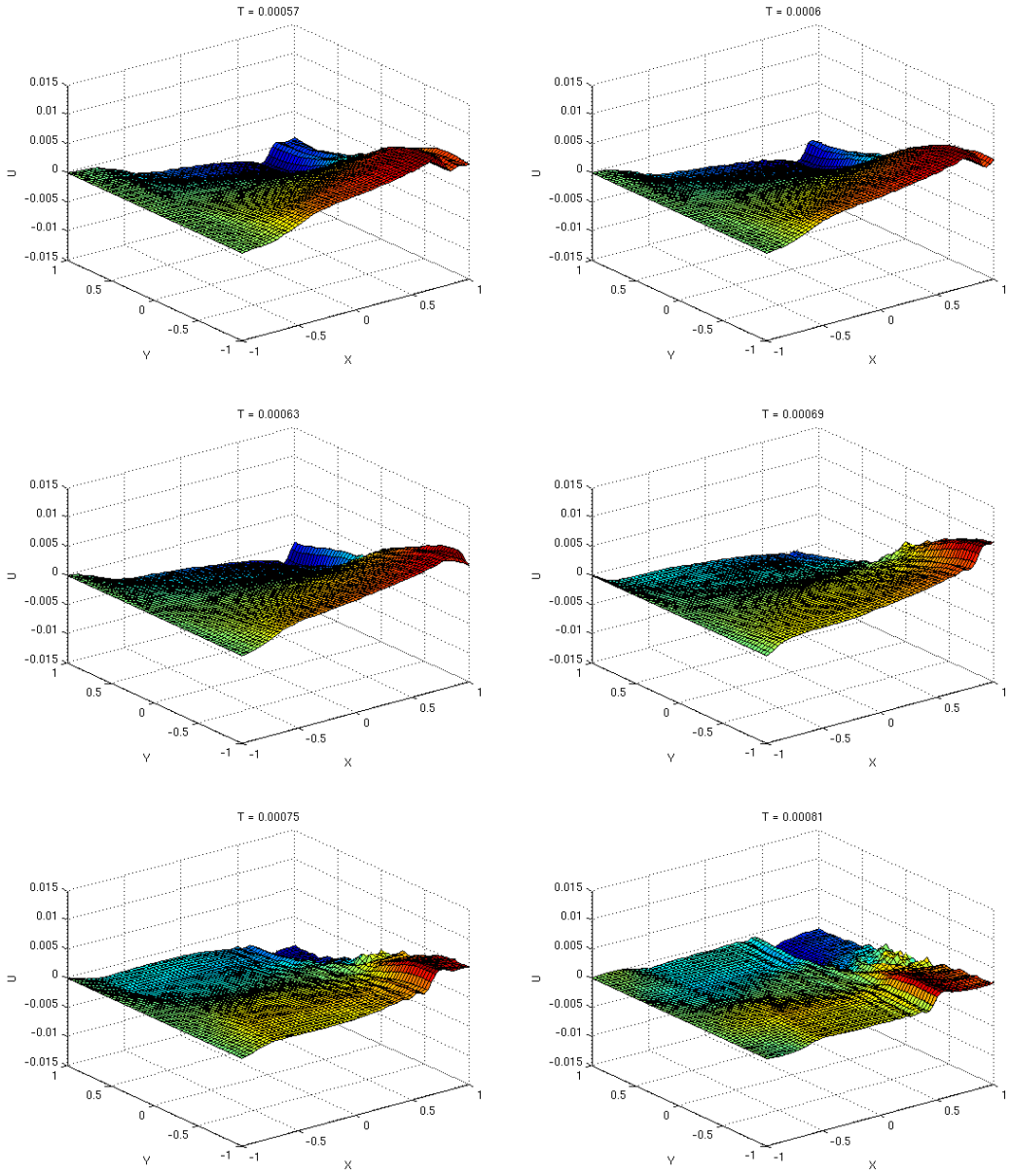

Figure 7.23: Interaction of elastic waves with a crack in the interval $[5.7e-04,\ 8.1e-04]$ for out-of-plane case.

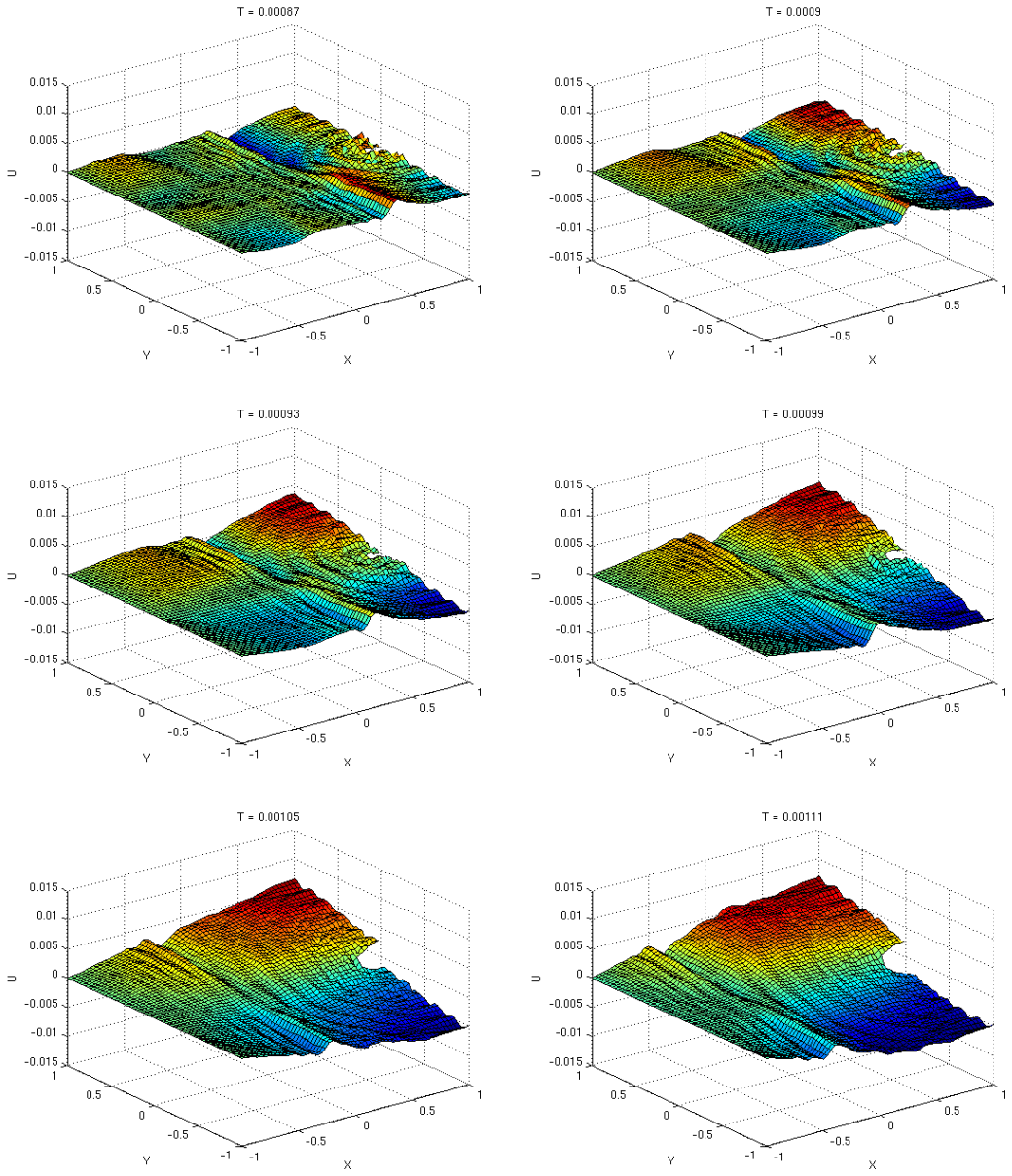

Figure 7.24: Interaction of elastic waves with a crack in the interval $[8.7e-04,\ 1.11e-04]$ for out-of-plane case.

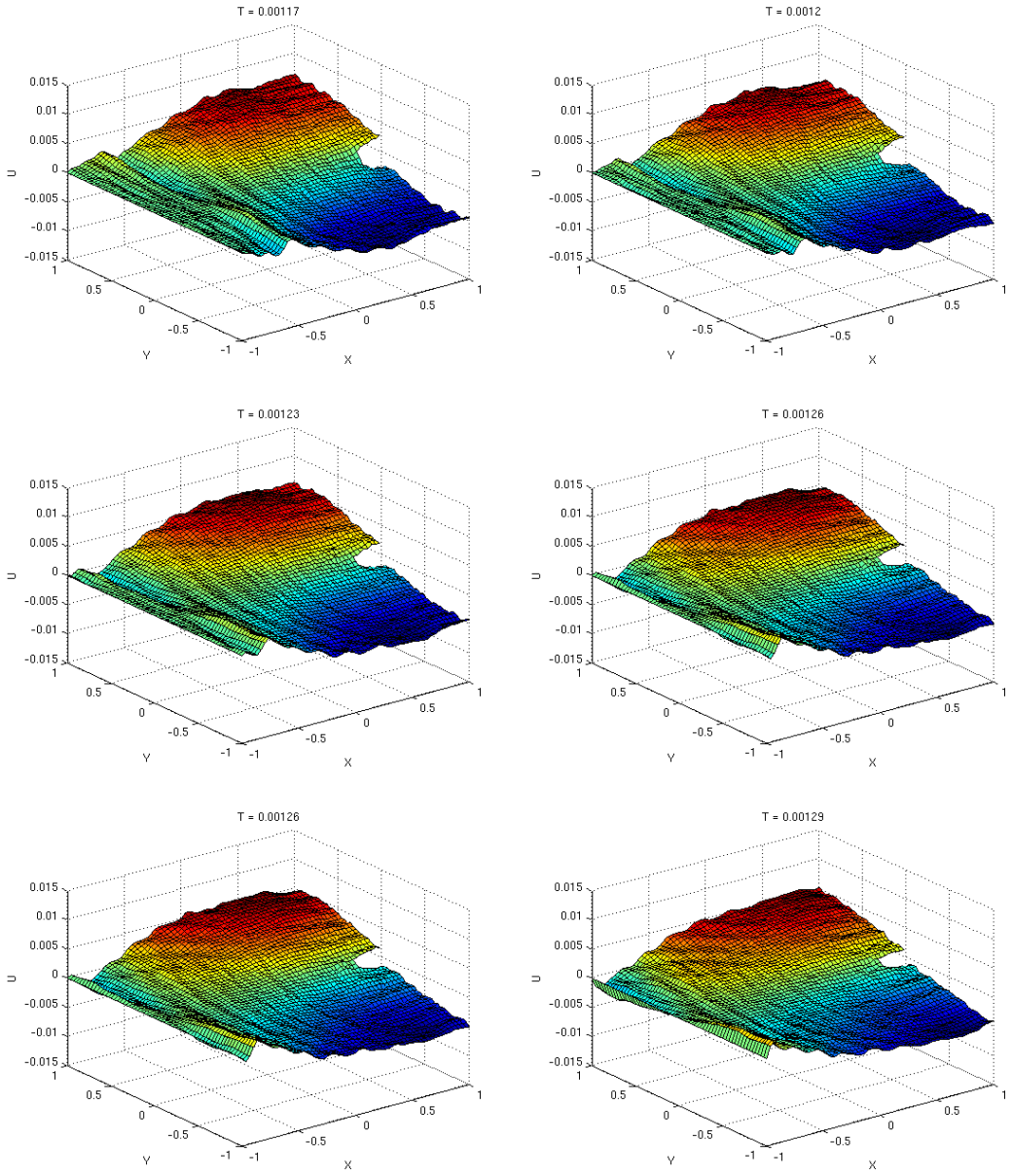

Figure 7.25: Interaction of elastic waves with a crack in the interval $[1.17e-04,\ 1.29e-03]$ for out-of-plane case.

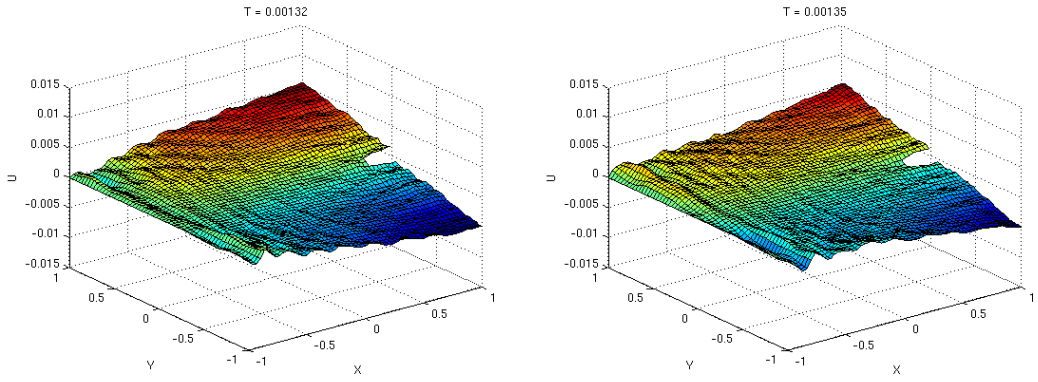

Figure 7.26: Interaction of elastic waves with a crack in the interval $[1.32e-03,\ 1.35e-03]$ for out-of-plane case.

7.3 Dynamical crack propagation for an in-plane state

In the previous sections we realised different successful numerical approximation methods for the coupled system problem (4.5)-(7.1). Now we try a more difficult coupled problem, namely, (5.6)-(6.26).

The unknowns h and u are coupled, through a system of an initial-boundary value problem for (5.6) and an initial value problem for an ordinary differential equation (6.26) derived from an energy balance law. Assuming that (4.49) is valid, it follows:

$$\Gamma(h,h') = \frac{1}{2\mu}\left[\frac{\left(1-\alpha_2(t)^2\right)\left(\alpha_1(t)\,k_I^2(t,h,h') + \alpha_2(t)\,k_{II}^2(t,h,h')\right)}{4\,\alpha_1(t)\,\alpha_2(t) - \left(1+\alpha_2(t)^2\right)^2}\right] = G(h,h') \qquad (7.9)$$

In a particular case of an opening mode crack ($k_{II} = k_{III} = 0$) the crack growth resistance $\Gamma(h,h')$, [8], [55], [93] is given by (5.1):

$$\Gamma(h,h') = \left(1 - \frac{h'(t)}{c_R}\right)\frac{(1-\nu^2)}{E}k_I(t,h,0)^2,$$

where c_R denotes the Rayleigh wave speed, ν and E are the elastic constants. $k_I(t,h,0)$ denotes the stress intensity factor for the mode I that would have resulted from the applied loading if the crack tip had always been at its instantaneous position represented by $h = h(t)$.

Therefore the latter problem reads:

Find $h = h(t)$ such that:

$$\Gamma(h,h') = \left(1 - \frac{h'(t)}{c_R}\right)\frac{(1-\nu^2)}{E}k_I(t,h,0)^2 = \frac{h'(t)^2}{2\,\mu\,c_2^2}\,\frac{\alpha_1(t)\,k_1^2(t,h,h')}{D} = G(h,h').$$

with $D = 4\,\alpha_1(t)\;\alpha_2(t) - \left(1+\alpha_2(t)^2\right)^2$.
Where $k_I(t,h,0)$ is the stress intensity factor for a quasi-static crack at the position h. $k_I(t,h,0)$ depends only on the applied loading and specimen geometry, and characterizes entirely the stress field in the vicinity of the crack tip. This equation describes quantitatively the experimental results for dynamic brittle fracture at slow crack velocities.

Note that $\dfrac{h'(t)^2\;\alpha_1(t)}{D} \to \dfrac{c_1^2 c_2^2}{2(c_1^2-c_2^2)} = (1-\nu)c_2^2$, as $h'(t) \to 0$.
This coincides with the energy release rate in the static case, hence the static Griffith criterion.

As far as we known, there are no general, reliable, efficient and accurate methods for the numerical solution of models where the elastic waves interact with cracks under dynamic loads. Techniques and results of our investigations devoted to the solution of dynamic crack propagation problems for an out-of-plane state are used here with certain adaptation for the solution of dynamic crack propagation problems in the in-plane-state.

7.3.1 Order reduction for the time-dependent problem.

The time-dependent problem (5.6) in two dimensions models the displacement $\vec{u}(y,t)$ of an elastic membrane with an interior straight crack.

Lemma 24. *If there are no body forces, $\vec{f} = 0$ then the system of second-order partial differential equations:*

$$(\lambda+\mu)\nabla(\nabla\cdot\vec{u}) + \mu\nabla^2\vec{u} = \rho\ddot{\vec{u}} \quad in\ \Omega_t,$$

can be broken into the following four first order equations, [26], before it can be solved by PDE2D [27]:

$$\begin{aligned}
\frac{\partial u_1}{\partial t} &= Du_1 \\
\rho\frac{\partial Du_1}{\partial t} &= \frac{\partial}{\partial y_1}[\mu\partial_1 u_1 + (\lambda+\mu)\,(\partial_1 u_1 + \partial_2 u_2)] + \frac{\partial}{\partial y_2}[\mu\;\partial_2 u_1] \\
\frac{\partial u_2}{\partial t} &= Du_2 \\
\rho\frac{\partial Du_2}{\partial t} &= \frac{\partial}{\partial y_1}[\mu\partial_1 u_2] + \frac{\partial}{\partial y_2}[\mu\partial_2 u_2 + (\lambda+\mu)\,(\partial_1 u_1 + \partial_2 u_2)]
\end{aligned} \tag{7.10}$$

Proof. The form of the 2D time-dependent system solved by PDE2D [27] is:

$$\begin{aligned}
C_{11}*\frac{\partial u_1}{\partial t}+C_{12}*\frac{\partial Du_1}{\partial t}+C_{13}*\frac{\partial u_2}{\partial t}+C_{14}*\frac{\partial Du_2}{\partial t}&=\frac{\partial A_1}{\partial y_1}+\frac{\partial B_1}{\partial y_2}-F_1\\
C_{21}*\frac{\partial u_1}{\partial t}+C_{22}*\frac{\partial Du_1}{\partial t}+C_{23}*\frac{\partial u_2}{\partial t}+C_{24}*\frac{\partial Du_2}{\partial t}&=\frac{\partial A_2}{\partial y_1}+\frac{\partial B_2}{\partial y_2}-F_2\\
C_{31}*\frac{\partial u_1}{\partial t}+C_{32}*\frac{\partial Du_1}{\partial t}+C_{33}*\frac{\partial u_2}{\partial t}+C_{34}*\frac{\partial Du_2}{\partial t}&=\frac{\partial A_3}{\partial y_1}+\frac{\partial B_3}{\partial y_2}-F_3\\
C_{41}*\frac{\partial u_1}{\partial t}+C_{42}*\frac{\partial Du_1}{\partial t}+C_{43}*\frac{\partial u_2}{\partial t}+C_{44}*\frac{\partial Du_2}{\partial t}&=\frac{\partial A_4}{\partial y_1}+\frac{\partial B_4}{\partial y_2}-F_4
\end{aligned} \tag{7.11}$$

where all coefficients can be functions of y_1, y_2, t, u_1, u_2 and the derivatives of u_1 and u_2. We set the following functions in (7.11):

$$\begin{aligned}
&C_{11}=1;\quad C_{12}=0;\quad C_{13}=0;\quad C_{14}=0;\quad F_1=-Du_1;\quad A_1=0;\quad B_1=0\\
&C_{21}=0;\quad C_{22}=\rho;\quad C_{23}=0;\quad C_{24}=0;\quad F_2=0;\\
&A_2=\mu\partial_1 u_1+(\lambda+\mu)*(\partial_1 u_1+\partial_2 u_2);\quad B_2=\mu*\partial_2 u_1\\
&C_{31}=0;\quad C_{32}=0;\quad C_{33}=1;\quad C_{34}=0;\quad F_3=-Du_2;\quad A_3=0;\quad B_3=0\\
&C_{41}=0;\quad C_{42}=0;\quad C_{43}=0;\quad C_{44}=\rho;\quad F_4=0;\\
&A_4=\mu\partial_1 u_2;\quad B_4=\mu*\partial_2 u_2+(\lambda+\mu)*(\partial_1 u_1+\partial_2 u_2)
\end{aligned}$$

and the order reduction (7.10) results. □

Since the Lamé Navier equation is second order in time, both the initial position and velocity of each portion of the membrane must be specified, so the initial conditions are:

$$\begin{aligned}
u_1(y,0)=k_I(h,h',0)\,\frac{(1+\alpha_2(0)^2)\,\sqrt{2r}}{\mu\,D}\Bigg[&\sqrt{\frac{\sqrt{\cos^2\varphi+\alpha_1(0)^2\sin^2\varphi}+\cos\varphi}{\cos^2\varphi+\alpha_1(0)^2\sin^2\varphi}}+\\
&-\frac{2\,\alpha_1(0)\,\alpha_2(0)}{(1+\alpha_2(0)^2)}\sqrt{\frac{\sqrt{\cos^2\varphi+\alpha_2(0)^2\sin^2\varphi}+\cos\varphi}{\cos^2\varphi+\alpha_2(0)^2\sin^2\varphi}}\Bigg],\\
u_2(y,0)=k_I(h,h',0)\,\frac{(1+\alpha_2(0)^2)\,\sqrt{2r}}{\mu\,D}\Bigg[&-\alpha_1(0)\sqrt{\frac{\sqrt{\cos^2\varphi+\alpha_1(0)^2\sin^2\varphi}-\cos\varphi}{\cos^2\varphi+\alpha_1(0)^2\sin^2\varphi}}+\\
&+\frac{2\,\alpha_1(0)}{(1+\alpha_2(0)^2)}\sqrt{\frac{\sqrt{\cos^2\varphi+\alpha_2(0)^2\sin^2\varphi}-\cos\varphi}{\cos^2\varphi+\alpha_2(0)^2\sin^2\varphi}}\Bigg]
\end{aligned} \tag{7.12}$$

and

$$\partial_t\vec{u}(y,0)=0. \tag{7.13}$$

From (7.12) can be seen that the values of $k_I(h,h',t)$ and $h'(t)$ at points near the crack tip affect the solution at y by the time t. It can be seen also that, as claimed earlier, if the coupled solutions between $k_I(h,h',t)$ and $h'(t)$ are badly behaved, the solution may be also.
On the boundary, the displacement vector is specified. The boundary conditions that model the latter situation are obtained by balancing the internal and external forces on the boundary. The homogeneous Dirichlet condition and homogeneous/non-homogeneous boundary conditions are shown in Figure 7.27.
Numerical simulations were carried out with 60×60 uniform mesh of 4000 elements. A FORTRAN expression for

$$TRIDEN(y_1,y_2) = \frac{1.0}{\sqrt{(y_1-h)^2+y_2^2}}$$

controls the grading of the triangulation. TRIDEN is largest where the triangulation is to be most dense, i.e at the crack tip $(h(t),0)$.

The computational domain consists of a cracked, finite, homogeneous, isotropic and linearly elastic solid, which is described by the square with vertices (-1,-1),(1,-1),(1,1) and (-1,1) and an interior crack σ_{t_0} from $(h(t_0),0)$ to (1,0) along the y_1-axis. The crack paths are shown in Figures 7.27.

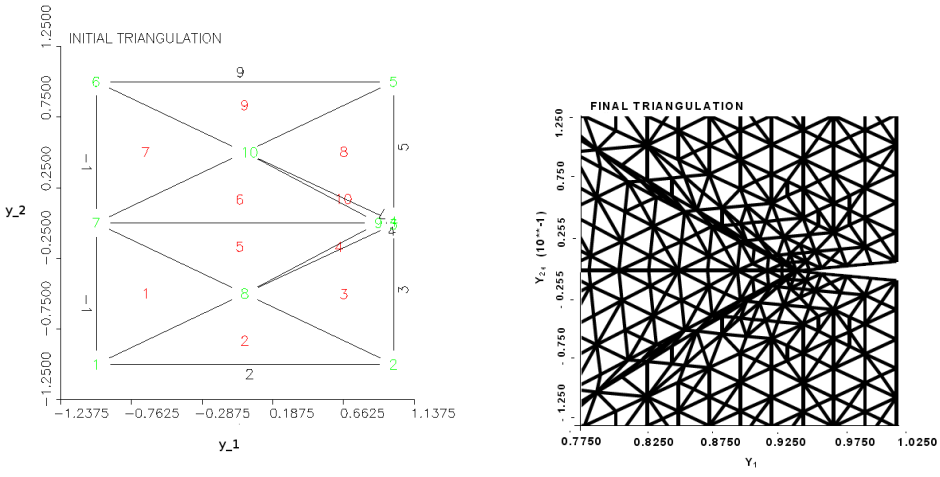

Figure 7.27: Initial/final triangulation.

The boundary conditions are:

$$\begin{aligned} &\vec{u}(y,t) = 0, \quad \text{at } y_1 = -1 \quad \text{(zero displacement at the wall)} \\ &\sigma\vec{n} = \text{prescribed function}, \quad \text{at } y_2 = -1 \text{and } y_2 = 1 \\ &\sigma\vec{n} = 0, \quad \text{at the crack} \\ &\sigma\vec{n} = 0, \quad \text{at } y_1 = 1 \end{aligned} \tag{7.14}$$

where

$$\sigma_{11} = \frac{E\left[(1-\mu)\partial_{y_1}u_1 + \mu\partial_{y_2}u_2\right]}{(1+\mu)(1-2\mu)}, \quad \sigma_{12} = \frac{E\left[\partial_{y_2}u_1 + \partial_{y_1}u_2\right]}{2\,(1+\mu)}, \quad \sigma_{22} = \frac{E\left[(1-\mu)\partial_{y_2}u_2 + \mu\partial_{y_1}u_1\right]}{(1+\mu)(1-2\mu)}.$$

The material properties are:

$\lambda = 3.12e09, \quad \nu = 0.34, \quad \mu = 1.47e09, \quad$ the dilatational wave speed $c_1 = 1970\dfrac{m}{seg}$,

the shear wave speed $c_2 = 1130\dfrac{m}{seg}$, the Rayleigh wave speed $c_R = 1017\dfrac{m}{seg}$,

The time discretization is done by the Crank-Nicolson method. The Galerkin method is used for the 2D space problem.

The strategy for solving dynamic fracture problems is to obtain the dynamically admissible displacement fields from the governing equation (7.10) subjected to the initial and boundary conditions, (7.12), (7.13), (7.14) and then to use the energy rate balance equation (6.26) at the crack tip equation to determine the crack speed. In other words, an iterative procedure to solve the nonlinear coupled problem is proposed by the flow-chart in Figure (7.28).

7.3.2 Crack propagation at constant speed in a finite body.

In order to evaluate the procedure (7.28), we want to get a first approach to describe the crack propagation in finite bodies under loading conditions. For simplicity the crack is assumed to be propagating at a specified velocity and also that only the mode I takes here place.
Uniformly distribuited tractions of magnitude $1000Pa$ are applied on the top and the bottom of the computational domain, i.e at the two sides paralell to the crack: $y_2 = -1$ and $y_2 = 1$. The plate dimensions are 2.0×2.0, and the crack, with an initial position at $(h_0(t),\, 0)$, with $h_0 = 0.1$ propagates with a constant velocity $h'(t) = 500m/s$ $(h'(t) < c_R)$. It is known that in Mode II fracture, the allowed velocities are sub-Rayleigh: $h'(t) \leq c_R$, as well as intersonic $c_2 < h'(t) < c_1$. In other words, the Rayleigh wave velocity is an upper limit of Mode I

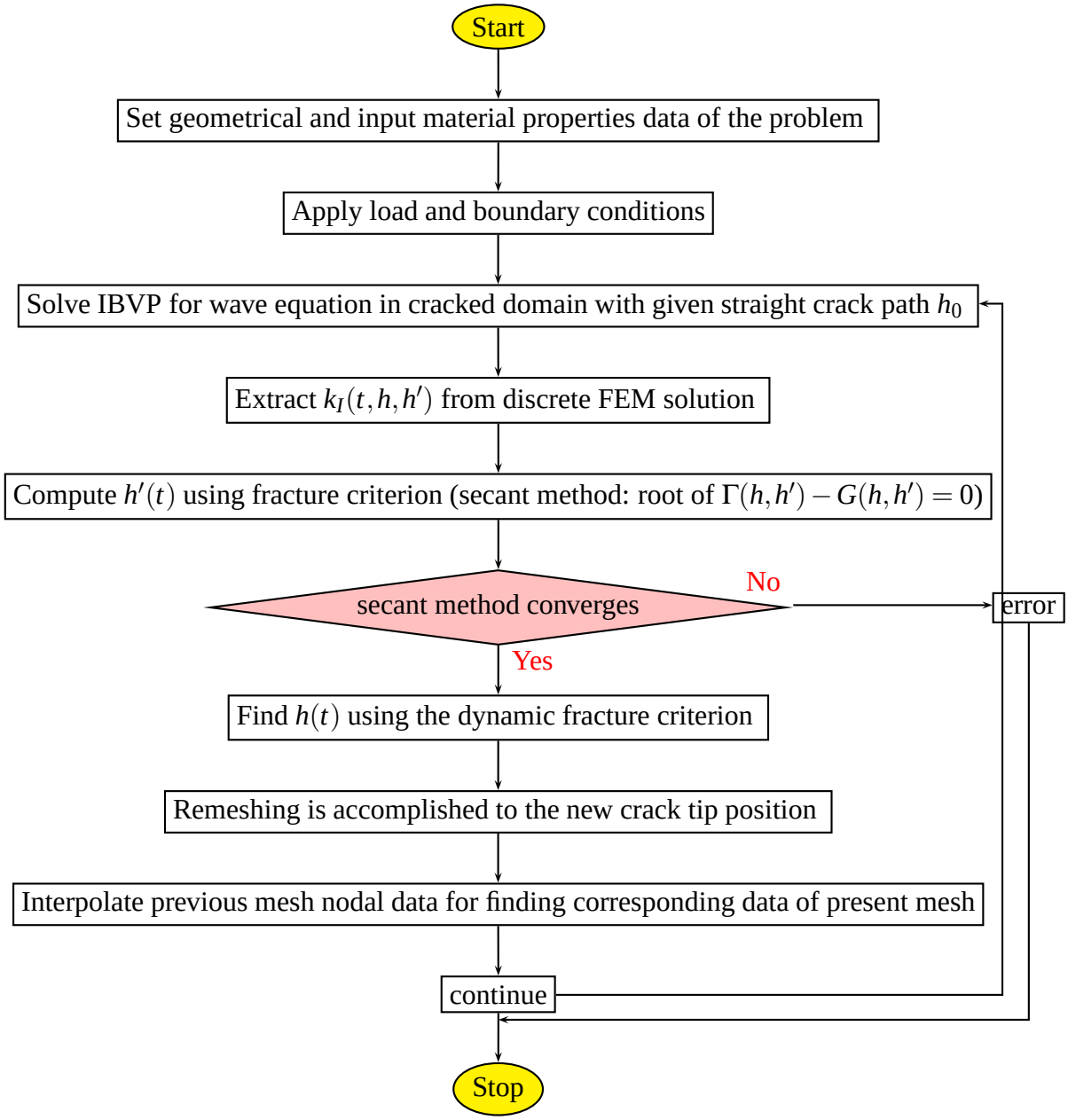

Figure 7.28: Flow-chart of the FEM algorithm of the problem

and II crack tip velocities in the subsonic or sub-Rayleigh region, i.e. $h'(t) \leq c_R$. This was originally shown by Barenblatt and Cherepanov (1960) [70] and Broberg (1960) [44] for Mode I and by Craggs (1960) [91] for Mode I and II. Note that, theoretically, the crack can reach velocities arbitrarily close to the Rayleigh wave velocities, but not propagate with this velocity.

The crack tip advances from right to left. Since the specimen is finite, we stopped the simulation before the propagating crack tip reaches the another extrem of the domain. The body is loaded by a tensile stress perpendicular to the crack face. The problems were run over a time corresponding to:

$$t_0 = (IPROB - 1) * DT0, \qquad t_F = IPROB * DT0,$$

with $IPROB = 1, \ldots, NPROB$. In this way we can solve several similar problems in the same run, i.e. we set NPROB equal to the number of problems we want to solve. Then NPROB loops through the main program will be done, and we can make the problem parameters vary with IPROB. Here NPROB = 25 and DT0=0.00003. The translation of the crack tip for each time step can take any value and is not related to the assumed discretization.

The Figures 7.29, 7.30, 7.31, 7.32, 7.33 show the first component U_1 of the displacement field as a crack moves at constant velocity.

The two types of waves, the longitudinal waves and the transversal ones, see Table 5.1 are independent in the interior of the solid. At boundaries, such as the faces of cracks, the two types of waves interact.

The wave reaches the crack at about $t = 6.9e^{-4}$s, Figure 7.32. The input waves are diffracted and scattered about the moving crack tip. When elastic waves are propagated, they are diffracted at an obstacle or geometric discontinuity and often give rise to a high elevation of local stress. These stress concentrations become extremely severe when the moving discontinuity is a crack.

The intensity factor is extracted from the FEM solutions by using (6.22). $k_I(t,h,h')$ is normalized with its initial value in order to obtain non-dimensional solution of the stress intensity factors. Figure 7.34 shows the value of normalized $k_I(t,h,h')$. It shows increasing the pathological oscillatory behaviour for $k_I(t,h,h')$ as the initial crack length increases.

$k_I(t,h,h')$ value moves from positive to negative with the increase of the crack length. The values for that $k_I(t,h,h') < 0$ would imply that the crack faces overlap. It also implies that the stress ahead of the crack are compressive and square root singular.

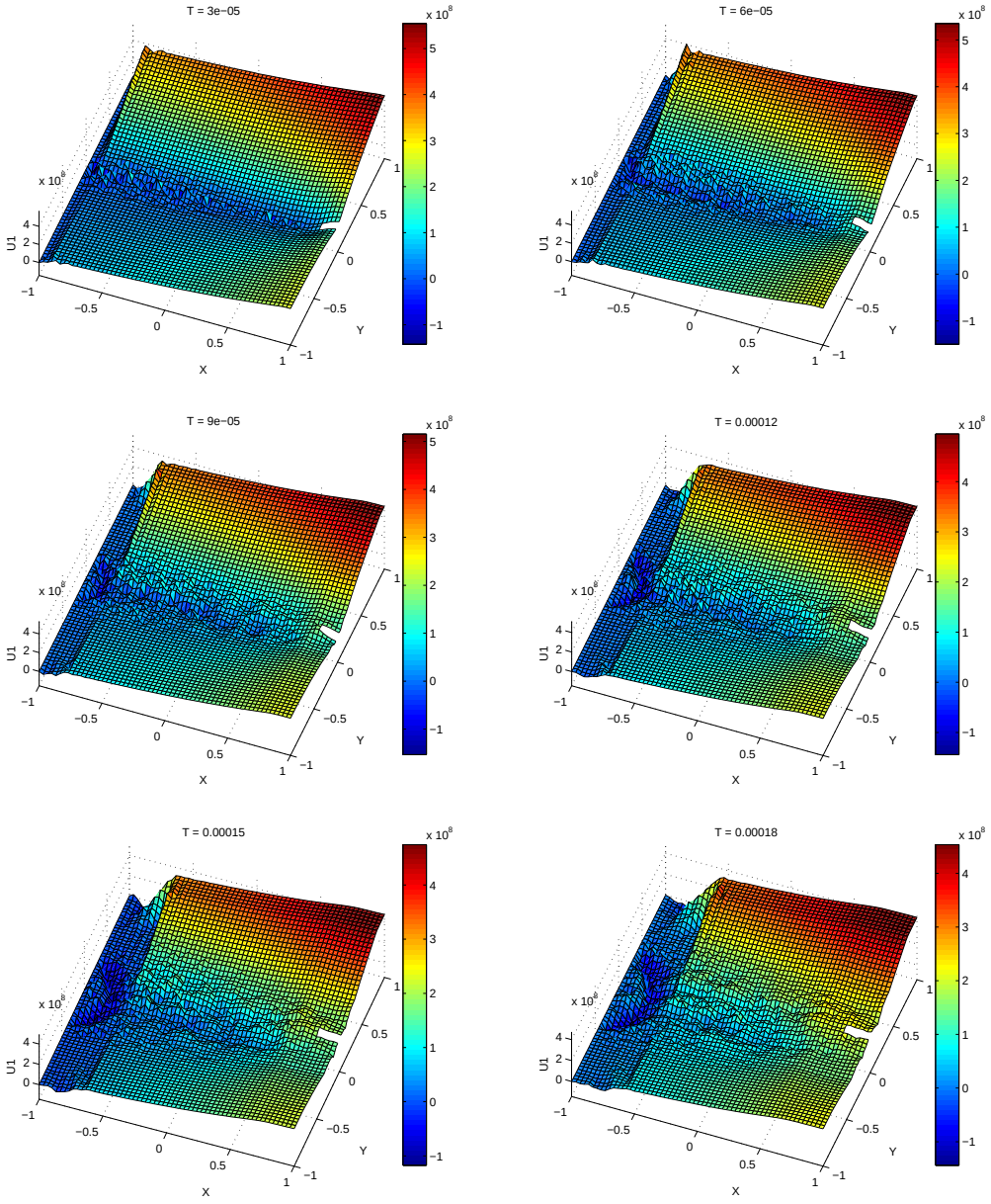

Figure 7.29: FEM solutions for (5.6). The first component U_1 for the displacement field is here shown for $t = 3e-05, \cdots, 1.8e-04$.

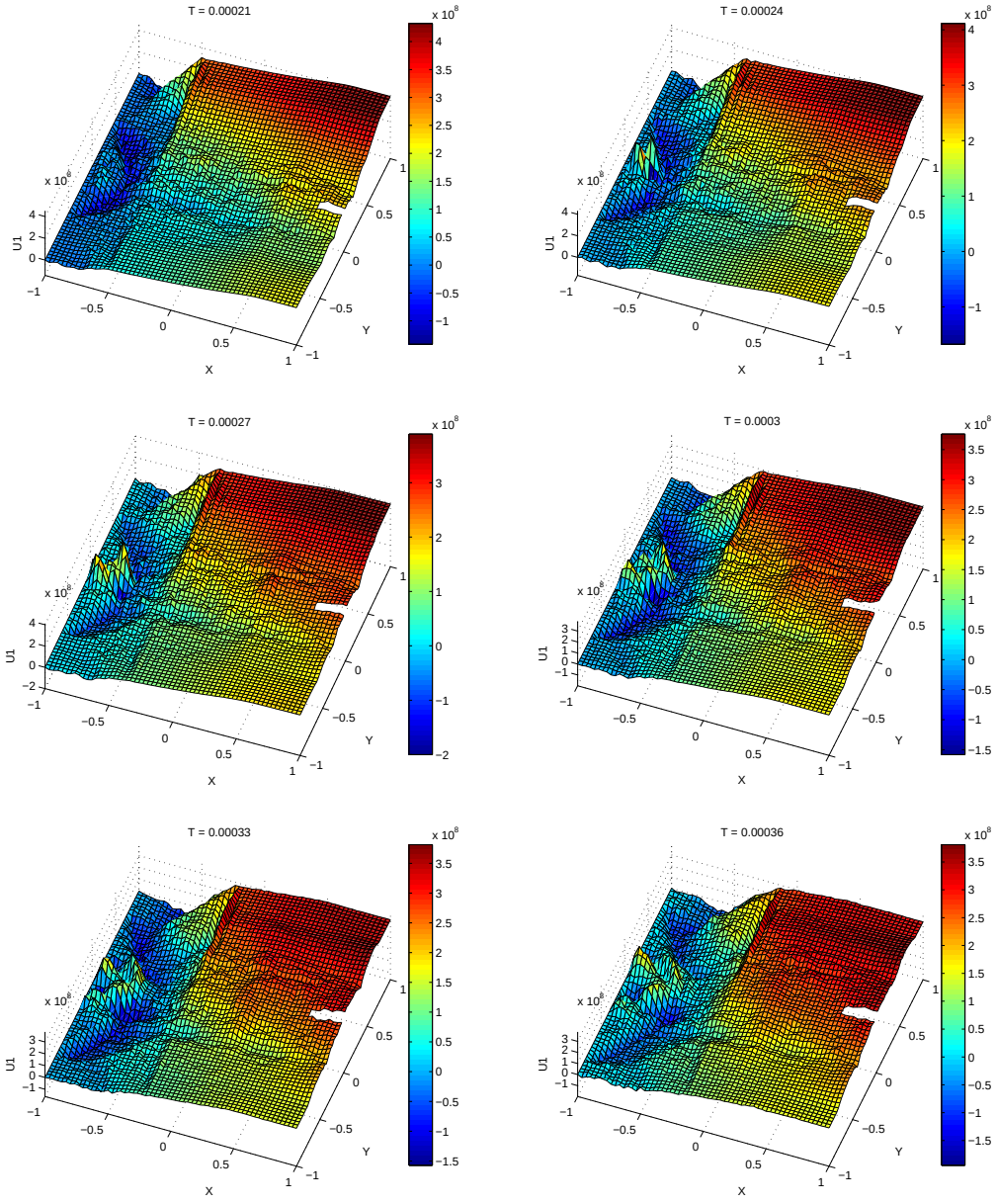

Figure 7.30: FEM solutions for (5.6). The first component U_1 for the displacement field is here shown for $t = 2.1e-04, \cdots, 3.6e-04$.

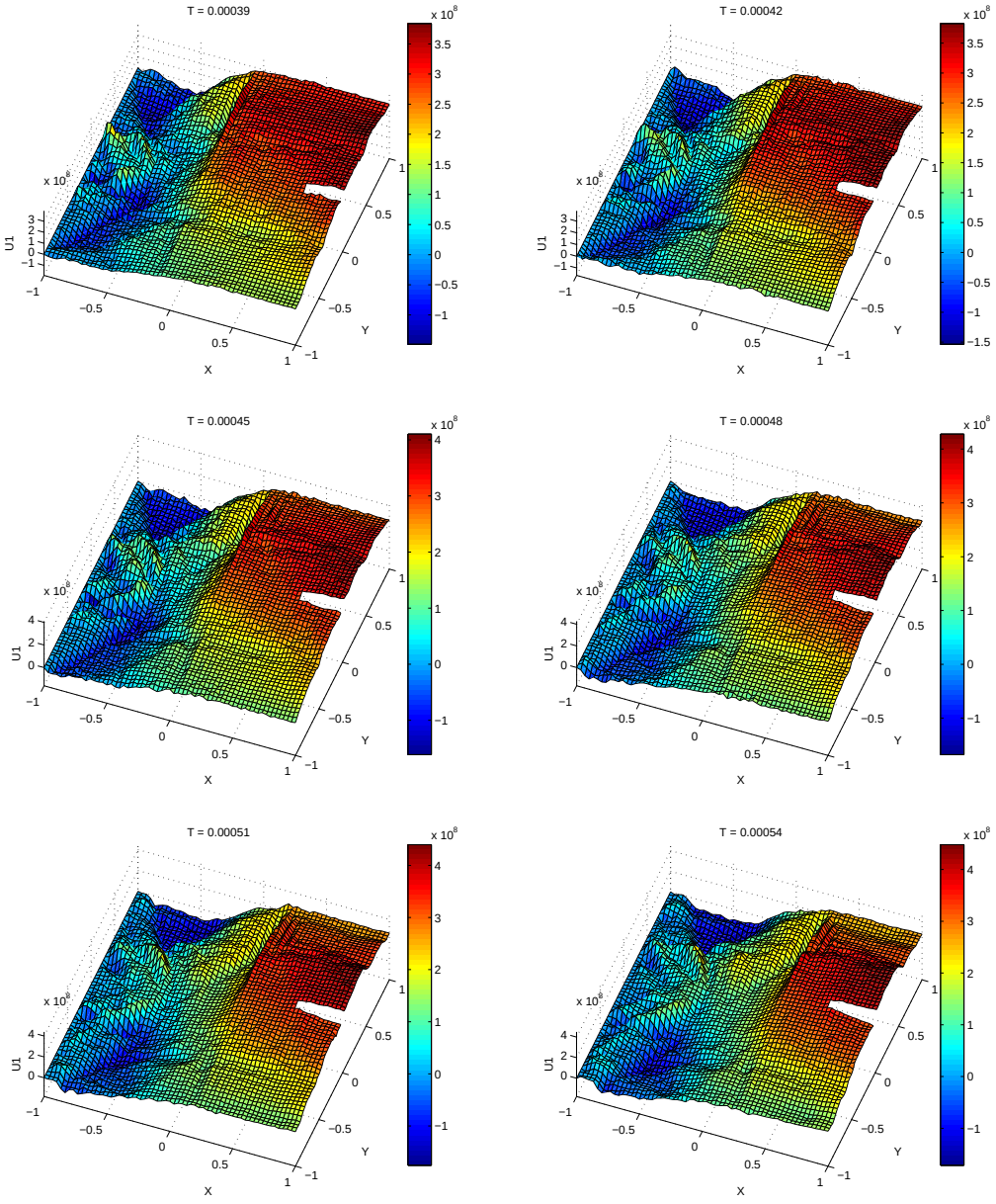

Figure 7.31: FEM solutions for (5.6). The first component U_1 for the displacement field is here shown for $t = 3.9e-04, \cdots, 5.4e-04$.

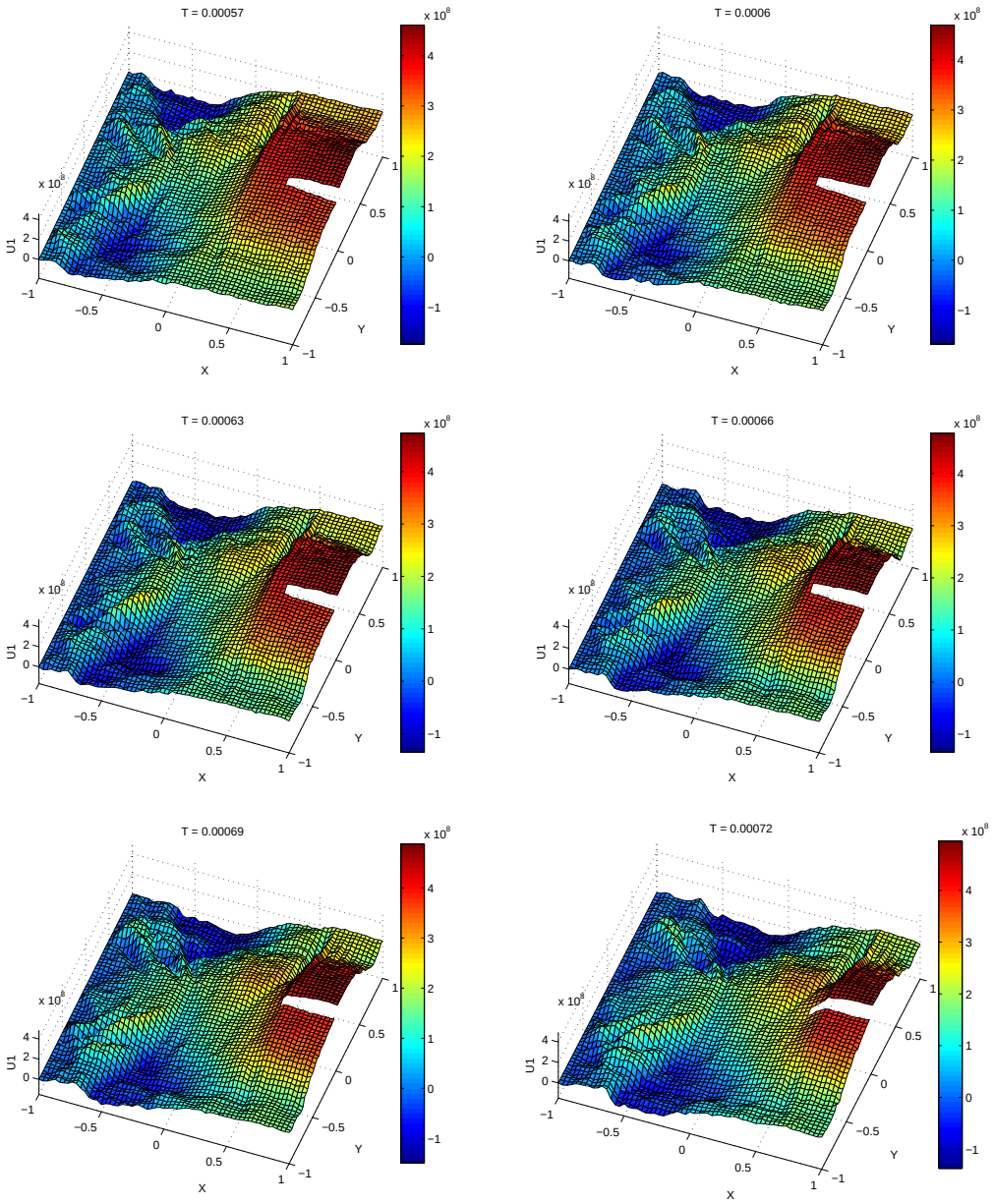

Figure 7.32: FEM solutions for (5.6). The first component U_1 for the displacement field is here shown for $t = 5.7e-04, \cdots, 7.2e-04$.

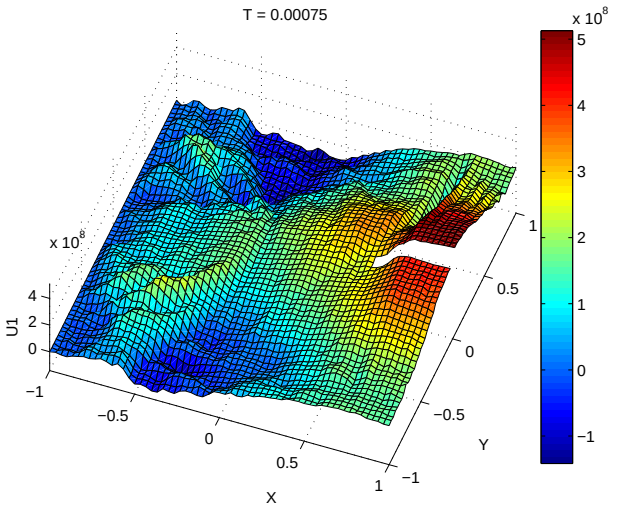

Figure 7.33: FEM solutions for (5.6). The first component U_1 for the displacement field is here shown for $t = 7.5e-04$..

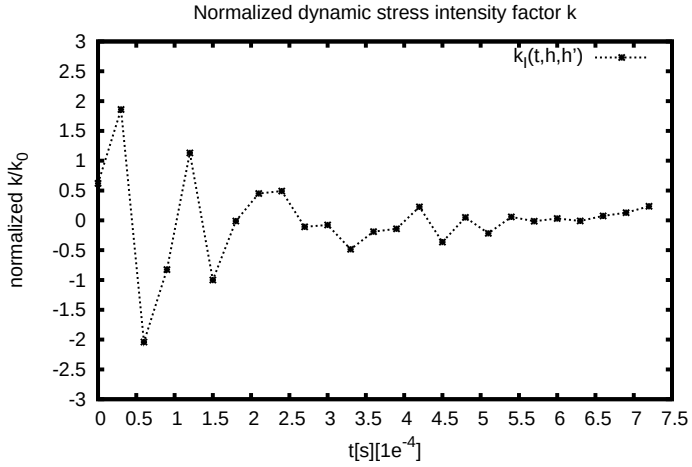

Figure 7.34: $k_I(t,h,h')$ for crack propagating with constant speed.

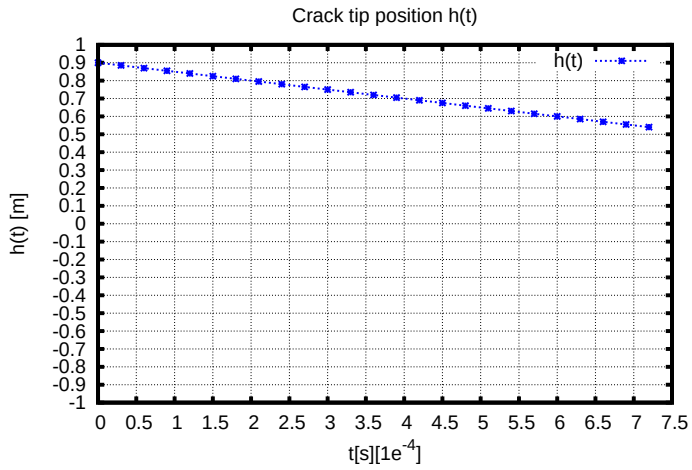

Figure 7.35: Crack evolution $h = h(t)$ for crack propagating with constant speed.

The evolution of the crack is shown in Figure 7.35.
Performing such a crack propagation simulation even through with constant speed is costly since the domain on which the elasticity equations have to be solved, changes in each iteration step thus requiring (at least local) remeshing. Additionally, since the solution exhibits a strong singularity at the crack tip, a strongly refined mesh is required near the crack tip. This technique requires considerable computing time because of the nature of the iteration. Because of that, the MPI-based parallel band solver implemented in PDE2D [27] was used. This is a parallel solver which runs efficiently on multiple processor machines, in our cases 8 processors were used, with the matrix distributed over the available processors. The CPU time required for these computations with 8 processors and only 25 iterations is: real time = 159m 49.16s with the mesh refinement at the crack tip.

7.4 Conclusions

In this thesis, it is assumed that the crack always propagates along a straight line and it does so even under the influence of a wave.
At first Mode III crack propagating in a finite domain is discussed and simulated.
A rigorous mathematical derivation of the crack tip motion under the influence of a wave is given in Section 4.2, which is a completion of the work in [77]. The expression for the total energy of the system is obtained. Assuming that a global energy equilibrium concept is valid, the equations of motion of the crack tip (7.1) is deduced, which governs the propagation of

the crack. This equation (7.1) is solved with two velocity-dependent resistances $\Gamma_1(h,h')$ and $\Gamma_2(h,h')$ (fracture toughnesses).

Numerical approximation methods for this coupled problem are developed in Section 7.1.1. We focus on the development of stable methods, as Crank Nicolson for the time discretization, Galerkin methods [12], [26]. An iterative procedure is derived for the coupled problem. The set of coupled equations (7.7) or (7.8) and (7.1) is solved by the program PDE2D, a commercially-available finite element code (www.pde2d.com). The mesh of the calculation must be particularly dense near the crack tip. A final triangulation of 4000 quadratic triangles is used. The analysis shows that -as expected- the coupled problem for the crack propagation with the interaction of a wave reproduces the characteristics of material behaviour, such as the stress intensity factor, the crack tip speed and the crack tip position.

The problems solved numerically in sections 7.1-7.2 for the out-of-plane case are exceptionally difficult for at least three reasons.

At first one has to calculate the stress intensity factor (4.43) with reasonable accuracy, given a numerical solution to an out-of-plane wave PDE. The computation of (4.43) represents a challenge even for the steady-state problem, because while $\frac{\partial u}{\partial y_2}$ is in theory infinite at the crack tip ($R(t)=h(t)$) for the numerical solution it is always finite, thus the product $\sqrt{(R(t)-h(t))}\frac{\partial u}{\partial y_2}$ numerically goes to 0 at $R(t)=h(t)$ and one needs to look at values of $R(t)$ close enough to $h(t)$ but not too close. One has to examinate the problem at small values of $R(t)$ whereas the grading of the triangulation is controlled to make sure there were still many triangles between the examined values and the crack tip. Additionally the time-depending function $\alpha_2(t)$ in (4.43) changes with the values of the crack tip speed $h'(t)$, which must therefore be known with reasonable accuracy.

Second and even more difficult problem: given an estimate of the stress intensity factor from (4.43), calculate $h'(t)$ from (7.1). This assumes the fracture toughness is known as a function of the crack tip speed. The first numerical experiments were done using the formula for the fracture toughness given by (7.3), which when solved for $h'(t)$ results in (7.5). The formula (7.3) was used because of the lack of a better, more experimentally justified formula for the fracture toughness but it produces monotonically increasing values of the crack tip velocities to a limit of c_2, [1]. Later on a second formula for the fracture toughness is used (7.4). This formula come from experiments published by University of Tokyo researchers and it gives us the formula (7.6) when solved for $h'(t)$. Besides the fact that this second formula is a published experimental relationship, it also has another advantage over the first formula: as can be seen in Figure 7.2 (or verified directly from 7.5-7.6) for the first formula the derivative of h' with respect to the stress intensity factor is infinite at $h'(t)=0$, which means when the crack speed is nearly 0, a very small increase in stress intensity leads to a very large increase

in h', which is probably the source of some inestability in the results. The second formula from University of Tokyo does not suffer from this stability problem.
A third difficulty is that one must treat a moving-singularity problem. Although PDE2D does not directly handle moving boundary problems, this was satisfactorily resolved by moving the crack in small increments, after each small increase in crack length, the solution was dumped and re-interpolated into the new problem with the new boundary (longer crack).
The influence of the geometry and of the length of the pre-existenting crack on the configuration could also be considered, for more details see [78].
The equation of motion of the crack tip under the influence of a wave was simulated here for given initial data, loading and other parameters. The simulation results and data can be used in the future in order to compute the crack tip propagation behaviour in other situations. In particular, the simulation can be done for other material dependent fracture resistances $\Gamma = \Gamma(h, h')$.

So far, to the authors' knowledge, no such simulations for crack propagation have been done. Although the obtained solutions are not high accurate, particularly at larges times, given the difficulty of the problem, the obtaining results are even qualitatively correct and a major achievement.

In section 7.3 an overview is given of how one could extend the out-of-plane algorithms to solve the in-plane state problem, with a similarly-computed variable crack velocity. For this even more complicate problem it is presented a first step forward, by solving an in-plane wave problem with a crack whose velocity $h'(t)$ is constant and given, and the stress intensity factor is computed as function of time in this case.

APPENDIX A

Appendix A

A.1 Useful equalities and transformations

Operators in polar coordinates:
The operators can be written in polar coordinates as follows:

$$\begin{aligned}
\nabla &= \frac{\partial^2}{\partial r^2} + \frac{1}{r}\frac{\partial}{\partial r} + \frac{1}{r^2}\frac{\partial^2}{\partial \omega^2} \\
\operatorname{grad}\vec{\mathrm{u}} &= \begin{pmatrix} \cos\omega \frac{\partial \mathrm{u}_1}{\partial r} - \frac{1}{r}\sin\omega \frac{\partial \mathrm{u}_1}{\partial \omega} & \sin\omega \frac{\partial \mathrm{u}_1}{\partial r} + \frac{1}{r}\cos\omega \frac{\partial \mathrm{u}_1}{\partial \omega} \\ \cos\omega \frac{\partial u_2}{\partial r} - \frac{1}{r}\sin\omega \frac{\partial u_2}{\partial \omega} & \sin\omega \frac{\partial u_2}{\partial r} + \frac{1}{r}\cos\omega \frac{\partial u_2}{\partial \omega} \end{pmatrix} \\
&= \left[\begin{pmatrix} \cos\omega & \sin\omega \\ -\sin\omega & \cos\omega \end{pmatrix} \begin{pmatrix} \frac{\partial}{\partial r} \\ \frac{1}{r}\frac{\partial}{\partial \omega} \end{pmatrix} \begin{pmatrix} u_1 & u_2 \end{pmatrix} \right]^\top \qquad \text{(A.1)} \\
\operatorname{div}\begin{pmatrix} \mathrm{u}_1(r,\omega) \\ \mathrm{u}_2(r,\omega) \end{pmatrix} &= \cos\omega \frac{\partial u_1}{\partial r} - \frac{1}{r}\sin\omega \frac{\partial u_1}{\partial \omega} + \sin\omega \frac{\partial u_2}{\partial r} + \frac{1}{r}\cos\omega \frac{\partial u_2}{\partial \omega} \\
&= \begin{pmatrix} \cos\omega & \sin\omega \\ -\sin\omega & \cos\omega \end{pmatrix} \begin{pmatrix} \frac{\partial}{\partial r} \\ \frac{1}{r}\frac{\partial}{\partial \omega} \end{pmatrix} \cdot \begin{pmatrix} u_1 \\ u_2 \end{pmatrix}.
\end{aligned}$$

The following relations hold:

$$\begin{aligned}
\partial_1 &= \cos\varphi\partial_r - \frac{\sin\varphi}{r}\partial_\varphi,\\
\partial_2 &= \sin\varphi\partial_r + \frac{\cos\varphi}{r}\partial_\varphi,\\
\partial_1^2 &= \cos^2\varphi\frac{\partial^2}{\partial r^2} + \frac{2\sin\varphi\cos\varphi}{r^2}\frac{\partial}{\partial\varphi} - \frac{2\sin\varphi\cos\varphi}{r}\frac{\partial^2}{\partial r\partial\varphi} + \frac{\sin^2\varphi}{r}\frac{\partial}{\partial r} + \frac{\sin^2\varphi}{r^2}\frac{\partial^2}{\partial\varphi^2},\\
\partial_2^2 &= \sin^2\varphi\frac{\partial^2}{\partial r^2} - \frac{2\sin\varphi\cos\varphi}{r^2}\frac{\partial}{\partial\varphi} + \frac{2\sin\varphi\cos\varphi}{r}\frac{\partial^2}{\partial r\partial\varphi} + \frac{\cos^2\varphi}{r}\frac{\partial}{\partial r} + \frac{\cos^2\varphi}{r^2}\frac{\partial^2}{\partial\varphi^2}.
\end{aligned} \tag{A.2}$$

The known trigonometrical formulas

$$\cos\left(\frac{3}{2}\varphi_{z^{(1)}}\right) = \cos\varphi_{z^{(1)}}\cos\frac{\varphi_{z^{(1)}}}{2} - \sin\varphi_{z^{(1)}}\sin\frac{\varphi_{z^{(1)}}}{2}, \tag{A.3}$$

$$\sin\left(\frac{3}{2}\varphi_{z^{(2)}}\right) = \sin\varphi_{z^{(2)}}\cos\frac{\varphi_{z^{(2)}}}{2} + \cos\varphi_{z^{(2)}}\sin\frac{\varphi_{z^{(2)}}}{2}, \tag{A.4}$$

$$\cos^2\frac{\varphi_{z^{(1)}}}{2} = \frac{1+\cos\varphi_{z^{(1)}}}{2} = \frac{\sqrt{\cos^2\varphi+\alpha_1^2\sin^2\varphi}+\cos\varphi}{2\sqrt{\cos^2\varphi+\alpha_1^2\sin^2\varphi}}, \tag{A.5}$$

$$\sin^2\frac{\varphi_{z^{(1)}}}{2} = \frac{1-\cos\varphi_{z^{(1)}}}{2} = \frac{\sqrt{\cos^2\varphi+\alpha_1^2\sin^2\varphi}-\cos\varphi}{2\sqrt{\cos^2\varphi+\alpha_1^2\sin^2\varphi}}. \tag{A.6}$$

The anisotropic Lamé equations

$$\begin{pmatrix} c_2^2\Delta+(c_1^2-c_2^2)\partial_1^2-h'(t)^2\partial_1^2 & (c_1^2-c_2^2)\partial_1\partial_2 \\ (c_1^2-c_2^2)\partial_1\partial_2 & c_2^2\Delta+(c_1^2-c_2^2)\partial_2^2-h'(t)^2\partial_1^2 \end{pmatrix}\begin{pmatrix} v_1 \\ v_2 \end{pmatrix} = \begin{pmatrix} 0 \\ 0 \end{pmatrix}, \tag{A.7}$$

can be written in spherical coordinates with $\vec{v} = \begin{pmatrix} v_r \\ v_\varphi \end{pmatrix} = \begin{pmatrix} r^\alpha g_1(\varphi) \\ r^\alpha g_2(\varphi) \end{pmatrix}$:

$$\begin{pmatrix} A/2-B/2\cos(2\varphi) & 0 \\ 0 & A/2-B/2\cos(2\varphi)+C \end{pmatrix}\begin{pmatrix} g_1'' \\ g_2'' \end{pmatrix} + \begin{pmatrix} (1-\lambda)B\sin(2\varphi) & C(\lambda-1)-A+B\cos(2\varphi) \\ C(1+\lambda)+A-B\cos(2\varphi) & (1-\lambda)B\sin(2\varphi) \end{pmatrix}\begin{pmatrix} g_1' \\ g_2' \end{pmatrix} +$$
$$\begin{pmatrix} (A/2+C)(\lambda^2-1)+B/2(\lambda-1)^2\cos(2\varphi) & -B(1-\lambda)\sin(2\varphi) \\ B(1-\lambda)\sin(2\varphi) & A/2(\lambda^2-1)+B/2(\lambda-1)^2\cos(2\varphi) \end{pmatrix}\begin{pmatrix} g_1 \\ g_2 \end{pmatrix} = \begin{pmatrix} 0 \\ 0 \end{pmatrix}, \tag{A.8}$$

with $A = 1+\dfrac{1}{\alpha_2(t)^2}$, $B = 1-\dfrac{1}{\alpha_2(t)^2}$ and $C = \dfrac{c_1^2-c_2^2}{c_2^2\alpha_2(t)^2} = \dfrac{1}{(1-2\nu)\alpha_2(t)^2}$.

APPENDIX B

Appendix B

B.1 Fortran Code

Distribution of the eigenvalue solved by PDE2D Program.

```
C     *************************
C     * PDE2D 9.2 MAIN PROGRAM *
C     *************************
C     *** 1D PROBLEM SOLVED (COLLOCATION METHOD) ***
C#############################################################################
C     Is double precision mode to be used?  Double precision is recommended   #
C     on 32-bit computers.                                                     #
C#############################################################################
      implicit double precision (a-h,o-z)
      parameter (neqnmx=  99)
C#############################################################################
C     NXGRID = number of X-grid lines                                          #
C#############################################################################
      PARAMETER (NXGRID = 100)
C#############################################################################
C     How many differential equations (NEQN) are there in your problem?       #
C#############################################################################
      PARAMETER (NEQN = 2)
```

```
C        DIMENSIONS OF WORK ARRAYS
C        SET TO 1 FOR AUTOMATIC ALLOCATION
      PARAMETER (IRWK8Z=           1)
      PARAMETER (IIWK8Z=           1)
      PARAMETER (NXP8Z=1001,KDEG8Z=1)
C#############################################################################
C     The solution is saved on a uniform grid of NX+1 points                 #
C                         XA + I*(XB-XA)/NX                                  #
C     I=0,...,NX.  Enter a value for NX (suggested value = 50).              #
C#############################################################################
      PARAMETER (NX = 50)
C#############################################################################
C     The solution will be saved (for possible postprocessing) at the NSAVE+1 #
C     time points                                                            #
C                           T0 + K*(TF-T0)/NSAVE                             #
C     K=0,...,NSAVE.  Enter a value for NSAVE.                               #
C                                                                            #
C     If a user-specified constant time step is used, NSTEPS must be an      #
C     integer multiple of NSAVE.                                             #
C#############################################################################
      PARAMETER (NSAVE = 200)
      common/parm8z/ pi,al    ,rnu   ,alpha2
      dimension xgrid(nxgrid),xout8z(0:nx),xcross(100),tout8z(0:nsave),u
     &out8z(0:nx,2*neqn,0:nsave),uout(0:nx,2,neqn,0:nsave),xres8z(nxp8z)
     &,ures8z(neqn,nxp8z)
      equivalence (uout,uout8z)
      allocatable iwrk8z(:),rwrk8z(:)
C      dimension iwrk8z(iiwk8z),rwrk8z(irwk8z)
      character*40 title
      logical linear,crankn,noupdt,nodist,fillin,evcmpx,adapt,plot,lsqfi
     &t,fdiff,econ8z,ncon8z,restrt,gridid
      common/dtdp14/ sint8z(20),bint8z(20),slim8z(20),blim8z(20)
      common/dtdp15/ evlr8z,ev0r,evli8z,ev0i,evcmpx
      common/dtdp16/ p8z,evr8z(50),evi8z(50)
      common/dtdp19/ toler(neqnmx),adapt
      common/dtdp30/ econ8z,ncon8z
      common/dtdp42/ nxa8z,kd8z
```

```
      common/dtdp43/ work8z(nxp8z+3)
      common/dtdp45/ perdc(neqnmx)
      common/dtdp46/ eps8z,cgtl8z,npmx8z,itype
      common/dtdp62/ amin8z(2*neqnmx),amax8z(2*neqnmx)
      pi = 4.0*atan(1.d0)
      nxa8z = nxp8z
      kd8z = kdeg8z
C#############################################################################
      NPROB = 1
      do 78755 iprob=1,nprob
C#############################################################################
C     You may now define global parameters, which may be referenced in any    #
C     of the "FORTRAN expressions" you input throughout the rest of this      #
C     interactive session.  You will be prompted alternately for parameter    #
C     names and their values; enter a blank name when you are finished.       #
C                                                                             #
C     Parameter names are valid FORTRAN variable names, starting in           #
C     column 1.  Thus each name consists of 1 to 6 alphanumeric characters,   #
C     the first of which must be a letter.  If the first letter is in the     #
C     range I-N, the parameter must be an integer.                            #
C                                                                             #
C     Parameter values are either FORTRAN constants or FORTRAN expressions    #
C     involving only constants and global parameters defined on earlier       #
C     lines.  They may also be functions of the problem number IPROB, if      #
C     you are solving several similar problems in one run (NPROB > 1).  Note  #
C     that you are defining global CONSTANTS, not functions; e.g., parameter  #
C     values may not reference any of the independent or dependent variables  #
C     of your problem.                                                        #
C                                                                             #
C     +++++++++++++++ THE "FINE PRINT" (CAN USUALLY BE IGNORED) +++++++++++++#
C     + If you define other parameters here later, using an editor, you must +#
C     + add them to COMMON block /PARM8Z/ everywhere this block appears, if  +#
C     + they are to be "global" parameters.                                   +#
C     +                                                                       +#
C     + The variable PI is already included as a global parameter, with an    +#
C     + accurate value 3.14159...                                            +#
C     ++++++++++++++++++++++++++ END OF "FINE PRINT" ++++++++++++++++++++++++++#
```

```
C#########################################################################
      al     =
     & pi
      rnu    =
     & 0.45
      alpha2 =
     & 1.0
C#########################################################################
C     A collocation finite element method is used, with cubic Hermite         #
C     basis functions on the subintervals defined by the grid points:         #
C              XGRID(1),XGRID(2),...,XGRID(NXGRID)                            #
C     You will first be prompted for NXGRID, the number of X-grid points,     #
C     then for XGRID(1),...,XGRID(NXGRID).  Any points defaulted will be      #
C     uniformly spaced between the points you define; the first and last      #
C     points cannot be defaulted.  The interval over which the PDE system     #
C     is to be solved is then:                                                #
C               XGRID(1) < X < XGRID(NXGRID)                                  #
C#########################################################################
      call dtdpwx(xgrid,nxgrid,0)
C        XGRID DEFINED
      XGRID(1) =
     & -al/2.
      XGRID(NXGRID) =
     & al/2.
      call dtdpwx(xgrid,nxgrid,1)
C        *******TIME-DEPENDENT PROBLEM
      itype = 2
C#########################################################################
C     Enter the initial time value (T0) and the final time value (TF), for    #
C     this time-dependent problem.  T0 defaults to 0.                         #
C#########################################################################
      T0 = 0.0
      T0 =
     & 0
      TF =
     & 4.0
C#########################################################################
```

```
C     Is this a linear problem? ("linear" means all differential equations    #
C     and all boundary conditions are linear)                                 #
C#############################################################################
      LINEAR = .TRUE.
C#############################################################################
C     Do you want the time step to be chosen adaptively?  If you answer       #
C     'yes', you will then be prompted to enter a value for TOLER(1), the     #
C     local relative time discretization error tolerance.  The default is     #
C     TOLER(1)=0.01.  If you answer 'no', a user-specified constant time step #
C     will be used.  We suggest that you answer 'yes' and default TOLER(1)    #
C     (although for certain linear problems, a constant time step may be much #
C     more efficient).                                                        #
C#############################################################################
      ADAPT = .FALSE.
      TOLER(1) = 0.01
      NOUPDT = .FALSE.
C#############################################################################
C     The time stepsize will be constant, DT = (TF-T0)/NSTEPS.  Enter a       #
C     value for NSTEPS, the number of time steps.                             #
C     +++++++++++++++ THE "FINE PRINT" (CAN USUALLY BE IGNORED) +++++++++++++#
C     + If you later turn on adaptive step control, the time stepsize will be+#
C     + chosen adaptively, between an upper limit of DTMAX = (TF-T0)/NSTEPS  +#
C     + and a lower limit of 0.0001*DTMAX.                                    +#
C     ++++++++++++++++++++++++++ END OF "FINE PRINT" ++++++++++++++++++++++++#
C#############################################################################
      NSTEPS =
     & 200
      dt = (tf-t0)/max(nsteps,1)
C#############################################################################
C     If you don't want to read the FINE PRINT, enter 'no'.                   #
C                                                                             #
C     +++++++++++++++ THE "FINE PRINT" (CAN USUALLY BE IGNORED) +++++++++++++#
C     + Is the Crank-Nicolson scheme to be used to discretize time?  If you  +#
C     + answer 'no', a backward Euler scheme will be used.                    +#
C     +                                                                       +#
C     + If a user-specified constant time step is chosen, the second order   +#
C     + Crank Nicolson method is recommended only for problems with very      +#
```

```
C     + well-behaved solutions, and the first order backward Euler scheme    +#
C     + should be used for more difficult problems.  In particular, do not   +#
C     + use the Crank Nicolson method if the left hand side of any PDE is    +#
C     + zero, for example, if a mixed elliptic/parabolic problem is solved.  +#
C     +                                                                      +#
C     + If adaptive time step control is chosen, however, an extrapolation   +#
C     + is done between the 1-step and 2-step answers which makes the Euler  +#
C     + method second order, and the Crank-Nicolson method strongly stable.  +#
C     + Thus in this case, both methods have second order accuracy, and both +#
C     + are strongly stable.                                                 +#
C     ++++++++++++++++++++++++++ END OF "FINE PRINT" ++++++++++++++++++++++++#
C#######################################################################
      CRANKN = .FALSE.
      FDIFF = .FALSE.
C#######################################################################
C     You may calculate one or more integrals (over the entire region) of     #
C     some functions of the solution and its derivatives.  How many integrals #
C     (NINT), if any, do you want to calculate?                                #
C                                                                              #
C     +++++++++++++++ THE "FINE PRINT" (CAN USUALLY BE IGNORED) +++++++++++++#
C     + In the FORTRAN program created by the preprocessor, the computed     +#
C     + values of the integrals will be returned in the vector SINT8Z.  If   +#
C     + several iterations or time steps are done, only the last computed    +#
C     + values are saved in SINT8Z (all values are printed).                 +#
C     +                                                                      +#
C     + A limiting value, SLIM8Z(I), for the I-th integral can be set        +#
C     + below in the main program.  The computations will then stop          +#
C     + gracefully whenever SINT8Z(I) > SLIM8Z(I), for any I=1...NINT.        +#
C     ++++++++++++++++++++++++++ END OF "FINE PRINT" ++++++++++++++++++++++++#
C#######################################################################
      NINT =          1
C#######################################################################
C     You may calculate one or more boundary integrals (over the entire       #
C     boundary) of some functions of the solution and its derivatives.  How   #
C     many boundary integrals (NBINT), if any, do you want to calculate?      #
C#######################################################################
      NBINT =          0
```

```
C#####################################################################################
C     If you don't want to read the FINE PRINT, enter 'no'.                          #
C                                                                                    #
C     +++++++++++++++ THE "FINE PRINT" (CAN USUALLY BE IGNORED) +++++++++++++++#
C     + Normally, interpolation is done to approximate the initial values    +#
C     + using cubic Hermites.  Since some derivatives must be interpolated,  +#
C     + if the initial values are not smooth (ie, have large or infinite     +#
C     + derivatives), the resulting cubic interpolants may have undesired    +#
C     + noise or large spikes.  Do you want to compute a least squares       +#
C     + approximation to the initial values, rather than an interpolant?     +#
C     + The least squares fit is generally much smoother, but requires one   +#
C     + extra linear system solution.                                        +#
C     ++++++++++++++++++++++++++ END OF "FINE PRINT" ++++++++++++++++++++++++++#
C#####################################################################################
      LSQFIT = .FALSE.
      RESTRT = .FALSE.
C     GRIDID = .FALSE. IF FINITE ELEMENT GRID CHANGES BETWEEN DUMP, RESTART
      GRIDID = .TRUE.
C#####################################################################################
C     If you do not have periodic boundary conditions, enter IPERDC=0.               #
C                                                                                    #
C     Enter IPERDC=1 for periodic conditions at X = XGRID(1),XGRID(NXGRID)           #
C#####################################################################################
      IPERDC =          0
C#####################################################################################
C     The solution is saved on a uniform grid of NX+1 points, covering the           #
C     interval (XA,XB).  Enter values for XA,XB.  These variables are usually        #
C     defaulted.                                                                     #
C     The defaults are XA = XGRID(1), XB = XGRID(NXGRID)                             #
C#####################################################################################
C        defaults for xa,xb
      xa = xgrid(1)
      xb = xgrid(nxgrid)
C        DEFINE XA,XB HERE:
      call dtdpx1(nx,xa,xb,hx8z,xout8z,npts8z)
C        *******allocate workspace
      call dtdp1q(nxgrid,neqn,ii8z,ir8z)
```

```
      if (iiwk8z.gt.1) ii8z = iiwk8z
      if (irwk8z.gt.1) ir8z = irwk8z
      allocate (iwrk8z(ii8z),rwrk8z(ir8z))
C        *******DRAW GRID POINTS?
      PLOT = .FALSE.
C        *******call pde solver
      call dtdp1x(xgrid, nxgrid, neqn, nint, nbint, xout8z, uout, tout8z
     &, iperdc, plot, lsqfit, fdiff, npts8z, t0, dt, nsteps, nout, nsave
     &, crankn, noupdt, itype, linear, rwrk8z, ir8z, iwrk8z, ii8z, restr
     &t, gridid)
      deallocate (iwrk8z,rwrk8z)
C        *******read from restart file to array ures8z
C       call dtdpr1(1,xres8z,nxp8z,ures8z,neqn)
C        *******write array ures8z back to restart file
C       call dtdpr1(2,xres8z,nxp8z,ures8z,neqn)
C        *******call user-written postprocessor
      call postpr(tout8z,nsave,xout8z,nx,uout,neqn)
C        *******LINE PLOTS
C#############################################################################
C     Enter a value for IVAR, to select the variable to be plotted or         #
C     printed:                                                                #
C         IVAR = 1 means G1  (possibly as modified by UPRINT,..)              #
C                2       G1x                                                  #
C                3       G2                                                   #
C                4       G2x                                                  #
C#############################################################################
      IVAR =          2
C        T IS VARIABLE
      ics8z = 2
C#############################################################################
C     One-dimensional plots of the output variable as a function of T         #
C     will be made, at the output grid points X closest to                    #
C                XCROSS(I), I=1,...,NXVALS                                    #
C                                                                             #
C     Enter values for NXVALS, XCROSS(1),...,XCROSS(NXVALS),                  #
C#############################################################################
      NXVALS =          1
```

```
      XCROSS(1) =
     & 0
C
      alow = amin8z(ivar)
      ahigh = amax8z(ivar)
C#########################################################################
C     Specify the range (UMIN,UMAX) for the dependent variable axis.  UMIN    #
C     and UMAX are often defaulted.                                           #
C                                                                             #
C     +++++++++++++++ THE "FINE PRINT" (CAN USUALLY BE IGNORED) +++++++++++++#
C     + By default, each plot will be scaled to just fit in the plot area.   +#
C     + For a common scaling, you may want to set UMIN=ALOW, UMAX=AHIGH.     +#
C     + ALOW and AHIGH are the minimum and maximum values over all output    +#
C     + points and over all saved time steps or iterations.                  +#
C     ++++++++++++++++++++++++++ END OF "FINE PRINT" ++++++++++++++++++++++++#
C#########################################################################
      UMIN = 0.0
      UMAX = 0.0
C#########################################################################
C     Enter a title, WITHOUT quotation marks.  A maximum of 40 characters     #
C     are allowed.  The default is no title.                                  #
C#########################################################################
      TITLE = ' '
      TITLE = 'Eigenvalue                                 '
      is8z = 0
      do 78756 ixv8z=1,nxvals
      call dtdpzx(xcross(ixv8z),xa,xb,nx,ix8z)
      call dtdpzp(ics8z,ivar,tout8z,nsave,xout8z,nx,uout8z,neqn,title,um
     &in,umax,ix8z,is8z)
78756 continue
C        *******LINE PLOTS
      IVAR =          1
C        X IS VARIABLE
      ics8z = 1
      ISET1 = 0
      ISET2 = NSAVE
      ISINC = 1
```

```
      ISET1 =
     & 50
      ISET2 =
     & 200
      ISINC =
     & 50
C
      alow = amin8z(ivar)
      ahigh = amax8z(ivar)
C#########################################################################
C     Specify the range (UMIN,UMAX) for the dependent variable axis.  UMIN    #
C     and UMAX are often defaulted.                                           #
C                                                                             #
C     +++++++++++++++ THE "FINE PRINT" (CAN USUALLY BE IGNORED) +++++++++++++#
C     + By default, each plot will be scaled to just fit in the plot area.   +#
C     + For a common scaling, you may want to set UMIN=ALOW, UMAX=AHIGH.     +#
C     + ALOW and AHIGH are the minimum and maximum values over all output    +#
C     + points and over all saved time steps or iterations.                  +#
C     ++++++++++++++++++++++++++ END OF "FINE PRINT" ++++++++++++++++++++++++#
C#########################################################################
      UMIN = 0.0
      UMAX = 0.0
C#########################################################################
C     Enter a title, WITHOUT quotation marks.  A maximum of 40 characters     #
C     are allowed.  The default is no title.                                  #
C#########################################################################
      TITLE = 'G1 '
      call dtdprx(tout8z,nsave,iset1,iset2,isinc)
      do 78757 is8z=iset1,iset2,isinc
      call dtdpzp(ics8z,ivar,tout8z,nsave,xout8z,nx,uout8z,neqn,title,um
     &in,umax,ix8z,is8z)
78757 continue
C        *******LINE PLOTS
C#########################################################################
C     Enter a value for IVAR, to select the variable to be plotted or         #
C     printed:                                                                #
C         IVAR = 1 means G1  (possibly as modified by UPRINT,..)              #
```

```
C                2       G1x                                                  #
C                3       G2                                                   #
C                4       G2x                                                  #
C#############################################################################
      IVAR =          3
C        X IS VARIABLE
      ics8z = 1
      ISET1 = 0
      ISET2 = NSAVE
      ISINC = 1
      ISET1 =
     & 50
      ISET2 =
     & 200
      ISINC =
     & 50
C
      alow = amin8z(ivar)
      ahigh = amax8z(ivar)
C#############################################################################
C     Specify the range (UMIN,UMAX) for the dependent variable axis.  UMIN    #
C     and UMAX are often defaulted.                                           #
C#############################################################################
      UMIN = 0.0
      UMAX = 0.0
C#############################################################################
C     Enter a title, WITHOUT quotation marks.  A maximum of 40 characters     #
C     are allowed.  The default is no title.                                  #
C#############################################################################
      TITLE = 'G2 '
      call dtdprx(tout8z,nsave,iset1,iset2,isinc)
      do 78758 is8z=iset1,iset2,isinc
      call dtdpzp(ics8z,ivar,tout8z,nsave,xout8z,nx,uout8z,neqn,title,um
     &in,umax,ix8z,is8z)
78758 continue
78755 continue
      call endgks
```

```
      stop
      end
C
      subroutine pdes8z(yd8z,i8z,j8z,kint8z,x,t,uu8z)
      implicit double precision (a-h,o-z)
      parameter (neqnmx=  99)
C        un8z(1,I),un8z(2,I),... hold the (rarely used) values
C        of UI,UIx,... from the previous iteration or time step
      common /dtdp4x/un8z(3,neqnmx)
      common /dtdp11/normx
      double precision normx,uu8z(3,neqnmx)
      common/parm8z/ pi,al    ,rnu   ,alpha2
      G1  = uu8z(1, 1)
      G1x = uu8z(2, 1)
      G1xx= uu8z(3, 1)
      G2  = uu8z(1, 2)
      G2x = uu8z(2, 2)
      G2xx= uu8z(3, 2)
                          if (i8z.eq.0) then
      yd8z = 0.0
C#########################################################################
C     Enter FORTRAN expressions for the functions whose integrals are to be   #
C     calculated and printed.  They may be functions of                       #
C                                                                             #
C       X,G1,G1x,G1xx,G2,G2x,G2xx and (if applicable) T                       #
C                                                                             #
C     +++++++++++++++ THE "FINE PRINT" (CAN USUALLY BE IGNORED) +++++++++++++#
C     + If you only want to integrate a function over part of the interval,  +#
C     + define that function to be zero on the rest of the interval.         +#
C     ++++++++++++++++++++++++++ END OF "FINE PRINT" ++++++++++++++++++++++++#
C#########################################################################
C                                                    INTEGRAL DEFINED
      if (kint8z.eq.    1) yd8z =
     & abs(G1)+abs(G2)
C#########################################################################
C     Enter FORTRAN expressions for the functions whose "integrals" (sum      #
C     over two boundary points) are to be calculated and printed.  They may   #
```

```
C     be functions of                                                          #
C                                                                              #
C       X,G1,G1x,G1xx,G2,G2x,G2xx and (if applicable) T                        #
C                                                                              #
C     The unit outward normal, NORMx (=1 at right endpoint, -1 at left),       #
C     may also be referenced.                                                  #
C                                                                              #
C     +++++++++++++++ THE "FINE PRINT" (CAN USUALLY BE IGNORED) +++++++++++++#
C     + If you only want to "integrate" a function over one boundary point,  +#
C     + define that function to be zero at the other point.                  +#
C     ++++++++++++++++++++++++++ END OF "FINE PRINT" ++++++++++++++++++++++++#
C##############################################################################
C                                                    BND. INTEGRAL1 DEFINED
C     if (kint8z.eq.-1) yd8z =
C    & [DEFAULT SELECTED, DEFINITION COMMENTED OUT]
                          else
C##############################################################################
C     Now enter FORTRAN expressions to define the PDE coefficients, which      #
C     may be functions of                                                      #
C                                                                              #
C        X,T,G1,G1x,G1xx,G2,G2x,G2xx                                           #
C                                                                              #
C     Recall that the PDEs have the form                                       #
C                                                                              #
C                  C11*d(G1)/dT + C12*d(G2)/dT = F1                            #
C                  C21*d(G1)/dT + C22*d(G2)/dT = F2                            #
C                                                                              #
C##############################################################################
      phi = x
      rlambda = t
      A = 1 + 1/alpha2**2
      B = 1 - 1/alpha2**2
      C = 1./(1-2*rnu)*alpha2**2
      F11 = A/2. - B/2.*cos(2*phi)
      F22 = A/2. - B/2.*cos(2*phi) + C
      D11 = (1-rlambda)*B*sin(2*phi)
      D12 = C*(rlambda-1) - A + B*cos(2*phi)
```

```
      D21 = C*(1+rlambda) + A - B*cos(2*phi)
      D22 = (1-rlambda)*B*sin(2*phi)
      E11 = (A/2.+C)*(rlambda**2-1) + B/2.*(rlambda-1)**2*cos(2*phi)
      E12 = -B*(1-rlambda)*sin(2*phi)
      E21 =  B*(1-rlambda)*sin(2*phi)
      E22 =     A/2.*(rlambda**2-1) + B/2.*(rlambda-1)**2*cos(2*phi)
                if (j8z.eq.0) then
      yd8z = 0.0
C                                                     C(1,1) DEFINED
      if (i8z.eq. -101) yd8z =
     & 0
C                                                     C(1,2) DEFINED
      if (i8z.eq. -102) yd8z =
     & 0
C                                                     F1 DEFINED
      if (i8z.eq.    1) yd8z =
     & F11*G1xx + D11*G1x + D12*G2x + E11*G1 + E12*G2 - exp(x)
C                                                     C(2,1) DEFINED
      if (i8z.eq. -201) yd8z =
     & 0
C                                                     C(2,2) DEFINED
      if (i8z.eq. -202) yd8z =
     & 0
C                                                     F2 DEFINED
      if (i8z.eq.    2) yd8z =
     & F22*G2xx + D21*G1x + D22*G2x + E21*G1 + E22*G2 - exp(-x)
                else
                endif
                          endif
      return
      end
c
      function u8z(i8z,x,t0)
      implicit double precision (a-h,o-z)
      common/parm8z/ pi,al    ,rnu   ,alpha2
      u8z = 0.0
C#############################################################################
```

```
C     Now the initial values must be defined using FORTRAN expressions.       #
C     They may be functions of X, and may also reference the initial time T0. #
C#############################################################################
C                                                    G10 DEFINED
      if (i8z.eq.    1) u8z =
     & 0
C                                                    G20 DEFINED
      if (i8z.eq.    2) u8z =
     & 0
      return
      end
c
      subroutine gb8z(gd8z,ifac8z,i8z,j8z,x,t,uu8z)
      implicit double precision (a-h,o-z)
      parameter (neqnmx=  99)
      dimension uu8z(3,neqnmx)
C        un8z(1,I),un8z(2,I),... hold the (rarely used) values
C        of UI,UIx,... from the previous iteration or time step
      common /dtdp4x/ un8z(3,neqnmx)
      double precision none
      common/parm8z/ pi,al    ,rnu   ,alpha2
      none = dtdplx(2)
      G1  = uu8z(1, 1)
      G1x = uu8z(2, 1)
      G2  = uu8z(1, 2)
      G2x = uu8z(2, 2)
      if (j8z.eq.0) gd8z = 0.0
C#############################################################################
C     Enter FORTRAN expressions to define the boundary condition functions,   #
C     which may be functions of                                               #
C                                                                             #
C              X,G1,G1x,G2,G2x and (if applicable) T                          #
C                                                                             #
C     Recall that the boundary conditions have the form                       #
C                                                                             #
C                           G1 = 0                                            #
C                           G2 = 0                                            #
```

```
C                                                                              #
C     Enter NONE to indicate "no" boundary condition.                          #
C##############################################################################
            if (ifac8z.eq. 1) then
C##############################################################################
C     First define the boundary conditions at the point X = XGRID(1).          #
C##############################################################################
                          if (j8z.eq.0) then
C                                                    G1 DEFINED
      if (i8z.eq.    1) gd8z =
     & G1
C                                                    G2 DEFINED
      if (i8z.eq.    2) gd8z =
     & G2
                          else
                          endif
            endif
            if (ifac8z.eq. 2) then
C##############################################################################
C     Now define the boundary conditions at the point X = XGRID(NXGRID).       #
C##############################################################################
                          if (j8z.eq.0) then
C                                                    G1 DEFINED
      if (i8z.eq.    1) gd8z =
     & G1
C                                                    G2 DEFINED
      if (i8z.eq.    2) gd8z =
     & G2
                          else
                          endif
            endif
      return
      end
c
      subroutine pmod8z(x,t,uu8z,uprint,uxprnt)
      implicit double precision (a-h,o-z)
      dimension uu8z(3,*),uprint(*),uxprnt(*)
```

```
      common/dtdp14/sint(20),bint(20),slim8z(20),blim8z(20)
      common/parm8z/ pi,al    ,rnu   ,alpha2
      G1  = uu8z(1, 1)
      G1x = uu8z(2, 1)
      G1xx= uu8z(3, 1)
      G2  = uu8z(1, 2)
      G2x = uu8z(2, 2)
      G2xx= uu8z(3, 2)
C#############################################################################
C     + Normally, PDE2D saves the values of G1,G1x,G2,G2x at the output      +#
C     + points.  If different variables are to be saved (for later printing  +#
C     + or plotting) the following functions can be used to re-define the    +#
C     + output variables:                                                    +#
C     +    define UPRINT(1) to replace  G1                                   +#
C     +           UXPRNT(1)             G1x                                 +#
C     +           UPRINT(2)             G2                                  +#
C     +           UXPRNT(2)             G2x                                 +#
C     + Each function may be a function of                                   +#
C     +                                                                      +#
C     +    X,G1,G1x,G1xx,G2,G2x,G2xx and (if applicable) T                   +#
C     +                                                                      +#
C     + Each may also be a function of the integral estimates SINT(1),...,   +#
C     + BINT(1),...                                                          +#
C     +                                                                      +#
C     + The default for each variable is no change, for example, UPRINT(1)   +#
C     + defaults to G1.  Enter FORTRAN expressions for each of the           +#
C     + following functions (or default).                                    +#
C#############################################################################
C        DEFINE UPRINT(*),UXPRNT(*) HERE:
      UXPRNT(1) = 0
      if (sint(1).ge.0.001) then
         UXPRNT(1) = log(sint(1))
      endif
      return
      end
C        dummy routines
      subroutine xy8z(i8z,iarc8z,s,x,y,s0,sf)
```

```
      implicit double precision (a-h,o-z)
      return
      end
      subroutine dis8z(x,y,ktri,triden,shape)
      implicit double precision (a-h,o-z)
      return
      end
      function fb8z(i8z,iarc8z,ktri,s,x,y,t)
      implicit double precision (a-h,o-z)
      fb8z = 0
      return
      end
      function axis8z(i8z,x,y,z,ical8z)
      implicit double precision (a-h,o-z)
      axis8z = 0
      return
      end
      subroutine tran8z(itrans,x,y,z)
      implicit double precision (a-h,o-z)
      return
      end
C
      subroutine postpr(tout,nsave,xout,nx,uout,neqn)
      implicit double precision (a-h,o-z)
      dimension xout(0:nx),tout(0:nsave)
      dimension uout(0:nx,2,neqn,0:nsave)
      common/parm8z/ pi,al    ,rnu   ,alpha2
      common /dtdp27/ itask,npes,icomm
      common /dtdp46/ eps8z,cgtl8z,npmx8z,itype
      data lun,lud/0,47/
      if (itask.gt.0) return
C     UOUT(I,IDER,IEQ,L) = U-sub-IEQ,  if IDER=1
C                          Ux-sub-IEQ, if IDER=2
C       (possibly as modified by UPRINT,..)
C       at the point XOUT(I)
C       at time/iteration TOUT(L).
C       ******* ADD POSTPROCESSING CODE HERE:
```

```
C       IN THE EXAMPLE BELOW, MATLAB PLOTFILES pde2d.m,
C      pde2d.rdm CREATED (REMOVE C! COMMENTS TO ACTIVATE)
      if (lun.eq.0) then
         lun = 46
         open (lun,file='pde2d.m')
         open (lud,file='pde2d.rdm')
      endif
      do 78753 l=0,nsave
         if (tout(l).ne.dtdplx(2)) nsave0 = l
78753 continue
      write (lud,78754) nsave0
      write (lud,78754) neqn
      write (lud,78754) nx
78754 format (i8)
      do 78755 i=0,nx
         write (lud,78760) xout(i)
78755 continue
      do 78759 l=0,nsave0
         write (lud,78760) tout(l)
         do 78758 ieq=1,neqn
         do 78757 ider=1,2
         do 78756 i=0,nx
            write (lud,78760) uout(i,ider,ieq,l)
78756    continue
78757    continue
78758    continue
78759 continue
78760 format (e16.8)
      write (lun,*) '% Read solution from pde2d.rdm'
      write (lun,*) 'fid = fopen(''pde2d.rdm'');'
      write (lun,*) 'NSAVE = fscanf(fid,''%g'',1);'
      write (lun,*) 'NEQN = fscanf(fid,''%g'',1);'
      write (lun,*) 'NX = fscanf(fid,''%g'',1);'
      if (itype.eq.2) then
         write (lun,*) 'L0 = 0;'
      else
         write (lun,*) 'L0 = 1;'
```

```
      endif
      write (lun,*) 'T = zeros(NSAVE+1,1);'
      write (lun,*) 'X = zeros(NX+1,1);'
      write (lun,*) 'U = zeros(NX+1,NSAVE+1,2,NEQN);'
      write (lun,*) 'for i=0:NX'
      write (lun,*) '   X(i+1) = fscanf(fid,''%g'',1);'
      write (lun,*) 'end'
      write (lun,*) 'for l=0:NSAVE'
      write (lun,*) 'T(l+1) = fscanf(fid,''%g'',1);'
      write (lun,*) 'for ieq=1:NEQN'
      write (lun,*) 'for ider=1:2'
      write (lun,*) 'for i=0:NX'
      write (lun,*)
     & '   U(i+1,l+1,ider,ieq) = fscanf(fid,''%g'',1);'
      write (lun,*) 'end'
      write (lun,*) 'end'
      write (lun,*) 'end'
      write (lun,*) 'end'
      write (lun,*) 'xmin = min(X(:));'
      write (lun,*) 'xmax = max(X(:));'
      write (lun,*) '% Plots of each variable'
      write (lun,*) 'for IEQ=1:NEQN'
      write (lun,*) 'IDER = 1;'
      write (lun,*) 'umin = min(min(U(:,L0+1:NSAVE+1,IDER,IEQ)));'
      write (lun,*) 'umax = max(max(U(:,L0+1:NSAVE+1,IDER,IEQ)));'
      write (lun,*) 'for L=L0:NSAVE'
      write (lun,*) '   figure'
      write (lun,*) '   plot(X,U(:,L+1,IDER,IEQ))'
      write (lun,*) '   axis([xmin xmax umin umax])'
      write (lun,*) '   xlabel(''X'')'
      write (lun,*) '   ylabel([''U'',num2str(IEQ)])'
      write (lun,*) '   title(['' T = '',num2str(T(L+1))])'
      write (lun,*) 'end'
      write (lun,*) 'end'
      return
      end
```

List of Figures

References

[1] ASTM E 1823-96. *Standard terminology relating to fatigue and fracture testing-Annual Book of ASTM Standards*, volume 03.01. American Society for Testing and Materials, West Conshohocken, 1996. 32, 139, 178

[2] Griffith A. A. The phenomena of rupture and flow in solids. *Philos. Trans. R. Soc. Lond.*, 221:163–198, 1920. 30

[3] Rössle A. Corner singularities and regularity of weak solutions for the Two-Dimensional Lamé equations on domain with angular corners. *Journal of Elasticity*, 60:57–75, 2000. 48

[4] Lalegname A. Sändig A.-M. and Sewell G. Analytical and numerical treatment of a dynamic crack model. *Int. J. Fracture*, 152:97–125, 2008. 8, 64, 65, 67, 88, 94, 133, 134

[5] Owen D. M. Zhuang S. Rosakis A.J. and Ravichandran G. Experimental determination of dynamic crack initiation and propagation fracture toughness in thin aluminum sheets. *Int. J. of Fracture*, 90:153–174, 1998. 33, 79, 141

[6] Kobayashi A.S. and Mall S. Dynamic fracture toughness of homalite 100. *Experimental Mechanics*, 18:11–18, 1978. 139

[7] Broberg K. B. *Cracks and Fracture*. [u.a.]:Academic Press, San Diego, Calif., 1999. 3, 79, 80

[8] Freund L. B. *Dynamic Fracture Mechanics*. Cambridge University Press, New York, 1990. 3, 11, 32, 33, 79, 80, 82, 114, 131, 139, 141, 165

[9] Friedman A. Hu B. and Velazquez J.J.L. The evolution of stress intensity factors and the propagation of cracks in elastic media. *Arch. Rational Mech. Anal.*, 152:103–139, 2000. 66

[10] Yang B. and Ravi-Chandar K. On the role of the process zone in dynamic fracture. *J. Mech. Phys. Solids*, 44:1955–1976, 1996. 140

[11] Kostrov B.V. Unsteady propagation of longitudinal shear cracks. *Appl. Math. Mech.*, 30:1241–1248, 1966. 139

[12] Großmann C. and Roos H.-G. *Numerische Behandlung partieller Differentialgleichungen.* B.G. Teubner Verlag, 2005. 178

[13] Rosakis A.J. Liu C. and Freund L.B. A note on the asymptotic stress field of a non-uniformly propagating dynamic crack. *Journal of Mechanics and Physics of Solids*, 50:R39–R45, 1991. 11, 157

[14] Zhang Ch. *On wave Propagation in Cracked Solids*. PhD thesis, TH Darmstadt, Germany, 1993. 10

[15] Zhang Ch. and Gross D. Interaction of antiplane cracks with elastic waves in transversely isotropic materials. *Acta Mechanica 101*, pages 231–247, 1993. 10, 11

[16] Eshelby J. D. The continuum theory of lattice defects. *Solid State Physics*, III:79–144, 1956. 31

[17] Gross D. *Bruchmechanik*. Springer-Verlag, Berlin, 1996. 3, 11, 79, 80, 113

[18] Malvern L. E. *Introduction to the mechanics of a continuous medium*. Englewood Cliffs, NJ : Prentice-Hall, 1969. 83

[19] Erdogan F. *Crack-Propagation Theories*, volume II. Academic Press, New York and London, liebowitz ed. edition, 1968. 157

[20] Malluck J. F. *Crack propagation in finite bodies*. PhD thesis, Georgia Institut of Technology, 1976. 113

[21] Zhou F. and Shioya T. Energy balance analysis on mode-III dynamic crack propagation in fixed sided strip. *Int. J. of Fracture*, 80:33–44, 1996. 33, 64, 140

[22] Fichera G. *Existence theorems in elasticity*. Springer-Verlag, Berlin, handbuch der physik, Vol. VIa/2 edition, 1972. 27

[23] Kozlov V. A. Maz'ya V. G. and Rossmann J. Spectral properties of operator pencils generated by elliptic boundary value problems for the Lamé system. *Rostocker Math. Kolloq.*, 51:5–24, 1997. 7, 100

[24] Lamé G. *Leçons sur la Théorie Mathématique de l'Elasticité des Corps Solides*. Bachelier, Paris, 1852. 90

[25] Rosakis A.J. Ravichandran G. Dynamic failure mechanics. *Int. J. of Solids and Structures*, 37:331–348, 2000. 11, 33, 79

[26] Sewell G. *The Numerical Solution of Ordinary and Partial Differential Equations*. John Wiley & Sons Inc, second edition, 2005. 49, 137, 166, 178

[27] Sewell G. *PDE2D*. University of Texas, El Paso, www.pde2d.com. 35, 48, 133, 137, 150, 166, 167, 177

[28] Hsiao G.C. and Wendland W. *Boundary Integral Equations*. Applied Mathematical Sciences 164, Springer, 2008. 17, 18

[29] version 4.0. GnuPlot. *Technical report, Pixar Corporation*. http://www.gnuplot.info/, 2004. 134

[30] Aliabadi M. H. and Rooke D.P. *Numerical Fracture Mechanics*. Computational Mechanics Publications, Boston, 1991. 11, 27, 114

[31] Liebowitz H. *Fracture*, volume 6 of *1*. Academic Press, New York, 1968. 30

[32] Love A. E. H. *A treatise on the Mathematical Theory of Elasticity*, volume 14. Cambridge University Press, Cambridge, 4th edition, 1952. 28

[33] Neuber H. Ein neuer Ansatz zu Lösung raumlicher Probleme der Elastizitätstheorie. *Z. Ang. Math.-Mech.*, 23:585–614, 1986. 90

[34] Ockendon H. and Ockendon J. *Waves and Compressible Flow*, volume 47. Springer, texts in applied mathematics edition, 2004. 91

[35] Wenzel H. and Meinhold P. *Gewöhnliche Differentialgleichungen*. B.G. Teubner Verlagsgesellschaft, Leipzig, 1994. 39, 40

[36] Viktorov I.A. *Rayleigh and Lamb Waves*. Plenum, New York, 1967. 115

[37] Betten J. *Kontinuumsmechanik. Elastisches und inelastisches Verhalten isotroper und anisotroper Stoffe*. 2. ed. Springer Verlag, 2001. 13

[38] Freund L.B. Duffy J. and A.J. Rosakis. *Dynamic fracture initiation in metals and preliminary results on the method of caustics for crack propagation measurements*. Cambridge University Press, New York, 1981. 11, 139, 141

[39] Rosakis A. J. Duffy J. and Freund L.B. The determination od dynamic fracture toughness of aisi 4340 steel by the shadow spot method. *Journal of Mechanics and Physics of Solids*, 32:443–460, 1984. 33, 64, 139, 141

[40] Schwalbe K.-H. Landes J.D. and Heerens J. Classical fracture mechanics methods, comprehensive structural integrity. online update. 11, 2007. 33, 64, 139

[41] Ravi-Chandar K. and Knauss W.G. An experimental investigation into the mechanics of dynamic fracture: I. crack initiation and arrest. *International Journal of Fracture*, 25:247–262, 1984. 68, 157

[42] Takahashi K. and Arakawa K. *Experimental Mechanics*, 27:195–199, 1987. 140

[43] Wieghardt K. Über das Spalten und Zerreien elastischer Körper. Auf Grund eines Ansatzes von A. Sommerfeld. *Zs. f. Math. u. Phys*, 55:60–103, 1907. 5

[44] Broberg K.B. The propagation of a brittle crack. *Arkiv för Fysik*, 18:159–192, 1960. 171

[45] Freund L.B. Crack propagation in an elastic solid subjected to general loading iii. stress wave loading. *Journal of the Mechanics and Physics of Solids*, 21:47–61, 1973. 11

[46] Freund L.B. and Rosakis A.J. The structure of the near tip field solution during transient elastodynamic crack growth. *J. of the Mechanics and Physics of Solids*, 40:699–719, 1992. 11, 32, 64

[47] Freund L.B. and Clifton R.J. On the uniqueness of plate elastodynamic solutions for running cracks. *Journal of Elasticity*, 4:293–299, 1974. 141, 144

[48] Malvern L.E. *Methods of theoretical physics*, volume I and II. McGraw-Hill, New York, 1953. 90

[49] Youngseog Lee and Vikas Prakash. Dynamic fracture toughness versus crack tip speed relationship at lower than room temperature for high strength 4340var structural steel. *J. Mech. Phys. Solids*, 46:1943–1967, 1998. 33, 64

[50] Bockniack M. and Sändig A.-M. Computation of generalized stress intensity factors for bounded elastic structures. *Math. Modelling and Numerical Analysis*, 33:853–878, 1999. 35

[51] Brokate M. and Khludnev A. On crack propagation shapes in elastic bodies. *Z. angew. Math. Phys.*, 55:318–329, 2004. 66

[52] Dauge M. *Elliptic Boundary Value Problems on Corner Domains*. Springer-Verlag, Berlin-Heidelberg, lecture notes in mathematics 1341-mr 91a:35078 edition, 1988. 64

[53] Dauge M. Elliptic boundary value problems on corner domains - smoothness and asymptotics of solutions. *Lecture Notes in Mathematics*, 1341, 1988. 34

[54] Giaquinta M. and Hildebrandt S. *Calculus of Variations*. Springer: Berlin, Heidelberg, 1996. 67

[55] Marder M. Molecular dynamics of cracks. *Comp. Sci. Eng.*, 1:48–55, 1999. 82, 131, 165

[56] Westergaard H. M. Bearing pressures and cracks. *Journal Applied Mech.*, 6:A49–A53, 1939. 5

[57] Gurtin M.E. *The linear theory of elasticity*. Springer-Verlag, Berlin, handbuch der physik, vol. via-2 edition, 1972. 27

[58] Gurtin M.E. On the energy release rate in quasi-static elastic crack propagation. *J. Elasticity*, 9:187–195, 1979. 30

[59] Gurtin M.E. *An introduction to Continuum Mechanics*. Academic Press, New York, 1981. 15

[60] Williams M.L. Stress singularities resulting from various boundary conditions in angular corners of plates in extension. *Journal Applied Mech.*, 19:526–528, 1952. 5

[61] Muskhelishvili N.I. *Some Basic Problems on the Mathematical Theory of Elasticity*. Noordhoff, Groningen, 1952. 27

[62] Cherepanov G. P. Crack propagation in continuous media. *J. Appl. Math. Mech.*, 31:503–512, 1967. 30, 54

[63] Destuynder P. and Jaoua M. Sur une interprétation mathématique de l'intégrale de rice en théorie de la rupture fragile. *Math.Methods Appl.Sci.*, 3:70–87, 1981. 66, 67

[64] Grisvard P. *Elliptic Problems in Nonsmooth Domains*. Pitman, London, 1985. 34, 64

[65] Grisvard P. Singularités en elasticité. *Arch. Rational Mech. Anal.*, 107:157–180, 1989. 46

[66] Grisvard P. *Singularities in Boundary Value Problems*. Masson, Paris, rma 22 edition, 1992. 21, 34

[67] Morse P. and Feshbach H. *Dynamics of Fracture*. Heidelberg [u.a.] : Springer Verlag, Berlin, 2000. 114, 139

[68] Papkovich P.F. The representation of the general integral of the fundamental equations of elasticity theory in terms of harmonic functions (in russian). *Izv.Akad. Nauk SSSR, Phys.-Math.Ser.*, 10:1425, 1932. 90

[69] Ciarlet P.G. *Mathematical Elasticity*. North Holland, Amsterdam, vol. I- three-dimensional elasticity edition, 1988. 27, 85

[70] Barenblatt G. I. & Cherepanov L. R. On the wedging of brittle bodies. *J. Appl. Math. Mech.*, 23. 171

[71] Irwin G. R. *J. Appl. Mech*, 24:361, 1957. 5, 114

[72] Leis R. *Initial Boundary Value Problems in Mathematical Physics*. B. G. Teubner. Stuttgart and John Wiley & Sons, Chichester, 1986. 19

[73] Rice J. R. Mathematical analysis in the mechanics of fracture. in fracture ii: Mathematical fundamentals. 113

[74] Rice J. R. A path-independent integral and the approximate analysis of strain concentration by notches and cracks. *J. Appl. Mech.*, 35:376–386, 1968. 31

[75] Charoenphan S. *Computer methods for modeling the progressive damage of composite material plates and tubes*. PhD thesis, University of Wisconsin-Madison, 2002. 136

[76] Nicaise S. About the Lamé system in a polygonal or a polyhedral domain and a coupled problem between the Lamé system and the plate equation. I: regularity of the solutions. *Annali della Scuola Normale Superiore di Pisa Classe di Scienze*, 19:327–361, 1992. 46, 47, 48

[77] Nicaise S. and Sändig A.-M. Dynamic crack propagation in a 2D elastic body: The out-of-plane case. *J. Math. Anal. Appl.*, 329:1–30, 2007. 8, 68, 70, 74, 88, 96, 100, 177

[78] Sändig A.-M. Nicaise S. and Lalegname A. Dynamic crack propagation in a 2d elastic body. the out-of plane case. *ICIAM 07. ETH Zürich*, 2007. 179

[79] Suresh S. *Fatigue of Materials*. Cambridge University Press, second edition, 1998. 140

[80] Nazarov S.A. and Plamenesvkii B.A. Elliptic problems in domians with piecewise smooth boundaries. *Expositions in Mathematics*, 13:MR 95h:35001, 1984. 64

[81] Nazarov S.A. and Plamenevskii B.A. *Elliptic Problems in domains with piecewise smooth boundary*. Englewood Cliffs, Walter de Gruyter, New York, 1991. 21, 40

[82] Kato T. Linear and quasilinear equations of evolution of hyperbolic type. *CIME II ciclo*, Cortona:125–191, 1976. 70

[83] Seelig Th. *Zur Simulation der dynamischen Rißausbreitung mit einer Zeitbereichs-Randelementmethode*. PhD thesis, TH Darmstadt, Germany, 1997. 10

[84] Sändig A.-M. Richter U. and Sändig R. Regularity of boundary value problems for the Lamé equations in polygonal domain. *Rostocker Math. Kolloq.*, 36:21–50, 1989. 35, 46

[85] Tvergaard V. and Hutchinson J. The relation between crack growth resistance and fracture process parameters in elastic-plastic solids. *J. Mech. Phys. Solids*, 40:1377–1397, 1992. 33, 79

[86] Kondrat'ev V.A. Boundary value problems for elliptic equations in domain with conical o angular points. *Trans. Moscow Math. Soc.*, 16:227–312, 1967. 5, 21, 34, 64

[87] Kovtunenko V.A. Sensitivity of cracks in 2D-Lamé problem via material derivatives. *Z. angew. Math. Phys.*, 52:1071–1087, 2001. 66

[88] Kozlov V.A. and Mazya V.G. On stress singularities near the boundary of a polygonal crack. *Proc. Roy. Soc. Ednburgh*, 117A:31–37, 1991. 21

[89] Kozlov V.A. Maz'ya V.G. and Rossmann J. *Spectral Problems associated with corner Singularities of Solutions to Elliptic Equations*. American Mathematical Society, 2001. 35, 49, 54, 55

[90] Mazya V.G. and Plamenevskii B. A. On the coefficients in the asymptotics of solutions of elliptic boundary value problems in domain with conical points. *Amer. Math. Soc. Transl.*, 123:57–88, 1984. 34, 47

[91] Craggs J. W. On the propagation of a crack in an elastic-brittle material. *J. Mech. Phys. Solids*, 8:66–75, 1960. 171

[92] Bratov V. Petrov Y. Application of incubation time approach to simulate dynamic crack propagation. *Int. J. Fract.*, 146:53–60, 2007. 33, 79

[93] Buehler M.J. Gao H. Huang Y. Atomistic and continuum studies of a suddenly stopping supersonic crack. *Computational Materials Science*, 28:385–408, 2003. 82, 131, 165

Curriculum vitae

Personal information

Name: **Dipl.-Math. Adriana E. Lalegname**.

Day of birth: **April 15, 1976**.

Place of birth: **Tucumán-Argentina**.

Career

1982-1988. **Primary School**, *Ejército Argentino*, Tucumán-Argentina, Standard-bearer.

1989-1993. **Secondary School**, *Escuela Nacional de Comercio N 1*, General Belgrano, Tucumán.

1994-1999. **National University of Tucumán**, *(U.N.T.)*, Degree in Mathematics, (5 years).

1997-1999. **Mathematics Tutor**, *Chair of Algebra*, U.N.T..

April-Jun 2001. **Member of the Committee for academicals evaluation**, *for Assistant Professor place at the Department of Mathematics of University Tucumán*.

2000-2003. **Assistant Professor**, *Chair of Algebra*, U.N.T..

2000-2006. **Assistant Professor**, *Chair of mathematical Analysis*, U.N.T..

2005-2006. **Research Assistant**, *Project: "Experimental, theoretical and computational analysis of behavior of brittle porous materials"*, U.N.T..

October 2005 **PhD student**, *at University Stuttgart*, Project: "Modeling, analysis and simulation 2D dynamic crack propagation".

01.10.2005-30.09.2006. **DAAD Fellowship**, *Deutscher Akademischer Austausch Dienst*, Institute for Applied Analysis and Numerical Simulation, University Stuttgart, Germany.

01.05.2007-30.04.2008. **DAAD Fellowship**, *Deutscher Akademischer Austausch Dienst*, Institute for Applied Analysis and Numerical Simulation, University Stuttgart, Germany.

2008-2009. **Teaching Assistant**, *Department of Mathematic*, IANS, Institut für Angewandte Analysis und Numerische Simulation, University Stuttgart.

Language Knowledge

Spanish **native**

German **good**

English **good**

IANS - Inst. für Angewandte Analysis und Numerische Simulation. – Pfaffenwaldring 57, D-70569, Stuttgart, Germany.

✉ *Adriana.Lalegname@mathematik.uni-stuttgart.de*

• *http://www.ians.uni-stuttgart.de/am/Lalegname*